TWENTIETH ANZIP

CONDENSED MATTER PHYSICS MEETING

WAGGA WAGGA

30 JANUARY - 2 FEBRUARY 1996

HANDBOOK

DISCLAIMER

Portions of this document may be illegible in electronic image products. Images are produced from the best available original document.

Australian and New Zealand Institutes of Physics

20th ANNUAL

CONDENSED MATTER PHYSICS MEETING

Charles Sturt University, Riverina

Wagga Wagga, NSW

30 January - 2 February 1996

CONFERENCE HANDBOOK

ISSN-1037-1214

ORGANISED BY: Trevor Finlayson, John Cashion, Michael Ling, Andrew Smith, Tuck Choy and Peter Derlet

Department of Physics, Monash University,
Clayton, Victoria 3168

CONTENTS

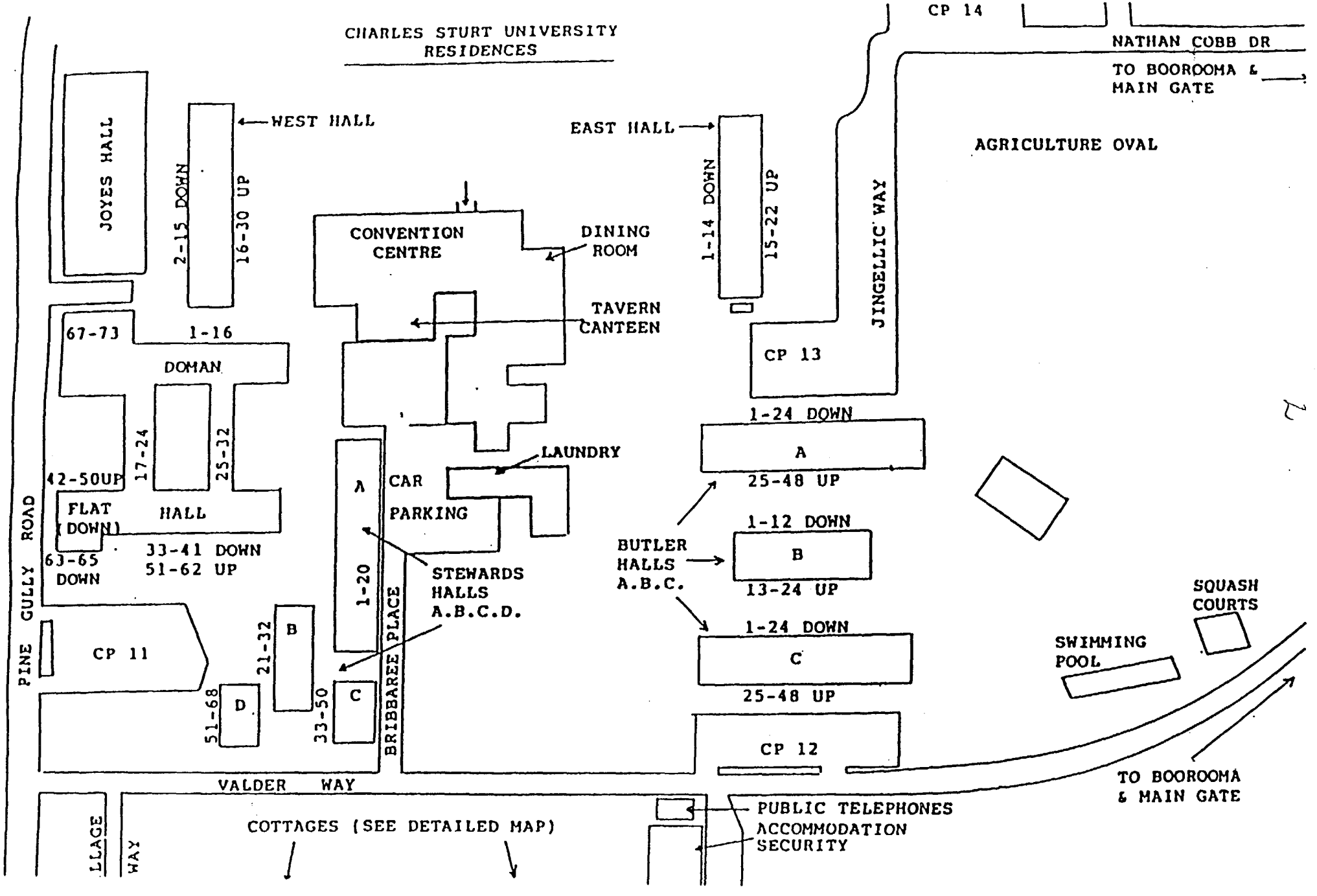
CHARLES STURT UNIVERSITY
RESIDENCES
CP 14
NATHAN COBB DR
TO BOOROOMA & MAIN GATE
AGRICULTURE OVAL
JOYES HALL
WEST HALL
2-15 DOWN
16-30 UP
EAST HALL
1-14 DOWN
15-22 UP
JINGELLIC WAY
CONVENTION CENTRE
DINING ROOM
TAVERN
CANTEEN
CP 13
67-73
1-16
DOMAN
1-24 DOWN
A
25-48 UP
17-24
25-32
42-50UP
FLAT (DOWN)
HALL
LAUNDRY
A
CAR
PARKING
63-65 DOWN
33-41 DOWN
51-62 UP
1-20
STEWARDS
HALLS
A.B.C.D.
BUTLER
HALLS
A.B.C.
1-12 DOWN
B
13-24 UP
SQUASH COURTS
SWIMMING POOL
1-24 DOWN
C
25-48 UP
PINE GULLY ROAD
CP 11
21-32
B
51-68
D
33-50
C
BRIBBAREE PLACE
CP 12
VALDER WAY
TO BOOROOMA & MAIN GATE
PUBLIC TELEPHONES
ACCOMMODATION
SECURITY
COTTAGES (SEE DETAILED MAP)
LLAGE
WAY

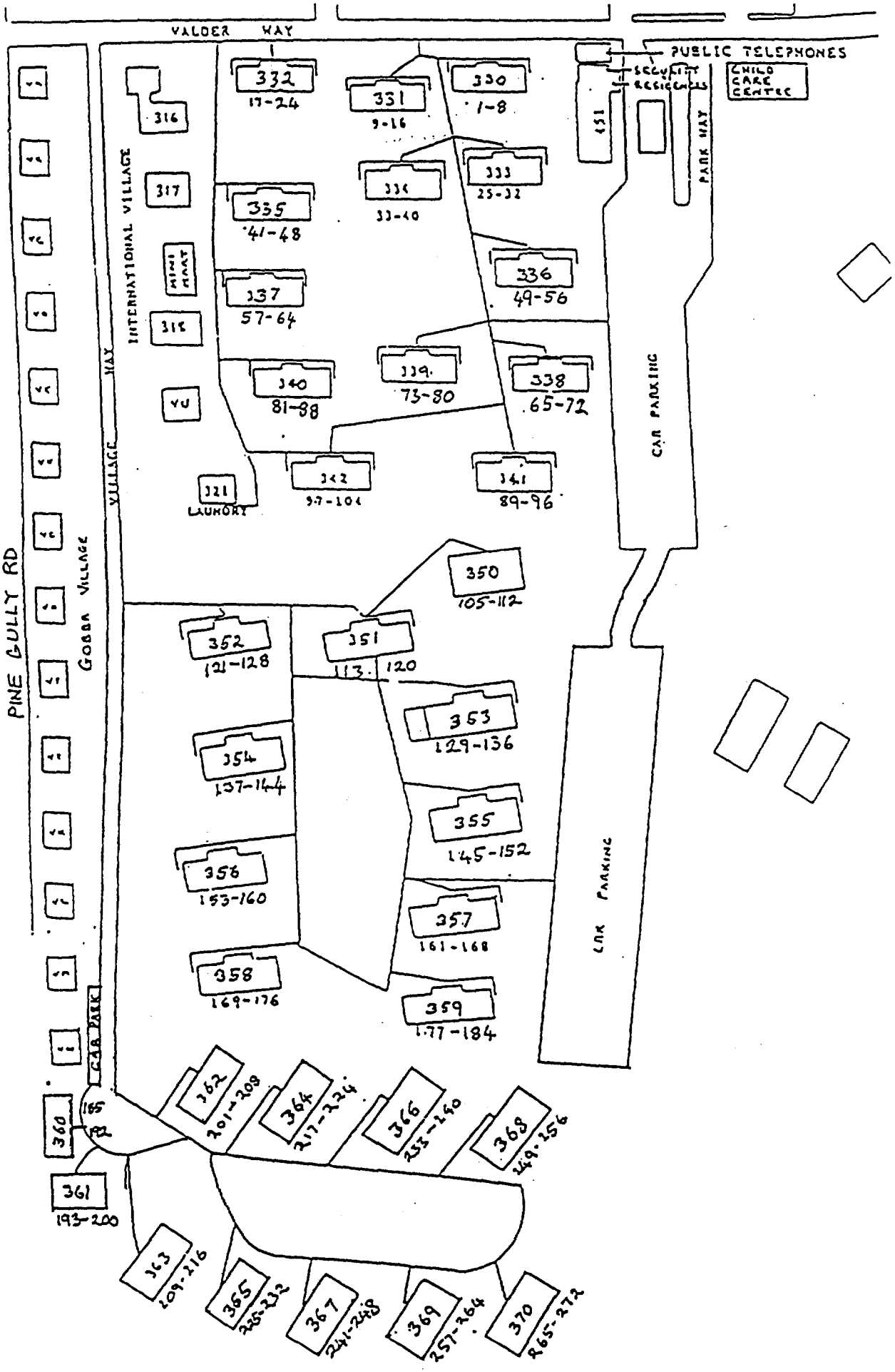
VALDER WAY
PUBLIC TELEPHONES
SECURITY RESIDENCES
CHILD CARE CENTRE
PARK WAY
CAR PARKING
INTERNATIONAL VILLAGE
VILLAGE WAY
PINE GULLY RD
GOGGA VILLAGE
CAR PARK
LAUNDRY
316
317
NIGHT HAWK
318
VU
321
332
17-24
331
9-16
330
1-8
333
25-32
334
33-40
335
41-48
336
49-56
337
57-64
338
65-72
339
73-80
340
81-88
341
89-96
342
97-104
350
105-112
351
113-120
352
121-128
353
129-136
354
137-144
355
145-152
356
153-160
357
161-168
358
169-176
359
177-184
360
185
361
193-200
362
201-208
363
209-216
364
217-224
365
225-232
366
233-240
367
241-248
368
249-256
369
257-264
370
265-272
451

WAGGA^2 '96

Welcome to Wagga^2 '96, the 20th Annual Australian/New Zealand Condensed Matter Physics Meeting. The 20th "Wagga", for the "staunch Wagga-ites", is certainly a significant milestone in the history of this conference which, as some of you will remember, began with the intention of creating an opportunity for the "condensed matter community" (including our post-graduate students) to come together for a few days in order to exchange ideas. The fact that the conference continues to achieve this objective is - in the terms of "Quality for the 1990s" - a significant measure of success.

This year's conference has been organised by a committee from the Department of Physics, Monash University, which, apart from two members on their third committee cycle, contains significant "new blood". So, from the administrative point of view, "Wagga^2"administration is "alive and well". The conference program this year incorporates a special symposium in memory of Dr. R. Lindsay Davis who will be sadly missed from "Wagga^2",after being an enthusiastic contributor to almost all previous meetings in this series. This "Lindsay Davis Memorial Symposium" is programmed for Thursday afternoon and we especially welcome to "Wagga '96" for this symposium, some of Dr. Davis' family, personal friends and professional colleagues. We trust that this symposium achieves the aims "to present some of the science conducted through the auspices of the Australian Institute of Nuclear Science and Engineering of which Dr. Davis was an integral part, and to include science in which he might have had a professional interest."

In assembling the program, we have tried to reaffirm the successful trend introduced at "Wagga '95", to include a significant number of oral talks by post-graduate students. (There are 10 in all, which represents about one quarter of the oral presentations.) We trust the plenary lectures offer you some of the significant "directions forward" for our discipline and provide all attendees some "food for thought" for their future research. For registration purposes, you should note that this conference handbook now has an ISSN reference number (ISSN-1037-1214) and for the information of all future organising committees, this number can now be retained for reference to all future Conference Handbooks in this Series, including any which will be at venues across the Tasman.

For the statisticians amongst you, the number of registrants at the time of writing is 195 and we have attempted to schedule 183 papers of which 40 are oral presentations. We are also pleased to welcome the input to our conference from nine industrial exhibitors and/or advertisers in this conference handbook.

We thank you all for your continuing support of the "Wagga^2" and we wish you a stimulating and productive "Wagga^2 '96".

The 1996 Committee (Trevor Finlayson, John Cashion, Michael Ling, Andrew Smith, Tuck Choy and Peter Derlet)

ACKNOWLEDGEMENTS

The Committee is grateful to Nick Savvides and his Committee for "Wagga^2 '95" for their advice and assistance in passing on the efficient "Wagga^2" organisation traditions; to Kathy Panarello, the Convention Centre Manager at CSU, for her assistance in the running of the conference, and to Julia Barnes and Maria Carter for their assistance in the data assembly. Also no conference of this nature could possibly be organised successfully without the support for the Organising Committee and the "Wagga^2" concept from the resources of the Department/Division in which it is based, which this time was the Department of Physics, Monash University.

We thank the "volunteer contacts" in the various institutions who have assisted with information distribution on which the success of "Wagga^2" depends: G.J. Bowden (UNSW), R. Buckley (IRL NZ), P.T. Callaghan (Massey), J. Ceremuga (JCU), D.J.H. Cockayne (Sydney), M.P. Das (ANU), S.X. Dou (Wollongong), A. Edgar (Victoria, NZ), P. Fisher (Wollongong), L. Folks (UWA), E. Grey (Griffith), E. Goldys (Macquarie), W. Huchison (ADFA), C. Jagadish (ANU), D.N. Jamieson (Melbourne), P.D. Killen (QUT), R. Leckey (LaTrobe), J.M. Long (Deakin), D.S. Maddison (DSTO), V. Maslen (CSIRO, MS&T), N. Savvides (CSIRO, DAP), C.A. Sholl (UNE), G.B. Smith (UTS), P.V. Smith (Newcastle), I. Snook (RMIT), E.R. Vance (ANSTO), T. Warminski (Telecom).

Finally, thanks are due to AINSE for its moral support of the concept of the "Lindsay Davis Memorial Symposium" and its financial support to some of the special guests.

GENERAL INFORMATION

Scientific Programme

All posters and lectures will be in the Convention Centre which adjoins the dining room (see maps). Chairpersons and speakers must keep to the lecture programme schedule. If slides are to be used during a session, please provides the projectionist with clearly marked slides at least 10 minutes before the relevant session. Preferably oversee their mounting and test one or two prior to the session. Overhead transparencies are, of course, catered for.

Posters must be mounted and removed at the time in the timetable.

Administration

Please wear your name tag at all times at the Convention Centre. Registration and all other administrative matters should be addressed to the registration desk or a committee member. For lost keys or if locked out of your room, contact the Accommodation and Security Office near the corner of Valder Way and Park Way or phone 2288 after hours.

Convention Centre Contact Numbers

Registration desk Phone (069) 33 2818 or (069) 33 2827
Convention Centre Office Phone (069) 33 2184
Fax (069) 33 2828
After hours emergencies, phone Security on (069) 33 2288

Meals, Coffee/Tea, Bar Facilities

All meals will be served in the dining room. You will receive a dining room pass on registration. *This must be produced at every meal.* It may also be required as ID for use of all other campus facilities (see below) which are at your disposal. Morning and afternoon tea will be served each day as indicated in the timetable. Coffee and tea-making facilities are also available in the Common Room of each building. In addition, at the time for author attendance at posters on Wednesday and Thursday, the Conference Bar will be open for author attendance at posters and on Wednesday only will reopen from 2000 until 2200. The Union bar at the rear of the centre is open all day and until late in the evening.

Sport and Recreational Facilities

The swimming pool is open from 0630 until 2200 as are the adjacent squash courts. Tennis courts opposite the oval are also available. A wide range of facilities such as exercise bikes, weight training, table tennis and basketball are available in the gymnasium. All of the facilities are free, i.e., covered by your registration fee.

SPONSORS

The Organising Committee gratefully acknowledges support from the following sponsor companies:

Alphatech International Pty Ltd

Balzers Australia

Cambridge University Press

Coherent Scientific

Domo-Technica Pty Ltd

Lastek Pty Ltd

Oxford Instruments

Oxford Scientific

Stanton Scientific

Some of the above companies are exhibiting their equipment and we encourage you to visit them during the course of the conference. Their sponsorships and those of other companies who have advertised in the handbook have helped to contain costs.

The financial support available to student members of the Australian and New Zealand Institutes of Physics, through the respective Branch Committees, to assist students to attend this conference is also acknowledged.

TIMETABLE

Tuesday 30 January

1400 onwards	Registration
1800 - 1900	*Dinner*
2000 - 2030	Posters WP to be mounted
2030	Poster session WP commences

Wednesday 31 January

0730 - 0830	*Breakfast*
0850 - 0900	Opening
0900 - 1030	Lecture session, Papers WM01 - WM05
1030 - 1100	*Morning Tea*
1100 - 1230	Lecture session, Papers WM06 - WM10
1230 - 1330	*Lunch*
1400 - 1515	Lecture session, Papers WA01 - WA04
1515 - 1635	Author attendance at Posters WP01 - WP36 *(Afternoon Tea)*
1600 - 1800	*Conference bar open*
1635 - 1800	Author attendance at Posters WP37 - WP72
1800 - 1900	*Dinner*
1900 - 1950	*Wine tasting*
2000 - 2115	Lecture session, Papers WE01 - WE03
2000 - 2200	*Conference bar open*
2115	Removal of WP Posters

Thursday 1 February

0730 - 0830	*Breakfast*
0730 - 0900	Mounting of TP Posters
0900	TP Poster session commences
0900 - 1030	Lecture session, Papers TM01 - TM04
1030 - 1100	*Morning Tea*
1100 - 1230	Lecture session, Papers TM05 - TM09
1230 - 1330	*Lunch*
1400 - 1540	Davis Symposium Lecture session, Papers TA01 - TA06
1540 - 1650	Author attendance at Posters TP01 - TP36 *(Afternoon Tea)*
1600 - 1800	*Conference bar open*
1650 - 1800	Author attendance at Posters TP37 - TP71
1800 - 1900	*Dinner*
2030 -	Trivia quiz: main Union Boorooma campus. Buses will be leaving outside the Accommodation and Security Office at regular intervals.

Friday 2 February

0730 - 0830	*Breakfast*
0900 - 1030	Lecture session, Papers FM01 - FM04
1030 - 1100	*Morning Tea*
1100 - 1215	Lecture session, Papers FM05 - FM08
1215 - 1230	Prizes and closing
1230 - 1330	*Lunch*
1230	Removal of TP posters

LECTURE SESSIONS

WEDNESDAY, 31 JANUARY

0850 - 0900 Opening: J.D. Cashion

Session WM

Chairperson: S.J. Campbell

0900 - 0930 WM01 *The Application of High Temperature Superconductors in Passive Microwave Devices*
D. Dew-Hughes (Invited Lecture)

0930 - 0945 WM02 *Flux Pinning and Vortex Dynamics in YBCO Melt-Textured Crystals*
Y. Zhao, H. Zhang, M. Xu, C.H. Choi and C. Andrikidis

0945 - 1000 WM03 *Advances in Development of Ag-Clad Bi-Based Superconducting Tapes*
S.X. Dou, M. Ionescu, W.G. Wang, Y.C. Guo, N.V. Vo, B. Zeimetz, H.K. Liu, I. Kusevic and E. Babic

1000 - 1015 WM04 *Electronic Raman Scattering in $Bi_2Sr_2CaCu_2O_{8+\delta}$*
J.W. Quilty, H.J. Trodahl and D. Pooke

1015 - 1030 WM05 *Processing and Fabrication of Ag-Clad Bi(Pb)-2223 Mono and Multifilamentary Tapes for Small Scale Coils Application*
N.V. Vo, S.X. Dou and H.K. Liu

Chairperson: N. Long

1100 - 1130 WM06 *Surface Alloy Structures*
D.J. O'Connor, J. Yao and Y.G. Shen (Invited Lecture)

1130 - 1145 WM07 *Nanometre Diameter Measurements on Silicon Spheres for Determination of the Avogadro Constant*
M.J. Kenny and E.C. Morris

1145 - 1200 WM08 *DNA Electrophoresis through Microlithographic Arrays*
E.M. Sevick and D.R.M. Williams

1200 - 1215 WM09 *Evolution of a Rolling Wear Track on Mg-PSZ*
G.L. Kelly and T.R. Finlayson

1215 - 1230 WM10 *Laser Raman Analysis Thresholds within Disordered Carbon Systems*
R.J. Walker, D.N. Barbara and K.W. Nugent

Session WA

Chairperson: N. Savvides

1400 - 1430	WA01	*Developments of High-T_c Oxide Superconducting Tapes and Coils at NRIM* H. Maeda (Invited Lecture)
1430 - 1445	WA02	*The High Temperature Approximation in NMR* G.J. Bowden, T. Heseltine and G.E. Ball
1445 - 1500	WA03	*Multiple Spin Echo Signal Formation from Ferromagnets* L.N. Shakhmuratova, D.K. Fowler, D.J. Isbister and D.H. Chaplin
1500 - 1515	WA04	*Magnetism and Atomic Short Range Order in Iron-rich B.C.C. Alloys* M.F. Ling, J.B. Staunton and D.D. Johnson

Session WE

Chairperson: G.A. Stewart

2000 - 2020	WE01	*Magnetic Properties of Fullerene Superconductors* V. Buntar (Invited Lecture)
2020 - 2040	WE02	*Detecting and Identifying Underground Nuclear Explosions* S. Spiliopoulos (Invited Lecture)
2040 - 2115	WE03	*A Skeptic Adrift on the Sea of Unreason* B. Williams (Invited Lecture)

LECTURE SESSIONS

THURSDAY, 1 FEBRUARY

Session TM

Chairperson: S.J. Kennedy

0900 - 0945 TM01 *Study and Engineering of Solid Surfaces on an Atomic Scale*
T.T. Tsong (Invited Lecture)

0945 - 1000 TM02 *The Differential Reflectance Microscope*
J. Tann and M. Gal

1000 - 1015 TM03 *High Magnetic Field Transport Measurements of a 2D-Hole System with an Unusual Landau Level Degeneracy*
E.E. Mitchell, R.G. Clark, V.A. Stadnik, R.B. Dunford, R.P. Starrett, A.S. Skougarevsky, F.F. Fang, P.J. Wang and B.S. Meyerson

1015 - 1030 TM04 *Tunneling Processes and Charge Accumulation in Triple Barrier Resonant Tunneling Structures*
L.D. Macks, S.A. Brown, R.G. Clark, R.P. Starrett, M.A. Read, M.R. Deshpande and W.R. Frensley

Chairperson: J. Liesegang

1100 - 1130 TM05 *The Physics of Granular Materials*
D.R.M. Williams (Invited Lecture)

1130 - 1145 TM06 *A New Hydrodynamics for Plasmons*
J.F. Dobson

1145 - 1200 TM07 *Hydrodynamic Plasmons on Wide Parabolic Quantum Wells*
H.M. Le and J.F. Dobson

1200 - 1215 TM08 *Studies of Quantum Spin Ladders at $T = 0$ and at High Temperatures*
Z. Weihong, J. Oitmaa and R.R.P. Singh

1215 - 1230 TM09 *Carbon K-Shell Near Edge Structure Calculations of Graphite using the Multiple Scattering Approach*
D.G. McCulloch and R. Brydson

Session TA **The Lindsay Davis Memorial Symposium**

Chairperson: J.B. Dunlop

1400 - 1410		*Introductory Remarks: Lindsay and "Wagga²"* J.B. Dunlop
1410 - 1430	TA01	*Neutron and X-ray Reflectometry: Solid Multilayers and Crumpling Films* A.S. Brown and J.W. White (Invited Lecture)
1430 - 1445	TA02	*Polarised Neutron Diffraction and the Spin Density in* $[As(C_6H_5)_4][TcNCl_4]$ P.A. Reynolds, J.B. Forsyth and B.N. Figgis
1445 - 1500	TA03	*Crystal Field Effects Using Polarised Neutron Spectroscopy* D.J. Goossens, S.J. Kennedy and T.J. Hicks
1500 - 1520	TA04	*Lindsay's Science on Reflection* M.M. Elcombe (Invited Comments)
1520 - 1535	TA05	*Small Angle Neutron Scattering from Hydrated Cement Pastes* T.M. Sabine, W.K. Bertram and L.P. Aldridge
1535 - 1550	TA06	*The Incommensurate Structure of* $Bi_2Sr_2CaCu_2O_{8+\delta}$ P.A. Miles, S.J. Kennedy. G.J. Russell, G. Gu, G.J. McIntyre and N. Koshizuka

Poster Papers TP65 - TP70 are also part of the Lindsay Davis Memorial Symposium

LECTURE SESSIONS

FRIDAY, 2 FEBRUARY

Session FM

Chairperson: J.F. Dobson

0900 - 0930	FM01	*Atomistic Simulation of Polymer/Solid and Polymer/Polymer Interfaces* I. Yarovsky (Invited Lecture)
0930 - 1000	FM02	*Macroscopic Properties of Model Disordered Materials* M.A. Knackstedt and A.P. Roberts (Invited Lecture)
1000 - 1015	FM03	*Dynamics of Polymers in a Good Solvent - a Molecular Dynamics Study using the Connection Machine* S.R. Shannon and T.C. Choy
1015 - 1030	FM04	*An Internal Configuration Bias Sampling Method for Dense Polymer Systems* A. Uhlherr

Chairperson: F. Green

1100 - 1130	FM05	*Semiquantum Systems from Supertransport to Giant Opalescence* E.P. Bashkin (Invited Lecture)
1130 -1145	FM06	*Mie Scattering in Heavy-Metal Fluoride Glasses* A. Edgar
1145 - 1200	FM07	*Two Photon Processes in Surface Photovoltage Spectroscopy* R.P. Craig and S.M. Thurgate
1200 - 1215	FM08	*Developments in Inverse Photoemission Spectroscopy* W. Sheils, R.C.G. Leckey and J.D. Riley
1215 - 1230		Closing: T.R. Finlayson

POSTER SESSIONS

Wednesday 31 January

Posters Up:	Tuesday 2000 - 2030
Author Attendance:	WP01 - WP36 1515 - 1635
	WP37 - WP72 1635 - 1800
Posters Down:	Wednesday 2110

WP01	The Structure of Gold Clusters in YBCO:Au	J.D.Cashion, D.Jinks, G.Jakovidis, G.Ganakas, L.J.Brown and M.J.Morgan
WP02	Crystal Field Interaction for the Superconducting Ceramics $TmBa_2Cu_3O_7$ and $TmBa_2Cu_4O_8$	G.A.Stewart, S.J.Harker and A.V.J.Edge
WP03	In Search of a Depinning Model for the Irreversibility Line in Conventional Superconductors	D.B.Lowe and T.R.Finlayson
WP04	High Temperature Pressing of Bi-2223 Tapes	P.A.Bain, Q.Y.Hu, D.Yu, H.K.Liu and S.X.Dou
WP05	Processing and Joining of Ag-sheathed Bi-2223 Superconducting Tapes	R.Bhasale, J.Horvat, H.K.Liu and S.X.Dou
WP06	Measuring Internal Friction at Sonic and Ultrasonic Frequencies in High Temperature Superconductors	A.R.Anderson and G.J.Russell
WP07	A High T_c Superconducting Current Limiting Device	C.Grantham, J.Beer, J.X.Jin and S.X.Dou
WP08	Testing a High T_c Superconducting High Voltage Generator	C.Grantham, J.Beer, J.X.Jin and S.X.Dou
WP09	High Temperature Superconducting Current Leads	B.Zeimetz, H.K.Liu and S.X.Dou
WP10	Thermopower of Magnetically Aligned $YBa_2Cu_3O_{7-\delta}$ Ceramic: A Measurement Approach for Anisotropic Transport of Ceramics	C. -J.Liu, H.J.Trodahl, J.Downes and M.P.Staines
WP11	Intrinsic Josephson Effects in Bi-2212	H.L.Johnson
WP12	Improvement of Critical Current Density by Control of Phase Evolution Prior to Sintering in Bi-2223 Tapes	W.G.Wang, P.Bain, J.Horvat, B.Zeimetz, Y.C.Guo, H.K.Liu and S.X.Dou
WP13	Cross-Sectional STEM Study of Cathodic Arc Deposited Amorphous Carbon and Carbon-Nitride Films	A.R.Merchant, D.G McCulloch, Y.Yin and D.R.McKenzie
WP14	Oxygen Ion and Electronic Conductivity in Doped Bismuth Oxides	N.J.Long and M.G.Fee
WP15	Measurement of Temperature Rise During Si Cleavage	D.Zhao, N.S.McAlpine and D.Haneman
WP16	Wave-function Mapping by (e,2e) Spectroscopy	S.A.Canney, M.Vos, P.J.Storer, A.Kheifets, I.E.McCarthy and E.Weigold

WP17	Electronic Structure of an Aluminium Oxide Film as Studied by (e,2e) Spectroscopy	X.Guo, M.Vos, Z.Fang, A.S.Kheifets, S.Canney, S.Utteridge, I.McCarthy and E.Weigold
WP18	Ultrasonic Absorption in Solid Specimens	P.J.W.Siwabessy and G.A.Stewart
WP19	Magnesium-Based Hydrogen Alloy Anodes for a Nickel-Metal Hydride Secondary Battery	N.Cui, B.Luan, H.J.Zhao, H.K.Liu and S.X.Dou
WP20	Effects of Cobalt, Aluminium, and Potassium-Boron Additions on the Performance of Titanium Based Alloy Electrodes	H.K.Liu, B.Luan, N.Cui and S.X.Dou
WP21	Shock Diffraction in Alumina Powder	G.Venz, P.D.Killen and N.W.Page
WP22	Cobalt-Doped Iron Oxides Prepared by Mechano-Chemical Activation	W.A.Kaczmarek
WP23	Formation of Zirconium Nitride Via Mechanochemical Decomposition of Zircon	T.Puclin and W.A.Kaczmarek
WP24	Examining the Effects of Fill Gas Pressure on the Distribution of Copper Atoms in a Hollow Cathode Lamp	D.R.Oliver and T.R.Finlayson
WP25	Thermal Expansion Anomalies in the Pre-cubic-to-tetragonal Phase-transition Range and the Quantum Paraelectric Regime of $SrTiO_3$	Mao Liu, Trevor R Finlayson and T Fred Smith
WP26	Effects of Aging on the Transformation Temperature in a Au-49.5at%Cd Alloy	Yoshihiro Kuroiwa, Mao Liu, Trevor R.Finlayson and T.Fred Smith
WP27	Electron and H-Atom Phototransfer: ESR Investigation in Doped Crystals and Glassy Matrices	George G Lazarev
WP28	An Electron Paramagnetic Resonance Study of the Behaviour of Copper (II) in Ageing Catechin-Based Model Wines	M.Mitri, G.R.Scollary, G.J.Troup, D.R.Hutton, C.A.Hunter and D.G.Hewitt
WP29	EPR Spectra of Synthetic, and Natural Australian Opals - A Pilot Study	D.R.Hutton, Mary Young G.J.Troup
WP30	Bernal Liquid Drop-Alpha Particle Models of Some Heavy Magic Number Nuclides	P D Norman
WP31	Magnetic Transitions in $La_{1-x}Y_xMn_2Si_2$ - Mössbauer Effect Study	X L Zhao, S J Campbell, J M Cadogan and Hong-Shuo Li
WP32	Detailed Comparison of Experiment with Theory for the Oscillatory Free Induction Decay in Gamma Detected NMRON	L.N.Shakhmuratova, W.D.Hutchison, D.J.Isbister and D.H.Chaplin
WP33	The Fermi Surface of Ferromagnetic Ni as Determined by Photoemission Spectroscopy: Resolution of the Spin Split Σ_1 Bands	S.Tkatchenko, J.A.Con Foo, A.P.J.Stampfl, B.Mattern, M.Hollering, R.Denecke, L.Ley, J.D.Riley and R.C.G.Leckey
WP34	Magnetic Disorder in Co-Mn and Ni-Mn Alloys	T.J.Hicks and M.F.Ling

WP35	Towards a Realistic Model of Fe-Cu-Fe Spin Valve Systems Using Tight-Binding Methods	Y.Hancock and A.E.Smith
WP36	Progress on 40 Tesla Hybrid Magnet at TML	H.Maeda
WP37	XPS Determination of Doping Mechanism in Amorphous Silicon	Jagriti Singh and R.C.Budhani
WP38	Use of NEXAFS for Thin Film Growth Morphology	Jagriti Singh
WP39	Electroluminescence of Spark-Processed Silicon	D.Haneman and J.Yuan
WP40	Stability of sp^2 Carbon Single Layer Nanostructures	L.N.Bourgeois and L.A.Bursill
WP41	Current Transport Mechanism and Effect of Hydrogen Plasma Treatment on A1-GaSb Schottky Diode	A.Subekti, V.W.L.Chin and T.L.Tansley
WP42	Photoconductive Decay in LCVD/PECVD Low Temperature Grown GaN	Bing Zhou, K.S.A.Butcher, Helen Zuo, Xin Li and T.L.Tansley
WP43	Studies in the Growth of ZnSe on GaAs(001)	J.D.Riley, D.Wolffframm, D.Westwood and A.Evans
WP44	The Determination of Poisson's Ratio of $Al_{0.3}Ga_{0.7}As$	B.F.Usher, A.S.Bloot, and G.W.Yoffe
WP45	Design and Performance Modelling of a Wavelength Specific Asymmetric Fabry-Perot Modulator	G.J. Nott, E.M.Goldys and K.J.Grant
WP46	Reflectance Spectroscopy in Very High Quality Shallow Quantum Wells	T.M.Silver and P.E.Simmonds
WP47	Zeeman Spectroscopy of Neutral Copper in Germanium	P.Fisher and R.E.M.Vickers
WP48	Far-Infrared Spectroscopy in Large Magnetic Fields	R.J.Heron, R.A.Lewis, R.G.Clark, R.P.Starrett and A.Skougarevsky
WP49	The Surface Band Structure of MBE Grown ZnSe{100}.	Y.Zhang, J.Xue, J.A.Con Foo, A.P.J.Stampfl, A.Ziegler, M.Hollering, R.Denecke, L.Ley, D.Wolframm, A.Evans, J.D.Riley and R.C.G.Leckey
WP50	Dopant Disorder-free 2DEG GaAs/AlGaAs Heterostructure FET Devices for Quantum Hall and Nanostructure Studies	Geoffrey R.Facer and Bruce E.Kane
WP51	Identification of the Common Electrically Detected Magnetic Resonance Signal from a Silicon Diode	D.J.Miller and Z.Xiong
WP52	Correlations and Finite Size Effects in Quasi One-dimensional Electron System	J.S.Thakur and D.Neilson
WP53	Electronic Structure of Perovskite $LaMnO_3$ and $CaMnO_3$	B.Chen, Y.Zhao and X.Zheng
WP54	A Theory of Paramagnetic Dynamic Susceptibility of Compositionally Disordered Alloys	M.F.Ling, J.B.Staunton and J.Poulter
WP55	Improved Bose Representation for One-dimensional Fermi Operators	G.B.Honner and M.P.Das

WP56	A Molecular Dynamics Study of Impurity Atoms in a Host Lattice	Marek Kijek and Ian Snook
WP57	The Structure of Glassy Carbon - A Model Based on Reverse Monte Carlo Analysis of TEM Data	Brendan O'Malley, Ian Snook and Dougal McCulloch
WP58	Goldstone Modes in the Edward's Polymer and How They Control the Corrections to Scaling	T C Choy and S R Shannon
WP59	Hysteresis in Ultrathin Ferroelectric Polymer Films Observed by Capacitance versus Voltage Measurements	Afifuddin and Ian L.Guy
WP60	Charge Transport of Doped Polypyrrole Films with Various Counter Anions	C.-J.Liu, A.B.Kaiser, W.T.Smith and J.S.Shapiro
WP61	High Exposure Hydrogen Chemisorption on the Si(111)7x7 Surface: A Semiempirical Cluster Study	Jian-Zhong Que, M.W.Radny and P.V.Smith
WP62	Boron, Hydrogen and Silicon Adatoms on the Si(111) Surface: An Ab Initio Hartree-Fock/Density Functional Cluster Study	Sanwu Wang, M.W.Radny and P.V.Smith
WP63	Elastic and Inelastic Scattering in Reflection High Energy Electron Diffraction (RHEED)	A.E.Smith
WP64	A Dielectric Matrix Calculation of the Surface-Plasmon Energy for the Silicon (100) Surface	A.J.Forsyth, A.E.Smith and T.W.Josefsson
WP65	Auger Photoelectron Coincidence Spectroscopy of Fe/Ni Alloys	S.M.Thurgate and C.P.Lund
WP66	Connection Between Electron Surface Barrier Resonance States in Metals and Surface Barrier Features in VLEED (Very-Low-Energy Electron Diffraction)	M.N.Read and A.S.Christopoulos
WP67	Magnetization Studies of Bi-2223 Tapes	K.-H.Müller, C.Andrikidis, H.K.Liu and S.X.Dou
WP68	Self-field AC Losses in Bi-2223 Superconducting Tapes	K.-H.Müller and K.E.Leslie
WP69	Noise Properties of High-Quality Step-Edge YBCO Josephson Junctions	Catherine P.Foley, Simon Lam, Graeme J.Sloggett, Nicholas Savvides, Alex Katsaros, Ling Hao, John C.Macfarlane, Colin M.Pegrum and Jan Kuznik
WP70	High-T_c Superconducting YBCO Thin Films for SQUIDS	Alex Katsaros, Nick Savvides and Cathy Foley
WP71	Microwave Properties and Microstructure of $Y_1Ba_2Cu_3O_7$ Thin Films	Nick Savvides, Alex Katsaros, David Reilly, Cathy Foley, Janina Ceremuga and Kenneth Leong
WP72	Does the Internet Improve Research Productivity?	D.S.Maddison

POSTER SESSIONS

Thursday 1February

Posters Up:	Thursday 0730 - 0900
Author Attendance:	TP01 - TP36 1540 - 1650
	TP37 - TP71 1650 - 1800
Posters Down:	Friday 1230

TP01	Preparation and Superconducting Critical Current of Melt-Textured YBCO with Large Size	Y.Zhao, C.H.Choi, C.C.Sorrell, B.Chen, M.La Robina and C.Andrikidis
TP02	The Search for Superconductivity in Rare Earth Nickel(III) and Nickel(I) Oxides	M.James and J.P.Attfield
TP03	Effect of Various Mechanical Deformation on the Properties of Silver-clad Bi-2223 Composites	Y.C.Guo, D.Akmacic, H.Wang, H.K.Liu and S.X.Dou
TP04	Particle and Powder Characterisation of Bi-Based Superconductors	M.Yavuz, Y.C.Guo, E.R.Vance, H.L.Liu and S.X.Dou
TP05	Formation of Weak and Strong Links in Ag/Bi-2223 Superconducting Tapes	J.Horvat, S.X.Dou and Y.C.Guo
TP06	A High T_c Superconducting Liquid Nitrogen Level Sensor	J.X.Jin, H.K.Liu, S.X.Dou, C.Grantham and J.Beer
TP07	High T_c Superconducting Winding	J.X.Jin, H.K.Liu, S.X.Dou, C.Grantham and J.Beer
TP08	A High T_c Superconducting Loss-free Resistor	J.X.Jin, J.Y.Chen and S.X.Dou
TP09	A Temperature Dependent Study of the Raman-active Phonon Modes in Ca and Zn doped $YBa_2Cu_3O_{7-x}$	J.W. Quilty, A. Simpson, H.J. Trodahl, N.Flower, M.Staines and J.Downes
TP10	Normal State Phase of CuO Planes in High T_c Superconductors	B.C.den Hertog and M.P.Das
TP11	Correlation of Micro-Raman and Optical Microscopy Analysis of Polycrystalline $YBa_2Cu_3O_{7-x}$	J.M.Long, T.R.Finlayson, C.S.Lim and T.P.Mernagh
TP12	XAS Study of Pu and Np Incorporation in Zirconolite	Bruce D.Begg and Eric R.Vance
TP13	Thermal Reorientation of Hydrogenic Pr^{3+} Centres	Glynn D. Jones
TP14	The Fermi Surface of Ordered and Disordered Cu_3Au as Determined by Angle Resolved Photoemission	J.A. Con Foo, S.Tkatchenko, A P. J.Stampfl, A.Ziegler, B.Mattern, M.Hollering, R.Denecke, L.Ley, J.D.Riley and R.C.G.Leckey
TP15	Surface Electrical Resistivity of Insulators	B.C.Senn and J.Liesegang
TP16	Imaging of Surface States and the Interpretation of STM Images from the GaAs Surface	L.D.Broekman, R.C.G.Leckey and J.D.Riley
TP17	Ellipsometric Studies of Anisotropic Thin Films	P.Moses, S.Dligatch and G.B.Smith
TP18	Direct Deposition of Quantum Scale Metal Structures in Oxide Matrices	S.Dligatch, M.R.Phillips, G.B. Smith and G.M.McCredie
TP19	Parameter Prediction for Microwave Garnets	Rodica Ramer
TP20	Nitridation of Si Using Mechano-Fusion Method	Z.L.Li, A.Calka and J.S.Williams

TP21	Preparation of Tungsten - Iron Carbide by Ball Milling	G.M.Wang, S.J.Campbell, A.Calka and W.A.Kaczmarek
TP22	Some Image Artefacts in Non-contact Mode Force Microscopy	B.P.Dinte, G.S.Watson, J.F.Dobson and S.Myhra
TP23	Conductor Shape Optimisation Using Thermographic Imaging	D.Jinks and P.Owen
TP24	An EPR Study of the Lacquer-Type Bottle Deposits from Red Wines	G.J. Troup, D.R.Hutton, J.R.Pilbrow, C.A. Hunter and D.G. Hewitt
TP25	The Possible Use of EPR Spectroscopy for Paint Pigment Identification	G.J.Troup, D.R.Hutton, M.Bacci, F.Lotti, A.Casini and M.Picollo
TP26	Blessed Niels Stensen: Dane, Florentine and Bishop; A Founding Father of Crystallography	A.E.Smith and G.J.Troup
TP27	Bacterial Leaching of Pyritic Gold Ores	Frank M.Gagliardi, John D.Cashion, L. Joan Brown and William H. Jay
TP28	Chemical and Morphological Changes During Production of Conducting Carbons from Ferrocene-Poly(Furfuryl Alcohol)	J.Ozaki, J.D.Cashion and L.J.Brown
TP29	Ball Milled Magnetic Powders	Sally G.Whitehead, John D.Cashion and L.Joan Brown
TP30	Review of Methods for Determining the Loaded Q-Factor of Microwave Resonators	Kenneth Leong, Robert Grabovickic and Janina Ceremuga
TP31	Invar Fe-Ni and the Santa Catharina Meteorite	Julia Chadwick
TP32	Magnetic Anisotropy of Amorphous Alloy Ribbons	Xiang-Yuan Xiong, Paul L.Rossiter and Trevor R.Finlayson
TP33	Nuclear Magnetic Resonance on Oriented Nuclei in $MnBr_2.4H_2O$	M.J.Prandolini, W.D. Hutchison, J.Leib, D.H.Chaplin and G.J.Bowden
TP34	Paramagnetic Probes to study $PrNi_5$	W.D.Hutchison, S.J.Harker, G.A.Stewart, D.H.Chaplin and N.Kaplan
TP35	Thulium Environment in the Ceramics Tm_2BaCoO_5 and Tm_2BaNiO_5	S.J.Harker, G.A.Stewart and A.V.J.Edge
TP36	Low-Field Magnetic Properties of $Fe_{3-x}Mn_xSi$ Alloys	T.Ersez, G.T.Etheridge and T.J.Hicks
TP37	Nanostructured Hexagonal Ferrites	W.A.Kaczmarek and B.W.Ninham
TP38	Interband Absorption in the Presence of a 2D Electron Gas: Fermi Edge Singularities and the Role of Negatively Charged Excitons	S.A.Brown, Jeff F.Young, J.A.Brum, P.Hawrylak and Z.Wasilewski
TP39	High Sensitivity to Temperature and Quantum Effects in Vanadium Oxide Diodes	V.A.Kuznetsov and D.Haneman
TP40	Spectroscopy of Beryllium Impurity in Gallium Arsenide	R.A.Lewis, T.S.Cheng, M.Henini and J.M.Chamberlain
TP41	Effect of Acoustic Phonon Scattering on the Width of the Electrical Multistability in a Double Barrier Structure	D.J.Fisher and C.Zhang

TP42	Stress-Enhancement of Certain Spectral Lines of Antimony in Germanium	R. J.Baker and P.Fisher
TP43	Minority Carrier Tunneling Resonances in Semiconductor Double Barrier Structures	M.L.F.Lerch, A.D.Martin, T.Silver, P.E.Simmonds and L.Eaves
TP44	Introduction to the La Trobe University II-VI MBE Facility	Y.Zhang, E.Huwald, J.D.Riley and R.C.G.Leckey
TP45	Illumination Effect on Transport Properties and Photo Conductivity Measurements of High Mobility 2D Hole Gas in Si-SiGe Heterostructures	V.A.Stadnik, E.E.Mitchell, R.G.Clark, F.F.Fang, P.J.Wang, B.S.Meyerson
TP46	Differential Reflectance Spectroscopy of Quantum Well Structures	Patrick Burke and Michael Gal
TP47	Direct and Indirect Optical Transitions in Strained $In_{0.15}Ga_{0.85}As/GaAs$ and in $In_{0.15}Ga_{0.85}As/Al_{0.15}Ga_{0.85}As$ Quantum Wells	E.M.Goldys, H.Zuo, M.R.Phillips, C.M.Contessa, M.R.Vaughan and T.L.Tansley
TP48	Mobility and Resistivity in GaAs Grown by MBE at Low Substrate Temperature	P.Arifin, E.M.Goldys, T.L.Tansley and M.R.Vaughan
TP49	Scientific Program of the Semiconductor Nanofabrication Facility	A.S.Dzurak, B.E.Kane and R.G.Clark
TP50	Understanding Noise Suppression in Heterojunction Field-Effect Transistors	F.Green
TP51	A Positron Annihilation Lifetime Spectroscopy Study of Porous Silicon Using a Continuous Lifetime Fitting Algorithm	P.M.Derlet and T.C.Choy
TP52	Green's Function Calculation of STM on Graphite Using a Pseudo Tight-Binding Model	B.A.McKinnon and T.C.Choy
TP53	Non-orthogonality in Tight-binding Models - a Derivation of the SWMc Parameters for Graphite	B.A.McKinnon and T.C.Choy
TP54	Series Expansion for the J_1-J_2 Heisenberg Antiferromagnet on the Square Lattice	J.Oitmaa and Zheng Weihong
TP55	Optical Absorption of a Quantum Plasma in a Magnetic Field and a Unidirectional Periodic Modulation	S.M.Stewart and C.Zhang
TP56	Theory of 2D Quantum Liquids	Miklos Gulacsi
TP57	Crystallization and Mechanical Properties of the Ultrafine Ferric Oxide-filled Polypropylene and Rheology of the Filled Polypropylene Melt	Gong Xiaoyi, Zeng Meizhen and Song Rongzhao
TP58	The Use of Piezoelectric Bimorph Transducers to Measure Forces in Colloidal Systems	A.M.Stewart
TP59	A Massively Parallel Molecular Dynamics Simulation of Phase Separation and Nucleation in a Simple Fluid	Steven Pickering and Ian Snook
TP60	A Parallel Molecular Dynamics Code Based on the Linked-Cell Method and its Application to Liquids	Aaron McDonough, Salvy Russo and Ian Snook
TP61	Electronic Charge Density of Si(111)2x1	B.Chen, Y.Zhao and D.Haneman
TP62	A Laboratory Based X-ray Reflectivity System	S.A.Holt, I.M.Jamie, T.L.Dowling, A.S.Brown and D.C.Creagh

TP63	A Molecular Dynamics Study of Hydrocarbons on the (001) Surfaces of Si and β-SiC	A.J.Dyson and P.V.Smith
TP64	The Jahn-Teller Effect and its Observation in Titanium Alum	Philip Tregenna-Piggott
TP65	Structural and Magnetic Features of the Novel Quaternary Compounds $NdTM_8SiB_3$(TM=Co, Ni)	Heng Zhang, S.J.Campbell, A.V.J.Edge and E.Wu
TP66	Leaching of Synroc in D_2O	E.R.Vance, N.Dytlewski, B.D.Begg, K.Prince and G.J.Thorogood
TP67	Neutron and Resonant X-ray Diffraction from Cuprate Superconductors	B.A.Hunter and C.J.Howard
TP68	A Neutron Diffraction Study of the Kinetics of Setting Cement	L.C.Jones, S.J.Kennedy and L.P.Aldridge
TP69	Plastic Deformation of Ce-ZrO_2 Studied by In-Situ Neutron Diffraction	E.H.Kisi, C.J.Howard and S.J.Kennedy
TP70	Development of Software in Labview for measurement of transport properties of High T_c Superconductors	David Reilly and Nick Savvides
TP71	Electron Emission from Materials at Low Excitation Energies	Nicoleta Urma, Marek Kijek and J.J.Millar

ABSTRACTS

LECTURES

WEDNESDAY POSTERS

THURSDAY POSTERS

THE APPLICATION OF HIGH TEMPERATURE SUPERCONDUCTORS IN PASSIVE MICROWAVE DEVICES

David Dew-Hughes
University of Oxford
Department of Engineering Science
Parks Road, Oxford, OX1 3PJ, UK

The front end of a microwave communications system is assembled form circuit elements comprising antennae, local oscillator, mixer and filters. Interconnection is by transmission line, into which delay may be incorporated. All of these components can, with advantage, be implemented in superconducting material. Superconductors, when operating below their crossover frequency, have values of surface resistance lower than those for normal metals such as copper and silver. This results in lower insertion loss for microwave components, allowing the design of smaller, more compact, yet at the same time more complicated, devices. The non-dispersive nature of superconductors can also be an advantage in enabling very high band-width signal processing. High temperature superconductors allow operating temperatures in the liquid nitrogen range, not too far below the ambient temperature in many communication satellites. HTS filters are already incorporated into mobile communications systems base stations in the US.

The Oxford microwave programme has concentrated on the implementation of all of the above devices from thin-film TI-2212, on MgO and $LaAlO_3$ substrates. The performance of resonators, delay line, antenna-mixers, and filters will be described. Of these, filters represent the greatest challenge, as they must be patterned to a higher degree of accuracy than the other components. An all-77K oscillator, stabilised by a superconducting resonator, has just been completed. A complete system front end is our next objective.

FLUX PINNING AND VORTEX DYNAMICS IN YBCO MELT-TEXTURED CRYSTALS

Y.Zhao[1], H.Zhang[2], M.Xu[3], C.H.Choi[1], and C.Andrikidis[4]

[1]School of Materials Science and Engineering, University of New South Wales, Sydney, NSW 2052, Australia

[2]Department of Physics, Peking University, Beijing 100871, P.R. China

[3]Ames National Laboratory, Iowa State University, Ames, Iowa, USA

[4]CSIRO Division of Applied Physics, National Measurement Laboratory, Lindfield, NSW 2047, Australia

Flux pinning and vortex dynamics in Melt-Textured-Growth (MTG) $YBa_2Cu_3O_{7-y}$ (Y123) crystals have been studied by measurements of magnetization from 4 to 90 K and up to 5 T, ac susceptibility, I-V characteristics, and TEM and SEM analyses. A fishtail or peak effect in the field dependence of the superconducting current density is observed in samples annealed in oxygen for a long time. It is found that the fishtail effect is sensitive to the oxygen distribution and dopants such as Nd at Y site or Ni at Cu(2) site, suggesting that the fishtail effect is independent of the magnetic impurities, but closely related to the microstructural defects. TEM analysis shown these samples have needle-shape defects with high density. The irreversibility line determined by I-V curve is consistent with that by magnetization and the I-V curves are found to obey the scaling behaviour of the vortex-glass transition. The mechanisms of fishtail effect and high critical current density of the samples are discussed.

References:

[1] Y.Zhao, et al, **Physics Letters A**, 203, 53-57 (1995).

ADVANCES IN DEVELOPMENT OF Ag-CLAD Bi-BASED SUPERCONDUCTING TAPES

S.X. Dou, M. Ionescu, W.G. Wang, Y.C. Guo, N. V. Vo, B. Zeimetz and H.K. Liu

Centre for Superconducting and Electronic Materials,

University of Wollongong, NSW 2522, Australia

I. Kusevic and E. Babic

Department of Physics, University of Zagreb, POB 162, Zagreb, Croatia

Significant advances in development of the Ag-clad Bi-based superconducting tapes have been recently achieved by the Wollongong group. These include understanding of the effect of initial phase composition on sintering temperature, formation mechanism of high T_c phase, control of sausaging formation during rolling and effect of atmosphere on microstructure of the tapes. Techniques such as "sandwich rolling" process have been developed to prevent the formation of sausaging and cracks in longitudinal direction of the Ag-clad Bi-based superconducting tapes. High J_c for Ag/Bi-2212 tapes achieved through MTG in the alternating oxygen and nitrogen atmosphere. While N_2 annealing on cooling ensures high T_c, O_2 treatment during melting period enhances the stability of 2212, allowing for grain growth with ample liquid formation. Direct observation of the interface achieved by removing Ag sheath with Hg alloy shows highly dense, textured and thin-film like structure. Ca_2PbO_4 was found to have significant effect of sintering temperature. Incorporation of Ca_2PbO_4 into 2212 phase can reduce the duration of 2223 tape process to below 100h, resulting high J_c with a record performance in magnetic field. 23.4% of zero field J_c value was retained in 1T. Grain growth in 2223 tape must be well controlled in order to optimise J_c. Features of 2212 tape and 2223 tape are compared in terms of their processing, microstructure and electromagnetic properties. Potential strong links in the tape are proposed to be the low angle tilt boundaries where the Cu-O planes are well connected. The pinning potential, U_o, for 2223 tape, determined by using magnetoresistance measurements, is larger than that for the best 2212 tape and epitaxial thin films while U_o for the latter is, in turn, higher than 2212 single crystal. This may be attributed to the difference in dislocation density in these materials.

AU9918113

ELECTRONIC RAMAN SCATTERING IN $Bi_2Sr_2CaCu_2O_{8+\delta}$

J.W. Quilty*, H.J. Trodahl* and D. Pooke†
*Victoria University of Wellington, New Zealand
† Industrial Research Limited, New Zealand

High–T_c superconductors exhibit a definite Electronic Raman Scattering (ERS) continuum, which most materials do not. Typically, the continuum is relatively flat in the normal state, while below T_c the ERS spectrum shows reduced scattering at the lowest Raman shifts and a peak close to the superconducting gap energy. The behaviour below T_c is due to the breaking of Cooper pairs and reflects the superconducting density of states, hence revealing the superconducting gap.

Through an appropriate choice of incident and scattered polarisation vectors, the electronic Raman continuum of high–T_c superconductors may also be used to reveal information on the symmetry of the superconducting gap.[1] Previous studies[2,3] of the electronic continuum show that a broad peak associated with the superconducting gap forms in the continuum below T_c in these materials, when compared to the normal–state.

We report temperature and polarisation dependent ERS measurements on differently–doped $Bi_2Sr_2CaCu_2O_{8+\delta}$ (Bi2212) single crystals, within a temperature range of 300K to 10K. The electronic continuum shows the expected peak below T_c (fig. 1), which changes in position and intensity with the doping of the crystal.

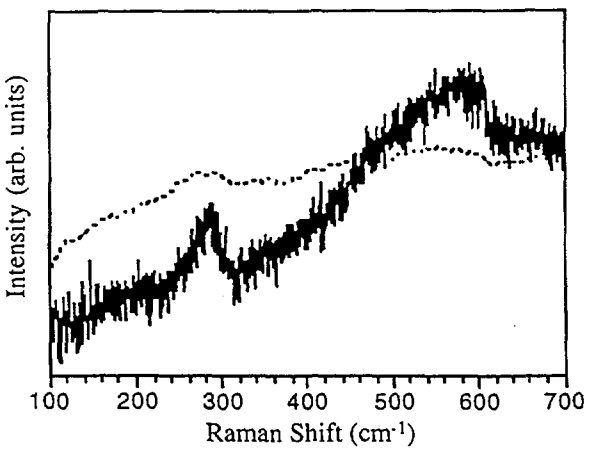

Figure 1 (left) shows two Raman spectra taken from an optimally doped single crystal of Bi2212. The dashed line is the electronic continuum at 300K, the solid line is the continuum at 10K. Note the peak at around 590cm^{-1} and the reduced scattering at low Raman shifts, compared to the 300K spectrum. The peak at 290cm^{-1} in both spectra is a phonon mode.

[1] T.P Deveraux, D. Einzel, B. Stadlober, et al., **Electronic Raman Scattering in High–T_c Superconductors: A Probe of d_{x-y} Pairing**, Phys. Rev. Lett. 72 (3), 396–399 (1994)
[2] C. Kendziora and A. Rosenberg, ***a-b* plane anisotropy of the superconducting gap in $Bi_2Sr_2CaCu_2O_{8+\delta}$**, Phys. Rev. B 52 (14), R9869–R9870 (1995)
[3] B. Stadlober, R. Nemetschek, O.V. Misochko, et al., **Electronic Raman scattering in differently doped high–T_c materials**, Physica B 194–196 (1994) 1539–1540

PROCESSING AND FABRICATION OF Ag-CLAD Bi(Pb)-2223 MONO AND MULTIFILAMENTARY TAPES FOR SMALL SCALE COILS APPLICATION

N.V. Vo, S.X. Dou and H.K. Liu

Centre For Superconducting and Electronic Materials, University of Wollongong, Northfields Avenue, Wollongong, NSW 2522, Australia.

Abstract

The processing of long length mono and multifilamentary silver clad Bi(Pb)-2223 tapes requires careful monitoring and controlling at every step of the production. The fate of the finished product relies on such factors as the quality of the precursor powder: reactivity, initial compositional phase and particle size, packing density, alternative alloys of silver as a cladding matrix, and thermal-mechanical (plastic) deformation: temperature of annealing and sintering, duration of sintering, pressing and/or rolling reduction ratio in between sintering stages, filling factor, filament distribution and stacking factor. Furthermore, these factors are found to be inter-related. Tapes prepared with different powder stoichiometric compositions show a slight variation in optimal parameters such as temperature and duration of heat treatment. With multifilamentary tapes in particular, different rolling reduction ratio zone between sintering periods can result from a change in the number and/or distribution of the individual filaments themselves.

With a systematic approach in processing of long lengths mono and multifilamentary Bi(Pb)-2223/Ag tapes successful high temperature superconducting singly and co-wounded pancake and solenoidal coils have been fabricated by react-wind and wind-react techniques. Current measurements are being conducted on these coils for future magnet applications.

Acknowledgement: The authors would like to acknowledge the financial support from The Australian Research Council, Metal Manufactures Ltd and The Energy Research and Development Corporation.

SURFACE ALLOY STRUCTURES

D.J. O'Connor, J. Yao and Y.G. Shen
Department of Physics, University of Newcastle, Callaghan, N.S.W. 2308

There have been numerous studies of the surface structure of bulk alloys and their properties when exposed to different environments. To better understand the driving forces in the dynamics of alloy surfaces, there has been greater interest in the growth of alloys from clean surfaces. In some instances, alloys of one atomic layer thickness are formed while in other, a region of 2-4 atomic layers of alloy has been observed. The physical and chemical properties of these surfaces can be significantly different to those of bulk terminated surfaces. In order to understand the importance of the structure on the chemical and physical properties, a series of alloy systems have been investigated to grow alloys controllably layer by layer.

This report will concentrate on the growth of alloy surfaces in systems for which there are stable bulk forms. The systems investigated include Ni_3Al, Cu_3Pd and Al_3Pd. Using Low Energy Ion Scattering the surface and near-surface composition was measured while the order was established by Low Energy Electron Diffraction. For Al/Ni(100) a three atomic layer deep alloy surface was formed and the order was the (2x2) structure expected for an ordered bulk termination of $Ni_3Al(100)$. The interesting aspect of this surface is that the alloy thickness formed appears to be independent of the availability of Al beyond some initial threshhold value.

The situation is different for Pd/Cu(100) where the surface was initially disordered. However, once the composition reached that of the bulk like termination a *p4g* structure was observed. This observation has been explained in terms of size differences between the Cu and Pd atoms. This structure has not been reported for the bulk terminated surface and arises from the growth from a Cu(100) substrate. The critical composition structure involves both the surface and the second layers comprising nearly 50% Cu and Pd.

To check these findings a similar system which is reported to develop a p4g structure is currently under investigation. The system involves Al/Pd(100) in which the Al and Pd have a similar difference in atomic sizes to that of the Cu and Pd. It is expected that this size difference will be the driving force to create this interesting surface difference. This series of studies is still underway however the *p4g* surface has again been observed. Although the measurements are not yet complete, it appears that the *p4g* structure is developed in a different manner to the Pd/Cu(100) as the surface composition of this system has remained 100% Pd under the ordered conditions. The compositions of the second and subsequent layers have yet to be confirmed.

These structures offer an interesting intermediate state between simple metals and ordered bulk alloy surfaces to test models of surface properties as well as the prospect of 'new surfaces' to explore for different chemical and physical properties.

Nanometre Diameter Measurements on Silicon Spheres for Determination of the Avogadro Constant

M.J.Kenny and E.C.Morris, CSIRO Division of Applied Physics, PO Box 218 Lindfield NSW 2070

The kilogram is the only remaining fundamental unit within the *SI* system which is defined in terms of an artefact (a Pt-Ir cylinder kept in Paris). It is proposed in the medium term to redefine the kilogram in terms of the Avogadro constant. By definition an Avogadro number of ^{12}C atoms weigh exactly 12 g, so the kilogram could be defined as the mass of 1000/12 ^{12}C atoms if the Avogadro constant is known to an accuracy of 1×10^{-8}.

The preferred method for determination of the Avogadro constant is to use a highly polished 1 kg silicon sphere manufactured with roundness to within ±30 nm. The parameters to be measured are lattice spacing and atoms per unit cell, mass and volume. It is also necessary to know the nature and composition of surface impurities such as oxide and water.

The nominal diameter of a 1 kg Si sphere is 94 mm. In order to obtain an accuracy of 1×10^{-8} in volume, the diameter must be known to ± 0.3 nm i.e. within one atom. This requires optical interferometry against a precision etalon using stabilised laser light. The measurements are sensitive to many parameters particularly temperature. An instability of ±5 mK will be sufficient to cause the silicon to expand and the refractive index of air to change beyond the accuracy limit. In addition alignment of all optical components is critical. The interference fringes are collected on the CCD of a video camera and transferred to computer for processing. An accuracy of ±1 millifringe is required.

If the lattice parameters are known, the mass of an atom is simply the product of atomic volume by density. The Avogadro constant is the ratio of molar mass to atom mass.

The paper describes the apparatus which is being set up for this series of measurements, the parameters which have to be considered and the role of surface impurities in the determination of the density.

DNA Electrophoresis through Microlithographic Arrays

E.M. Sevick and D.R.M. Williams, Department of Chemcial Engineering, University of Colorado and Institute of Advanced Studies, The Australian National University

Electrophoresis is one of the most widely used techniques in biochemistry and genetics for size-separating charged molecular chains such as DNA or synthetic polyelectrolytes. The separation is achieved by driving the chains through a gel with an external electric field. As a result of the field and the obstacles that the medium provides, the chains have different mobilities and are physically separated after a given process time. The macroscopically observed mobility scales inversely with chain size: small molecules move through the medium quickly while larger molecules move more slowly. However, electrophoresis remains a tool that has yet to be optimised for most efficient size separation of polyelectrolytes, particularly large polyelectrolytes, e.g. DNA in excess of 30-50 kbp. Some advances have occurred through trial and error exploration; however these improvements are not sufficient and changing the media morphology may provide the greatest effects upon separation. Unfortunately, gels provide only a small window of random morphologies and are difficult to control, let alone optimize for the electrophoretic process.

Microlithographic arrays etched with an ordered pattern of obstacles would provide an attractive alternative to gel media and provide wider avenues for size separation of polyelectrolytes and promote a better understanding of the separation process. Its advantages over gels are (1) the ordered array is durable and can be re-used, (2) the array morphology is ordered and can be standardized for specific separation, and (3) calibration with a marker polyelectrolyte is not required as the array is reproduced to high precision. Most importantly, the array geometry can be graduated along the chip so as to expand the size-dependent regime over larger chain lengths and postpone saturation. The high precision available in today's silicon chip industry promises accurate and controllable electrophoretic arrays with minimum length scale of 1 micron. Recent advances in nanolithography promise even smaller dimensions.

What is the optimal array geometry for separation of DNA? In order to predict the effect of obstacles upon the chain-length dependence in mobility and hence, size separation, we study the dynamics of single chains using theory and simulation. We present recent work describing:

- The release kinetics of a single DNA molecule hooked around a point, frictionless obstacle and in both weak and strong field limits.
- The mobility of a chain impinging upon point obstacles in an ordered array of obstacles, demonstrating the wide range of interactions possible between the chain and the point obstacle. Despite the range of glancing and head on impact that a chain may suffer with the obstacle, our simulations demonstrate a surprisingly simply universal description of the interaction kinetics. This universal description allows prediction of chain length dependence of mobility as a function of row spacing of obstacles.
- The escape kinetics of a single DNA molecule impinging upon a barrier wall perforated with holes in both weak and strong field limits.

EVOLUTION OF A ROLLING WEAR TRACK ON MG-PSZ

G.L. Kelly and T.R. Finlayson

Department of Physics, Monash University, Clayton, Vic. 3168, Australia

Mg-PSZ (Magnesia Partially Stabilized Zirconia) combines the hardness and high melting point of traditional ceramics with a high toughness, making it a useful engineering material. The microstructure consists of cubic grains with lenticular tetragonal precipitates. The high toughness is attributed to the stress-induced tetragonal to monoclinic phase transformation.

The phase transformations and surface morphologies resulting from contact between a steel roller and an Mg-PSZ disc have been characterised by a variety of methods. Micro-Raman spectroscopy has been used to monitor the tetragonal to monoclinic and tetragonal to orthorhombic transformation zones.

The rolling contact results in the formation of both the monoclinic and orthorhombic phases with the transformation zone of the monoclinic product extending in excess of 100 μm below the worn surface. Under the more severe conditions used in these tests, the resulting wear surface is rough with cracks and fracture evident on a grain-size scale. Wear mechanisms operating include fatigue and possibly intergranular fracture.

LASER RAMAN ANALYSIS THRESHOLDS WITHIN DISORDERED CARBON SYSTEMS

Russell J. Walker, Damien N. Barbara and Kerry W. Nugent
MicroAnalytical Research Center (MARC), School of Physics, University of Melbourne, Parkville, Victoria, 3052, Australia

Recent years have seen Laser Raman Microprobe Spectroscopy increasingly utilised as the 'tool of choice' in the analysis of carbon systems such as diamond, graphite, glassy carbon and others, due to its ease of use and its particular sensitivity to crystal and atomic structure. In this work we show, however, that amorphous carbon systems (specifically the example of an ion implanted carbon layer in fused quartz) may be readily annealed by a focused argon ion (514.5 nm) laser operating at powers typical of those used for conventional laser Raman spectroscopy. Microcrystallites of disordered graphite within the region of the laser spot focus are produced by the annealing process. Analysis of the raman spectra has been carried out by performing a deconvolution of the spectra into two separate Lorentzian functions to obtain the D (disorder) and G (graphitic) contributions. We have determined there exist two distinct annealing thresholds. The first threshold corresponds to the formation of disordered graphitic microcrystallites from the amorphous carbon background. The positions and intensity ratios of the graphite peaks remain essentially constant as the energy density at the annealed region is increased across an order of magnitude, until the second threshold is reached when the size and ordering of the crystals increases dramatically. Again, this profile remains essentially constant as the energy density is increased, until eventually ablation of the quartz occurs. These thresholds compare well with previously published work (for example, ref. [1]) and, within limits, do not rely greatly on factors such as implantation energy, dose or the matrix within which the amorphous carbon resides. The mechanisms responsible for these processes are discussed and power density limits for laser raman analysis of such systems are recommended.

[1] M. Bowden, D.J. Gardiner and J.M. Southall, J. Appl. Phys. 71 (1992) 521

DEVELOPMENTS OF HIGH-T_c OXIDE SUPERCONDUCTING TAPES AND COILS AT NRIM

H. Maeda
National Research Institute for Metals, Tsukuba Magnet Laboratories
Sengen, Tsukuba 305, Japan

We have been studying Bi- and Y-oxide superconducting tapes (or thick films on metallic tapes) and coils.

Bi-2212/Ag composite tapes about 60 m in length, were prepared by a combination of the continuous dip-coating process and melt-solidification treatment. Superconducting layers are formed on both sides of the Ag tape. The layers are highly textured with the (001) crystal plane parallel to the Ag tape surface. The tapes have critical current densities, J_cs, more than 2 x 10^5 A/cm^2 at 4.2 K above 20 T. Double-stacked pancake coils were fabricated using the tapes. One of the coils (20 mm inner bore x 98 mm outer diameter) generated 2.6 T at 4.2 K and also 1.5 T at 20 K. The other (13 mm inner bore x 46.5 mm outer diameter) was used as an inserted coil of a conventional superconducting magnet system and generated 0.9 T in a bias field of 20.9 T, i.e., a total of 21.8 T at the center of the magnet, which is the highest field in a fully superconducting system. J_c of the coil is 4.7 x 10^4 A/cm^2 (I_c = 310 A) with a criterion of 10^{-13} Ωm in the bias field. These results clearly indicate that Bi-2212 coils are promising for high-field magnets, and also are good candidates for a magnets operated by a cryocooler without liquid helium.

Bi-2223 tapes were prepared by the powder-in-tube method using Ag-10 at%Cu-x at%M alloy sheaths with M of Ti, Zr or Hf and x less than 0.1%. The small additions of the elements into the Ag-Cu alloy sheath modify the grain structures of Bi-2223 crystals. The grains are large, dense and more aligned, especially at the sheath/core interface, being very effective in increasing J_c, for instance, up to 9 x 10^4 A/cm^2 at 4.2 K and 14 T, with reproducibility. Futhermore, it is very interesting that amorphous, disc-like regions, less than 5 nm in thickness, parallel to the (001) plane are incorporated in the Bi-2223 crystal lattice. The regions will be one of the possible pinning centers in Bi-oxide superconductors.

On the other hand, highly in-plane-textured, Y-123, thick films of about 1 μm thickness, were deposited on metallic tapes with a highly (200)-oriented, polycrystalline, yttria-stabilized zirconia (YSZ) buffer layer, using the pulsed-laser-ablation method. The highly textured, buffer layer was deposited on both sides of Ni-based, polycrystalline, metallic tape using the modified bias-sputtering technique. J_cs about 10^5 A/cm^2 at 77 K and 0 T can be successfully obtained. The Y-123 films show three-dimensional, terraced, island growth, with several turns of the screws, with the screw edges still along the ⟨200⟩ axis of YSZ. These terraced islands seem to coalesce in the films.

THE HIGH TEMPERATURE APPROXIMATION IN NMR

G. J. Bowden, T. Heseltine, and G. E. Ball*
School of Physics, University of New South Wales
*School of Chemistry, University of New South Wales
Sydney, NSW 2052

Recently, Warren S. Warren has challenged one of the basic assumptions of NMR at ambient temperatures known as the High Temperature Approximation (HTA). In a series of papers (eg.1) Warren et al., presented convincing evidence for the need to include the second, and higher order, terms in the density matrix expansion:

$$\rho \propto e^{-\beta H} = 1 - \beta g \mu_N \mathrm{H} \sum_i I_z(i) + \frac{\beta^2}{2!} \sum_i \sum_j I_z(i) I_z(j) + \ldots.$$

In particular, gradient selective double quantum 2D NMR experiments were used to show that double quantum states of the form $I_x(i)I_x(j)$ must be present right after a single 90° rf-pulse, which could only come from the third term in the density matrix expansion. An alternative explanation has been provided by Bowden et al., (2) who show that Warren's results could be explained in therms of multiple spin echoes re-focused in the presence of magnetic field gradients.

In this paper, new experiments designed to test for the existence or otherwise of higher order terms in the expansion of ρ are presented and discussed. Using the UNSW 600MHz spectrometer we found, to our astonishment, strong multiple quantum signals in excess of $\Delta m = \pm 2$, in accord with Warren, However, by partially de-tuning the tank circuit, all of the $\Delta m > \pm 2$ peaks could be made to disappear. This points to "radiation damping", as the source of the high-order peaks, but at this stage other mechanisms cannot be ruled out. In Jan. 1996, further experiments will be performed at the Bruker Research Centre at Karlsruhe, using the new Q-switching Facility.

(1) W. Richer, S. Lee, and W.S. Warren, Science **267** (1995) 654-7.
(2) G.J.Bowden, T.Heseltine, and M.J. Prandolini, Chem.Phys.Letters. **233** (1995) 639-43.

AU9918122

MULTIPLE SPIN ECHO SIGNAL FORMATION FROM FERROMAGNETS

L.N. Shakhmuratova, D.K. Fowler, D.J. Isbister and D.H. Chaplin
School of Physics, University College, The University of New South Wales,
Australian Defence Force Academy, Canberra, ACT, 2600, Australia

The method of concatenation of perturbation factors in statistical tensors is applied to conventional one pulse and two pulse NMR in multi-domain ferromagnets in the limit of extreme inhomogeneous broadening. It is shown that the single pulse echo has a fundamental origin which is neither solely due to off-resonant nor pulse phase distortion effects but arises from severe simultaneous inhomogeneity in the Larmor and Rabi frequencies. It is shown that for severe Larmor inhomogeneous broadening along with a distribution in the ferromagnetic enhancement factor, there are four two-pulse stimulated T_1 echoes (peaks 1-4 in the diagram below) and nine T_2 echoes. All thirteen fundamental echoes are observed for the most general case of low radiofrequency power and unequal pulse durations. These thirteen echoes are truly resonant echoes rather than being due to nonresonant effects and are completely separate to quadrupolar effects. The theoretical predictions are well verified in a comprehensive experimental study in ternary (^{59}Co**CoFeNi**), binary (^{51}V**Fe**) and pure elementary (enriched ^{57}Fe**Fe**) ferromagnets. For the single pulse echo severe inhomogeneities in both Larmor and Rabi frequencies are essential for its occurrence rather than pulse distortions. The time-resolved thirteen echoes to the right of the second pulse (for unequal pulses) are shown below for (^{59}Co**CoFeNi**) together with the single pulse echo appropriate to the first pulse.

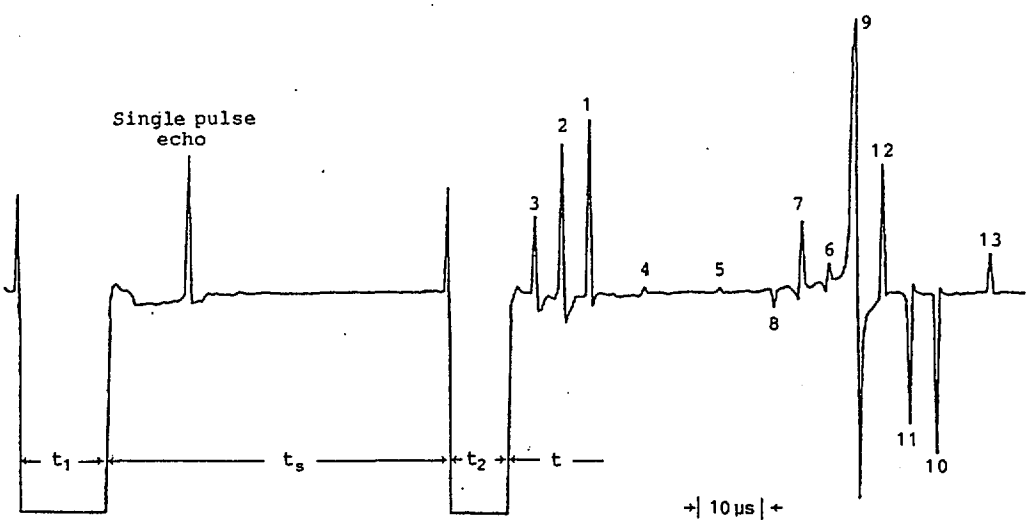

The echo-signals are formed at t equal to (1) t_1, (2) t_2, (3) $t_1 - t_2$, (4) $t_1 + t_2$, (5,13) $t_s \mp (t_1 + t_2)$, (6,12) $t_s \mp (t_1 - t_2)$, (7,11) $t_s \mp t_2$, (8,10) $t_s \mp t_1$, (9) t_s.

MAGNETISM AND ATOMIC SHORT RANGE ORDER IN IRON-RICH B.C.C. ALLOYS

M.F. Ling

Department of Physics, Monash University,

Clayton, Victoria 3168, Australia.

J.B. Staunton

Department of Physics, University of Warwick,

Coventry CV4 7AL, United Kingdom.

and

D.D. Johnson,

Computational Materials Science Division 8341,

Sandia National Laboratories, Livermore,

CA94551-0969, U.S.A.

Magnetism and the ordered structures that iron alloys form are closely interrelated via their underlying electronic structure. Since the Curie temperatures of iron-rich b.c.c. alloys are often comparable with their compositional ordering or phase segregation transition temperatures, the magnetic state can play a crucial role in determining the type of alloy formed and its dependence on its thermal history. Long-range magnetic order spin-polarises the electronic structure producing different electronic mechanisms for arranging the atoms from those set by the paramagnetic alloy in which the effects of spin-fluctuations are important.

We illustrate this close relationship between magnetism and atomic short range order in iron-rich b.c.c. alloys by presenting details of the application of our "first-principles" theory of compositional and magnetic correlations to $Fe_{75}Al_{25}$, $Fe_{80}Al_{20}$, and $Fe_{87}V_{13}$ ferromagnetic alloys. For the first time, the magnetic and compositional correlations have been treated on equal basis within a theoretical framework. We further suggest that measurement of atomic short range order in metallic alloys be used to test models of spin fluctuations in the paramagnetic state of metallic magnets. In such systems, the longstanding controversy of whether there is massive or modest amount of magnetic short-range order could be resolved.

MAGNETIC PROPERTIES OF FULLERENE SUPERCONDUCTORS

Victor Buntar
Atomic Institute of the Austrian Universities,
Schüttelstr. 115, A-1020 Vienna, Austria

Review of the present experimental situation with regards to magnetization measurements of the fullerene superconductors is made. Typical results of magnetization curves are shown and the evaluation of the superconducting fraction from these measurements is discussed. We also discuss results of the evaluation of the critical fields and characteristic lengths by different techniques. New results on measurements of the lower critical fields of crystalline K_3C_{60} and $RbCs_2C_{60}$ fullerene superconductors are presented. It is shown that the trapped magnetization appears at characteristic fields H*, which are much smaller that the values of H_{c1} expected for these compounds. We suppose that these values of H* can be interpreted as the values of the lower critical fields.

This work was supported by Fonds zur Förderung der Wissenschaftligen Forschung, Vienna, Austria.

DETECTING AND IDENTIFYING UNDERGROUND NUCLEAR EXPLOSIONS

S. Spiliopoulos
Australian Geological Survey Organisation,
Department of Primary Industry, Anzac Park, Constitution Avenue, A.C.T. 2600

To monitor both earthquakes and underground nuclear explosions, the Australian Geological Survey Organization (AGSO) operates, or assists with the operation of a network of seismic stations around Australia and in Antartica. These seismic stations include two arrays of seismic sencors in central Australia - one near Alice Springs and the othe near Tennant Creek. Data from all of these seismic stations are telemetered to AGSO's Australian Seismological Centre, in Canberra. The data from the Alice Springs installation are telemetred by landline, and for all other stations, by satellite.

The monitoring of underground nuclear explosions involves, first determining that the signals have originated from a test site and if so, then a pattern recognition analysis is undertaken to determine whether the signals originate from an explosion rather than an earthquake. In this we are aided by seismic observations of previous explosions from each test site.

To determine the origin of a signal use is first made of the two seismic arrays in central Australia. Each of these arrays consists of 20 spatially separated sensors (seismometers), and each of which can provide a preliminary estimate of the location of the source. In practise this is done automatically by inserting delays into the output of each of the sensors to compensate for a seismic signal taking a finite time to cross the array, and then adding the output of each sensor to form what are called "array beams". When the correct delays for a particular azimuth and wavespeed (corresponding to a particular source location) have been inserted, the signals recorded by each sensor will be in phase and the energy in the array beam will be a maximum. Because the seismic background noise at each sensor is not correlated, this beamforming also improves the signal-to-noise ratio. In this sense a seismic array is equivalent to other arrays of sensors - e.g. a radar antenna.

Having determined that a signal originates from somewhwere near a test site a more precise location can be obtained from the times that the signal arrives at different seismic stations. As an example, whether a French underground explosion has been detonated at Mururoa or Fangataufa can be determined from the differences in relative arrival times at the two Australian arrays and at Mawson in the Antartica. If further location precision is required, waveform data (and thus arrival times) can be extracted over the Internet from overseas seismic arrays, in particular from arrays in Canada, Germany and Scandinavia.

STUDY AND ENGINEERING OF SOLID SURFACES ON AN ATOMIC SCALE

T.T. Tsong
Institute of Physics, Academia Sinica,
Taipei, Taiwan. 11529

Using scanning probe microscopes, it is now possible to move surface atoms and to transfer atoms from the probe tip to the surface or from the surface to the probe tip, using high-field effects. Atomic manipulation is an exciting new development in condensed matter science. The principles of these techniques and current progress in their utilisation will be reviewed.

AU9918127

THE DIFFERENTIAL REFLECTANCE MICROSCOPE

J. Tann and M. Gal
School of Physics, The University of New South Wales, Sydney 2052

We have developed a sensitive optical technique that allows two-dimensional mapping of subsurface inhomogeneities of semiconductors. Using this contactless, room temperature technique, which is based on *differential reflectance spectroscopy*, we have been able to generate relief maps which show the spatial distribution of damage/defects in III-V compounds and Si.

Conventional microscopes are not sensitive to subsurface structures or inhomogeneities in opaque or highly reflective materials. This lack of sensitivity makes optical microscopy a seldom used diagnostic tool in semiconductor technology. We have developed a scanning optical microscope which is able to detect even minute subsurface variations in the refractive index of the semiconductor sample and is insensitive to the overall reflectivity of the sample. The differential reflectance signal is a strong function of the surface and near-surface inhomogeneities, and, unlike other modulation spectroscopies, it *increases* with increasing damage.

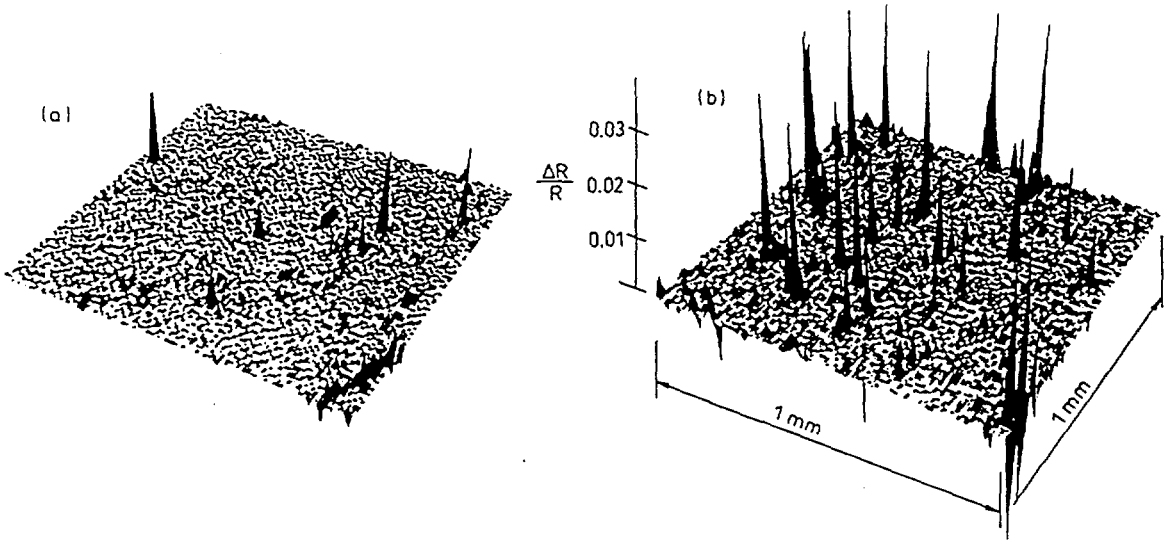

Differential reflection maps of a 1 mm x 1 mm sample of Si (a) before, and (b) after B implantation.

AU9918128

HIGH MAGNETIC FIELD TRANSPORT MEASUREMENTS OF A 2D-HOLE SYSTEM WITH AN UNUSUAL LANDAU LEVEL DEGENERACY

E.E. Mitchell[a], R.G. Clark[a], V.A. Stadnik[a], R.B. Dunford[a], R.P. Starrett[a], A.S. Skougarevsky[a], F.F. Fang[b], P.J. Wang[b] and B.S. Meyerson[b]

[a]*National Pulsed Magnet Laboratory, School of Physics, University of New South Wales, Sydney 2052, Australia*
[b]*IBM T.J. Watson Research Centre, P.O. Box 218, Yorktown Heights, NY 10598, USA*

Recent advances in growing p-type modulation doped Si_xGe_{1-x} layers on Si substrates[1] has lead to a reduction in the lattice mismatch and improved the hole mobility to $8000cm^2V^{-1}s$ (amongst the highest reported for these systems) so that transport studies of the high quality two-dimensional hole system (2DHS) in these Si-based heterostructures are now possible.

We have extended low temperature magneto-transport measurements to study the 2DHS in p-type Si/Si_xGe_{1-x} ($x\sim0.12$) heterostructures and results have revealed, together with the Integer Quantum Hall Effect (IQHE), two unexpected insulating regions at Landau level filling factors $\nu \sim 1.5$ and $\nu<0.5$.

Fig.1 shows the longitudinal resistivity data (ρ_{xx}) for a p-type Si/Si_xGe_{1-x} sample ($n=3.9\times10^{11}cm^{-2}$) with the field normal and at 72° to the 2D layer at 0.3K. The data reveal a number of interesting features: (i) A notably large, unexpected insulating phase (IP) at $\nu \sim 1.5$ which increases with decreasing temperature (~40kΩ at 30mK, 0°); (ii) Only odd integer QHE states are present in the low field region ($\nu>2$); (iii) A weak minimum forms in ρ_{xx} close to, but not exactly at $\nu=2$ and the corresponding quantized plateau in the Hall resistivity (ρ_{xy}) is absent; (iv) Several local minima are observed below 100mK reminiscent of, but not attributed to the fractional QHE.

These features can be correlated with the unusual Landau level (LL) degeneracy which occurs because the spin splitting ($g^*\mu_B B_T$) in this Si system is comparable in size to the cyclotron energy ($\hbar eB/m^*$). As a result the extended states of opposite spin from different LLs overlap (inset, fig.1). We have increased the IP resistance by tilting the sample in a magnetic field (fig.1) which changes the spin splitting and enhances the degeneracy. The IP region could be quenched by illuminating the sample, which changes the population of spin-up and spin-down states and lifts the degeneracy. Initial studies of the second, more resistive IP at $\nu \sim 0.5$ have been carried out in pulsed fields to 50T.

1. F.F. Fang *et al.* Surf.Sci. 263, 175 (1992).

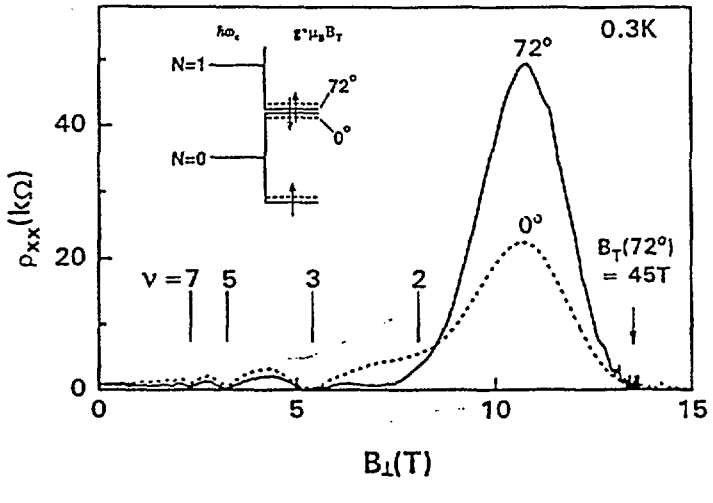

Figure 1 Longitudinal resistivity (ρ_{xx}) vs. the magnetic field normal to the 2D hole layer for a p-type Si/SiGe heterostructure at 0.3K. Inset: schematic of the LL degeneracy.

TUNNELING PROCESSES AND CHARGE ACCUMULATION IN TRIPLE BARRIER RESONANT TUNNELING STRUCTURES

L. D. Macks[a], S. A. Brown[a], R. G. Clark[a], R. P. Starrett[a], M. A. Reed[b], M. R. Deshpande[b] and W. R. Frensley[c]

[a]National Pulsed Magnet Laboratory, School of Physics, University of NSW, Sydney, NSW 2052, Australia.
[b]Departments of Electrical Engineering and Applied Physics, Yale University, New Haven, CT 06520, USA.
[c]Eric Jonsson School of Electrical Engineering and Computer Science, University of Texas at Dallas, Richardson TX 75083, USA.

Tunneling processes in semiconductor double barrier (single quantum well) resonant tunneling structures have been studied in great detail since the pioneering experiments of Chang, Esaki and Tsu [1]. The application of a bias voltage across the structure shifts the energy levels in the well relative to occupied states in the emitter electrode. Alignment of a well level with occupied emitter states results in resonant transmission of electrons through the emitter barrier. The rate of subsequent tunneling out of the well (through the collector barrier) will only vary significantly from the rate of tunneling into the well when the collector barrier is thicker than the emitter barrier. In this case, electrons will accumulate in the well, distorting the potential profile across the structure [2].

We present a study of tunneling processes in GaAs/AlAs *triple* barrier (double quantum well) structures, which demonstrates the critical role played by the second well. In sample I, when the emitter and first well are on resonance, the lowest level in the second well is at lower energy and electrons tunnel freely through the structure. At the same resonance condition in sample II, the level in the second well is at higher energy, thus the second well appears as part of a thick collector barrier and charge accumulates in the first well. As the bias voltage is further increased, a 'double resonance' condition (simultaneous alignment of both well levels with occupied emitter states) is achieved and the accumulated charge flows freely through the structure to the collector. The double resonance condition is then lost due to the resulting potential redistribution. As a mechanism for limiting the amount of charge accumulation, a multiple resonance is unique to multiple quantum well structures, and we believe it to be identified for the first time in the experiments reported here.

[1] L. L. Chang, L. Esaki and R. Tsu, Appl. Phys. Lett. 24, 593, (1974).

[2] M. L. Leadbeater et al, Semicond. Sci. Tech. 3, 1060, (1988); T. J. Foster et al, Phys. Rev. B 39, 6205, (1989).

TI TERIALS

David R.M. , A.N.U., Canberra.

The term "grani ostances such as sand, cornflakes, wheat, coal and most ores. This is an important area for two main reasons. First, these substances exhibit many interesting and novel physical effects. Second, they are important in a wide range of industries: mining, agriculture, food processing and pharmaceuticals. Early workers on this subject included Coulomb and Faraday and the area has recently undergone a revival of interest amongst physicists. The first half of this talk will present on overview of the subject and a discussion of some of the more interesting physical effects [1], such as clustering, heaping and avalanching. Amongst the most interesting of these is size-segregation [2]. If particles of two sizes are placed in a rotating cylinder two different kinds of behaviour are seen. At some rotation speeds the particles mix uniformly. However, for a certain range of speeds the particles segregate into a series of stripes.

The second half of the talk will focus on a simple model of granular materials: the driven dissipative gas [3,4]. In this system each particle is individually excited and undergoes inelastic collisions with the other particles. The dissipative interactions lead to equilibrium clustering in one-dimension. In two dimensions this gives rise to phase separation at a critical density, from a gas phase at low densities (left) to a liquid and a gas phase in coexistence (right) , at higher densities[4].

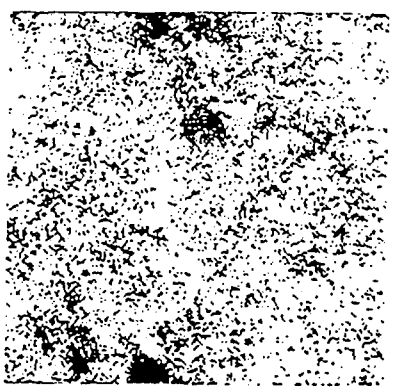

1. Jaeger, H.M. and Nagel, S.R., Science, 222 (1992) 1523.
2. Hill. K.M. and Kakalios, J., Phys. Rev. E., 4393 (1995) 52.
3. Williams, D.R.M. and MacKintosh, in "Fractal Aspects of Materials" ed. F. Family MRS (1995).
4. Williams, D.R.M., (preprint: submitted to Physica A)

A NEW HYDRODYNAMICS FOR PLASMONS

John F. Dobson
School of Science. Griffith University
Nathan, Queensland 4111, Australia
J.Dobson@sct.gu.edu.au

Plasma oscillations (plasmons) in solids are collective electron charge-density oscillations. They are observed, e.g., as peaks in the electromagnetic absorption spectra of thin metal films, where several types of plasmon mode occur (bulk, surface, standing, two-dimensional). Metallic plasmons typically have frequencies in the ultraviolet region, but in the epitaxial GaAlAs system, the plasmons lie in the far infrared because of the small electron effective mass and high dielectric constant of the underlying semiconductor. Plasmons are therefore of interest for possible far-IR-active devices. They may also be a limiting factor in the design of ultrasmall (nanosized) transistors and other electronic components. An understanding of the mutual plasmons of separated nanostructures is a key to prediction of van der Waals or dispersion forces, with applications ranging into chemistry and biology.

There are several types of approximate formalism for describing plasmons, such as hydrodynamics, time dependent Hartree (or classical Vlasov) theory, and time-dependent density functional theory. While exact description is usually impossible because one is dealing with a quantal many-body problem, an important exception is the case of many interacting electrons confined by a **harmonic** external potential, which is well-realized experimentally in epitaxially grown parabolic quantum wells, in some quantum dots and to a lesser degree in positively charged metal clusters or metal films. For this case one can prove a **"harmonic potential theorem"** [1]. This states that, despite the Coulomb interaction between the electrons, there is a mode in which the entire electron gas, including its highly inhomogeneous edge regions, moves rigidly at the bare harmonic-well frequency. This motion has proved to be a crucial test case for approximate theories of time-dependent many-body phenomena. In particular, the author has shown [1] that this test is failed both by the usual approximations for the ∇n pressure term in hydrodynamics, and by the most sophisticated expressions for the exchange-correlation kernel f_{xc} in time-dependent density functional theory. To rectify these failures the author has proposed modified theories. In the hydrodynamic case one replaces the usual linearized pressure force by

$$\vec{F} = -\frac{\hbar^2}{m}(3\pi^2)^{2/3}\vec{\nabla}[\{n_0(\vec{r})\}^{-1/3}\{\frac{3}{5}\delta n_1(\vec{r},t)+\frac{1}{3}\delta n_2(\vec{r},t)\}].$$

Here $n_0(\mathbf{r})$ is the equilibrium electron density, and the density perturbation is $\delta n = \delta n_1 + \delta n_2$. The partial densities δn_1 and δn_2 are defined in terms of the fluid displacement $\mathbf{x}(\mathbf{r},t)$ by

$$\delta n_1 = -n_0(\vec{r})\vec{\nabla}\cdot\vec{x}(\vec{r},t), \qquad \delta n_2 = -(\vec{\nabla}n_0(\vec{r}))\cdot\vec{x}(\vec{r},t)\ .$$

δn_1 is the density perturbation due to compression of the plasma, while δn_2 is the density perturbation which would occur in rigid displacement of the equilibrium density profile.

The present talk will motivate this form of "high-frequency" hydrodynamics, while the following talk by H. Le will demonstrate its success in obtaining the plasmon spectra of some epitaxial quantum wells.

[1] J.F. Dobson, Phys. Rev. Lett. **73**, 2244 (1994)

HYDRODYNAMIC PLASMONS ON WIDE PARABOLIC QUANTUM WELLS

Hung M. Le (H.Le@sct.gu.edu.au) and John F. Dobson
School of Science. Griffith University
Nathan, Queensland 4111, Australia

We report progress towards a simple, reliable theory of plasmons on mesoscopic structures of arbitrary geometry. Fully microscopic many-body quantum theories are usually too cumbersome, and quantum hydrodynamics is an attractive option. Simple hydrodynamics has been widely used, e.g. for thin metal films [1]. In most such calculations, the equilibrium electron gas has been assumed uniform up to a sharp boundary. In describing the plasmon motions, hard-wall boundary conditions at the electron gas edge have usually been added in an ad hoc fashion. Experiment and microscopic theoretical work [2] have shown, however, that the details of the nonuniform equilibrium electron density near the edge of the sample are crucial in determining the dispersion of surface plasmons. Once this inhomogeneity of the electron gas is included, simple hydrodynamic models fail, and one requires a new form of hydrodynamics, as shown in the previous talk.

Here we report tests of the new hydrodynamics using the parabolic quantum well, a system well-understood both experimentally and from microscopic theory [3], and for which the usual hydrodynamics fails to give the known frequency of the Kohn or sloshing plasmon mode. GaAa/GaAlAs parabolic quantum wells have been grown [3] by molecular beam epitaxy with the Al content varying during growth in such a way that conduction electrons feel an effective parabolic potential $V(z) = (\text{const})z^2$ where z is the space coordinate in the layer growth direction. By remote doping, a highly mobile electron gas layer is formed which partly fills the parabolic well, and this situation can be proved isomorphic [3] to a non-neutral slab of electron gas with excess positive background extending outside the electron gas. Microscopic theory shows that this electron gas, when IR-irradiated at finite surface-parallel wavenumber q via a grating coupler, exhibits absorption peaks at 2D plasmon, Kohn-mode and bulk standing plasmon frequencies The new hydrodynamics yields all these modes with use of one natural boundary condition. No other hydrodynamic theory has been able to do this.

Our initial step involved self-consistent solution of the static Poisson and Thomas Fermi equations to obtain for the first time the smooth static electron TF density profile $n_0(z)$ of the parabolic well. (Thomas-Fermi theory is the static limit of the simplest hydrodynamic theory). Then we solved the new hydrodynamic equations for the nonuniform gas, obtaining the dispersion relations of all the plasmon modes in good agreement with microscopic theory.

Currently we are looking at a corrected version of a higher-order hydrodynamics including further gradient terms (dynamic TF-von Weizsacker theory). This will be needed for a credible hydrodynamic theory of the whole gamut of plasmons on neutral metallic surfaces, for which the electrons are precariously bound and for which Thomas-Fermi theory correspondingly gives a poor description. (No such difficulty occurs for the tightly-bound electrons of the parabolic well). We have also considered the effects of spatially varying effective mass, important if the GaAlAs Kohn mode is to be exploited technologically.

[1] A.G. Eguiluz, Phys. Rev. B **19**, 1689 (1979)
[2] K.D. Tsuei et al, Surf. Sci. **247**, 302 (1991)
[3] J. F. Dobson, Australian J. Phys. **46**, 391 (1993)

STUDIES OF QUANTUM SPIN LADDERS AT T = 0 AND AT HIGH TEMPERATURES

Zheng Weihong and J. Oitmaa
School of Physics, The University of New South Wales
Sydney NSW 2052, Australia

Rajiv R.P. Singh
Department of Physics, University of California,
Davis, CA 95616, USA

Compounds have recently been found[1] which, to a first approximation, can be regarded as "spin ladders", i.e. 2 or 3 coupled chains of $S = \frac{1}{2}$ ions. These are $(VO)_2P_2O_7$ and $SrCu_2O_3$ (2 chains), and $SrCu_3O_5$ (3 chains).

A number of striking theoretical predictions[2] have been made for such systems. Ladders with an even number of legs have an energy gap, short range correlations and a "spin liquid" ground state. Ladders with an odd number of legs, on the other hand, have gapless excitations and quasi long range order. Experiments appear to confirm these features, which are analogous to the Haldane gap in integer chains.

We have carried out extensive series studies of 2-chain and 3-chain ladder systems, both at $T = 0$ and at high temperatures. Our results confirm the existence of a gap in the 2-chain system and identify the structure of the phase diagram. The dispersion law for excitations is estimated. For the 3-chain system we are unable to exclude the possibility of a small gap, although our results are quite consistent with a gapless spectrum. We estimate the high temperature magnetic susceptibility and compare with previous calculations and with experiment.

---

1. D.C. Johnston et al., Phys. Rev. B**35**, 219 (1987). M. Azuma et al., Phys. Rev. Lett **73**, 3463 (1994).
2. T.M. Rice, S. Gopalan & M. Sigrist, Europhys. Lett. **23**, 445 (1993). S.R. White, R.M. Noack & D.J. Scalapino, Phys. Rev. Lett. **73**, 886 (1994).

CARBON K-SHELL NEAR EDGE STRUCTURE CALCULATIONS OF GRAPHITE USING THE MULTIPLE SCATTERING APPROACH

D.G. McCulloch[1] and R. Brydson[2]

[1]Electron Microscope Unit & Australian Key Centre for Microscopy and Microanalysis, University of Sydney, NSW 2006, Australia.

[2]Department of Materials Science and Engineering, University of Surrey, Guildford Surrey GU2 5XH, U.K.

The ability of electron energy loss spectroscopy (EELS) to accurately determine chemical compositions from inner-shell loss edges is well known. In addition to elemental concentrations, each characteristic absorption edge exhibits structure which provides information on the atomic environment of the absorbing atom[1]. The strong oscillations which occur within about 40 eV of the Fermi energy are known as near edge structure (NES) and reflect the local density of unoccupied states. In the present work, the near edge absorption fine structure of carbon in graphite has been calculated using the multiple scattering approach. The effects of both a neutral carbon absorber and taking into account the effect of the core hole by using a nitrogen (Z+1) absorber atom are considered. The best agreement with experiment was obtained for the case of the nitrogen absorber and a cluster of 150 atoms, with the calculated NES containing the main features observed experimentally. A splitting near the onset of the σ^* peak, similar to that seen experimentally[2], was found to occur in the calculated NES for one of the two inequivalent carbon atoms in the graphite structure. This splitting was not observed in the calculated NES for a single sheet of graphite supporting the proposition that it only occurs in well ordered graphite. This result supports the proposition that the splitting originates from a sharp σ^* peak and a dipole allowed bandlike contribution associated to the Γ_2^- branch of the free-electron-like interlayer states[2].

[1] Vvedensky D.D., *Unoccupied Electronic States*, Topics in Applied Physics Vol. 69, ed. Fuggle F.J. and Inglesfield J.E., chap. 5, 139 (Springer-Verlag, Berlin-New York 1992).

[2] Batson P.E., Phys. Rev. B, **48**, 2608 (1993).

NEUTRON AND X-RAY REFLECTOMETRY: SOLID MULTILAYERS AND CRUMPLING FILMS.

Anthony S. Brown and John W. White.
Research School of Chemistry
Australian National University

Australia has a significant stake in the newly commissioned neutron reflectometer, known as SURF, at the Rutherford Appleton Laboratory in the U.K., as well as easy access to the older and higher resolution instrument known as CRISP. Our own laboratory, in collaboration with the Australian Defence Force Academy and the University of Queensland, is currently commissioning Australia's first x-ray reflectometer, designed as a prototype for possible implementation at the Australian National Beamline at the Photon Factory in Japan.

Specular reflection of neutrons and x-rays from interfaces provide a useful probe of the variation of refractive index through the interface and normal to it. The refractive index is a function of the scattering length density or electron density in the neutron and x-ray cases, respectively, and reflectivity measurements thus provide structural information difficult to obtain by other means. The differences in the scattering of neutrons and x-rays mean that neutron and x-ray reflectometry provide complementary means of elucidating interfacial and film structures.

An introduction to the basic principles of neutron and x-ray reflectometry will be given at a level suitable for those not familiar with the technique. Our recent neutron reflectivity work on polymer films spread at the air-water interface will also be presented. These films show marked temperature and molecular weight dependences in their properties, and undergo interesting transitions from monolayer to multilayer structures at higher surface pressures. A brief indication will be given of how it is envisaged that x-ray reflectivity measurements will provide complementary data to maximize our information retrieval from the neutron data.

During recent commissioning experiments, x-ray reflectivity measurements have been made for a Langmuir-Blodgett film composed of thirty one layers of barium arachidate deposited on a silicon substrate. A comparison of these preliminary results with simulations will be presented. The talk will conclude with a brief speculation about the future directions of reflectometry in our research effort.

Reference: P.M. Saville, I.R. Gentle, J.W. White, J. Penfold and J.R.P. Webster. *"Specular And Off-Specular Neutron Reflectivity Of A Low Molecular Weight Polystyrene Surfactant At The Air-Water Interface."* J. Phys. Chem. **98**, 5935-5942 (1994)

POLARISED NEUTRON DIFFRACTION AND THE SPIN DENSITY IN $[As(C_6H_5)_4][TcNCl_4]$

Philip A. Reynolds[a], J. Bruce Forsyth[b] and Brian N. Figgis[c].

a) *Research School of Chemistry, Australian National University*

b) *ISIS facility, Rutherford-Appleton Laboratory, United Kingdom*

c) *Department of Chemistry, University of Western Australia*

The study of magnetism in large single crystals of paramagnets by polarised neutron diffraction (PND) measures Fourier components of the crystal magnetisation density. Over the last few years we have used this to study magnetic exchange pathways, spin canting, metal ion anisotropies and, particularly, metal-ligand bonding.

In complexes of heavy transition metals the bonding is not well understood and the detailed data potentially available from PND would provide a stringent test of theory. Suitable materials are rare, but one such is $[As(C_6H_5)_4][TcNCl_4]$, in which magnetically independent, square pyramidal, spin-half $TcNCl_4^-$ ions exist in a simple crystal structure [1]. Preliminary PND [2] showed extensive covalent delocalisation of the single unpaired spin from the technetium onto the chlorine ligands.

We have now collected an extensive PND data set on this material which shows, inter alia, that the spin-density on the technetium complex is extremely delocalised and highly anisotropic. A simplified interpretation is that there is preferential occupation of the Tc $4d_{xy}$ orbital with covalent delocalisation into Cl 3p, but only in the Cl_4 plane. The Tc-N bond is strongly spin-polarised, a correlation effect. Other detail is not so simply explained, and good quality *ab-initio* quantum mechanical calculations do not reproduce the observations.

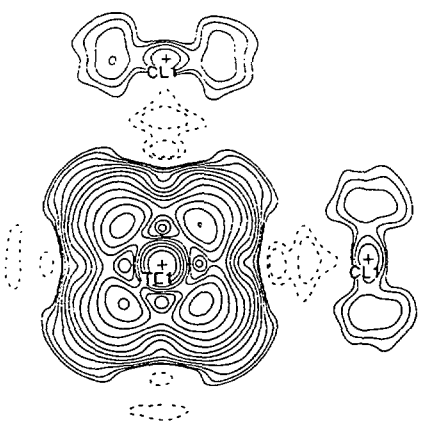

Experimental spin density in $TcCl_2$ plane.
Contours geometric, start 0.01 μ_B Å^{-3}, increment $\sqrt{2}$, negative dashed.

1)B.N.Figgis, P.A.Reynolds, F.K.Larsen, G.A.Williams, B.Moubaraki and K.S.Murray *Aust.J.Chem.*, in press.

2)B.N.Figgis, P.A.Reynolds and J.W.Cable *J.Chem.Phys.*, **98**, 7743 (1993)

Crystal Field Effects Using Polarised Neutron Spectroscopy

D. J. Goossens, S. J. Kennedy and T. J. Hicks.

Monash University, Melbourne, Australia

The ground state of a Pr^{3+} ion is ninefold degenerate. In the hexagonally symmetric crystal field that the ion experiences in $PrAl_3$, this degeneracy is partially lifted and three doublets and three singlets come about. Transitions take place between these levels. As each level has a different magnetic moment, a transitions alters the magnetic induction in the sample. The energy of the transition can therefore be measured using magnetic neutron scattering.

If polarised neutrons are used, and the polarisation vector is parallel to the scattering vector, magnetic neutron scattering occurs with neutron spin flip. Nuclear scattering will be non-spin flip. This means that an instrument fitted with both polarisation and energy analysis should be useful in the measurement of crystal field transitions, as it can discriminate nuclear from magnetic scattering.

One such instrument is the LONGPOL long wavelength polarised neutron scattering instrument at Lucas Heights. In this experiment, LONGPOL was used to measure transition energies in $PrAl_3$. The transitions were successfully seen. The ground state transition was found to be of energy 4.5 ± 0.4 meV, and a second transition was seen at ~3.5 meV. Further, nuclear and magnet elastic scattering were seen, the latter quasielastic. Analysis of these features was aided by the polarisation analysis, as it could immediately distinguish the magnetic components of the scattering from the nuclear.

The results were enough to suggest that LONGPOL could make a useful contribution to the study of crystal field effects.

LINDSAY'S SCIENCE ON REFLECTION

M.M. Elcombe
Australian Nuclear Science & Technology Organisation,
Private Mailbag 1, Menai, N.S.W. 2234

In this presentation, some of the contributions to condensed matter research by Dr. Lindsay Davis, particularly during his time as a Research Scientist with the Australian Institute of Nuclear Science and Engineering, based at the Lucas Heights Research Reactor, will be reviewed. In this capacity, he interacted and collaborated with many users of the neutron scattering facilities, particularly from Australian universities.

SMALL ANGLE NEUTRON SCATTERING FROM HYDRATED CEMENT PASTES

T.M. Sabine, W.K. Bertram, and L. P. Aldridge
Materials Division ANSTO (Australian Nuclear Science and Technology Organisation)

Small angle neutron scattering (SANS) was used to study the microstructure of hydrating cement made with, and without silica fume. Some significant differences were found between the SANS spectra of pastes made from OPC (ordinary Portland cement) and DSP (made with silica fume and superplasticiser).

The SANS spectra are interpreted in terms of scattering from simple particles (as shown below). Particle growth was monitored during hydration and it was found that the growth correlated with the heat of hydration of the cement.

SANS spectra were fitted to I(Q) by the equation,

$$I(Q) = nV^2 \left|\rho_a - \rho_b\right|^2 F(QR)^2$$

where n is the number of particles per unit volume, V is the volume of the particle, ρ_a is the mean coherent scattering length density of a particle in a medium with mean coherent scattering length density ρ_b, R is the particle radius, and F(QR) is the structure factor of the scattering particles.

$$F(QR)^2 = \left(\sqrt{1+\frac{(QR)^2}{3}}\right)^{-p}$$

p= 1 for rod shaped particles, 2 for discs and 4 for spheres.

THE INCOMMENSURATE STRUCTURE OF $Bi_2Sr_2CaCu_2O_{8+\delta}$

P.A.Miles[1], S.J.Kennedy[2], G.J.Russell[1], G.Gu[4], G.J.McIntyre[3], N.Koshizuka[4]

[1]Advanced Electronic Materials, Physics Department, University of NSW, PO Box 1 Kensington NSW 2033, Australia

[2]Australian Nuclear Science & Technology Organisation, PMB 1 Menai, NSW 2234 Australia

[3]Institut Laue-Langevin, Grenoble, France.

[4]ISTEC, 10-13 Shinonome, I-chome, Koto-ku, Tokyo 135, Japan

Despite numerous attempts to resolve the incommensurate crystal structure of the Bi(2212) superconductor, some controversy remains as to the correct space group, the description of the incommensurate modulation vector, and the crystallographic defect distributions. This is due to observation of different satellite reflections and diffuse peaks by different single crystal x-ray and neutron diffraction studies. In addition to this some temperature dependence of the incommensurate strucutre has been suggested in some reports.

In this study two Bi(2212) crystals were examined using the D19 diffractoemeter at ILL, Grenoble and 2TanA at HIFAR, Lucas Heights, Sydney. One crystal had a large mozaic spread while the other was a near perfect crystal. Crystallographic structure factors were measured between 12K and room temperature to high order reflections (e.g. (8,4,0) & (0,0,42)) and several diffuse features were also scanned. The incommensurate lattice structure was found to have space group *N Bbmb/IÎI*. Our results also indicate that the widely reported 'diffuse' features are strongly sample dependent, and that in the near perfect crystal many are actually absent. No structural changes were eveident between 12K and RT.

Refined Structure:

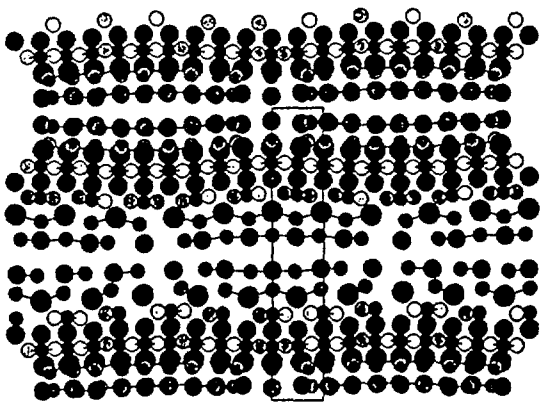

ATOMISTIC SIMULATION OF POLYMER/SOLID AND POLYMER/POLYMER INTERFACES

I Yarovsky

BHP Research
245 Wellington Rd., Mulgrave, Vic. 3170, Australia

Atomistic simulation techniques have been used to provide a molecular level perspective on the phenomena which control adhesion at metal oxide/polymer and polymer/polymer interfaces relevant to steel coating systems. Two simulation methodologies illustrated by relevant examples will be discussed.

The physisorption of an epoxy resin (widely used as the basis of primer paint systems for metallic structural materials) onto alumina and chromia surfaces was compared. Initial model conformations of an epoxy resin oligomer were generated using the Theodorou-Suter technique [1] and the metal oxide surfaces were represented by the low index Miller planes of Al^{III} and Cr^{III} oxides. The simulated complexes of a single oligomer and various metal oxide surfaces were compared both geometrically and energetically and revealed the basis for better adhesion to the chromia surface.

In order to simulate adhesion at polymer/polymer interfaces fully periodic amorphous models of interfaces were constructed and submitted to molecular dynamics. Using this technique adhesion between corona discharge treated polyethylene (CDPE) and a polyester resin was studied. Changes in the chemical composition of the CDPE (depending on the extent of corona discharge treatment [2]) result in clear changes in the calculated energy of adhesion and in the structural properties of the interface as characterised by radial distribution functions for specific functional groups.

The results of these studies are in general agreement with experimental observations and provide the basis for developing a better understanding of the factors controlling adhesion at metal oxide/polymer and polymer/polymer interfaces.

[1] Theodorou D N and Suter U W, *Macromolecules*, 19 (1986) 139

[2] Lane J M, Hourston D J, *Progress in Organic Coatings*, 21 (1993) 269

MACROSCOPIC PROPERTIES OF MODEL DISORDERED MATERIALS

Mark A. Knackstedt* and A.P. Roberts
Department of Applied Mathematics, Research School of Physical Sciences and Engi neering, Australian National University

Disordered materials are ubiqitous in nature and in industry. Soils, sedimentary rocks, wood, bone, polymer composites, foams, catalysts, gels, concretes and ceramics have properties that depend on material structure. Present techniques for predicting properties are limited by the theoretical and computational difficutly of incorporating a realistic description of material structure. For this reason, current models of material properties are largely empirical, without sound theoretical connections to material microstructure. In the absence of any general theory, mechanical properties (elasticity, fracture toughness), and transport properties (thermal and electrical conductivity, permeability and diffusivity) of porous solids are usually correlated to the volume fraction of pore space (porosity) of the solid by the form:

$$\frac{\sigma}{\sigma_s} = C\phi^n = C(\frac{\rho}{\rho_s})^n. \tag{1}$$

Here σ is the physical property (thermal or electrical conductivity, elasticity, fracture toughness, diffusivity, permeability), ϕ is the porosity or volume fraction of the cellular solid, ρ is the density and the subscript s designates a property of the solid material. Most experimental and theoretical work has been devoted to establishing the phenomenological correlation coefficients n and C for different classes of material.

A general model for microstructure was recently proposed by Berk [*Berk, Phys.Rev.A,* 44 *5069 (1991)*]. The model is based on level cuts of a Gaussian random field with arbitrary spectral density. The freedom in specifying the parameters of the model allows the modeling of physical materials with diverse morphological characteristics. We have shown that the model qualitatively accounts for the principal features of a wider variety of disordered materials including geologic media, membranes, polymer blends, ceramics and foams. Correlation functions are derived for the model microstructure. From this characterisation we derive mechanical and conductive properties of the materials. Excellent agreement with experimentally measured properties of disordered solids is obtained. The agreement provides a strong hint that it is now possible to correlate effective physical properties of porous solids to microstructure. Simple extensions to modelling properties of non-porous multicomponent blends; metal alloys, ceramics, metal/matrix and polymer composites are also discussed.

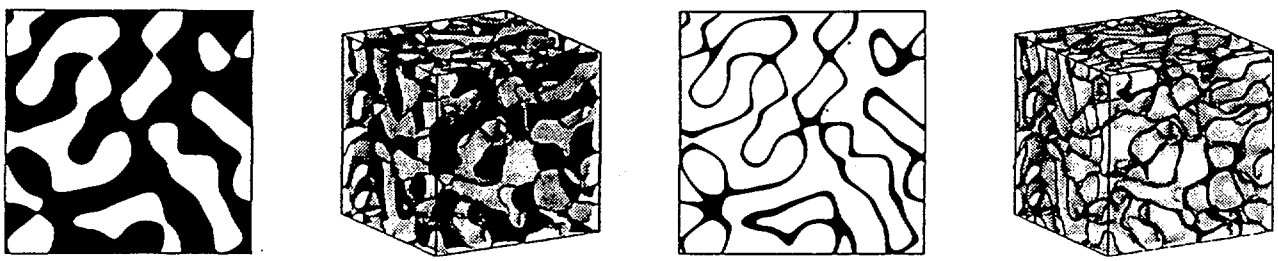

Figure 1: *Examples of two model morphologies given by the level-cut model: Figures show both a two-dimensional cut and the three-dimensional Image.*

Dynamics of Polymers in a good solvent - a Molecular Dynamics Study using the Connection Machine

S.R. Shannon and T.C. Choy
Department of Physics
Monash University
Clayton, Victoria 3168

In recent times the use of molecular dynamics simulations has become an important tool in modelling and understanding the dynamics of interacting many-body systems. With recent advances in computing power it is now feasible to perform modelling of systems which contain a large number of interacting particles, and thus to simulate the behaviour of real systems reasonably. Motivated by our earlier discoveries of anomalous corrections to scaling behaviour of the Edward's polymer[1,2], we apply this approach to study the dynamical behaviour of two dimensional polymer systems - either a single chain immersed in a fluid, a pure polymer melt, or with any concentration of polymers in the fluid. By choosing a suitable interaction potential between the fluid particles and the monomers, we are able to study the experimentally observable time dependent structure factor of polymers in a good solvent. Simulations were performed using the Connection Machine CM5 supercomputer at the ANU which due to its fast multi-processor nearest neighbour communications facility, enables us to easily model large systems of at least 3000 fluid plus monomer particles. Our study is based on a finite difference solution of Newton's equations of motion i.e. the Verlet algorithm, and the results are used to test current theories of polymer dynamics[3,4], which were based primarily on the earlier models proposed by Rouse(1953) and Zimm (1956). In particular dynamical scaling predictions is scrutinised to examine the effects due to the anomalous corrections-to-scaling behaviour found in an earlier work[1] using finite-size scaling analysis of Monte-Carlo data and now understood via a new perturbation concept[2].

References

1. S.R. Shannon, T.C. Choy and R.J. Fleming , Phys. Rev. **B53**, No 5 , (1996)
2. S.R. Shannon, T.C. Choy and R.J. Fleming, J. Phys. A, (submitted).
3. M. Doi and S.F. Edwards, "The Theory of Polymer Dynamics" , Oxford University Press, Oxford (1986).
4. P.G. DeGennes, "Introduction to polymer dynamics", Cambridge University Press, Cambridge (1992).

AN INTERNAL CONFIGURATION BIAS SAMPLING METHOD FOR DENSE POLYMER SYSTEMS

Alfred Uhlherr

CSIRO Division of Chemicals & Polymers, Private Bag 10, Rosebank MDC, Clayton 3169

A new internal configuration bias (ICB) scheme for Monte Carlo (MC) sampling of any number of internal degrees of freedom in chain molecules with arbitrary fixed bond lengths and angles is proposed, extending recent methods restricted to lattice chains,[1] freely jointed chains[2] or short segments[3]. The move is described pictorially in Fig.1 for the case of a linear chain; the method may also be readily generalised to branched chains or networks. Its application to a "phantom" hexadecane backbone with no interatomic potential (Fig.2) confirms that it satisfies detail balance. Its application in a strategy for atomistic simulation of bulk polymeric systems is depicted in Fig.3. Unlike previous polymer MC schemes[4,5] ICB is not dependent on the presence of chain ends, making it potentially highly suitable for the kinds of dense, entangled, high molecular weight & crosslinked systems relevant to applications in the polymer industry.

1. M. Dijkstra, D. Frenkel & J.-P. Hansen, *J. Chem. Phys.* **101** (1994) 3179.
2. F. A. Escobedo & J. J. de Pablo, *J. Chem. Phys.* **102** (1995) 2636.
3. L. R. Dodd, T. D. Boone & D. N. Theodorou, *Mol. Phys.* **78** (1993) 961.
4. D. Frenkel, G. C. A. M. Mooij & B. Smit, *J. Phys.: Condens. Matter* **4** (1992) 3053.
5. P. V. K. Pant & D. N. Theodorou, *Macromolecules* **28** (1995) 7224.

Fig 1. Schematic of a single ICB Monte Carlo move.

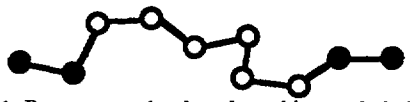

1. Remove randomly selected internal chain section

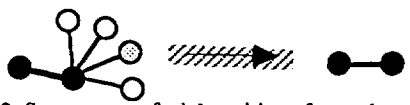

2. Suggest set of trial positions for each atom in turn, & select one biased by interatomic energy + fictitious "spring" to other end

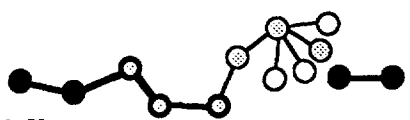

3. Use same method to generate initial guess positions for last 3 atoms

4. Refine cartesian coordinates of last 3 atoms by Newton-Raphson algorithm until all bond length & angle constraints are satisfied

5. Regenerate original chain conformation to calculate necessary probability terms

Fig 2. Normalised histogram of torsion angles in a phantom C_{16} chain after 2×10^7 MC moves

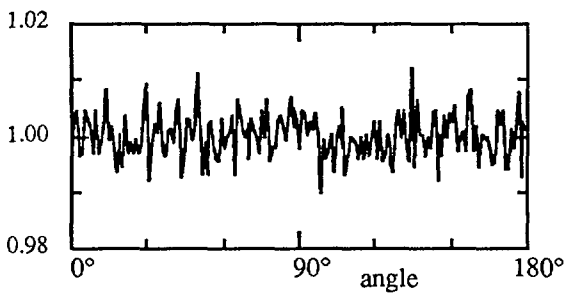

Fig 3. Schematic of a bulk MC simulation scheme based on the ICB method. All atoms in the highlighted region are removed and replaced sequentially by adding to one of the currently active "growth" sites (shaded).

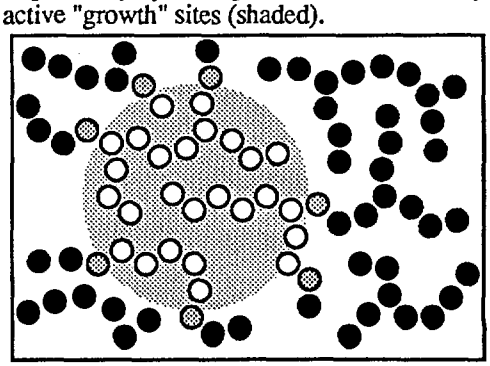

SEMIQUANTUM SYSTEMS FROM SUPERTRANSPORT TO GIANT OPALESCENCE

Eugene P Bashkin
Department of Physics
University of Western Australia

The concept of the semiquantum system, i.e. of a system which exhibits macroscopic quantum-mechanical phenomena within the classical temperature range, is discussed and illustrated by numerous examples. Unusual long-range correlations of fundamentally quantum mechanical origin come into effect even at high temperatures and lead to a large variety of collective phenomena in such systems. Thermodynamics, transport, unique magnetic properties, and weakly-damped collective modes in various semiquantum systems are described. Under certain conditions even a rarefied Maxwell-Boltzmann gas, the most classical matter in physics, can display a fundamentally quantum behaviour. The large magnitude of the effects in question makes the semiquantum systems very attractive for experimental study.

The applications of the theory to condensed matter physics and materials science, atomic spectroscopy, molecular and electron beams, surface phenomena and neutron optics are considered. The most typical objectives for experimental study include helium and hydrogen systems, semiconductors, plasmas, conducting media with point and linear defects, layered electron structures, some classic fluids, spin-polarised systems, Rydberg atoms, etc. The present "state of the art" of and the new prospects for both theoretical and experimental studies are discussed.

MIE SCATTERING IN HEAVY-METAL FLUORIDE GLASSES

A. Edgar
Physics Department
Victoria University of Wellington
New Zealand

"Heavy-metal fluoride glasses" [1] comprise mixtures of heavy-cation fluorides such as those of zirconium, barium, and lanthanum together with some stabilising fluorides such as AlF_3. For particular relative proportions, the mixtures form a glass rather than a polycrystalline material when quenched from the melt. The particularly useful features of these glasses are the wide spectral region (~200nm-8000nm) over which they are transparent, the low minimum attenuation at the centre of the spectral window , and the ease with which optically-active rare-earth ions can be incorporated, leading to potential applications in passive and active fibre optics.

The minimal attenuation, which is potentially lower than for silica fibre, is generally limited by wavelength-independent scattering by particle and gas bubble inclusions. We have observed a new *wavelength-dependent* scattering effect in fluoride glass of the well-known composition ZLABN20. Glass samples which have been prepared at VUW under particular thermal and chemically reducing conditions are coloured, ranging from pink to yellow, with some samples showing the novel characteristic of appearing blue when viewed in transmitted light but rose-red in scattered light. The differing colours arise from different relative magnitudes of a strong scattering peak in the yellow-red region of the spectrum, and a λ^{-n} background absorption. The scattering effect is similar to that reported in "ruby glass", which contains colloidal particles of gold, where Mie scattering from the particles together with the complex refractive index of gold combine to give strong scattering of red light from this composite material.

In this paper, we report on work in progress on the optical extinction and scattering spectrum of the fluoride glasses, and discuss the spectra in terms of Mie's scattering theory. The chemical nature of the scattering centres in these nominally "pure" glasses is at present a puzzle, and relative merits of various possible models will be compared.

1) I D Aggarwal and G Lu, " Fluoride Glass Fibre Optics", Academic Press Inc, (1991), ISBN 0-12-044505-0

AU9918146

Two photon processes in Surface Photovoltage Spectroscopy

Richard P. Craig and Stephen M. Thurgate
School of Physical Sciences, Engineering & Technology
Murdoch University Western Australia

Abstract:

A significant mid-gap effect has been found in Surface Photovoltage Spectroscopy measurements of cleaved GaAs, InP and Si wafer which is normally interpreted as arising from transitions between surface states and band edges[1]. This large mid-gap effect common to various materials is puzzling as such a high proportion of mid-gap states seems unlikely. Most theories of surface states predict states that tail from the band edges into the gap or states that have a well defined energy in the gap. None propose a large state exactly at $E_G/2$. We recently investigated the variation in SPS spectra with flux density. We find a non-linear correlation in the magnitude of Band-Bending arising from mid-gap and band-gap photon energies. We suggest that the mid-gap feature is due to a two photon absorption process leading to carrier pair generation mediated by mid-gap states in the continuum of band-gap surface states.

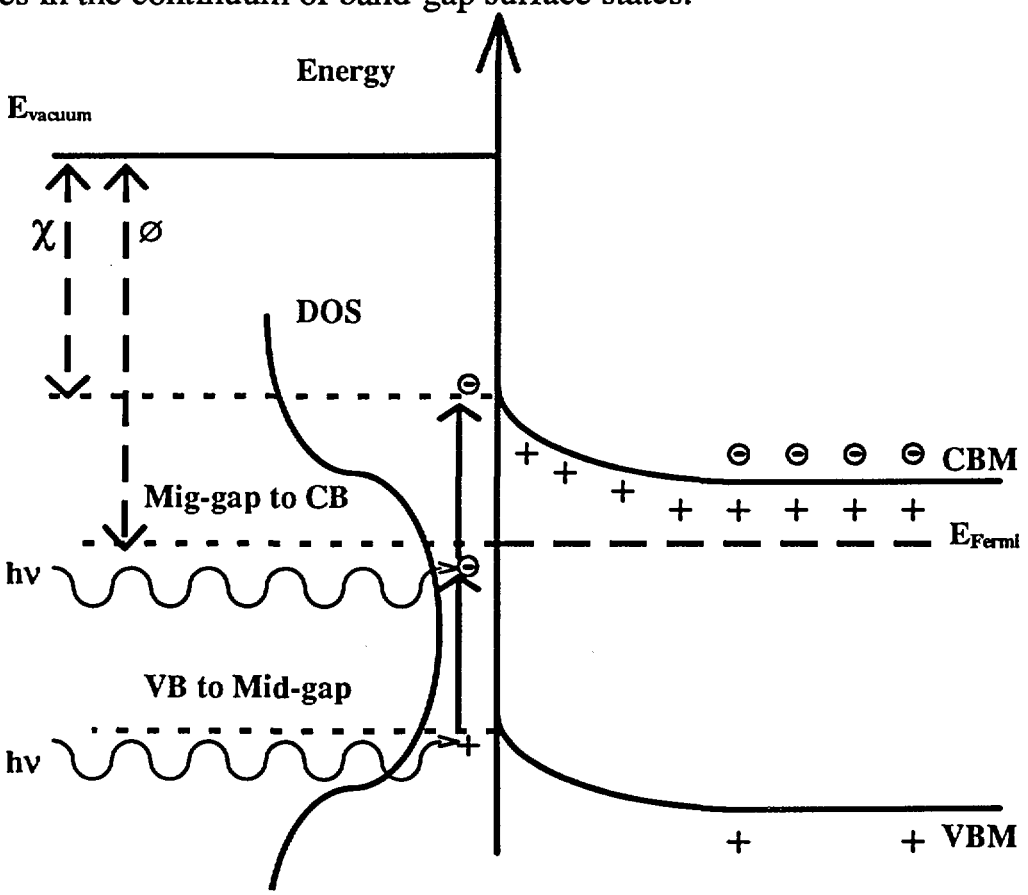

1. S. M. Thurgate et al, Surface Science 310(1994) 103-112

DEVELOPMENTS IN INVERSE PHOTOEMISSION SPECTROSCOPY

W. Sheils, R.C.G. Leckey, and J.D. Riley

Physics Department, La Trobe University, Bundoora, Victoria. 3083

In the 1950's and 1960's, Photoemission Spectroscopy (PES) established itself as the major technique for the study of the occupied electronic energy levels of solids. During this period the field divided into two branches: X-ray Photoemission Spectroscopy (XPS) for photon energies greater than ~1000eV, and Ultra-violet Photoemission Spectroscopy (UPS) for photon energies below ~100eV. By the 1970's XPS and UPS had become mature techniques.

In comparison, while activity in PES was expanding, investigations of the unoccupied states languished. The 'complementary' technique to XPS that probes the unoccupied states is Bremsstrahlung Isochromat Spectroscopy (BIS). Like XPS, BIS (at x-ray energies) does not have the momentum-resolving ability of UPS that has contributed much to the understanding of the occupied band structures of solids. BIS moved into a new energy regime in 1977 when Dose employed a Geiger-Muller tube to obtain density of unoccupied states data from a tantalum sample at a photon energy of ~9.7eV. After the demonstrations of the momentum-resolution provided by working at this energy, the amount of experimentation increased rapidly. At similar energies, the technique has since become known as Inverse Photoemission Spectroscopy (IPS), in acknowledgment of its complementary relationship to UPS and to distinguish it from the higher energy BIS. Drawing on decades of UPS expertise, IPS has quickly moved into areas of interest where UPS has been applied; metals, semiconductors, layer compounds, adsorbates, ferromagnets, and superconductors.

At La Trobe University an IPS facility has been constructed. This presentation reports on developments in the experimental and analytical techniques of IPS that have been made there. The results of a study of the unoccupied bulk and surface bands of GaAs are presented.

THE STRUCTURE OF GOLD CLUSTERS IN YBCO:Au

J.D.Cashion, D.Jinks, G.Jakovidis, G.Ganakas, L.J.Brown and M.J.Morgan
Physics Department, Monash University, Clayton 3168

The addition of a small amount of gold to superconducting $YBa_2Cu_3O_{7-\delta}$ increases its critical temperature[1]. The Au is incorporated[1,2] into the Cu(1) sites and can be precipitated as Au^0. At an oxygen concentration of 7.02 the substitutional Au is Au^{3+}, and reducing the concentration to 6.40 produces complete reduction of the Au^{3+} to principally Au^+, but with also some conversion to Au^0. The nature of the gold clusters is important because they presumably act as weak pinning centres in the superconductor. Recently Storey et al.[3] deduced, from simulations of TEM images that, when in the Au^{3+} state, the gold is in the form of rods of gold atoms in the Cu(1) sites along the [100] direction, with intervening interstitial oxygen atoms, and when in the Au^+ state, it is in the form of rods of gold atoms, with intervening oxygen vacancies along [010].

Combining these results with our own ^{197}Au Mössbauer measurements, we propose the following model. The gold atoms form an approximately square array in the Cu(1) sites on the (001) plane, with approximate dimensions 4 x 4 atoms. In the fully oxygenated state, interstitial oxygen atoms join pairs of gold atoms along [100] so that there are half as many interstitial oxygen atoms as gold atoms. Thus the majority of gold atoms are five-coordinated to oxygens, although some end atoms may be only four-coordinated. The first stage of de-oxygenation removes these interstitial atoms to give square-planar coordination.

Removal of the next oxygen is accompanied by a change in the gold valence to Au^+. Removal of the second O(1) atom allows the Au^+ to achieve its preferred linear coordination with oxygen vacancies along [010]. Our model explains the observed TEM rod-like images of ref. 3 while, at the same time, providing a simple mechanism of getting from one state to the other.

1. M.Z.Cieplak, et al., *Phys. Rev.* **42** 6200 (1990).
2. M.Eibschütz et al., *Appl. Phys. Lett.* **62** 1827 (1993).
3. B.G.Storey, M.A.Kirk and L.D.Marks, *Physica C* **246** 46 (1995).

CRYSTAL FIELD INTERACTION FOR THE SUPERCONDUCTING CERAMICS $TmBa_2Cu_3O_7$ and $TmBa_2Cu_4O_8$

G. A. Stewart, S. J. Harker and A. V. J. Edge

School of Physics, University College, The University of New South Wales, Australian Defence Force Academy, Canberra ACT 2600

For most high temperature ceramic superconductors, the rare earth ions are situated close to the Cu-O planes in which the superconducting carriers are believed to be located. The crystal electric field acting at these rare earth ions is sensitive to the structural arrangement of the oxygen nearest neighbours and their associated charge distribution. The charge distribution is dependent on the degree of charge transfer which, in turn, is closely linked with the existence (or non-existence) of superconductivity. Because of this, considerable experimental effort has been directed at characterising the rare earth crystal field for 1:2:3-type ($RBa_2Cu_3O_7$ R=rare earth) superconductors, and at investigating how the crystal field is influenced by oxygen deficiency. More recently, crystal field data have become available for the related 1:2:4-type ($RBa_2Cu_4O_8$) superconductors. The oxygen stoichiometry of the 1:2:4 systems is much more stable than for the 1:2:3 systems. The 1:2:3- and 1:2:4-type superconductors are the first (n = 0) and third (n = 2) members respectively of a homologous series of compounds with the general formula $R_2Ba_4Cu_{6+n}O_{14+n}$, and the local rare earth site symmetry is very similar for the two types.

The most reliable crystal field parameter determinations in the literature appear to be those based on inelastic neutron scattering measurements, although other techniques have been employed. This work compares the crystal field parameters available for both types of superconductors and tests them against existing ^{169}Tm Mössbauer measurements for $TmBa_2Cu_3O_7$ [1, 2] and $TmBa_2Cu_3O_6$ [2], and new measurements (this work) for $TmBa_2Cu_4O_8$.

[1] P. C. M. Gubbens, J. J. van Loef, A. M. van der Kraan and D. M. Leeuw, J. Magn. Magn. Mater. 76-77(1988)615.

[2] M. Bergold, G. Wortmann and G. A. Stewart, Hyperfine Interactions 55(1990) 1205-1212.

IN SEARCH OF A DEPINNING MODEL FOR THE IRREVERSIBILITY LINE IN CONVENTIONAL SUPERCONDUCTORS

D. B. Lowe and T. R. Finlayson
Department of Physics, Monash University, Clayton, Victoria, 3168

The behaviour of magnetic flux lines in superconductors is of both a fundamental interest and a practical relevance. With the discovery of high temperature superconductors (HTSs) and the observation of their more novel magnetic behaviour, some of the traditional theories concerning flux pinning and flux motion in a type II superconductor have needed to be re-examined. More specifically, the HTSs exhibit relatively large magnetic relaxations compared to conventional materials, and an appreciable magnetically reversible region near the upper critical field in the magnetic phase diagram. The boundary marking the crossover from magnetic irreversibility to reversibility has been called the "irreversibility line".

Interestingly, researchers have since reported similar behaviour in conventional type II superconductors and furthermore, some have argued that the irreversibility line is actually a melting line of the same kind observed in HTSs. However, it is not clear why such materials, some that are strongly pinning, should exhibit such a melting transition.

We have been investigating the same phenomena in various conventional superconductors with different pinning properties. We have chosen to probe the magnetic behaviour using both a vibrating sample magnetometer (VSM) and the newly installed Quantum Design SQUID magnetometer, as functions of temperature and field, to test the validity of various theories. We also offer an alternative model based upon conventional flux pinning concepts.

AU9918151

HIGH TEMPERATURE PRESSING OF Bi-2223 TAPES

P.A.Bain, Q.Y.Hu, D.Yu, H.K.Liu, S.X.Dou

Centre for Superconducting and Electronic Materials, University of Wollongong, Northfields Avenue, Wollongong, 2522, Australia.

Silver clad $(Bi,Pb)_2Sr_2Ca_2Cu_2O_{10}$ superconducting monofilamentary and multifilamentary tapes have been uni-axially pressed at various temperatures ranging from 750° to 850°C under various pressures ranging from 5MPa to 20 MPa. The pressing was performed at various stages of thermomechanical processing consisting of alternate cold pressings and sinterings. SEM, J_c and J_c behaviour in magnetic field were performed to assess induced changes. These were compared with measurements of tape undergoing the same thermomechanical treatment to the exclusion of high temperature pressing. All the obtained microstructural and electromagnetic properties of high temperature pressed tapes show improvements over non-treated tapes. In particular, powder texture, powder density and consequently Jc show significant improvements. A substantial inprovement of Jc behaviour in magnetic field also indicates a possible beneficial effect of high temperature pressing on flux pinnng behaviour. All aspects of both treatments have been thoroughly investigated and analysed.

PROCESSING AND JOINING OF Ag-SHEATHED Bi-2223 SUPERCONDUCTING TAPES

R. Bhasale, J. Horvat, H.K. Liu, S.X. Dou
Centre for Superconducting and Electronic Materials,
University of Wollongong, Wollongong NSW 2522 Australia.

Long length Ag-sheathed Bi-2223 multifilamentary superconducting tapes upto 45 metres long having a transport current of upto 15A over the entire length have been fabricated. Multiprobe measurements show that the transport current has a variation of not more than 10% along the length. A solenoid coil fabricated by the react and wind procedure maintained the uniformity of the transport current along its length.

The degree of reduction in thermomechanical processing has a considerable effect on the critical current density of the tapes. The development of strong links has been seen to be strongly influenced by the degree of reduction in thermomechanical processing.

An investigation of different angle joining of tapes showed that zero degree joining retained about 75% of critical current. It was also observed that nearly 95% of critical current was maintained if the joining was done after first sinter.

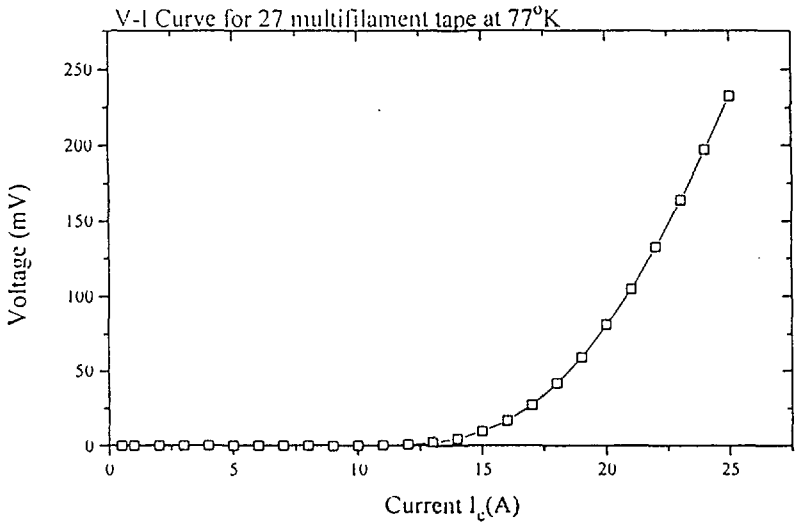

sample	deformation	J_c (kA/cm^2)	I_{c0} (A)	I_{c0}' (A)	I_{c0}'/I_{c0}	a	H_0 (T)
RM1	50%	5.0	6.1	0.75	0.12	0.96	0.24
RM2	30%	8.9	15.6	2.90	0.19	0.95	0.23
RM4	20%	8.8	16.7	3.17	0.19	0.86	0.21
RM3	10%	6.5	13.7	2.94	0.21	0.69	0.20
HP	10%	22.0	20.0	6.57	0.33	0.59	0.18

AU9918153

MEASURING INTERNAL FRICTION AT SONIC AND ULTRASONIC FREQUENCIES IN HIGH TEMPERATURE SUPERCONDUCTORS

A.R. Anderson and G.J. Russell
School of Physics, The University of NSW, Sydney. 2052

Internal friction measurements provide a sensitive means for probing some structural properties of materials. Defect relaxation processes and phase changes are frequently reflected in internal friction measurements as a function of temperature. Relaxation processes associated with oxygen content have been observed in YBCO and BSCCO (2212). By measuring the internal friction at different frequencies activation energies associated with relaxation processes can be determined. Structural changes are temperature dependent and independent of frequency.

To cover the widest range from megahertz to subsonic frequencies a variety of techniques are available. Most authors have usually concentrated on one method, however the present paper describes composite bar and flexural vibration methods covering the frequency range from 600 Hz to 120 kHz providing an adequate frequency range for activation energy determination.

The composite bar technique developed employs a piezoelectric quartz bar (with lengths of 2 cm or 3 cm and resonant frequencies of approximately 85 kHz or 120kHz) with a resonant bar of HTSC attached to one end. The quartz bar is suspended at its nodal points and the system excited electrically using a regenerative feedback system.

The composite bar method can also be used at low kilohertz frequencies by attaching the HTSC specimen used in the previous technique to the end of a much longer (eg 30 cm) fused silica rod which has very low damping. The resulting composite bar can be excited electrostatically or electromagnetically at frequencies below 10 kHz. The internal friction can be measured by scanning through the resonant frequency and measuring the bandwidth or by observing the decay of free oscillation in the bar. The advantage of using the two composite bar techniques is that the measurements can be made on the same specimen at different frequencies.

Flexural vibrations have been extensively used for measuring internal friction at low kilohertz frequencies. The advantage of this method is that small samples can be used (eg 10-30 mm x 5 mm x 0.3 mm) while overtone measurements provide coverage of a range of frequencies. Background damping due to suspension losses can be high using flexural methods, however the use of thin specimens and careful mounting can improve the situation.

A HIGH T_c SUPERCONDUCTING CURRENT LIMITING DEVICE

C. Grantham and J. Beer
Dept. of Electric Power
University of NSW, Sydney 2052, Australia

J.X. Jin and S.X. Dou
Center for Superconducting and Electronic Materials
University of Wollongong, Wollongong, NSW 2522, Australia

A newly built 3.5 kVA rated current limiting device is introduced with a newly developed high T_c superconducting (HTS) coil. The device is based on a magnetic core saturable reactor, and is intended to demonstrate the principle of an electrical power system fault current limiter. A high current ampere-turns dc winding required to saturate magnetic cores in the device is prepared by a $(Bi,Pb)_2Sr_2Ca_2Cu_3O_{10+x}$ HTS coil, which is used as a hybrid coil with another copper coil to be the dc bias winding. The electrical reactance of the device ac limiting winding is related to the dc bias ampere-turns. The magnetic field generated by the dc bias winding is about 0.15 T at 20 kilo-AT. The technological possibility is provided for such a practical device, since at this value of the magnetic field, the used HTS maintains about 50% zero-field critical current I_c at 77 K. The 10^{-13} Ωm criterion is normally selected for the HTS which is much less than 1.68×10^{-8} Ωm for a normal copper conductor at room temperature. Under this criterion, the advantage of using a HTS coil is that there is a factor about 10^{-5} in the calculation of thermal loss ratio of the HTS over normal copper in the conductor design.

References

[1] J.X. Jin, C. Grantham, H.K. Liu and S.X. Dou, "Prototype fault current limiter built with high T_c superconducting coils", Journal of Electrical and Electronics Engineering, Australia, Vol. 15, No. 1, pp. 117-124, March 1995.

[2] J.X. Jin, S.X. Dou, C. Grantham and H.K. Liu, "Preparation of high T_c superconducting coils for consideration of their use in a prototype fault current limiter", IEEE Transactions on Applied Superconductivity, Vol. 5, No. 2, pp. 1051-1054, June 1995.

TESTING A HIGH T_c SUPERCONDUCTING HIGH VOLTAGE GENERATOR

C. Grantham and J. Beer
Dept. of Electric Power
University of NSW, Sydney 2052, Australia

J.X. Jin and S.X. Dou
Center for Superconducting and Electronic Materials
University of Wollongong, Wollongong, NSW 2522, Australia

Based on a R, L, C resonant circuit and using a high T_c superconducting (HTS) inductor, very high voltages and currents can be produced. Theoretically, an infinite high voltage can be achieved by continually reversing a dc power source in such a resonant circuit. An electronic switch has been built with a thyristor-bridge to enable the necessary switching to be carried out. A $(Bi,Pb)_2Sr_2Ca_2Cu_3O_{10+x}$ HTS wire has been used to make the superconducting inductor. The generator is a high voltage source suitable for a high impedance load, and therefore can be used for partial discharge testing and insulation resistance testing. It could also be used as a testing method for the HTS itself with respect to the critical current and AC loss measurements.

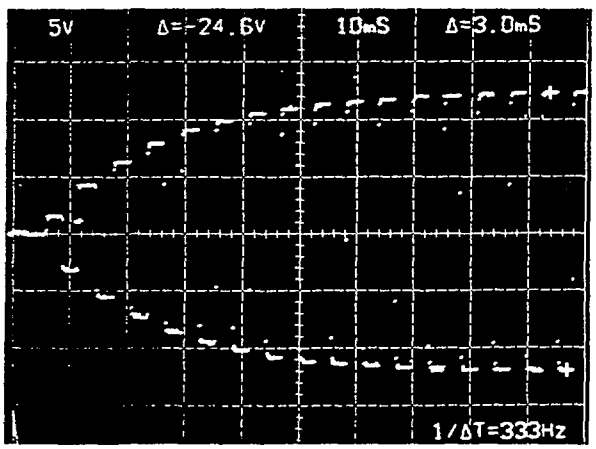

(Y -- 50 V/d, X -- 10 ms/d)

Figure1 Generated voltage with a small HTS inductor.

Reference

[1] C. Grantham, J.X. Jin, S.X. Dou, H.K. Liu and K.J.S. Holder, "Novel electronic high voltage generator with high T_c superconducting coils", The Second International Power Engineering Conference, Vol. 1, pp. 234-238, Singapore, 27 Feb.-1 March, 1995.

HIGH TEMPERATURE SUPERCONDUCTOR CURRENT LEADS

B. ZEIMETZ, H. K. LIU, S. X. DOU

CENTRE FOR SUPERCONDUCTING AND ELECTRONIC MATERIALS,

DEPARTMENT OF MATERIALS ENGINEERING,

UNIVERSITY OF WOLLONGONG

ABSTRACT

The use of superconductors in high electrical current applications (magnets, transformers, generators etc.) usually requires cooling with liquid Helium, which is very expensive. The superconductor itself produces no heat, and the design of Helium dewars is very advanced. Therefore most of the heat loss, i. e. Helium consumption, comes from the current lead which connects the superconductor with its power source at room temperature. The current lead usually consists of a pair of thick copper wires. The discovery of the High Temperature Superconductors makes it possible to replace a part of the copper with superconducting material. This drastically reduces the heat losses because a) the superconductor generates no resistive heat and b) it is a very poor thermal conductor compared with the copper. In this work silver-sheathed superconducting tapes are used as current lead components. The work comprises both the production of the tapes and the overall design of the leads, in order to a) maximize the current capacity ('critical current') of the superconductor, b) minimize the thermal conductivity of the silver clad, and c) optimize the cooling conditions.

THERMOPOWER OF MAGNETICALLY ALIGNED $YBa_2Cu_3O_{7-\delta}$ CERAMIC: A MEASUREMENT APPROACH FOR ANISOTROPIC TRANSPORT OF CERAMICS

C.-J. Liu and H. J. Trodahl
Victoria University of Wellington, Physics Department, P. O. Box 600,
Wellington, New Zealand

J. Downes and M. P. Staines
New Zealand Institute for Industrial Research and Development,
P. O. Box 31-310, Lower Hutt, New Zealand

We present for the first time the thermopower within *ab*-plane and *c*-axis of magnetically aligned $YBa_2Cu_3O_{7-\delta}$ ceramic with different oxygen contents ranging from the superconducting to the insulating regimes. The following features have been observed. (1) The magnitude of thermopower (TEP) becomes more positive with decreasing oxygen content. (2) For the sample with almost fully loaded oxygen content (δ=0.05), TEP within the *ab*-planes behaves distinctly from that of the *c*-axis. The *ab*-planes TEP is very small; the *c*-axis TEP decreases linearly with decreasing temperature. (3) For samples with larger oxygen deficiency ($\delta \geq 0.22$), the *ab*-planes and *c*-axis TEP both show broad hump behaviour; the *c*-axis TEP tends to level off at high temperatures. The broad hump behaviour is also seen for *a*- and *b*-axis TEP in an untwinned single crystal with δ=0.3.[1] (4) For all the samples, TEP of the *ab*-planes is smaller than that of the *c*-axis. (5) The broad maximum of TEP tends to shift to higher temperatures with increasing oxygen deficiency. It is found that both of the *ab*-planes and *c*-axis TEP behaviour for the δ=0.05 magnetically aligned sample bear similarities to the literature data of twinned single crystals,[2] which indicates the ceramic is well aligned along their crystallographic direction. This also makes available the anisotropic property measurements of ceramic samples by aligning polycrystallites using magnetic forces.

1. C. K. Subramaniam, H. J. Trodahl, A. B. Kaiser, and B. J. Ruck, Phys. Rev. B 51, 3116 (1995).
2. M. F. Crommie, A. Zettl, T. W. Barbee, and M. L. Cohen, Phys. Rev. B 37, 9734 (1988); M. Sera, S. Shamoto, M. Sato, Solid State Commun. 68, 649 (1988).

INTRINSIC JOSEPHSON EFFECTS IN Bi-2212

H. L. Johnson

CSIRO Division of Applied Physics, Lindfield, NSW 2070, Australia.

The interesting physics that is seen in the behaviour of a Josephson junction (a weak connection between two superconductors) can be exploited in a wide range of devices. For example the inverse AC Josephson effect underpins today's voltage standard, SQUID technology is based on quantum interference between two Josephson junctions and the AC Josephson effect has the potential to be used to produce microwave sources. Up till now these devices have used *extrinsic* junctions fabricated for example from sandwich structures, step edges or grain boundaries.

Recently, however, it has been shown that a variety of layered superconductors form *intrinsic* Josephson junctions as a direct consequence of the highly anisotropic nature of their crystal structure. One such layered superconductor is $Bi_2Sr_2CaCu_2O_8$ in which the CuO_2 planes act as the superconducting electrode and the non-superconducting Bi_2O_3 and SrO layers act as the barrier.

We report here on a study of intrinsic Josephson effects in single crystals of $Bi_2Sr_2CaCu_2O_8$. The I-V characteristic shows behaviour consistent with the DC Josephson effect. Indeed, close examination reveals a branching pattern in which the difference between adjacent branches corresponds to a switching of one atomic scale junction to the resistive state. We also discuss the microwave response and the possibility of using single crystals of $Bi_2Sr_2CaCu_2O_8$ as sub-millimetre sources.

AU9918159

IMPROVEMENT OF CRITICAL CURRENT DENSITY BY CONTROL OF PHASE EVOLUTION PRIOR TO SINTERING IN BI-2223 TAPES

W. G. Wang, P. Bain, J. Horvat, B. Zeimetz, Y. C. Guo, H. K. Liu, and S. X. Dou

Centre for Superconducting and Electronic Materials
University of Wollongong,
Wollongong, NSW 2522

The critical current density of tapes prepared using various pre-sintering thermal-mechanical treatments was compared. It was found that the phase state before sintering controls the rate of 2223 phase growth, texture and final transport properties. The difference in optimum required sintering processes to achieve high J_c using the same powder source reported by different researchers as well as powder processed using different methods can consequently be clearly explained. The optimum phase before sintering is textured Pb-2212 with a small amount of non-superconducting phase with very small particle size. Jc above 30,000A/cm^2 in self field and a J_{c0}/J_c ratio of above 20% in 1T magnetic field (B//ab) are obtained reproducibly using short sintering times by controlling the phase of the oxide core prior to sintering. The details of the process are reported.

CROSS-SECTIONAL STEM STUDY OF CATHODIC ARC DEPOSITED AMORPHOUS CARBON AND CARBON-NITRIDE FILMS

A.R.Merchant[1], D.G. McCulloch[1], Y.Yin[2], D.R.McKenzie[2]

[1]Electron Microscope Unit & Australian Key Centre for Microscopy and Microanalysis, University of Sydney, NSW 2006, Australia.

[2]School of Physics & Australian Key Centre for Microscopy and Microanalysis, University of Sydney, NSW 2006, Australia.

The VG601 high resolution dedicated Scanning Transmission Electron Microscope (STEM) located at the University of Sydney has the capability of providing structural information with a spatial resolution of less than one nanometre. Compositional information can be obtained using either Energy Dispersive Spectroscopy (EDS) or Electron Energy Loss Spectroscopy. Each characteristic absorption edge in EELS also exhibits structure which provides information on the atomic environment of the absorbing atom. The combination of EELS and STEM therefore provides a powerful tool for analysing structure at the nanometre scale. In this work we investigate the structure of cathodic arc deposited carbon and carbon-nitride films using this EELS/STEM combination. By preparing the films in cross-section and collecting a number of spectra in a line through the film thickness (line profile), it is possible to investigate the deposition process in great detail since variations in structure with depth in the film provide information on the "history" of film growth. In the case of carbon based materials, this technique provides a direct measure of the variations in both density and proportion of diamond-like bonding. These measurements will be used to help understand the mechanisms of film growth by cathodic arc deposition.

OXYGEN ION AND ELECTRONIC CONDUCTIVITY IN DOPED BISMUTH OXIDES

N.J. Long and M.G. Fee
New Zealand Institute for Industrial Research and Development,
PO Box 31-310, Lower Hutt, New Zealand.

We have studied bismuth oxide based materials which in particular may be useful as oxygen separation membranes. These materials form a number of phases with high oxygen ion conductivity. For example the material $Bi_xPb_{1-x}O_y$ (BPO) forms a body centred cubic β-phase at temperatures above 590°C which has an ionic conductivity, $\sigma_i \approx 1\ \Omega^{-1}cm^{-1}$[1]. This phase is also present in other Bi-Pb based materials Bi-Pb-(Ca,Sr,Ba,Cd). These materials may also form rhombohedral and face centred cubic phases with high ionic conductivity[2]. We examine the domains of stability of some of these phases using high temperature XRD and differential thermal analysis (DTA). We determine the total conductivity using AC conductance measurements and measure the ratio of ionic to electronic conduction using oxygen concentration cell measurements.

An oxygen separation membrane can operate in two basic configurations:
(1) An active mode where an applied voltage pumps the oxygen across the membrane.
(2) A passive mode where a partial pressure difference pumps the oxygen across the membrane. Shorting the membrane surfaces externally or using a mixed ionic and electronic conductor provides a return path for the electric charge. We examine how we could use the Bi based materials in either of these configurations.

For example doping BPO with Ni forms a mixed ionic and electronic electrolyte with an ionic conductivity comparable to that of the undoped material. By varying the Ni concentration we can tune the ionic transference number ($t_i = \sigma_{ionic} / \sigma_{total}$) between 0.5 and 1. Ideally $t_i = 0.5$ for an oxygen separation membrane operated using configuration (2) described above.

1. F. Honnart, J. C. Boivin, D. Thomas and K. J. de Vries, Solid State Ionics 9-10 (1983) 921.
2. A. M. Azad, S. Larose, S. A. Akbar, J. Mater. Sci. 29 (1994) 4135.

MEASUREMENT OF TEMPERATURE RISE DURING SI CLEAVAGE

D. Zhao, N. S. McAlpine and D. Haneman

School of Physics, University of New South Walse, Sydney, NSW 2052

A transient temperature change has been measured during the cleavage of Si(100) wafers both in air and in vacuum(5×10^{-6} torr). A fine thermocouple(TC)(E-type) formed by wires of diameter 25μm was placed in a groove cut on the (100) surface where the crack was to occur, as shown in Fig.1. A tiny drop of thermal transfer compound was applied to enhance the thermal conduction between TC and sample surface. The thermocouple signal was recorded by a digital storage adaptor after an amplification of 10,000 by a special low noise amplifier. A typical graph of signal verses time is shown in Fig.2. The width of the pulse appeared to be narrower in vacuum than in air. The difference is ascribed to effects of adsorption. Great care was taken to avoid spurious effects. The technique was tested by experiments on perspex and glass, where the results show reasonable agreement with those from previous work. Theoretical analysis of the measurements shows that the freshly cleaved surface can temporarily attain high temperatures, which is very significant for formation of surface structures.

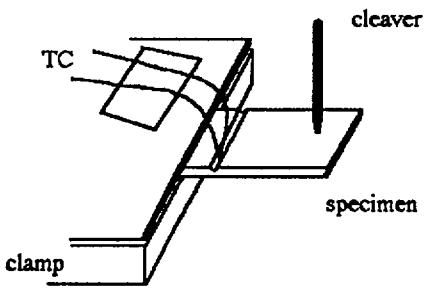

Fig. 1 Schematic diagram of cleavage apparatus

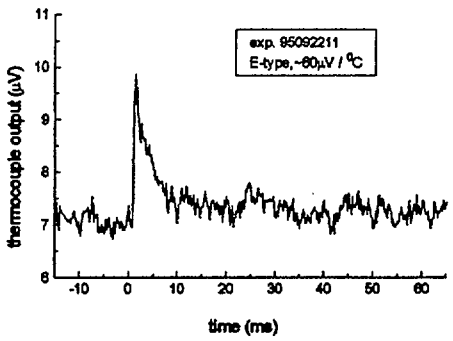

Fig. 2 Thermocouple reading during cleavage of Si in air. The force which induced the cleavage also produced a trigger signal at time zero

WAVE-FUNCTION MAPPING BY (E,2E) SPECTROSCOPY

S.A. Canney, M. Vos, P.J. Storer, A. Kheifets. I.E. McCarthy and E. Weigold*

ESM Centre, Flinders University of South Australia, GPO Box 2100, Adelaide, 5001, South Australia.
*RSPhysSE, The Australian National University, Canberra.

In an (e,2e) experiment the energy-resolved electron momentum density of free standing targets is measured. This spectral momentum density is proportional to the absolute square of the momentum-space wave-function. In an (e,2e) event an incoming electron knocks out an electron from the target and subsequently the two outgoing electrons are detected in coincidence. Our spectrometer measures a range of the binding energies and momenta of the target electrons in parallel. The energy of the incident electrons is 20keV, with the scattered and ejected electrons emerging from the free standing film with 18.8keV and 1.2keV respectively. The lower energy and hence shorter mean free path of the ejected electron ensures that the experiment is surface sensitive. Experiments are performed with an energy resolution better than 1.5 eV and momentum resolution of 0.15 a.u.

We report the results of several experiments carried out on amorphous, polycrystalline and crystalline samples in this spectrometer. For graphite we were able to measure the momentum density directed both in and out of the basal plane. We have also observed the electron dispersion in amorphous silicon, germanium and polycrystalline aluminium films. Carbon films were also exposed to an oxygen plasma and the wave-function of the adsorbed oxygen was measured. These examples illustrate very clearly the detailed information that is obtained about the electronic structure of materials using the (e,2e) technique.

AU9918164

Electronic Structure of an Aluminium Oxide Film as Studied by (e, 2e) Spectroscopy.

X. Guo, M. Vos, Z. Fang, A.S. Kheifets, S. Canney, S. Utteridge, I. McCarthy and E. Weigold*

ESM Centre, Flinders University of South Australian, Adelaide.
* RSPhysSE, The Australian National University, Canberra.

Electronic structure of aluminium oxide(Al_2O_3) has been widely studied experimentally and theoretically because of its importance in microelectronics applications. However, there is no general agreement theoretically and experimentally on its band structure details[1]. We report here on our recent investigations on electronic structure of an aluminium oxide layer on polycrystalline film by (e, 2e) spectroscopy.

The (e, 2e) spectroscopy, a new spectroscopic technique, can measure *real* electron momentum directly and visualize the dispersion relation between energy and momentum of electrons in solids[2]. The (e, 2e) spectrometer[3] in this experiment has been set up at non-coplanar asymmetric geometry. The incident electron energy is 20keV. The two outgoing electrons have energies of 18.8 keV and 1.2 keV, and are measured with two electron analysers each measuring simultaneously a range of angles and energies at polar angles of 14^0 and 76^0 respectively. With this kinematics the spectrometer is surface sensitive to about 2 nm layer on the sample and has an overall measurable energy range of 56 eV with a resolution of 1.0 eV and momentum range from -3.5 to 3.5 a.u. with a resolution of 0.15 a.u.

The sample was prepared by ion beam thinning of a substrate-free aluminium film obtained using vacuum evaporation deposit. An aluminium oxide layer(2-3nm) remained on the aluminium surface because of the vacuum condition used in the ion beam thinning. A count rate of 35 (e, 2e) coincidence counts per minute was achieved

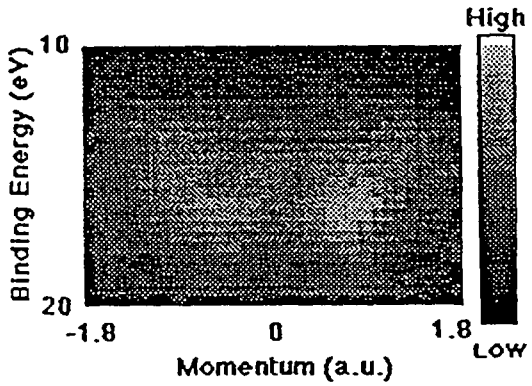

Fig. 1. The spectral momentum density of the upper valence band electrons of aluminium oxide as measured by (e, 2e) spectroscopy.

Fig. 1. shows the measured spectral momentum density of the aluminium oxide layer. A "dual parabola" dispersion patten spanning ~6eV has been observed in the upper valance band, in contrast with previous (e, 2e) measurement[4] by which a dispersionless structure in the upper valence band was reported. Theoretical efforts are being made to explain the observed dispersion patten in the spectral momentum density.

References:

[1] Yong-Nian Xu and W.Y. Ching, Phys. Rev., B43, 4461(1991); and references therein.
[2] I.E. McCarthy and E. Weigold, Rep. Prog. Phys., 54, 789(1991).
[3] P. Storer, R.S. Caprari, S.A.C. Clark, M. Vos and E. Weigold, Rev. Sci. Instrum., 65, 2214(1994).
[4] P. Hayes, M.A. Bennett, J. Flexman and J.F. Williams, Phys. Rev. B38, 13371(1988).

ULTRASONIC ABSORPTION IN SOLID SPECIMENS

P. J. W. Siwabessy+ and G. A. Stewart*

+Poka Marine Science Centre, Fakultas Perikanan,
Unpatti, Kampus Poka, Ambon, Indonesia
*School of Physics, University College, The University of New South Wales,
Australian Defence Force Academy, Canberra ACT 2600

As part of a project to measure the absorption of high frequency (50 - 500 kHz) sonar signals in warm sea-water, a laboratory apparatus has been constructed and tested against room temperature distilled water and various solutions of $MgSO_4$ (chemical relaxation of $MgSO_4$ is the major contribution to absorption below 200 kHz). The technique involves monitoring the decay of an acoustic signal for different sizes of vessels of water suspended in an evacuated chamber. So far, all containing vessels used have been spherical in shape. Extrapolation of the results to infinite volume yields the absorption due to the water alone. In order to accommodate variations in temperature and pressure, and to make the system more robust (e.g. for ship deck usage), it is desirable to employ stainless steel vessels. However, it was found that the quality of the data was greatly improved when pyrex glass spheres were used.

The stainless steel spheres were manufactured by welding together mechanically spun hemispheres. In some cases, the "hemispheres" were not deep enough so that it was necessary to weld an additional equatorial strip into place. Therefore it was suspected that the different thermal and mechanical histories of the individual stainless steel spheres were responsible for the poorer quality of the extrapolated data. In order to test this hypothesis, independent acoustic absorption measurements were performed on an irregularly-shaped block of stainless steel which was submitted to a variety of thermal treatments. Advantages of such measurements are that they monitor absorption alone (scattering plays no role) and that there is no longer a contribution due to the containing vessel. However, unlike water, there is a mixture of compressional wave propagation and shear wave propagation so that a mixed absorption coefficient is obtained. Nevertheless, the linear frequency dependence characteristic of acoustic absorption in solids was observed (in contrast to the quadratic frequency dependence of acoustic absorption in water), and the acoustic absorption was found to depend strongly on the thermal history of the steel.

MAGNESIUM-BASED HYDROGEN ALLOY ANODES FOR A NICKEL-METAL HYDRIDES SECONDARY BATTERY

N. Cui, B. Luan, H. J. Zhao, H. K. Liu and S. X. Dou

Center for Superconducting and Electronic Materials, University of Wollongong, Northfields Avenue, Wollongong, NSW 2522, Australia

Abstract

In the past decade, a novel secondary battery, nickel-metal hydride (Ni-MH) battery using a hydrogen storage alloy as the negative electrode material have received much attention because of their high energy density, superior charge-discharge characteristics and freedom from poisonous materials. Most recent research in this area is focused on the developing superior negative electrode materials, mainly on rare-earth (misch metal) system and Laves-phase multicomponent hydrogen storage alloys.

Magnesium-based alloys have been used as hydrogen storage alloys since 70s. This type alloys are superior to other hydrogen storage alloys in respect to their high hydrogen storage capacity, light weight and low cost. Nevertheless, magnesium-based hydrogen storage alloys have never been used as electrode materials in a secondary battery since their slow hydriding-dehydriding kinetics and poor corrosion resistance in alkaline aqueous solution.

Extensive work has been carried out in our group to try utilizing magnesium-based hydrogen storage alloys as a low cost and high performance anode materials for Ni-MH battery. It was found that the modified Mg_2Ni alloy anodes were able to be charged-discharged effectively in a KOH aqueous solution at ambient temperature. The discharge capacity and cycle have been substantially improved in four ways: (1) by partial substitution of La, Ti, V, Zr, Ca for Mg and Fe, Co, Cu, Al, Si, Y, Mn for Ni in Mg_2Ni; (2) by composite of Mg_2Ni with another hydrogen storage alloys; (3) by room-temperature surface microencapsulation and, (4) by ultrasound treatment of alloy powders. A discharge capacity of 170 mAh/g has been obtained from the modified Mg_2Ni-type alloy electrode, and the cycle life has exceeded 350 cycles. The high-rate dischargeablity was also significantly improved by the modification. It was concluded that magnesium-based hydrogen storage alloys would become promising anode materials for Ni-MH secondary battery with further improvement of discharge capacity and cycling performance.

EFFECTS OF COBALT, ALUMINIUM, AND POTASSIUM-BORON ADDITIONS ON THE PERFORMANCE OF TITANIUM BASED ALLOY ELECTRODES

H.K. Liu, B. Luan, N. Cui and S.X. Dou

Centre for Superconducting & Electronic Materials,
University of Wollongong, Wollongong NSW 2522

Ti_2Ni intermetallic compound is one of the most remarkable alloys owing to its relatively high theoretical value of specific capacity and also the appropriate stability for reversible cycling. It is of interest for application in the field of rechargeable batteries and has drawn great attention recently. However, as the cycle life of Ti_2Ni hydrogen storage alloy electrode is rather short when exposed to electrolyte for cycling, the industrial application using this alloy as the negative electrode of a Ni-MH battery is therefore suspended. To solve this problem, many approaches have been taken such as microencapsulation of alloy powder, mixing of Ti_2Ni and TiNi alloys and also addition of metallic additives into the alloy. In this paper, we report the study on the effects of cobalt, aluminium, and potassium-boron additions on the performance of titanium based hydrogen storage alloy electrodes.

(1) The cycle life of Ti_2Ni electrodes increases significantly with cobalt addition. Charge/discharge cycle life measurements show that the specific capacity of Ti_2Ni electrodes increases with cobalt addition, reaches a maximum at a cobalt content of 0.67 at. % ($Ti_2Ni_{0.98}Co_{0.02}$), and then falls with further addition.

(2) The cycle life of Ti_2Ni electrodes greatly increases with increasing addition of aluminium. The specific capacity of the electrode severely decreases with increasing aluminium content.

(3) Addition of potassium-boron to Ti_2Ni hydrogen storage alloy is effective in increasing the specific capacity and the charge/discharge cycle life of the electrode.

SHOCK DIFFRACTION IN ALUMINA POWDER

G. Venz*, P.D.Killen* and N.W.Page$.
* Queensland University of Technology, Brisbane
$ The University of Newcastle, Newcastle

In order to produce complex shaped components by dynamic compaction of ceramic powders detailed knowledge of their response under shock loading conditions is required. This work attempts to provide data on release effects and shock attenuation in 1 μm and 5 μm α-alumina powders which were compacted to between 85% and 95% of the solid phase density by the impact of high velocity steel projectiles. As in previous work, the powder was loaded into large cylindrical dies with horizontal marker layers of a contrasting coloured powder to provide a record of powder displacement in the recovered specimens. After recovery and infiltration with a thermosetting resin the specimens were sectioned and polished to reveal the structure formed by the passage of the projectile and shock wave. Al'tshuler et al (1960) has shown that the shock formed in the target material is progressively weakened by relief waves originating at the edge of the projectile where the one dimensional shock pressure cannot be maintained and that the region affected by this is influenced by the speed of sound behind the shock. Therefore, if initial conditions such as the velocity and shock response of the projectile and the density of the target powder are known, analysis of the shocked structure will provide good estimates of the shock pressure and the sound speed in the high density material at the shock pressure and will also give an indication of the impact conditions required for successful densification of the powdered material. Results indicate that the shock pressures generated were of the order of 0.5 to 1.4 GPa and higher, with shock velocities and sound speeds in the ranges 650 to 800 m/s and 350 to 400 m/s respectively.

References

1. Al'tshuler, L.V., Kormer, S.B., Brazhink, M.I., Vladimirov, L.A., Speranskaya, M.P., and Funtikov, A.I. (1960) The isentropic compressibility of aluminium, copper, lead and iron at high pressures Soviet Physics JETP Vol.11, pp766-775
2. Killen, P.D., Page, N. W., Thornton D, Shock Diffraction Effects in Powdered Materials. Paper accepted for ACAM-96
3. Petrie, M.W. and Page, N.W. (1991) An equation of state for shock loaded powders. J.Appl.Phys. Vol.69, pp.3517-3524.
4. Page, N.W. (1994) Particle morphology and packing effects on the shock loading of powders. Shock Waves, pp73-80.

COBALT-DOPED IRON OXIDES PREPARED BY MECHANO-CHEMICAL ACTIVATION

W. A. Kaczmarek

Institute of Advanced Studies, Research School of Physical Sciences and Engineering
Australian National University, Canberra, A.C.T. 0200, Australia. wak110@phys.anu.edu.au

A mechano-chemical preparation method has been used successfully to produce equiaxial nanoparticles (10-100 nm) of Co-doped Fe_3O_4, and after annealing at 550 K for 2 hours, $CoFe_2O_4$-γ-Fe_2O_3 composites directly from a mixture of hematite and Co-hydroxide powders. This study is a continuation of a previously reported remarkable and highly efficient room temperature hematite to magnetite reduction process. The experimental results given there [1] clearly show that the complete transformation from hematite to magnetite is possible by room temperature and water assisted mechanical activation of α-Fe_2O_3 powder in oxygen free conditions. Microstructural analysis of the X-ray diffraction data indicated average crystal block sizes for the milled products of <D> ~ 30 nm [2]. Further evidence from Mössbauer spectroscopy shows that the ratio of iron in the octahedral and tetrahedral sites in the Fe_3O_4 produced by milling (Fe_B/Fe_A ~ 1.4) is less than that typically found (~1.8) in bulk crystalline material [3]. The same process offers the possibility of further modifications and particularly preparation of fine Co-doped Fe_3O_4 and γ-Fe_2O_3 composite particles. In this presentation, on the basis of XRD, DSC, FMR and VSM studies we discuss this possibility in detail.

References

[1] W. A. Kaczmarek and B. W. Ninham, IEEE Trans. Magn. MAG-30 (1994) 732.

[2] W. A. Kaczmarek, I. Onyszkiewicz and B. W. Ninham, IEEE Trans. Magn. MAG-30 (1994) 4725.

[3] S. J. Campbell, W. A. Kaczmarek and G-M. Wang, J. Nanostruc. Mat. (1995) in press.

WP23

FORMATION OF ZIRCONIUM NITRIDE VIA MECHANOCHEMICAL DECOMPOSITION OF ZIRCON

T. Puclin and W.A. Kaczmarek

Institute of Advanced Studies, Research School of Physical Sciences and Engineering, The Australian National University, Canberra, ACT 0200, Australia
e-mail: tpp110@rsphysse.anu.edu.au

Over the last few years mechanochemistry has become well established as a new method of advanced materials preparation. Mechanochemistry can often provide a pathway for processes such as gas-solid chemical reactions, which would normally be considered unfavourable or impossible at room temperature. Recently we have demonstrated a mechanochemically activated process for extraction of zirconia from the mineral zircon ($ZrSiO_4$) [1,2].

Formation of metal nitrides usually requires the use of expensive starting materials and processing, such as pure metals, high temperatures and plasma nitriding equipment. As a continuation of our zircon studies, in this paper we report some results of the Mechanochemical reduction of zircon, and for the first time subsequent reaction with nitrogen to form zirconium nitride (ZrN). This process can be described by the equation:

$$3ZrSiO_4 + 8Al + 1.5N_2 = 4Al_2O_3 + 3ZrN + 3Si$$

Milling was carried out in three steps: 1) low speed grinding of $Al+ZrSiO_4$ in vacuum, 2) high speed milling to effect the reduction, and 3) continued milling after the addition of nitrogen. Powders produced were examined by X-ray diffraction. The first step showed no reaction occurred during low speed grinding. The second step proved to be a slow reaction without the "ignition" often seen in other mechanochemical reduction works [3]. The final step was also gradual, and did not always go to full nitridation over the duration of the experiment, giving a product of composition $ZrN_{0.6}$ to $ZrN_{1.0}$. This is quite acceptable as transition metal nitrides are often non-stoichiometric [4].

These results show that the formation of a useful hard material such as ZrN can be formed from a raw mineral by two stage mechanochemical processing. Further investigations are currently being undertaken to eliminate Fe contamination and produce pure ceramic oxide-nitride composites.

1 T. Puclin, W. A. Kaczmarek and B.W. Ninham, *Mater. Chem. Phys.* **40** (1995) 105.
2 International PCT Patent Application, The Australian National University.
3 L.L. Wang, Z.A. Munir, and Y.M. Maximov, Review. "Thermite reactions: their utilization in the synthesis and processing of materials" *J. Mat. Sci.* **28** (1993) 3693.
4 "Ullmann's Encyclopedia of Industrial Chemistry", (VCH Verlagsgesellschaft, Weinheim) vol. A17 pp352-4.

EXAMINING THE EFFECTS OF FILL GAS PRESSURE ON THE DISTRIBUTION OF COPPER ATOMS IN A HOLLOW CATHODE LAMP

D.R. Oliver and T.R. Finlayson

Department of Physics, Monash University, Clayton VIC 3168, Australia.

A modified Copper Hollow Cathode lamp has been used to examine the effects of fill gas pressure on the distribution of sputtered Copper atoms in the body of the lamp. The lamp was modified by placing a quartz disc above the cathode, perpendicular to both the cathode bore and the cathode-anode axis. While the lamp is operating, some of the Copper that has been sputtered out of the cathode bore is deposited on the disc.

Modified Hollow Cathode Lamp

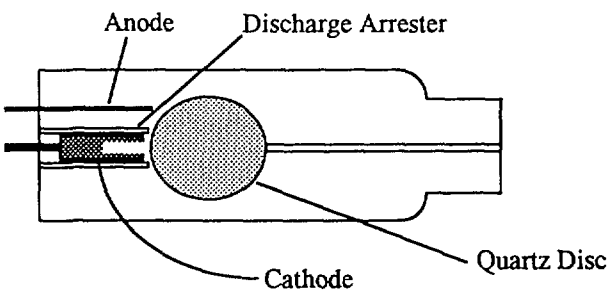

Modified lamps have been operated at a variety of pressures, and the resulting deposition profiles recorded using an optical microscope. A summary of the variations between different pressures are presented.

THERMAL EXPANSION ANOMALIES IN THE PRE-CUBIC -TO-TETRAGONAL PHASE-TRANSITION RANGE AND THE QUANTUM PARAELECTRIC REGIME OF $SrTiO_3$*

Mao Liu and Trevor R. Finlayson

Department of Physics, Monash University, Clayton, Victoria 3168

T. Fred Smith

Vice-Chancellor's Department, La Trobe University, Melbourne, Victoria 3083

High-resolution dilatometry measurements have been made for $SrTiO_3$ along the tetragonal-phase *a* and *c* axes and the cubic-phase [100] direction, for which a moderate stress field has been used accordingly to align the domains of the low-temperature tetragonal phase or to force a single domain. Anisotropy in thermal expansion just above the cubic to tetragonal transformation in the cubic phase for the measurements along the *a* and *c* directions has been observed. No structural change or strain anomaly has been detected in the low-temperature quantum-paraelectric (QPE) regime (K. A. Müller, W. Berlinger and E. Tosatti, *Z. Phys.*, B84 (1991) 277). However, the continuing expansion of the tetragonal *c* axis with decrease of temperature is arrested below 10 K, which can be related to the QPE state.

* The providing of a $SrTiO_3$ single crystal for this work by Dr. J. G. Bednorz is acknowledged.

EFFECTS OF AGING ON THE TRANSFORMATION TEMPERATURE IN A Au-49.5at%Cd ALLOY

Yoshihiro KUROIWA, Mao LIU and Trevor R. FINLAYSON
Department of Physics, Monash University, Clayton, Vic. 3168, Australia

T. Fred SMITH
Department of Vice-Chancellor, La Trobe University, Melbourne, Vic. 3083, Australia

Some martensitic alloys are found whose reverse-transformation temperatures, A_s and A_f, from the martensite phase to the parent phase are changed somewhat, after aging the alloys in the martensite phase.[1,2] This phenomenon has become known as the aging effect. This effect often gives rise to serious errors in the operation of devices, where the mechanism of shape memory is applied to a switch.

In this study, the aging effect in Au-49.5at%Cd has been investigated as a function of aging temperature, by observing the surface martensite-bands in an optical microscope equipped with a cryostat. A Au-49.5at%Cd alloy undergoes reverse-transformation from the trigonal, ζ'_2 martensite phase to the CsCl-type β_2 parent phase at around room temperature.[3] The transformation temperature of our particular sample was typically 36°C. The aging effect in this alloy was first measured by DSC following aging at room temperature,[4] and also the rubber-like behaviour associated with the aging of martensite was found.[5] A single crystal of Au-49.5at%Cd was kindly supplied by Professor T. Ohba of Teikyo University in Japan. The surface bands were observed on the electro-polished, {100} surfaces as stripes along the ⟨100⟩ or ⟨110⟩ directions. When the sample was aged at 20°C, there was no effect on either A_s or A_f until 3 hours aging. After 3 hours aging, the effect suddenly appeared, and both A_s and A_f increased with aging time, reaching maximum values of 49°C and 51°C, respectively. However, in the case of aging at 33°C, the effect appeared for very short aging time, and in the case of aging at -50°C, there was no effect even after long aging time. On the other hand, no obvious effect was observed in the parent to martensite transformation, following aging in the parent phase. This phenomenon is discussed in relation to the 'pinning of martensite-plate boundaries' and the 'reordering of the martensite'.

References

[1]G. Scarsbrook, J. M. Cook and W. M. Stobbs, Met. Trans. **15A**, 1977 (1984).
[2]T. Tadaki, H. Okazaki, Y. Nakata and K. Shimizu, Mater. Trans. JIM **31**, 941 (1990).
[3]T. Ohba, Y. Emura and K. Otsuka, Mater. Trans. JIM **33**, 29 (1992).
[4]Y. Murakami, S. Morito, Y. Nakajima, K. Otsuka, T. Suzuki and T. Ohta, Mater. Lett. **21**, 275 (1994).
[5]Y. Nakajima, S. Aoki, K. Otsuka and T. Ohba, Mater. Lett. **21**, 271 (1994).

ELECTRON AND H-ATOM PHOTOTRANSFER: ESR INVESTIGATION IN DOPED CRYSTALS AND GLASSY MATRICES.

George G. Lazarev

Physics Department, Monash University, Clayton, Victoria 3168, Australia

The radical pairs formation as a result of electron and hydrogen atom phototransfer was investigated. These intermediate radical pairs are, as a rule, sufficiently stable at low temperatures, and it is easy to detect them by ESR spectroscopy. Moreover, information concerning the structure of those radicals which form pairs can be obtained by this technique. Typical spectra of radical pairs arise if the distance between two radicals is not more than 7 A to 10 A. In this case, the dipole-dipole magnetic interaction of the electron spins is large enough to cause a detectable splitting in the ESR spectrum. In crystal matrix, anisotropy interactions, as a rule, do not take part within the width of lines, and it is possible to see the hyperfine splitting more distinctly, so giving more information about the nature of the radicals in the pair.

Ultraviolet irradiation of aromatic ketones in the presence of hydrogen or electron donors leads to photochemical reduction of the carbonyl group. Among the photochemical reactions of quinones, photoreduction plays an important role in electron transfer processes during photosynthesis and photophosphorylation.

The present report discusses the investigation of intermediate products in photoactive molecules which can be included in organic crystals as impurity. This method in doped crystals allows to obtain new results in the field of photoreactions of quinones, quinone diazides, iminoquinones and another acceptors of electron or H-atom. Asymmetric relaxation effects were observed in X-band spectra of some radical pairs. Anisotropy of electron transfer in photoreactions of porphyrins was investigated in glassy matrices at 77 K. The data obtained are explained by anisotropy of dark tunnel recombination of ion-radical pairs. Polarized light was used to produce oriented spin probes: radical complexes of phenol and quinones in frozen organic solutions. Kinetics of reorientation of these probes in time range from 10 min. to several months were measured at different temperatures (77 K - 140 K). Correlation between the molecular mobility of oriented radical complexes and the rate of radical reactions in the same frozen matrices were found. Photochemical transfer of electron and proton across the interface in microemulsion were investigated.

The preliminary results obtained using pulsed and 2-Dimensional ESR BRUKER 380E spectrometer in cooperation with Professor John Pilbrow and Dr. Y.C.Zhong will be discussed.

References: Chem.Phys.Lett. 95(1983)262, 170(1990)94, 181(1991)512, 185(1991)375, 199(1992)29, 212(1993)319, 215(1993)375,
J.Am.Chem.Soc. 116(6447)1994.

AN ELECTRON PARAMAGNETIC RESONANCE STUDY OF THE BEHAVIOUR OF COPPER(II) IN AGEING CATECHIN-BASED MODEL WINES

M. Mitri[1], G.R. Scollary[1], G.J. Troup[2], D.R. Hutton[2], C.A. Hunter[3] and D.G. Hewitt[4]

[1]School of Chemistry, The University of Melbourne, Parkville, 3052.

[2]Physics Department, [3]Anatomy Department, [4]Chemistry Department, Monash University, Clayton, 3168.

Copper is regarded as a problem metal in wine as, at too high a concentration, it appears to enhance the rate of oxidation and can also lead to haze formation. The critical copper concentration is the subject of debate and anecdotal reporting and the published mechanisms for the role of copper in wine oxidation are highly speculative, frequently invoking free radical processes without evidence for the copper/free radical chemistry.

This poster reports an epr study of copper in a model white wine. The model consists of a saturated 12% ethanol solution of potassium hydrogen tartrate solution (the "wine base") containing copper and catechin (Figure 1) as the oxidizable substrate. Ascorbic acid, as a supposed anti-oxidant, was added to some solutions. A Varian E-12 epr spectrometer (~9.1 GHz frequency) with quartz sample tubes was used and spectra were recorded at liquid nitrogen temperature to avoid polar water losses. Solutions were examined on four successive days whilst kept at room temperature and subsequently every third day when stored at 45°C. Variations in signal intensity, linewidth and form will be shown and the changes related to the degree of browning, as measured by visible absorption spectroscopy at 440 nm.

Figure 1. Structure of catechin

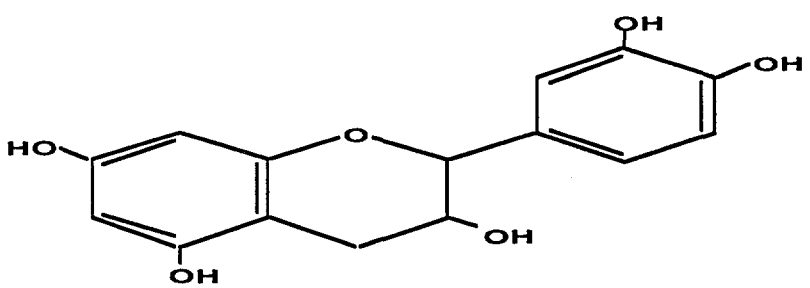

Brown deposits which were obtained from the copper-catechin solutions were also examined by epr. The spectra reveal that the copper(II) ion is in a low symmetry site and a well-defined free radical signal was also observed. A free radical signal was not found in solutions containing copper and catechin, indicating that a high degree of polymerization of the oxidized catechin is required to stabilize the free radical species.

EPR SPECTRA OF SYNTHETIC, AND NATURAL AUSTRALIAN OPALS - A PILOT STUDY

D.R. Hutton*, Mary Young † and G.J. Troup*

*Physics Department, Monash University, Clayton 3168 Victoria

†Gold Craft Creative Jewellery, South Oakleigh 3167 Victoria

The EPR spectra of some synthetic opals, and of some Australian natural opals of various provenance, have been obtained, with the use of a Varian E-12 EPR spectrometer operating at ~9.2 Ghz. The synthetic opals, from Swiss Gilson showed here a broad ESR signal in the g = 2 region, with little identifiable structure . The natural Australian opals from Coober Pedy, Lightning Ridge, and Mintabie all showed the clear presence of Fe^{3+}, Mn^{2+} and a free radical like signal, suspected to be localised on an Al atom. Examples of the various spectra will be presented. It is not yet certain how the spectra correlate with provenance, but the synthetic spectra are quite different from the natural ones.

We thank Mr Andrew Cody of Cody Opal, 119 Swanston Street, Melbourne for the loan of the synthetic and some natural specimens.

Bernal Liquid Drop - Alpha Particle Models of some Heavy Magic Number Nuclides

DR. P D NORMAN, Senior Lecturer (Retired), Physics Department, Monash University, Frankston, 3199, Victoria, Australia.

Models of the bond structures of nickel 56, strontium 88, tin 120, cerium 140, lead 208 and uranium 240 nuclides based on Bernal's models of dense liquid drops show good agreement between the binding energy data and shell structures when alpha particles are considered to be the densely packed hard spheres of Bernal's models. These models of the time-averaged structures of several closed shell nuclides have been developed as pedagogical aids for conceptualising some of the major aspects of nuclear matter and energy. These concepts include nuclear shape, size, charge density, quadrupole moment, viscosity, binding energy, coulomb repulsion, energy levels, magic numbers, shells and sub-shells; nucleon separation, bonding, pairing and clustering ; nucleosynthesis, radioactivity and fission.

As early as 1915 Harkins noted that some of the most abundant and stable nuclides appear to consist of integral numbers of alpha particles. Gamow, in 1929, carefully developed alpha particle models of a number of stable nuclides. Since then many other researchers have followed his lead, despite various difficulties, because the very existence of alpha decay, alpha capture, helium fusion, oxygen fusion, carbon fusion and silicon fusion have prompted their search.

The models discussed below are based on those proposed by Bernal to account for the properties of normal liquids. Bernal's models have also been extended by others to explain the nature of metallic glasses considered as supercooled liquids. In Bernal's tetrahedral model of a normal liquid drop, a hard sphere representing an atom, ion, or molecule is added at whatever available position is closest to the centre of the existing cluster of spheres so that the densest possible configuration is created. Accordingly, two spheres form a dumbbell, three spheres form a triangle and four spheres form a tetrahedron and so on.

REFERENCES

Norman, P.D. 1995, Liquid Drop - Alpha Particle Models of some Common Nuclides. Proc. ANA 95 (Lucas Heights) 125.

Norman, P.D. 1993, Models of the meson bond structures of the most abundant products of stellar nucleosynthesis. Eur J. Phys. 14,36.

Robson, D. 1978, Alpha particle clustering and the quark structure of elementary particles, Proc. of the 3rd Int. Conference on clustering aspects of nuclear structure and nuclear reactions (Winnepeg, AIP) 348.

Kukulin, V.I. 1991, A new physics in the problem of nucleon - nucleon interaction, Proc. of meeting re Pauli principle in few-body systems, (Tokyo, Inst. Nuclear Study).

Pearson, J.M. 1986, Nuclear Physics: Energy and matter, (Bristol, A. Hilger).

AU9918178

Magnetic Transitions in $La_{1-x}Y_xMn_2Si_2$ - Mössbauer Effect Study

X.L. ZHAO, S.J. CAMPBELL, J.M. CADOGAN[+] and Hong-Shuo LI[+]

School of Physics, University College, The University of New South Wales, Australian Defence Force Academy, Canberra, ACT 2600, Australia

[+] School of Physics, The University of New South Wales, Sydney, NSW 2052, Australia

Investigation of ternary rare-earth manganese silicides (RMn_2Si_2) with the tetragonal $ThCr_2Si_2$ structure (space group I4/mmm) continues to attract a great deal of interest due to the large variety of magnetic behaviours which they exhibit [see eg 1]. This interest has been further stimulated by the recent revision of the magnetic structure in some RMn_2Si_2 compounds based on neutron diffraction and magnetic measurements [see eg 2]. Here we outline our recent investigations of a series of $La_{1-x}Y_xMn_2Si_2(^{57}Fe)$ compounds using Mössbauer effect spectroscopy over the temperature range 4.2 - 520 K. The aim is to study the temperature- and concentration- induced magnetic phase transitions in these compounds as the antiferromagnetism of YMn_2Si_2 (T_N ~ 516 K) gives way to the predominant ferromagnetism of $LaMn_2Si_2$ (T_C ~ 306 K) around the critical concentration x ~ 0.2.

The set of $La_{1-x}Y_xMn_2Si_2(^{57}Fe)$ samples (x = 0.00, 0.10, 0.15, 0.20, 0.25, 0.30, 0.50 and 1.00) was prepared using conventional argon-arc melting and examined by x-ray diffraction. One of the striking features of our results is that the ordering temperatures of the compounds with low Y concentration (x < 0.3) are significantly higher than previously reported values [1], while, also at low Y concentrations, a transferred magnetic hyperfine field associated with ^{57}Fe atoms on the Si sites is found to persist well above T_C. These observations are in general agreement with the new findings of a high temperature antiferromagnetic phase in $LaMn_2Si_2$ [2,3]. Magnetic phase transitions (as indicated by distinct temperature- and concentration-dependent anomalies in the hyperfine magnetic field and quadrupole splitting), have been determined for the $La_{1-x}Y_xMn_2Si_2(^{57}Fe)$ samples, leading to clarification of the magnetic phase diagram. Around the critical concentration (x~0.2) which separates the predominant antiferromagnetic and ferromagnetic regions, the Mössbauer spectra exhibit broadened lines indicative of a spin glass-like or frustrated magnetic system.

[1] Szytula A and Leciejewicz J, **1989** *Handbook on the Physics and Chemistry of Rare Earths*, (Elsevier Science Publisher B.V.) Gschneidner Jr. K A and Eyring L (Editors), Vol.**12**, Chapter 83, pp 133.

[2] Venturini G, Welter R, Ressouche E and Malaman B, **1994** *J. Alloys and Cpds* **210** 213.

[3] Nowik I, Levi Y, Felner I and Bauminger E R, **1995** *J. Magn. Magn. Mater.* **147** 373.

AU9918179

DETAILED COMPARISON OF EXPERIMENT WITH THEORY FOR THE OSCILLATORY FREE INDUCTION DECAY IN GAMMA DETECTED NMRON

L.N. Shakhmuratova*, W.D. Hutchison, D.J. Isbister and D.H. Chaplin

School of Physics, University College, The University of New South Wales

Australian Defence Force Academy, Canberra, ACT, 2600, Australia

*Kazan State Pedagogical University, Kazan, Russia

At the Wagga '93 meeting the first theoretical developments (utilizing concatenation of perturbation factors in statistical tensor theory) and the first pulsed Nuclear Magnetic Resonance on Oriented Nuclei(NMRON) experiments on ^{60}Co**Fe** were reported for the Oscillatory Free Induction Decay(OFID) when detected by higher rank tensors other than first rank[1]. At that stage of theoretical development progress was limited to second rank detection tensors along with the effects of severe damping of the oscillations (the period of the OFID is related to the Rabi frequency) due to the metallic skin effect[2]. In the interim the analytical theory has been extended by one of us (LNS) to include third rank (for pedagogical reasons) and fourth rank (~ 5% correction to properly model ^{60}Co**Fe** data) detection tensors; additionally the degree of softness of the obligatory second "read" pulse that projects fast (transverse) coherences onto the slow, population-sensitive (longitudinal) nuclear radiation detection direction has been numerically modelled(DJI) and included to allow detailed comparison with experiment. In this paper it is demonstrated how the skin-effect damped oscillations of the OFID may be restored within a metal host, by employing the newly discovered two-pulse nutational stimulated echo criterion of two equal pulses[3]. For these conditions, dephasing of nuclear spins due to the skin effect during the first pulse is partially restored at the end of the second (equal area) pulse which has the dual role of acting as "read" pulse and refocussing the spins. The adjustable variable in the experiment is the pulse separation and the experimental signal is the change in gamma anisotropy at the trailing edge of the "read" pulse. All experiments are performed on a time scale short compared with nuclear spin-spin and spin-lattice relaxation times. Excellent fits of experimental data with the extended theory are obtained for a wide variety of unequal and equal pulses.

1) L.N. Shakhmuratova, D.J. Isbister and D.H. Chaplin, Hyp Int **80** (1993) 1167.
W.D. Hutchison, N. Yazidjoglou, D.J. Isbister, D.H. Chaplin and L.N.Shakhmuratova, Hyp Int **80** (1993) 1173.

2) D.J. Isbister and D.H.Chaplin, Z. Naturforsch **45a** (1990) 43.

3) L.N. Shakhmuratova, W.D.Hutchison, D.J. Isbister and D.H.Chaplin, Proceedings of HFI X, Leuven, Belgium, August 1995.

THE FERMI SURFACE OF FERROMAGNETIC Ni AS DETERMINED BY PHOTOEMISSION SPECTROSCOPY: RESOLUTION OF THE SPIN SPLIT Σ_1 BANDS.

S. Tkatchenko, J. A. Con Foo and A. P. J. Stampfl
School of Physics, La Trobe University, Victoria 3083, Australia

B. Mattern, M. Hollering, R. Denecke and L. Ley
Universität Erlangen-Nürnberg, 91058 Erlangen, Germany

J. D. Riley and R. C. G. Leckey
School of Physics, La Trobe University, Victoria 3083, Australia

The Fermi surface of Ni has been mapped using an angle resolved photoemission spectroscopic technique [1]. Our results compare well to previously reported de Haas van Alphen measurements and to the results of recent calculations. We have also clearly resolved the spin split Σ_1 bands without the use of a spin detector: previous reports only just resolve the bands ($\Delta E_{ex} \sim 0.2$ eV). Our method uses the tunablity of synchrotron light to excite only one band at a time: in this way the bands are separated by $\hbar\omega \sim 7$ eV. This is an important result as it will allow us to measure the temperature dependence of ΔE_{ex}. There is quite a lot of controversy as to what happens to these bands as the temperature approaches the Curie point: do the bands collapse to one band or do local moments persist ? We are presently attempting to acquire the necessary data to answer these questions.

[1] J. A. Con Foo, A. P. J. Stampfl et. al. Submitted to Phys. Rev. B

Magnetic Disorder in $Co-Mn$ and $Ni-Mn$ Alloys

T.J. Hicks and M.F. Ling

Department of Physics, Monash University,

Clayton, Victoria 3168, Australia.

Based on the diffuse neutron scattering measurements on $Co-Mn$ and $Ni-Mn$ alloys by Cable et al., we have modelled the magnetic disorder in these alloys and obtained new values for their average magnetic moments. The diffuse neutron scattering from the paramagnetic phase of these alloys is closely related to their generalised susceptibilities. The model is a mean field approximation to the susceptibility generalised to incorporate a non-uniform response.

AU9918182

TOWARDS A REALISTIC MODEL OF FE-CU-FE SPIN VALVE SYSTEMS USING TIGHT-BINDING METHODS

Y. Hancock and A.E. Smith

Department of Physics, Monash University, Clayton, Victoria 3168, Australia

Magnetic multilayer materials are becoming technologically important as they provide a more efficient means of magnetic reading and storage through utilisation of their giant magnetoresistence and oscillatory magnetic coupling [1,2,3]. This study presents preliminary tight-binding calculations with a view of developing a consistent tight-binding model of "spin valve" Fe-Cu-Fe tri-layer materials (Fig. 1) [3]. Further work involves using a self-consistent tight-binding approach [4] to obtain a more accurate picture of this system and a better understanding of surface effects at the Fe-Cu interface.

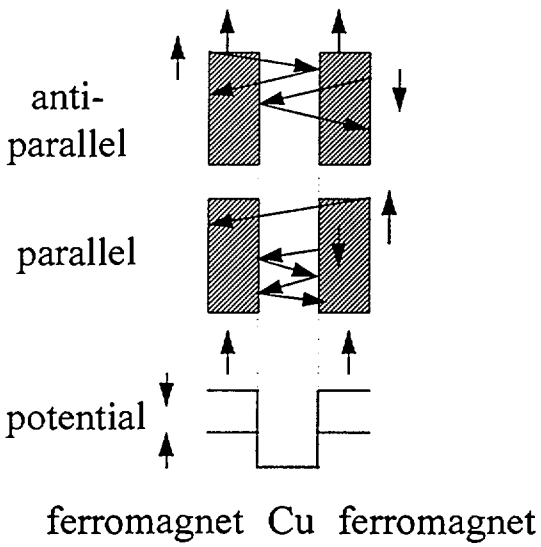

Fig. 1. Reflection of electrons at the interface of a spin valve for various magnetic configurations. A potential step confines the electrons at E_F to the Cu layer [3].

1. J.E. Ortega and F.J. Himpsel, Appl. Phys. Lett. **64** (1994) 1.
2. D.M. Deaven, D.S. Rokhsar and M. Johnson, Phys. Rev. B. **44** (1991) 11.
3. F.J. Himpsel and O. Rader, Appl. Phys. Lett. **67** (1995) 8.
4. F. Liu, Phys. Rev. B. **52** (1995) 15.

PROGRESS ON 40 TESLA HYBRID MAGNET AT TML

H. Maeda
Tsukuba Magnet Laboratories - National Research Institute for Metals
Sengen, Tsukuba 305, Japan

We have developed several high-field magnets, e.g., long-pulsed magnets, a 40 T class hybrid magnet, a 21 T superconducting magnet, several high-resolution magnets, etc.

At last,very recently, the 40 T class hybrid magnet (40 THM), composed of a 15 T superconducting magnet with a room-temperature clear bore of 400 mm (15 TSM) and a 25 T polyhelix-type, water-cooled magnet with a 30 mm bore (25 TWM), succeeded to generate a central field of 36.04 T which is a new world record for steady magnetic fields. The 15 TSM is composed of 58 double-pancake coils; each pancake is made of Nb-Ti and $(Nb,Ti)_3Sn$ multifilamentary superconducting wires. The magnet is operated to be cryogenically stabilized in full operation at 4.2 K under the maximum current of 1476 A and a stored energy of 63.37 MJ. The 25 TWM is composed of 18 coaxial, helical coils with a 30 mm clear bore, made of Cu-Al_2O_3 alloy having a high conductivity of 89 % IACS and a high strength of 420 MPa, which is much higher than the designed, maximum hoop stress of 337 MPa. The 40 THM system has a 15 MW dc power supply, a 15 MW water-cooling system, and a helium refrigerator (150 l/hr or 450 W at 4.4 K). The magnet is designed to generate 25 T at an operating current of 33.3 kA, in a back-up field of 15 T. The flow rate and the flow velocity of cooling water are about 650 l/hr and 18 m/s, respectively. We first excited the outer 15 TSM to generate 14.01 T at the center, then excited the inner 25 TWM to generate 22.03 T with gradually increasing its operation current up to 29.3 kA and holding for 30 minutes at the current, thus, successfully generating a total central field of 36.04 T in a clear bore of 30 mm. We have also another inserted 20 T polyhelix-type, water-cooled magnet with a 50 mm bore (20 TWM), composed of 15 polyhelix coils. The 35 T hybrid magnet inserting the 20 TWM also succeeded to generate 32.1 T in a clear bore of 50 mm. The magnets are now used for measurements such as magnetization, dHvA, etc.

For future hybrid magnets generating above 40 T we shall have to develop helical coils with higher strength/higher conductivity than those of Cu-Al_2O_3 alloy; for example, using Cu-Ag alloys. We have already developed Cu-Ag wires with high strength (>1 GPa) and high conductivity (>80 % IACS) sufficiently useful for pulsed magnets and also tapes useful for Bitter-type, water-cooled, resistive magnets.

XPS DETERMINATION OF DOPING MECHANISM IN AMORPHOUS SILICON

Jagriti Singh

Department of Applied Physics, Royal Melbourne institute of technology,Melbourne, Victoria 3001, Australia.

and

R. C. Budhani

Brookhaven National Laboratory, Upton, New York NY11973, USA

Abstract

The doping of amorphous tetrahedrally bonded semiconductors has been well established through conductivity and thermopower [1]. However, a basic understanding of the microscopic origin, in terms of topological and chemical environment of the impurity and concomitant changes in the distribution and type of the gap, tail and extended states is still being explored [2-4].The empirical observation that large amounts of impurities (as compared to crystalline semiconductors) are required to dope the amorphous material [1], even in the case of low mid-gap density material such as amorphous hydrogenated silicon (a-Si:H), challanges the singular assignment of the role of the impurity atom namely that of doping action.

The present paper is directed towards unfolding the doping mechanism in amorphous hydrogenated nitrogenated silicon (a-Si:H:N) thin films prepared by reactive ion beam sputtering (RIBS) technique. From the analysis of infrared (IR) absorption spectra and Si-2p core level shape, measured with X-ray photoelectron spectroscopy (XPS),the fine interplay between doping and alloying effects has been studied. XPS has been used to provide direct evidence of the movement of the fermi-level and the doping mechanism. XPS has also been used to determine upper solid solubility limit of nitrogen in amorphous silicon matrix.

1. P.G.LeComber and W.E. Spear, Topics in Applied Physics, Amorphous Semiconductors, Vol 36, p.251 (Edited by M.H. Brodsky) Springer-Verlag, Berlin (1979).
2. M. Stutzmann and R.A. Street, Phys. Rev. Lett. 54, 1836, (1985).
3. Jagriti Singh and R.C. Budhani, Solid State Commun.64(3), 349, (1987).
4. Jagriti Singh and R.C. Budhani, Communicated.

USE OF NEXAFS FOR THIN FILM GROWTH MORPHOLOGY

Jagriti Singh

Department of Applied Physics, Royal Melbourne Institute of Technology, Melbourne, Victoria 3001, Australia.

Abstract

The useful properties of thin films for various applications depend on the structure of the film which is sensitively dependent on initial growth of the adsorbate on the substrate. Most of the techniques used for studying thin film structure such as XRD, Neutron diffraction, electron microscopy, XPS and IR give information about crystal structure, physical topography, or chemical nature of the bonding of the adsorbate atoms. The present paper describes the first use of NEXAFS for studying growth morphology in terms of adsorbate orientation and its influence on oncoming species. For the purpose NEXAFS spectra of physisorbed ethylene on Cu{100} surface using monochromatic synchrotron radiation is used.

AU9918186

Electroluminescence of Spark-processed Silicon

D.Haneman and J.Yuan
School of Physics, University of New South Wales, Sydney 2052, Australia

We have successfully fabricated spark-processed silicon[1,2] to produce electroluminescence that can be readily seen under semi-dark conditions when about 10V pulses with a duty cycle of 50% are applied to the sample. The samples were lightly spark-processed with the system as described in Fig.1. After spark-processing, a layer of semitransparent metal was evaporated onto the surface of the sample as electrode and a layer of Al on the back as ohmic contact. The electroluminescence spectrum is measured with narrow band filters and a Si diode detector plus pre-amplifier. From the spectrum

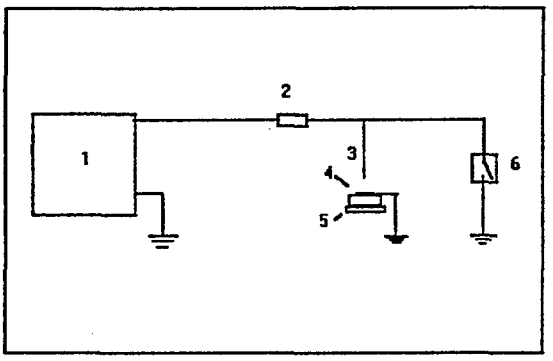

Fig 1. Experimental setup. 1. high voltage generator;2. resistor; 3.tungsten tip; 4.silicon wafer; 5.3-D movement unit ; 6.sparking time controlling unit.

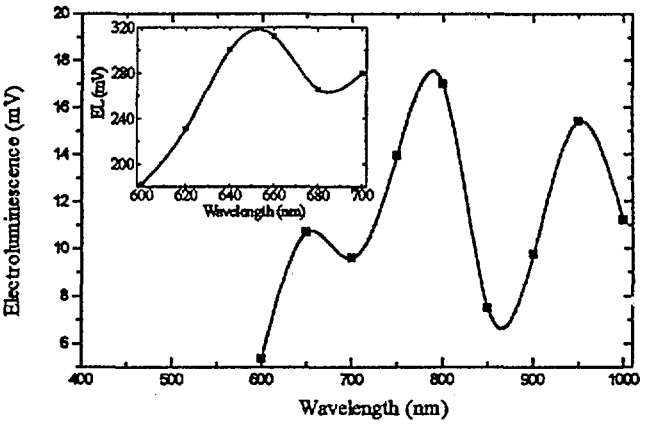

Fig.2. Typical electroluminescence intensity vs wave length. Inset shows result measured by using PMT and narrower band optical filters.

as shown in Fig.2, the peak around 650 nm matches what is seen with the naked eye. More investigation is needed about the infrared part. Photoluminescence, that shows only one peak around 650 nm, was also measured. XPS measurements show that the sample is composed mostly of Si and a few percent of oxygen. FTIR analysis indicates the existence of only Si-O species.

At this stage , we suspect that the visible light emission from spark-processed silicon may be due to some kinds of nanostructure, either nanosize silicon or nanosize silicon particles in silicon dioxide or both. However the real blue shifting mechanism for this material and also for porous Si is still not fully clarified.

[1]. R.E. Hummel and S.S.Chang Appl.Phys.Lett., 61,1965(1992)
[2]. J.Yuan and D.Haneman Appl.Phys.Lett., 67,1(1995)

STABILITY OF SP^2-CARBON SINGLE LAYER NANOSTRUCTURES

L.N. Bourgeois and L.A. Bursill

School of Physics, The University of Melbourne, Parkville 3052 VIC, Australia

Sp^2-hybridised carbon is quite versatile in its ability to build atomic structures. Although graphite is the most common and best known sp^2-carbon compound, recent discoveries of the C_{60} molecule and the related nanotubes have shown that networks of three-fold coordinated carbon atoms may result in a wide range of geometries. This has led to the postulation that structures such as the negatively curved schwarzites and tori may also be synthesized. In particular, theoretical calculations have shown the cohesive energy of schwarzites to be higher than that of C_{60}.

Presented here is an analytical model[1,2] describing the energetics of the most common sp^2-carbon single nanostructures as well as the hypothetical P-schwarzite. An expression for the energy with respect to a flat graphite sheet is written as the sum of a strain energy term (arising from curving of the carbon network) and a dangling bond energy term (not negligible in an inert environment).

The relative stability of carbon spheres, tubes, planes and minimal surfaces is then investigated as a function of the dangling bond energy. In an inert atmosphere (large dangling bond energy), the cylinder appears to be the most stable geometry up to a certain size (about 40 atoms only). Above this number of atoms, the sphere is found to be energetically favoured. In a reactive environment, flat sheets are found to have the lowest energy, as expected. The other structures appeared to be always less stable than tubes, spheres and planes. However, small proportions of negatively curved sheets may occur at high temperatures.

These results are compared with known experimental facts.

References:

1. L.N. Bourgeois and L.A. Bursill, *Mod. Phys.* **B10**, in press (1995).

2. L.N. Bourgeois and L.A. Bursill, *Mod. Phys.* **B**, in press (1996).

Current Transport Mechanism and Effect of Hydrogen Plasma Treatment on Al-GaSb Schottky Diode

A. Subekti, V.W.L. Chin and T.L. Tansley
Semiconductor Science and Technology Laboratories,
School of Mathematics, Physics, Electronics and Computing,
Macquarie University,
NSW 2109, Australia

Abstract

The aluminium Schottky contact to n-GaSb was fabricated using standard photolithography and lift-off techniques. The ohmic contact of low resistance was first formed by evaporating Ge-Au-Ni-Au (88% Au - 12% Ge by weight) on GaSb surface then followed by heat treatments. The I-V-T measurements were performed with a cryogenic system. The current transport mechanism of this non-ideal Al-GaSb Schottky diode was modelled for a wide temperature range. The conduction in both Γ and L valleys was included in the calculation of the thermionic emission current component. The contribution of thermionic emission, recombination and other current transport mechanisms were evaluated. The I-V characteristic at 300 K had an ideality factor of about 2 since the recombination dominates the current transport. However, at higher temperatures the thermionic emission becomes important and the ideality factor decreases below 2. We also examined the electrical properties of this diode after exposure on hydrogen plasma.

Photoconductive decay in LCVD/PECVD low temperature grown GaN

Bing Zhou, K. S. A. Butcher, Helen Zuo, Xin Li, and T. L. Tansley.

Semiconductor Science and Technology Laboratories

School of Mathmatics, Physics, Computting and Electronics

Macquarie University NSW 2109, Australia

Abstract

Photoconductive decay in undoped GaN has been investigated at room temperature using an ArF excimer laser as illuminative source and a boxcar integrator for detection of decay signals. GaN films were grown by combined laser and microwave plasma enhanced chemical vapour deposition at 550°C. The respective room temperature electron concentration and Hall mobility of the films were measured to be in the range 10^{15}-10^{16} cm^{-3} and up to 200 cm^2/Vs. Two time constants, 0.8 and 6 μs, are distinguishable in typical photoconductive decay curves and are associated with a dominant fast recombination and a weaker, slower process via unidentified defect state respectively. Near-band photoluminescence dominates the emission spectrum with little contribution from the sub-bandgap process often found in the presence of high-density defects.

Studies in the Growth of ZnSe on GaAs(001)

J Riley *, D Wolfframm, ♦ D Westwood ♣ & A Evans ♦

* School of Physics, La Trobe University, Bundoora VIC 3083, Australia

♦ Department of Physics, North East Wales Institute, Plas Coch, Wrexham, UK

♣ Department of Physics and Astronomy, University of Wales Cardiff,
P O Box 913, Cardiff CF2 3YB, UK

This paper reports a study of the Molecular Beam Epitaxial (MBE) growth of Zn Se on GaAs substrates using elemental sources. Growth rates of ZnSe as a function of Zn:Se flux ratio for constant Zn flux were determined over a wider range of values than previously reported. Careful measurements of atomic fluxes and sample thickness lead to a determination of the sticking coefficients of Zn and Se which are at variance with many previously reported values.

The temperature dependence of the sticking coefficients of Zn and Se have been measured carefully and provide evidence for a greater desorption of As from the growing surface that previously thought, an effect which persists at low growth temperatures. Measurements at high flux ratio supports the use of a precursor model to describe MBE growth of ZnSe on GaAs substrates.

THE DETERMINATION OF POISSON'S RATIO OF $Al_{0.3}Ga_{0.7}As$

B.F. Usher, A.S. Bloot* and G.W. Yoffe,
School of Electronic Engineering,
La Trobe University,
BUNDOORA, Victoria 3083.

*Physics Department,
Eindhoven University of Technology,
P.O. Box 513,
5600 MB Eindhoven, The Netherlands.

Abstract

As-grown semiconductor heteroepitaxial layers are never exactly lattice matched to their growth substrate and suffer distortion as a consequence. The relationship between the distortion and the relaxed lattice parameter depends on Poisson's Ratio ν. X-ray diffraction is commonly used to determine the chemical composition of a layer via measurements of the distorted lattice parameter and therefore it is essential to have an accurate value of Poisson's Ratio. Controversy surrounds the correct value for Poisson's Ratio, particularly for the technologically significant Aluminium Arsenide-Gallium Arsenide system. Previous studies[1-6] have made a number of untested assumptions in the course of determining a value for ν, including that the relationships between lattice constant and Aluminium fraction, and Poisson's Ratio and Aluminium fraction, are linear. The present study makes no such assumptions and instead precisely measures the unit cell structure in an $Al_{0.3}Ga_{0.7}As$ layer in two strain states. The first is the as-grown state, where the interfacial structure is coherent, while the second partially relaxed state is achieved by chemically releasing the epitaxial layer from its growth substrate. X-ray diffraction measurements made on the sample in both states yield a value for Poisson's Ratio directly.

(1) M.D. Lind, C.W. Farley, G.J. Sullivan and R.W. Grant, J. Appl. Phys. **74**, 5910 (1993).
(2) M.S. Goorsky, T.F. Kuech, M.A. Tischler and R.M. Potemski, Appl. Phys. Lett **59**, 2269, (1991).
(3) K.H. Chang, C.P. Lee, J.S. Wu, D.G. Liu, D.C. Liou, M.H. Wang, L.J. Chen and M Marais, J. Appl. Phys. **70**, 4877 (1991).
(4) B.K. Tanner, A.G. Turnbull, C.R. Stanley, A.H. Kean and M. McElhinney, Appl. Phys. Lett. **59**, 2272 (1991).
(5) M. Krieger, H. Sigg, N. Herres, K. Bachem and K. Kohler, Appl. Phys. Lett **66**, 682 (1995).
(6) C. Bocchi, C. Ferrari, P. Franzosi, A. Bosacchi and S. Franchi, J. Cryst. Growth **132**, 427 (1993).

DESIGN AND PERFORMANCE MODELLING OF A WAVELENGTH SPECIFIC ASYMMETRIC FABRY-PEROT MODULATOR

G. J. Nott[1], E. M .Goldys[1], and K. J. Grant[2]

[1]Semiconductor Science and Technology Laboratories, School of MPCE, Macquarie University NSW 2109
[2]Communications Division, DSTO, PO Box 1500, Salisbury SA 5108

Asymmetric Fabry-Perot modulators (AFPM's) combine the nonlinear effects present in multiple quantum well (MQW) structures with the interferometric operation of a Fabry-Perot cavity, thus increasing the modulator performance over simple transmission or reflection devices[1]. Parameters commonly used to evaluate the performance of a multiple quantum well optical modulator are its contrast ratio, dynamic range, and insertion loss. We present the design analysis of a GaAs/AlGaAs AFPM for operation at 850nm with respect to these performance parameters.

The reflectivity of the Bragg stack forming the back mirror of the AFPM was found for different layer materials. The number of layers and the materials used, was determined to ensure a mirror with a high maximum reflectivity over a range of wavelengths. A high reflectivity back mirror minimises the insertion loss while a broad reflectivity maxima reduces the dependence of device operation on the growth quality of the stack. Computations of transition energies of the MQW showed that for device operation at 850nm, a well width of 84.8Å (30 atomic monolayers) was required. Our calculations confirm those reported elsewhere[2], that show for this well width the barrier width may be reduced to approximately 50Å without superlattice coupling causing a serious degradation in the width of the excitonic peaks. The characteristics of the primary exciton peak have a large effect on the performance of the AFPM. Calculations indicated that narrow linewidths and large Stark shifts are required for an optimised contrast ratio, dynamic range and insertion loss. We demonstrate that with exciton linewidths of 3nm and Stark shifts of 15nm, contrast ratios of 900 are achievable. Of greater importance to the performance of the AFPM is the quality of the epitaxial growth and the accuracy of the cavity phase matching. It was found that if the thickness of the cavity deviates by only 10 monolayers either side of the optimum value the contrast ratio falls from approximately 27 to 7dB. The dynamic range and insertion loss are less dependent on the phase conditions, both requiring deviations of ±20 monolayers before they begin to fall off appreciably. The final design of an AFPM for operation at 850nm is presented.

---

[1]R. H. Yan, R. J. Simes, and L. A .Coldren, *IEEE Photon. Technol. Lett.*, 1, 9, pp273-275, 1989.
[2]P. Zouganeli, P. J. Stevens, D. Atkinson, and G. Parry, *IEEE J. Quantum Electron.*, 31, 5, pp927-943, 1995.

AU9918193

REFLECTANCE SPECTROSCOPY IN VERY HIGH QUALITY SHALLOW QUANTUM WELLS

T.M. Silver and P.E. Simmonds
Dept. of Physics, University of Wollongong

Optical properties of very shallow quantum wells have been studied between 5°and 150°K. The structures incorporate relatively wide GaAs wells set in (AlGa)As barriers of very low aluminum content (between 1% and 4.5%). Shallow quantum well structures are of technological interest as optical modulators because they show the desirable optical properties of quantum wells together with rapid carrier sweepout over the low barriers. (In conventional deep quantum wells carrier trapping limits the modulation frequency.) High resolution reflectivity and photoluminescence measurements of the heavy and light hole excitons show clear evidence of two-dimensional behavior even at the lowest barrier heights of $\leq$ 10 meV. Very narrow exciton linewidths were found, especially for the samples with the lowest aluminum content. In these cases the linewidths were comparable to those expected from purely homogeneous broadening, down to 60 μeV for the 1% Al samples. These narrow linewidths allowed the acoustic phonon contribution to broadening to be studied at temperatures below 80°K and linewidth temperature coefficients of approximately 3μeV/°K were measured. These values are considerably smaller than for bulk broadening and establish the quantum well character of these excitons. A detailed comparison of experimental and model exciton reflectivity lineshapes showed that optical polarizability (oscillator strength) tended to rise with barrier height, consistent with the measured increase in binding energy[1]. The work was carried out in collaboration with investigators at the University of Sheffield and Defense Research, Malvern UK.

1. M.J. Birkett, M.S. Skolnick, W.I.E. Tagg, P. Sobkowicz, G.W. Smith, D. M. Whittaker, *Phys. Rev. B* **50**, 11251 (1994).

ZEEMAN SPECTROSCOPY OF NEUTRAL COPPER IN GERMANIUM*

P. Fisher and R.E.M. Vickers
The Department of Physics, University of Wollongong, Wollongong, N.S.W. 2522.

A resurgence of interest has occurred in the more complex impurities, neutral zinc ($Zn^{(o)}$), a double acceptor, and neutral copper ($Cu^{(o)}$), a triple acceptor, in Ge.[1-3] For $Zn^{(o)}$ this has centred on identifying which of the two-hole ground states generated by $\{1\Gamma_8^+ \times 1\Gamma_8^+\} = 1\Gamma_1^+ + 1\Gamma_3^+ + 1\Gamma_5^+$ is the lowest. A theoretical treatment,[4] which takes into account various interactions but initially excludes dynamic many-body effects, favours the combination $1\Gamma_3^+ + 1\Gamma_5^+$ as being lower than $1\Gamma_1^+$ in conformity with Hund's rule. However, adjustment of a parameter gives agreement with the piezospectroscopic observations[5] which clearly indicate that the $1\Gamma_1^+$ state is the lowest. Recently, a model invoking a dynamic Jahn-Teller effect[1] directly supports the experimental conclusion.

In the past year, high-field Zeeman spectroscopy[3] of $Zn^{(o)}$ has confirmed that the $1\Gamma_1^+$ state is indeed the lowest. During this period, piezospectroscopy of $Cu^{(o)}$, has been extended to high stresses, yielding some unique results.[2] The ground state of this acceptor accommodates three holes and hence has the symmetry $\{1\Gamma_8^+ \times 1\Gamma_8^+ \times 1\Gamma_8^+\} = 1\Gamma_8^+$.[6] The excitation of one hole results in excited states represented by $\{1\Gamma_8^+ \times 1\Gamma_8^+\} \times n\Gamma_f^- = (1\Gamma_1^+ + 1\Gamma_3^+ + 1\Gamma_5^+) \times n\Gamma_f^-$, where f = 6, 7 or 8 and n = 1, 2, 3,....; thus these states are quite complex if $1\Gamma_1^+$, $1\Gamma_3^+$ and $1\Gamma_5^+$ are closely spaced. The piezospectroscopy of $Cu^{(o)}$ at moderate stresses is, however, relatively simple.[7] It has been conjectured[5] for $Cu^{(o)}$ that, like the two holes in the ground state of $Zn^{(o)}$, after the excitation of one hole the new configuration of the other two holes bound to the copper ion energetically favours the $1\Gamma_1^+$ state. Thus, the excited states of $Cu^{(o)}$ would be simply $1\Gamma_1^+ \times n\Gamma_f^- = n\Gamma_f^-$ and optical transitions from the ground state to an excited state would be given by $1\Gamma_8^+ \rightarrow n\Gamma_f^-$, which in terms of symmetry are the same as those for group III impurities. Here, we report the results of our recent high field Zeeman measurements of the D line of $Cu^{(o)}$ in Ge for B||<100>. These results determine unambiguously the nature of the excited states of this impurity.

**Work supported by the Australian Research Council and the University of Wollongong Board of Research and Postgraduate Graduate Studies.*

1 F. S. Ham and C. Leung, *Phys. Rev. Lett.* **71**, 3186 (1993).
2 O. D. Dubon, J. W. Beeman, L. M. Falicov, H. D. Fuchs, E. E. Haller and C. Wang, *Phys. Rev. Lett.* 72, 2231 (1994).
3 D. S. Ryan, P. Fisher and C.A. Freeth, *ibid.*, p. 2343.
4 A. Giesekus and L. M. Falicov, *Phys Rev. B* 42, 8975 (1990).
5 D. Labrie, I. J. Booth, M. L. Thewalt and E. E. Haller, *Phys. Rev. B* 38, 5504 (1988).
6 K. J. Duff and E. H. Salib, *Phys. Rev. B* 33, 1275 (1986).
7 E. H. Salib, P. Fisher and P.E. Simmonds, *Phys. Rev. B* 32, 2424 (1985).

FAR-INFRARED SPECTROSCOPY IN LARGE MAGNETIC FIELDS*

R. J. Heron and R. A. Lewis
Department of Physics, University of Wollongong, Wollongong NSW 2522, Australia

R. G. Clark, R. P. Starrett and A. Skougarevsky
National Pulsed Magnet Laboratory, School of Physics, University of New South Wales, Sydney NSW 2052, Australia

A far-infrared spectroscopy facility has recently been established at the National Pulsed Magnet Laboratory. The radiation source consists of a mid-infrared CO_2 laser (>80 lines, peak power >40 W) optically pumping a far-infrared cavity (peak power >150 mW). Choice of suitable lasing gas, pressure, and pump line, allow a variety of lasing lines of wavelengths from 40 to 1200 μm to be utilised.

The laser radiation is conducted into the magnet room through metal light pipes. A dedicated top-loading probe, incorporating suitable optical filtering, conducts the light to the sample in the bore of the magnet. This arrangement permits photoconductivity measurements in fields up to 60 T and at temperatures down to 300 mK. A second probe which will permit absorption and reflection measurements in fields up to 30 T has been designed and is under construction.

A variety of materials have been investigated using this facility. A preliminary report concerning organic conductors has already been given [1]. Earlier work on the far-infrared photoconductivity of these failed to find any spectral features which shifted systematically with field, apart from an overall change in intensity [2]. Our results are similar and indicate the importance of heating effects in these materials. Similar bolometric effects were evident in a multiple quantum well sample we have investigated. The present material being studied is high-mobility bulk n-type GaAs. We have observed sharp impurity transitions in complementary low-field (<7 T) far-infrared absorption measurements. The polarisation features are in agreement with the established selection rules and the magnitude of the Zeeman splitting in accord with that measured by others.

Work supported by the Australian Research Council, the University of Wollongong and the University of New South Wales.

[1] R. H. McKenzie *et al.*, *19th. ANZIP Cond. Matter Physics Meeting*, Wagga (1995).

[2] J. Lefebvre *et al.*, *Phys. Rev. Lett.* **72**, 3417 (1994).

THE SURFACE BAND STRUCTURE OF MBE GROWN ZnSe{100}.

Y. Zhang, J. Xue, J. A. Con Foo and A. P. J. Stampfl
School of Physics, La Trobe University, Victoria 3083, Australia

A. Ziegler, M. Hollering, R. Denecke and L. Ley
Universität Erlangen-Nürnberg, 91058 Erlangen, Germany

D. Wolframm and A. Evans
Department of Physics, University of North West Wales

J. D. Riley and R. C. G. Leckey
School of Physics, La Trobe University, Victoria 3083, Australia

The surface state band structure of the technologically important MBE grown II-VI semiconductor compound ZnSe {100} has been determined by angle resolved photoemission spectroscopy. Results were taken from the Se-rich (2×1) surface. Three surface resonance bands were observed in the first 3 eV from the top of the valence band to disperse over most of the Brillouin zone. One surface state band was observed in the gap at around 6 eV and another weak surface related feature was observed at $\overline{\Gamma}$ around the valence band maximum. Our data are compared to the results of two recent calculations for the {100} surface and a discussion is given of the likely surface structures for this reconstruction.

AU9918197

DOPANT DISORDER-FREE 2DEG GaAs/AlGaAs HETEROSTRUCTURE FET DEVICES FOR QUANTUM HALL AND NANOSTRUCTURE STUDIES

Geoffrey R. Facer, Dr Bruce E Kane
National Pulsed Magnet Laboratory, University of New South Wales

Two-dimensional electron gas (2DEG) GaAs/AlGaAs heterostructures have been grown by molecular beam epitaxy (MBE) in which gate-induced accumulation of carriers replaces the more usual modulation doping[1]. These novel devices have the advantages of reduced disorder and a high degree of tunability in the carrier density. Because modulation doping is not used, disorder effects in the 2DEG due to nearby dopants are eliminated. Mean free paths for electrons exceed 30 μm at low temperatures. Electron densities are accurately tunable over nearly two orders of magnitude, from 9×10^9 cm^{-2} to 4×10^{11} cm^{-2}. Very high electron mobilities, exceeding 3×10^6 cm^2/Vs at 4.2 K, are obtained. With such a combination of density tunability and low disorder, these layers provide unique opportunities for studying low dimensional systems following further lithography. Nanolithography with feature sizes under 50 nm will be possible at UNSW in early 1996.

In preparation for 1-dimensional and 0-dimensional structure fabrication, the 2DEG samples have been characterised in steady fields at temperatures ~50 mK. Recent theory has explained the fractional quantum Hall effect at electron filling factor ν=½ in terms of composite fermions (made up of interacting electrons) behaving as if they are a non-interacting system at B=0. The question of the mobility μ_c of composite fermions in the new devices, and how it varies as the electron density varies, has been studied. Preliminary measurements at ν=½ yield $\mu_c\sim10^4$ cm^2/Vs. The composite fermion mobility is nearly independent of electron density beyond an apparent threshold $N = 0.5\times10^{11}$ cm^{-2}, and independent of temperature in the range 50 to 200 mK. The electron N threshold coincides with the crossover of the carrier Fermi wavelength and the mean free path.

---

[1] B.E. Kane, L.N. Pfeiffer, K.W. West. *Applied Physics Letters*, 67,9, pp 1262-1264; 1995.

AU9918198

IDENTIFICATION OF THE COMMON ELECTRICALLY DETECTED MAGNETIC RESONANCE SIGNAL FROM A SILICON DIODE

D. J. Miller and Z. Xiong

School of Physics
The University of New South Wales
Sydney NSW 2052

Electrically detected magnetic resonance (EDMR) is method for investigating paramagnetic recombination centres in semiconductors [1]. It provides much greater sensitivity than other magnetic resonance techniques while providing the same information, which allows the identification of the atomic structure of the centre under favourable circumstances.

The EDMR method relies on changing the occupations of the energy sub-levels formed a magnetic field. In general the recombination rates from the various sub-levels will be different and information about the recombination centre can be obtained by disturbing, in a controlled way, the equilibrium occupations of the sub-levels and hence the overall recombination rate. One way of achieving this is to place the sample in the resonant microwave cavity of an electron paramagnetic spectrometer. When the magnetic field is scanned to the appropriate value, transitions are induced between sub-levels by the microwave power and the resulting change in the recombination rate can be measured by measuring the conductivity of the sample - typically by monitoring the voltage across the semiconductor at constant current using lock-in detection. It is also possible to change the occupation of the sub-levels in the absence of microwave stimulation if pairs of sub-levels can be caused to cross in the magnetic field [2].

The present results are for an EDMR signal which has been reported from various Si structures over the years but which has not been identified previously. The signal was obtained from a common type of Si diode and structure was resolved and measured for different orientations of the magnetic field in the (111) plane. The results show that the centre has C_{3v} symmetry with $\Delta g_{\parallel} > 0$ and $\Delta g_{\perp} \approx 0$. It is proposed that the signal is due to a broken bond, or combination of co-linear broken bonds, in a vacancy cluster which acts as a recombination centre. The most likely cluster is the divacancy in the configuration in which an electron has been captured in the antibonding state formed from the most distant broken bonds and a hole has been captured in a bonding state associated with the divacancy.

[1] Z. Xiong and D. J. Miller, J. Appl. Phys. **77**, 5201 (1995).
[2] D. J. Miller and J. Lobb, Appl. Phys. Lett. **65**, 1391 (1994).

CORRELATIONS AND FINITE SIZE EFFECTS IN QUASI ONE-DIMENSIONAL ELECTRON SYSTEM

J.S. Thakur and D. Neilson

School of Physics, The University of New South Wales, Sydney 2052, Australia

Correlation effects for quasi one-dimensional electron systems in thin wires in semiconductor heterostructures are found to be very sensitive to the diameter of the wire. We use the STLS many-body approach to determine local fields, pair correlation functions, static and dynamic structure factors and the dispersion curves of the plasmon. The effect of weak and strong disorder is also investigated. The signature of electrons localization is observed for stronger disorder.

[1] J. Sólyom, Adv. Phys. **28**, 201 (1979).

[2] D. Haldane, J. Phys. C**14**, 2585 (1981).

[3] Ben Yu-Kuang and S. Das Sarma, Phys. Rev. Lett. **68**, 1750 (1992).

[4] Q.P. Li and S. Das Sarma, Phys. Rev. B**43**, 11768 (1991).

[5] S. Sas Sarma and W.Y. Lai, Phys. Rev. B**32**, 1401 (1985).

[6] H.J. Schulz, Phys. Rev. Lett. **71** 1864 (1993).

AU9918200

ELECTRONIC STRUCTURE OF PEROVSKITE $LaMnO_3$ AND $CaMnO_3$

B. Chen, Y. Zhao

School of Materials Science and Engineering, University of New South Wales, Sydney, NSW 2052 Australia

and

X. Zheng

School of Chemistry, University of Sydney, NSW 2006, Australia

Abstract

Perovskite structured lanthanum manganite ($LaMnO_3$) can be made to exhibit both strong ferromagnetism and metallic conductivity by partial substitution of La ions (3+ valence) with 2+ valence ions such as Ca. The electronic structures of $LaMnO_3$ and $CaMnO_3$ were calculated using HF-LCAO and Local Density-Molecular Dynamics programs. The band structure show that both are isolators. The valence energy bands are highly degenerated at Γ point in reciprocal space for $LaMnO_3$. The conduction bands are partly degenerated in both structures. The dispersion of valence band of $LaMnO_3$ is about 1.7 eV and the dispersion of conduction band is about 2.0 eV from Γ point to M point. The top two valence bonds of $CaMnO_3$ are quite flat. The conduction band disperse down significantly, this behaviour could give some reasons why Ca doped $LaMnO_3$ is metallic conductor. The energy gap was obtained but overestimated as expected. The total density of states was found and compared with experimental results. The electronic images show that the interactions between Mn, Ca and three O are stronger than that between La and O. The bonding of Mn-O is pdσ bond.

A THEORY OF PARAMAGNETIC DYNAMIC SUSCEPTIBILITY OF COMPOSITIONALLY DISORDERED ALLOYS

M.F. Ling

Department of Physics, Monash University,

Clayton, Victoria 3168, Australia.

J.B. Staunton

Department of Physics, University of Warwick,

Coventry CV4 7AL, United Kingdom.

and

J. Poulter

Department of Mathematics,

Mahidol University,

Bangkok, Thailand.

Experimentalists in the field of quasi-elastic and inelastic neutron scattering measurements have long found a theory of dynamic susceptibility of metallic alloys wanting. We have developed the theoretical framework and computational codes for calculating the paramagnetic dynamic susceptibility of compositionally disordered alloys. The theory is based on "first-principles", multiple scattering formalism within a Stoner RPA set-up. We will report on our initial test results on Pd and discuss the extension of our work to alloys.

IMPROVED BOSE REPRESENTATION FOR ONE-DIMENSIONAL FERMI OPERATORS

G. B. Honner and M. P. Das

Department of Theoretical Physics
Research School of Physical Sciences and Engineering
The Australian National University, Canberra ACT 0200

Bosonization has proved a useful method for solving a large class of one-dimensional interacting electron systems. The method relies crucially on the identification of some regime in which the chiral density fluctuations $\rho_{pk\sigma}$, $p = \pm$, satisfy bosonic commutation relations

$$[\rho_{pk\sigma}, \rho_{p'k'\sigma'}] = \delta_{p,p'}\delta_{k,-k'}\delta_{\sigma,\sigma'}\frac{pkL}{2\pi}, \qquad \rho_{pk\sigma} = \sum_{p\bar{k}>0} c^{\dagger}_{\bar{k}-\frac{k}{2}\sigma} c_{\bar{k}+\frac{k}{2}\sigma}$$

with L the system length. Tomonaga[1] discovered that the bosonic relations obtain in a low-energy long-wavelength subspace defined with a bandwidth cutoff $k_0 < k_F$. The system Hamiltonian may be diagonalized in this subspace and its correlation functions determined by expressing Fermi operators $\psi_\sigma(x)$ in terms of the $\rho_{pq\sigma}$. We derive representations for Fermi operator pairs and use them to calculate the Green's function and momentum distribution. The representations take the form of series in Bose phase fields $\phi_\pm = \phi_\pm(\rho_{pk})$, for example,

$$\psi^{\dagger}_{\sigma}(x)\psi_{\sigma'}(x') \longrightarrow \frac{k_0}{2\pi}\Big[e^{-ik_F(x-x')}\Big\{e^{\gamma}e^{-i\phi_{+\sigma}(x)}e^{i\phi_{+\sigma'}(x')}$$

$$+e^{2\gamma}e^{ik_0(x-x')}e^{-i\sqrt{2}\phi_{+\sigma}(x)}e^{i\sqrt{2}\phi_{+\sigma'}(x')} + \cdots\Big\} + e^{ik_F(x-x')}\Big\{k_0 \to -k_0, \phi_+ \to \phi_-\Big\}\Big]$$

and at second-order go beyond the well-known Luttinger model Bose representation[2] which reproduces only asymptotic approximations to the correlation functions for realistic one-dimensional electron systems.

---

[1] Tomonaga S 1950 Prog. Theor. Phys. **5** 544

[2] Schotte K D and Schotte U 1969 Phys. Rev. **182** 479, Luther A and Peschel I 1974 Phys. Rev. B **9** 2911, Mattis D C 1974 J. Math. Phys. **15** 609

A Molecular Dynamics Study of Impurity Atoms in a Host Lattice

Marek Kijek and Ian Snook

Department of Applied Physics, RMIT, Melbourne

A single impurity atom was placed in an otherwise perfect host FCC lattice and the dynamical behaviour of the lattice and impurity were followed by use of the Molecular Dynamics (MD) technique. It was found that an impurity atom of relative diameter 1.06 has a significant effect on the behaviour of the mean square displacement and velocity autocorrelation function of the host lattice and , hence, on diffusive behaviour. If the relative diameter of the impurity was made as large as 1.12 then much larger effects were seen. In fact, under some conditions the lattice was amorphized and could not be "annealed" to return to a perfect lattice by replacement of the impurity atom by a host lattice atom.

AU9918204

The Structure of Glassy Carbon - A Model Based on Reverse Monte Carlo Analysis of TEM Data

Brendan O'Malley[#], Ian Snook[#] and Dougal McCulloch[*]

[#]Computational Physics Group, Department of Applied Physics, RMIT, Melbourne and Electron Microscope Unit, Sydney University, NSW

Glassy carbon is an amorphous form of carbon produced by the heat treatment of highly cross-linked polymers. It has been proposed by various authors that its microstructure consists of a tangle of graphitic ribbons containing many pores within the ribbon network. The structure factor of glassy carbon, produced at two temperatures 1000 and 2500 C, has been obtained by TEM. The Reverse Monte Carlo procedure has been used to model the static structure factor of glassy carbon in order to investigate the consistency of this model with the diffraction data and to provide details on the structure of the 'ribbons'. The resulting structures consist of well coordinated but buckled graphite basal planes. This buckling of the basal planes and their random stacking in the c-axis direction can account for the observed absence of reflections in the diffraction pattern of glassy carbon such as the intense (101) graphite reflection which is dependant on the correct ABA stacking of the graphite basal planes.

AU9918205

Goldstone Modes in the Edward's Polymer and how they control the corrections to scaling

T.C. Choy and S. R. Shannon
Department of Physics
Monash University
Clayton, Victoria 3168

Abstract

Writing $\langle R_N^2 \rangle = AN^{2\upsilon}(1+BN^{-\Delta_1}+CN^{-1}+...)$ for the mean square end-to-end length $\langle R_N^2 \rangle$ of a self-avoiding polymer chain of N links, we have previously reported compelling evidence for $\Delta_1 = 1/2$, in two dimensions[1,2]. This is based on a new *finite* perturbation expansion based on the ground state of Edward's selfconsistent solution[3], which predicts the (exact) $\upsilon=3/4$ exponent and is supported by careful finite size scaling analysis of data generated for the continuum using a biased Monte Carlo algorithm as well as a re-analysis of exact data for two-dimensional lattices. We noted that the scaling behaviour of lattice and continuum data differ markedly in that the latter show no sign of a universal crossing for all N. We present some new physical interpretations of these results based on the concept of spontaneous symmetry breaking and Goldstone excitations in the renormalised Edwards polymer. Our study suggests that spontaneous symmetry is completely broken in two dimensions, and as such the corrections to scaling is controlled solely by the associated Goldstone modes. We argue that in three dimensions, this is not the case and that mode coupling to fluctuations on all length scales are involved.

References

1. S.R. Shannon, T.C. Choy and R.J. Fleming , Phys. Rev. **B53**, No 5 , (1996)
2. S.R. Shannon, T.C. Choy and R.J. Fleming, J. Phys. A, (submitted).
3. S.F. Edwards, Proc. Phys. Soc. London **85**, 613 (1965).

HYSTERESIS IN ULTRATHIN FERROELECTRIC POLYMER FILMS OBSERVED BY CAPACITANCE VERSUS VOLTAGE MEASUREMENTS

Afifuddin and Ian L. Guy
Semiconductor Science and Technology Laboratories
School of Mathematics Physics Computing and Electronics
Macquarie University
NSW 2109 AUSTRALIA

Ferroelectric polymer films with thickness down to 50 nm have been prepared by spin coating a solution of the polymer onto electroded, glass substrates. Switching in the films has been observed both by measuring hysteresis loops and by capacitance (1kHz) versus voltage plots. The 50 nm films have a higher coercive field and a lower maximum polarisation than the those observed in films of the same materials with thickness above one micron. There appears to be a surprisingly small amount of fatigue in these films, when compared with thicker films. As the frequency of capacitance measurement increases to 1 MHz, it is found that the C-V characteristics change in nature. At 1 MHz, the capacitance maximum at the coercive field is not observed, but the capacitance shows a small increase at the highest field values. We conjecture that this increase is due to a field-induced increase in crystallinity in the films. This change is crystallinity is not permanent and disappears when the field is removed. Leakage currents in the thin films show a similar behaviour to that of thick films, both in terms of field dependence and in displaying a relaxation which persists for times in excess of one hour.

AU9918207

CHARGE TRANSPORT OF DOPED POLYPYRROLE FILMS WITH VARIOUS COUNTER ANIONS

C.-J. Liu[a], A. B. Kaiser[a], W. T. Smith[b], and J. S. Shapiro[b]
[a]Victoria University of Wellington, Physics Department, P. O. Box 600, Wellington, New Zealand
[b]Macquarie University, School of Chemistry, North Ryde, NSW, Australia, 2109

We have measured the electrical conductivity and thermopower as a function of temperature of electrochemically synthesized polypyrrole films with various counter anions, e.g., dodecylbenzene sulfonate ($DDBS^-=C_{12}H_{25}C_6H_4SO_3^-$), perchlorate ($ClO_4^-$), dodecylsulfate ($DDS^-=C_{12}H_{25}O_4S^-$), hexafluorophosphate ($PF_6^-$), and p-toluenesulfonate ($p\text{-}TsO^-=CH_3C_6H_4SO_3^-$). For all the doped polypyrrole films, the resistivity increases with decreasing temperature and exhibits a nonmetallic behaviour; the thermopower decreases with decreasing temperature and shows nearly linear temperature dependence below 280 K, which is slightly different from the reported results of nearly constant TEP above 230 K.[1,2] The analysis of the temperature dependence of normalized conductivity shows that samples with different counter anions vary in favouring the fits to the $(T_0/T)^v$-law (v = 1/2, 1/3, and 1/4), e.g., PPy-DDBS favours v=1/2, PPy-DDS v=1/4, PPy-pTsO (3 min. deposition) v=1/2, and PPy-pTsO (5 min. deposition) v=1/3. Furthermore, the strong temperature dependence of the normalized conductivity, e.g., $\sigma(295K)/\sigma(5K) = 10^4 - 10^5$, suggests that these samples are far from the metal-nonmetal transition regime, where the variable range hopping process is valid.[3] However, the absolute value of thermopower ($S \leq 15\ \mu V/K$) at 280 K is comparable to or even smaller than the 'new' polyacetylene.[4] Therefore, it seems to be inadequate to describe the transport by using the variable range hopping process without taking into consideration the microstructure and morphology of doped polypyrrole samples.

1. S. Masubuchi, S. Kazama, R. Matsushita, and T. Matsuyama, Synthetic Metals 69, 345 (1995).
2. D. S. Maddison, R. B. Roberts, and J. Unsworth, Synthetic Metals 33, 281 (1989).
3. C. O. Yoon, M. Reghu, D. Moses, and, A. J. Heeger, Phys. Rev. B 49, 10851 (1994).
4. A. B. Kaiser, Synthetic Metals 45, 183 (1991).

HIGH EXPOSURE HYDROGEN CHEMISORPTION ON THE Si(111)7x7 SURFACE: A SEMIEMPIRICAL CLUSTER STUDY

Jian-Zhong Que, M.W. Radny and P. V. Smith

Physics Department, University of Newcastle,
Callaghan, NSW, Australia, 2308

The various equilibrium structures of the hydrogen chemisorbed Si(111)7x7 surface are investigated using the semiempirical molecular orbital Austin 1 calculational method (AMI). Up to five hydrogen atoms are allowed to adsorb near the corner adatom, center adatom and restatom adsorption sites of the 7x7 surface. The results obtained from minimizing the energy of the system show very little difference between the chemisorption processes occurring at the two different adatom sites. In both cases, as progressively more hydrogen atoms are chemisorbed, the hydrogen bonded adatom is found to move from its original 3-fold (T_4) site (one hydrogen atom), to an adjacent bridge site (two and three hydrogen atoms), and then on-top of a neighbouring first layer silicon atom (more than three hydrogen atoms). The lowest calculated desorption energy is 0.65 eV and corresponds to SiH_3 at a center adatom site. In contrast to an adatom, a hydrogen bonded restatom is found to remain close to its original 3-fold equilibrium position. The smallest desorption energy for this site is 0.52 eV and also corresponds to an SiH_3 surface complex.

AU9918209

BORON, HYDROGEN AND SILICON ADATOMS ON THE Si(111) SURFACE: AN AB INITIO HARTREE-FOCK/DENSITY FUNCTIONAL CLUSTER STUDY

Sanwu Wang, M.W. Radny and P.V.Smith
Physics Department, University of Newcastle,
Callaghan, NSW, Australia 2308

Silicon and boron adatoms on the Si(111) surface have been studied using atomic clusters and the Hartree-Fock/Density Functional Theory components of the Gaussian94/DFT package. The binding energies for the adatom, Si(A), located at the T_4 position, and the Si(A)H species formed by the chemisorption of a single hydrogen atom, have been obtained for the corresponding equilibrium minimum energy configurations. We find that the most stable adatom structure results from boron occupying the S_5 substitutional position in the second layer directly below the Si adatom (B-S_5 topology). The binding energy of the Si adatom in this case is 7.49eV while the binding energy for the Si adatom without the boron (Si-T_4 topology) is only 6.34 eV. When a boron atom is chemisorbed in the T_4 position, instead of a silicon atom (B-T_4 structure), the binding energy is found to be 5.56 eV. The chemisorption of atomic hydrogen onto these clusters stabilizes the Si-T_4 geometry through the formation of a silicon adatom-hydrogen Si(A)H complex located at the three-fold T_4 position with a binding energy of 5.18 eV. In contrast to this, a hydrogen bonded Si adatom of the B-S_5 structure is observed to move away from its 3-fold T_4 position to an adjacent bridge site and give an Si(A)H binding energy of 4.68 eV. Similar reconstruction has been observed when a hydrogen atom chemisorbs onto a boron adatom in the B-T_4 topology with the binding energy of the BH complex being 5.03 eV. An interpretation of these results will be given in the context of the available experimental data.

ELASTIC AND INELASTIC SCATTERING IN RHEED

A.E. Smith, Department of Physics, Monash University, Clayton, Victoria 3168.

Reflection High Energy Electron Diffraction (RHEED) has become a widely employed technique in surface structure and growth characterisation. Recent work has been carried out on the layered transition metal dichalcogenides which are of great fundamental and technological importance [e.g. 1]. In particular, polytype structure of niobium diselenide close to the surface has been analysed by use of the fine structure oscillations which are superimposed on the main diffraction peaks [2]. The comparison between the determination of the precise surface structure using a variety of RHEED computation methods [e.g. 3] is part of a Round Robin series of calculations under the auspices of the International Union of Crystallography [4]. Recent precise energy-filtered RHEED measurements [5] have indicated that previous unfiltered results should be treated with caution. For instance, at very low incident angles relative diffraction peak intensities may have been overestimated by as much as a factor of three. A theoretical description of inelastic scattering at extremely low angles is outlined. This is based on the spatial inelastic potential profile, formulated in terms of the dielectric response of the surface plasmon excitation.

[1] J.A. Wilson and A.D. Yoffe, Adv. Physics 18, 193 (1969).

[2] A.E. Smith, Y. Horio, H. Iwashige and A. Ichimiya, Surface Polytypic Determination of Niobium Diselenide by RHEED, to be published in Surface Science (1996).

[3] A.E. Smith and D.F. Lynch, Acta Cryst. A 44, 780 (1988); T. Kawamura, A. Ichimiya and P.A. Maksym, Japan J. Appl. Phys. 27, 1098 (1988); A. Ichimiya, Surface Science 235, 75 (1990); Y. Ma, S. Lordi, P.K. Larsen and J.A. Eades, Surface Science 306, 252 (1994); J.M. McCoy, U. Korte, P.A. Maksym and G. Meyer-Ehmsen, Surface Science 306, 247 (1994); G.R. Antis and X.S. Gan, Surface Science, 314, L919 (1984).

[4] A. Ichimiya, Round Robin of RHEED Dynamical Calculations, Winter Workshop on Electron Diffraction and Imaging at Surfaces, Scotsdale, USA (1996) and to be published in Surface Review and Letters (1996).

[5] Y. Horio, Y. Hashimoto and A. Ichimiya, A New Type of RHEED Apparatus Equipped with An Energy Filter, to appear in Surface Science (1996).

A dielectric matrix calculation of the surface-plasmon energy for the silicon (100) surface.[1]

A. J. Forsyth, A. E. Smith
Department of Physics, Monash University, Clayton, Victoria 3186.

T. W. Josefsson
School of Physics, University of Melbourne, Parkville, Victoria 3052.

As an extension of previous work[2], we present preliminary calculations for the dielectric properties of the silicon (100) surface. In particular, the $|\mathbf{q}|\rightarrow 0$ and $|\mathbf{q}|=2\pi/a(1,0,0)$ surface loss function, and corresponding surface plasmon energies have been calculated within a simple model for the silicon surface. The results have been obtained from the Adler[3] and Wiser[4] dielectric matrix (DM). The bandstructure used for the calculation was based on the highly successful empirical pseudopotential method of Cohen and Chelikovsky[5]. We have used a 59 plane wave basis for the bandstructure, and have chosen a DM size of 59 × 59. Results are compared and contrasted with volume plasmon calculations, free electron calculations and experiment.

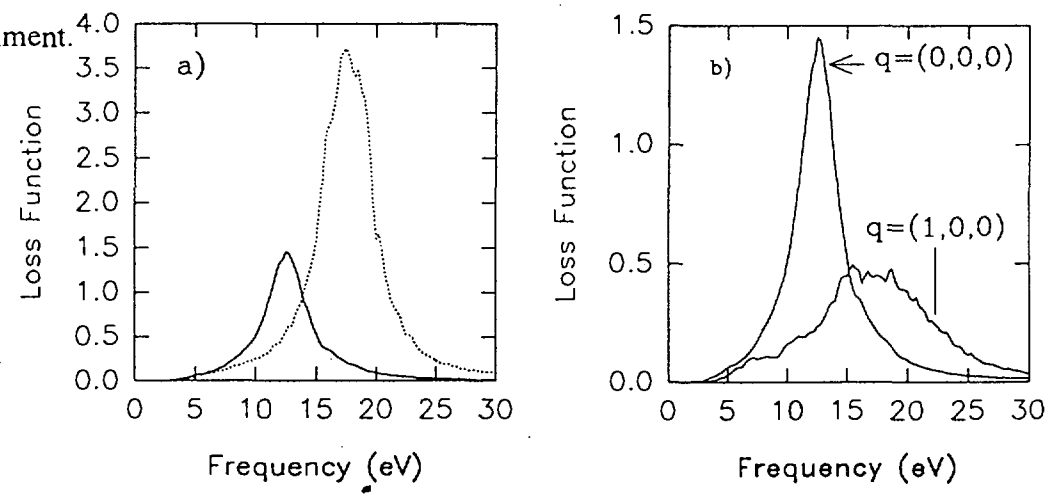

Figure 1 a) The calculated loss function for bulk silicon (dotted line), and the silicon surface (solid line) for $|\mathbf{q}|=0$. b) Comparison of the surface loss function for $\mathbf{q}\rightarrow 0$ and $\mathbf{q}=2\pi/a(1,0,0)$.

---

[1] A. J. Forsyth, A. E. Smith and T. W. Josefsson, *A dielectric matrix calculation of the surface plasmon energy for the silicon (100) surface,* Surface Science (*in press*)

[2] A. J. Forsyth, T. W. Josefsson and A. E. Smith, *A dielectric matrix calculation of the volume-plasmon dispersion relation in silicon,* Submitted for publication to Phys. Rev. B.

[3] S. Adler, Phys. Rev. **126** (1962) 413.

[4] N. Wiser, Phys. Rev. **129** (1963) 62.

[5] M. L. Cohen and J. R. Chelikovsky, *Electronic structure and Optical Properties of Semiconductors,* 2nd ed. (Springer-Verlag, Berlin , 1989).

Auger Photoelectron Coincidence Spectroscopy of Fe/Ni Alloys

S.M. Thurgate and C.P. Lund
School of Physical Sciences, Engineering and Technology
Murdoch University
Murdoch, Western Australia

Auger photoelectron coincidence spectroscopy (APECS) is a technique where two electron spectrometers are used to record the response of a particular atom when irradiated by x-rays[1]. One spectrometer records the photoelectron while the other records the Auger electron [2]. In this way, one can determine the correlations between the features in the XPS and AES spectra.

In this work, we report on APECS measurements of Ni/Fe alloys[3]. Several interesting effects are seen clearly in this data. They include:

1. The high kinetic energy side of the L_3VV peak is better resolved in APECS as the partly overlapping intensity from the L_2VV line is missing in the spectrum in coincidence with the $2p_{3/2}$ photoelectron line.
2. The contribution to the background from initial state shake up/off is greater in the alloy than in the pure material. This is however almost completely compensated for from an decrease in final state shake up/off. Hence the APECS spectra show large differences while the regular singles spectra are all but identical.
3. The probability of the Coster Kronig process L_2L_3V is decreased in the alloy systems.

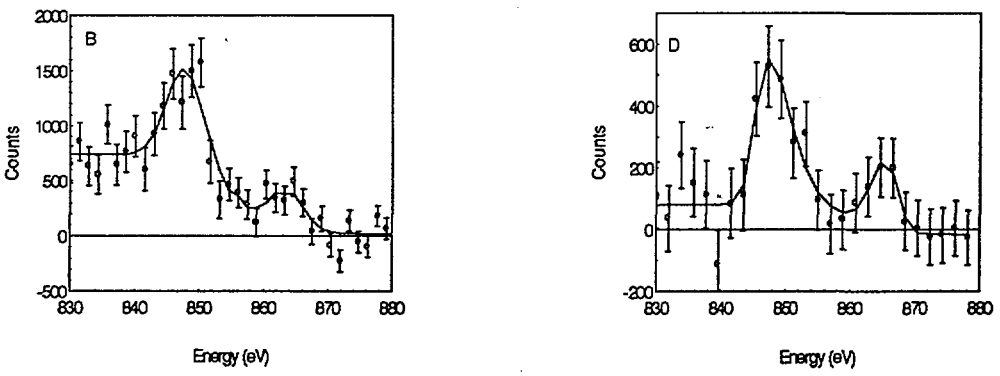

a) Pure Ni b) 50% Ni/Fe alloy

APECS spectrum of Ni L_3VV with $2p_{1/2}$.

References

1 S. M. Thurgate and C. P. Lund, Journal of Electron Spectroscopy and Related Phenomena **72**, 289 (1995).

2 S. M. Thurgate, B. Todd, B. Lohmann, *et al.*, Review of Scientific Instruments **61**, 3733 (1990).

3 S. M. Thurgate, C. P. Lund, and A. B. Wedding, Physical Review B **50**, 4810 (1994).

CONNECTION BETWEEN ELECTRON SURFACE BARRIER RESONANCE STATES IN METALS AND SURFACE BARRIER FEATURES IN VLEED (VERY-LOW-ENERGY ELECTRON DIFFRACTION)

M. N. Read and A. S. Christopoulos
Department of Theoretical Physics
School of Physics
University of New South Wales
Sydney NSW 2052
Australia

In the past there has been some uncertainty about whether the fine-structure features appearing in VLEED (very-low-energy electron diffraction) from metal surfaces are interference effects due to a few scattering events at the surface barrier, or are due to the electron temporarily occupying a surface barrier resonant state.

We have calculated the reflectivity profiles for VLEED on W(001)-1x1 surface for polar angles of incidence of $\Theta = 0^\circ$ to 48°and azimuthal angle of $\Phi = 0^\circ$ for 00 beam from 0 to 13 eV using a realistic model for the surface barrier form. It is found that sustained multiple scattering occurs for $\Theta = 6^\circ$ to 26° from a detailed analysis of the number of scattering events between substrate and barrier and that the electron is temporarily trapped in a barrier resonance state. The angles of incidence used correspond to the electron having reduced momentum along $\bar{\Gamma}(\bar{\Delta})\bar{X}$.

We have used our plane-wave scattering method [M. N. Read and A. S. Christopoulos, Phys. Rev. B **45**, 13 729 (1992)] to calculate the surface barrier resonance band structure of W(001)-1x1 for 10.5 eV above the vacuum level and along $\bar{\Gamma}(\bar{\Delta})\bar{X}$ and using the same surface barrier model. We observe a strong resonance band starting at 10.2 eV at $\bar{\Gamma}$ and which is most likely the lowest n = 1 member of the Rydberg series of image resonances. A Shockley resonance occurs between 0 and 4 eV.

The correlation between the observable features in the two methods is discussed with a view to determining information about the structure of the surface barrier.

MAGNETIZATION STUDIES OF Bi-2223 TAPES

K.-H. Müller, C. Andrikidis, H.K. Liu* and S.X. Dou*

CSIRO, Division of Applied Physics, Sydney 2070.

* Centre for Superconducting and Electronic Materials, University of Wollongong, Wollongong 2522.

Superconducting Bi-2223 silver sheathed tapes show a critical current density large enough for power transmission line applications where the magnetic fields involved are small. Unfortunately, the performance of these tapes at 77 K in large fields is quite poor and a better understanding of magnetization data might help to elucidate the reasons for the limitation of the tape's current carrying capacity.

We have investigated by means of magnetic moment measurements on monofilamentary Bi-2223 tapes, using a Quamtum Design SQUID magnetometer, the correlation between intergranular critical current density J_c^J which is flowing over the entire tape, and the intragranular critical current density J_c^G which is flowing inside grains. The experimental data reveal that J_c^J depends strongly on the magnetic history of grains and the value of J_c^G. The anomalous peak seen in magnetization loops of tapes correlates well with the peak seen in the critical current density measured electrically in a decreasing magnetic field. The position of the anomalous peak does not shift further to higher fields when the applied field exceeds the field of full grain penetration. By separating the silver cladding from the superconductor we found that, opposite to common believe, the current does not flow mainly near the superconductor-silver interface but is more homogeneously distributed throughout the filament.

SELF-FIELD AC LOSSES IN Bi-2223 SUPERCONDUCTING TAPES

K.-H. Müller, K. E. Leslie

CSIRO, Division of Applied Physics, Sydney 2070.

The self-field AC loss in Bi-2223 silver sheathed tapes for AC currents of up to 100 A was measured at 77 K and frequencies of 60 Hz and 600 Hz using a lock-in amplifier. The frequency dependence indicated a purely hysteretic loss which can be well described in terms of the critical state model for a flat superconducting strip [1]. The only parameter needed to predict the self-field AC loss is the critical current of the critical state. Because the loss voltage is extremely small compared with the inductive voltage, a very high accuracy of the lock-in amplifier phase setting is required. Unlike in loss measurements on cylindrical superconducting samples, in the case of the tape the measuring circuit leads have to be brought out from the surface forming a loop where the changing magnetic field induces an additional voltage. Only if the loop formed by the leads at the voltage tabs is large enough will the apparent power dissipation approach the real AC loss associated with the lenght of the sample probed [2].

[1] W. T. Norris, J. Phys. D 3, 489 (1970).

[2] J. Clem, T. Pe and J. McDonald, (1995) to be published.

Noise Properties of High-Quality Step-Edge YBCO Josephson Junctions

Catherine P. Foley, Simon Lam, Graeme J. Sloggett, Nicholas Savvides, Alex Katsaros, Ling Hao[a],
John C. Macfarlane[a], Colin M. Pegrum [a]and Jan Kuznik[b]

CSIRO Division of Applied Physics, PO Box 218 Lindfield, NSW 2070, Australia
[a]Dept. Physics and Applied Physics, University of Strathclyde, Glasgow, UK.
[b] Czech Academy of Sciences, Prague, Czech Republic.

Abstract -We report the results of noise and other measurements on YBCO step-edge Josephson junctions whose morphology closely approaches the ideal of a homogeneous tilt angle grain boundary. The junctions exhibit near-perfect single-junction RSJ current voltage characteristics and magnetic field dependence(1). Excess noise in the junctions was comparable to the best bicrystal types previously measured(2), the normalised amplitude of the critical current fluctuations, $S_i^{1/2}$, being less than $1x10^{-4}$ $Hz^{-1/2}$ at 1 Hz and 77 K. $S_i^{1/2}$ was found to be independent of temperature(3) and also independent of magnetic field provided the zero-field critical current was used for normalisation.

1. C.P. Foley, G.J. Sloggett, K.-H. Muller, S. Lam, N. Savvides, A. Katsaros and D. N. Matthews, IEEE Trans. Applied Superconduct., to be published.
2. M. Kawasaki, P.Chaudhari and A. Gupta, Phys. Rev. Lett. 68, 1065 (1992).
3. A.H. Miklich, J. Clarke, M.S. Colclough and K. Char, Appl. Phys. Lett 60, 1899 (1992).

High-J_c Superconducting YBCO Thin Films for SQUIDs

Alex Katsaros, Nick Savvides and Cathy Foley
CSIRO Applied Physics, Sydney 2070

High critical current density, J_c, and reproducibility of film quality are major issues in high-T_c superconducting device technology. Because many factors such as substrate quality, deposition parameters and film stochiometry impact on film quality the growth of high-Jc $YBa_2Cu_3O_7$ thin films suitable for devices is a demanding task. For optimum device performance c-axis epitaxial films are required with smooth surfaces, controlled microstructure and crystalline orientation, high T_c (> 87 K) and high J_c (> $1x10^6$ A cm^{-2}). Consequently a stable platform in film quality is critical in developing and maintaining world class device technology.

In previous "Wagga" meetings and elsewhere we presented details of our thin film deposition system, results of film growth studies, techniques of film characterisation and SQUID performance [1-5]. In this paper we present transport properties and lattice parameters for a large number of films deposited over a period of ten months using a single target and under similar sputtering conditions. The data serve to illustrate the level of reproducibility of our deposition technology while closer examination of the data reveal some interesting "correlations" among properties. We have used these correlations to assist us to control both the deposition of films and subsequent processing into test structures and SQUIDs.

[1] See for example, CMPM Conf. Proc. 1992-1995.
[2] N Savvides and A Katsaros, Appl. Phys. Lett. 62 (1993) 1993; Physica C 226 (1994) 23.
[3] N. savvides, A. Katsaros, CP Foley and GJ Sloggett, Adv. Cryogenic Eng. 40 (1994) 409.
[4] GJ Sloggett, DL Dart, CP Foley, RA Binks, N Savvides and A Katsaros, Supercon. Sci. Tech. 7 (1994) 260.
[5] CP Foley, S Lam, GJ Sloggett, N Savvides, A Katsaros, L Hao, JC Macfarlane, CM Pegrum and J Kuznik, (this conference).

MICROWAVE PROPERTIES AND MICROSTRUCTURE OF $Y_1Ba_2Cu_3O_7$ THIN FILMS

Nick Savvides, Alex Katsaros, David Reilly and Cathy Foley
CSIRO Applied Physics, Sydney 2070

Janina Ceremuga and Kenneth Leong
Electrical and Computer Eng., James Cook University, Townsville 4811

The quality of high-T_c thin films for microwave applications is determined by the microwave surface resistance, R_s, and the penetration depth, λ. For good quality $Y_1Ba_2Cu_3O_7$ thin films R_s is much smaller than that of metals such as copper and gold for frequencies up to 200 GHz. Also the penetration depth (0.45 mm at 77 K) is much smaller than the skin depth (equivalent to λ) of metals and is independent of frequency. Consequently $Y_1Ba_2Cu_3O_7$ thin film microwave devices operating at 77 K outperform their pure metal counterparts: superconducting lines have much smaller attenuation, filters have a much higher Q factor and interconnects for digital systems operate at much higher speed.

The microwave resistance of $Y_1Ba_2Cu_3O_7$ thin films is very susceptible to the film microstructure such as grain boundaries, impurity phases, outgrowths and other large scale structural defects. We have investigated the effect of microstructure on the microwave properties of thin films at 77 K. The epitaxial c-axis $Y_1Ba_2Cu_3O_7$ thin films, deposited onto MgO (100) substrates by magnetron sputtering [1], had a range of microstructural defects but similar transport properties ($T_{c\infty}$ = 87-88 K and J_c = (2-3) x10^6 A cm^{-2}). Microwave properties were measured at 77 K using a sapphire dielectric resonator operated in the TE_{011} mode. Films relatively free of large scale microstructural defects have low microwave loss (R_s = 0.8 mOhm at 10 GHz) while films with large scale defects such as outgrowths have much higher loss (R_s = 3 - 4 mOhm).

[1] N. Savvides and A. Katsaros, Appl. Phys. Lett. 62 (1993) 528;
Thin Solid Films 228 (1993) 182; Phys. C 226 (1994) 23.
[2] J. Ceremuga, 19th ANZIP Cond. Mater Physics Meeting, Wagga 1995.

This page(s) is (are) intentionally left blank.

PREPARATION AND SUPERCONDUCTING CRITICAL CURRENT OF MELT-TEXTURED YBCO WITH LARGE SIZE

Y.Zhao[1], C.H.Choi[1], C.C.Sorrell[1], B.Chen[1], M.La Robina[2], C.Andrikids[3]

[1]School of Materials Science and Engineering, University of New South Wales, Sydney, NSW 2052, Australia

[2]Australian Nuclear Science and Technology Organization, Advanced Materials Program, PMB 1, Menai, NSW 2234, Australia

[3]CSIRO Division of Applied Physics, National Measurement Laboratory, Lindfield, NSW 2047, Australia

A new Melt-Textured-Growth (MTG) method was developed to fabricate $YBa_2Cu_3O_{7-y}$ (Y123) crystals by using horizontal furnace, Y_2BaCuO_5 (211) substrate, "super-critical control" at the peritectic reaction point. Compared with the normal MTG technique, the processing time was reduced up to 30 percent, the 211 particle size was reduced from 8 μm to 1.5 μm, and the Y123 single-domain size was increased up to 27 mm with no porosity and cracks. Owing to the very fine size and highly homogeneous distribution of the 211 particles in the Y123 matrix, samples prepared by the new method have strong flux pinning and high critical current density (J_c). At 77 K, J_c reaches $6x10^4$ A/cm^2 in zero field, and $1x10^4$ A/cm^2 in 2 Tesla field.

The effects of the contact area as well as the weight fraction of 211 substrate to Y123 matrix is also investigated. It is found that a proper control of the mass transfer (or liquid phase absorption) from Y123 to 211 substrate is very important for growing high quality crystals.

References:

[1] Y.Zhao, et al, **Physics Letters A**, 203, 53-57 (1995).

[2] Y.Zhao, et al, **International Ceramic Monographs** 1, 1172-76 (1994).

THE SEARCH FOR SUPERCONDUCTIVITY IN RARE EARTH NICKEL(III) AND NICKEL(I) OXIDES.

M. James[1,2] and J. P. Attfield[2]
[1]*A.N.S.T.O., Private Mail Bag 1, Menai, N.S.W. 2234, Australia.*
[2]*Department of Chemistry, University of Cambridge, Lensfield Road, Cambridge, U.K.*

Recently there has been a great deal of interest in rare earth nickel oxide phases with the K_2NiF_4 structure as they show structural, magnetic and electrical properties similar to high T_c copper oxide materials. In particular, the properties of the $Ln_{2-x}Sr_xNiO_{4-\delta}$ solid solutions have been extensively studied for the larger lanthanide ions Ln = La ($0 \leq x \leq 1.6$) [1], Nd ($0 \leq x \leq 1.4$) [2], Pr ($0 \leq x \leq 1.0$), Sm ($0.5 \leq x \leq 1.0$) and Gd ($x = 1.0$)[3].

We have undertaken a systematic study of the $Ln_{2-x}Sr_xNiO_{4-\delta}$ system over the entire lanthanide range, focusing on doping levels above x = 1.0. It was observed that for samples prepared under flowing O_2 at 1100 °C, the upper solid solution limit was x = 1.67. The lower solubility limit increased with decreasing ionic radii for Ln = Nd^{3+} - Gd^{3+}, forming essentially point phases $Ln_{0.33}Sr_{1.67}NiO_{3.67}$ ($LnSr_5Ni_3O_{11}$) for Ln = Y^{3+}, Dy^{3+} - Tm^{3+} [4,5]. Thermogravimetric analysis of these phases indicated that they contained nickel in a 3+ oxidation state. Rietveld refinement of the structure of these materials using powder X-ray diffraction data showed that each adopted the tetragonal K_2NiF_4 structure(*I4/mmm*), with Ln^{3+} and Sr^{2+} disordered over the K sites and oxygen vacancies occuring predominantly in the NiO_2 planes. Electrical conductivity measurements of $YSr_5Ni_3O_{11}$ indicate semiconducting behaviour which is able to be modelled by variable range hopping. Magnetic susceptibility measurements between 6 K and 300 K show Curie-Weiss behaviour, with substantially lower effective moments than expected from spin only low-spin Ni(III) due to the delocalisation of the nickel electrons.

Partial thermogravimetric reduction of $LnSr_5Ni_3O_{11}$ (Ln = Y, Dy - Tm) led to a series of nickel(I) oxides: $LnSr_5Ni_3O_8$ [6,7]. Rietveld refinement of the structure of these materials using powder X-ray diffraction data indicated a transition from a tetragonal K_2NiF_4 to an orthorhombic Sr_2CuO_3 (*Immm*) arrangement, in which $^1/_3$ of the bridging oxygen atoms were missing from the chains of apex-linked nickel oxide square planes. Bond valence calculations supported the notion of nickel being present as Ni^+.

[1] Takeda, Y.; Kanno, R.; Sakano, M.; Yamamoto, O.; Takano, M.; Bando, Y.; Akinaga, H.; Takita; K.; Goodenough, J. B., *Mater. Res. Bull.* (1990), **25**, 293.
[2] Takeda, Y.; Nishijima, M.; Imanishi, N.; Kanno, R.; Yamamoto, O.; Takano, M. *J. Solid State Chem.* (1992), **96**, 72.
[3] Chen, S. C.; Ramanujachary, K. V.; Greenblatt, M., *J. Solid State Chem.*, (1993), **105**, 444.
[4] James, M.; Attfield, J. P. *J. Solid State Chem.*, (1993), **105**, 287.
[5] James, M.; Attfield, J. P.; Rodriguez-Carvajal, J. *Chem. Mater.*, (1995), **7**, 1448.
[6] James, M.; Attfield, J. P. *J. Chem. Soc., Chem. Comm.*, (1994), 1185.
[7] James, M.; Attfield, J. P. *Physica C.*, (1994),.**235-240**, 751.

EFFECT OF VARIOUS MECHANICAL DEFORMATION ON THE PROPERTIES OF SILVER-CLAD BI-2223 COMPOSITES

Y.C. Guo, D. Akmacic, H. Wang, H.K. Liu and S.X. Dou
Centre for Superconducting and Electronic Materials
The University of Wollongong
Northfields Ave., Wollongong, NSW 2522

Silver-clad Bi-2223 composite wires were prepared by either square-rolling or drawing silver tube packed with superconductor precursor powder. Wires were then turn into flat tapes using different mechanical deformation techniques including flat-rolling, transverse-rolling and uniaxial pressing. The silver/core interface of differently prepared tapes was examined by optical and scanning electron microscopy. While the wire processing method was found to produce no noticeable difference in the silver/core interface, the tape forming technique resulted in significantly different interface. Pressing produced more wavy silver/core interface (sausaging) than flat-rolling and transverse rolling. Cracks were also found common in pressed samples, but rare in flat-rolled and transverse-rolled samples. Furthermore, the direction of sausaging was found to be dependent on the mechanical deformation technique used, i.e., along the length of tape in pressed and transverse-rolled samples and along the width of tape in flat-rolled tapes.

The green tapes were heat treated using a thermomechanical process consisting of alternate mechanical deformation and sintering. For comparison, a control tape in which no deformation was used between sinterings was also prepared using the same sintering conditions. After each step of heat treatment, tapes were characterised in terms of high-T_c phase fraction, microstructure and critical current density (J_c). The results indicated that the mechanical deformation accelerated the Bi-2223 phase formation rate, in particular, the pressed samples showed the fastest Bi-2223 phase formation rate. For the J_c, pressing yielded the highest value, probably due to the high density and excellent grain alignment in the pressed tapes.

PARTICLE AND POWDER CHARACTERISATION OF BI-BASED SUPERCONDUCTORS

M.Yavuz, Y.C.Guo, E.R. Vance*, H.L.Liu, and S.X. Dou

Center for Superconducting and Electronic Materials, University of Wollongong, NSW 2522, Australia

* Division of Advanced Materials, ANSTO, New Illawarra Road, Lucas Heights, NSW 2234, Australia

Superconductor precursor powder was ground in a planetary and an attrition mill using various combinations of grinding container, balls and carrier (dry and wet). Dry milling was found to be more effective than wet milling for reducing particle size irrespective of container and ball materials used in the planetary milling. On the other hand, wet milling was found more effective in the attrition milling. Serious Si contamination was observed in powders milled using agate grinding materials. Some C from polypropylene container was found after milling, but no Zr from YSZ balls. Effect of particle size on the property of Bi2223/Ag tapes was investigated in terms of critical current density (J_c). Fine particle size was found to show high J_c.

FORMATION OF WEAK AND STRONG LINKS IN Ag/Bi-2223 SUPERCONDUCTING TAPES

J. Horvat, S. X. Dou and Y. C. Guo

Centre for Superconducting and Electronic Materials, University of Wollongong, Wollongong 2522

The formation of weak and strong links between the superconducting grains in Ag-sheathed Bi-2223 superconductors was monitored as a function of sintering time. The samples were pressed after 20, 50, 110, 190 and 285 hours of sintering and critical current measured at each of the stages. The critical current was measured with 1μV/cm criterion, at 77K. The value of the critical current was used as a measure of the connectivity between the grains. The critical current through strong links (I_c^s) was distinguished from the total critical current (I_c). The molar fractions of Bi-2223 and Bi-2212 phases formed upon the sintering was estimated using X-ray diffraction. The molar fraction of Bi-2223 phase (X_{2223}) increases in the first 110 hours, after which it retains a value of about 90%. I_c^s, and to a lesser extent I_c, continue increasing with further sintering, even though X_{2223} does not change. Both, I_c^s and I_c decrease slightly if samples are pressed at 190 hours of sintering and then sintered for further 95 hours. However, there is a substantial increase of I_c^s and I_c if the samples are further sintered without any pressing at 190 hours. I_c^s triples by the last sintering stage, whereas I_c doubles. This shows that the links between the grains are mostly formed in the last stages of sintering, after the grains are fully formed. There should be no further mechanical deformation of the samples after the grains are formed, because the resulting cracks can be no longer healed with further sintering. Longer sintering times are particularly important for the formation of strong links, which can result in samples retaining higher I_c in the field.

AU9918224

A HIGH T_c SUPERCONDUCTING LIQUID NITROGEN LEVEL SENSOR

J.X. Jin, H.K. Liu and S.X. Dou
Center for Superconducting and Electronic Materials
University of Wollongong, Wollongong, NSW 2522, Australia

C. Grantham and J. Beer
Dept. of Electric Power
University of NSW, Sydney 2052, Australia

The dramatic resistance change in the superconducting-normal transition temperature range enables a high T_C superconductor to be considered for designing a liquid nitrogen level sensor. A $(Bi,Pb)_2Sr_2Ca_2Cu_3O_{10+x}$ Ag clad superconducting wire is selected and tested as a continuous liquid nitrogen level sensor to investigate the possibility for this application. The $(Bi,Pb)_2Sr_2Ca_2Cu_3O_{10+x}$ Ag clad superconducting wire has approximately 110 K critical temperature, with more flexible and stable properties compared with bulk shape ceramic high T_C superconductors. The voltage drops across the sensor are tested with different immersion lengths in liquid nitrogen. The accuracy of the HTS sensor is analysed with its dR/dT in the superconducting-normal transition range. The voltage signal is sensitive to liquid nitrogen level change, and this signal can be optimized by controlling the transport current. The problems of the Ag clad superconductor are that the Ag sheath thermal conductivity is very high, and the sensor normal resistance is low. These are the main disadvantages for using such a wire as a continuous level sensor. However, a satisfactory accuracy can be achieved by control of the transport current. A different configuration of the wire sensor is also designed to avoid this thermal influence.

TP7

HIGH T_c SUPERCONDUCTING WINDING

J.X. Jin, H.K. Liu and S.X. Dou
Centre for Superconducting and Electronic Materials
University of Wollongong, Wollongong, NSW 2522, Australia

C. Grantham and J. Beer
Dept. of Electric Power
University of NSW, Sydney 2052, Australia

$(Bi,Pb)_2Sr_2Ca_2Cu_3O_{10+x}$ Ag clad high T_c superconducting (HTS) wires behave well on applicable performance, therefore, the HTS wires are prepared to produce HTS windings and considered for use in electrical applications. HTS coils are made, and their critical currents (I_c) and magnetic fields generated by the produced coils are measured at 77 K. Since for most electrical applications, HTS are likely to be used as a magnetic core bias winding, magnetic cores were then added to the HTS coils for investigation. The magnetic core influence on the HTS windings is investigated by measuring I-V characteristic changes of the HTS coils with different magnetic cores and different core air gaps. A 0.15 T magnetic field can be selected to design the HTS bias winding ampere-turns, at which about 50% I_c can be maintained at 77 K. Therefore the HTS bias winding ampere-turns NI at 77 K is evaluated with its dimension by $B = \mu_o NI \cdot [2(R_2-R_1)]^{-1} \cdot \ln\{[R_2+(R_2^2+L^2)^{1/2}]/[R_1+(R_1^2+L^2)^{1/2}]\} = 0.15$. The achieved I_c of the HTS short wires at 77 K, are suitable for satisfying some low field applications. However, for high magnetic field applications, the existing $(Bi,Pb)_2Sr_2Ca_2Cu_3O_{10+x}$ HTS wires have to work below 77 K to increase flux pinning potential in the HTS materials, resulting in higher I_c.

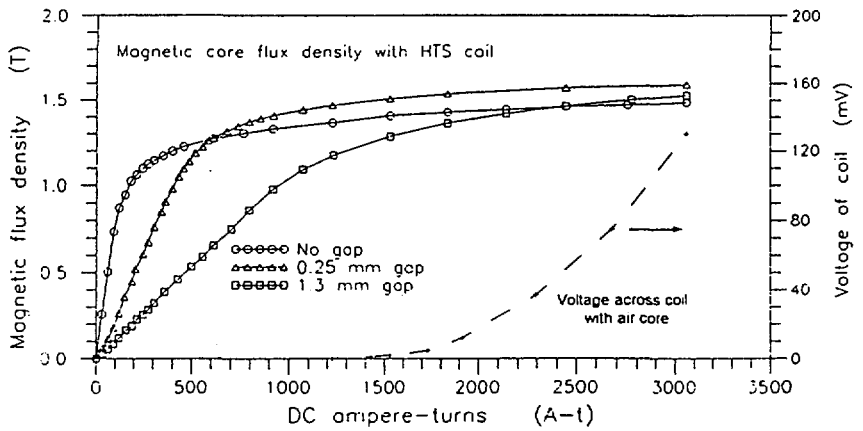

Figure 1 Fields generated by a HTS winding at 77 K with different magnetic cores

A HIGH Tc SUPERCONDUCTING LOSS-FREE RESISTOR

J.X. Jin, J.Y. Chen and S.X. Dou
Center for Superconducting and Electronic Materials
University of Wollongong, Wollongong, NSW 2522, Australia

A loss-less resistor (LLR) is introduced as a novel concept with consideration of using a high T_c superconducting (HTS) inductor. This LLR resistor mainly consists of an electronic switch bridge and a inductor L. By controlling the electronic switch bridge, an equivalent resistance R(i) can be generated, and its value is R(i) = (L/i)di/dt, which allows the LLR resistor have a resistive voltage-current characteristic i.e. V(t) = i(t)R, but without thermal loss across this LLR resistor if a superconducting inductor is selected. With a HTS winding and therefore a HTS inductor, this LLR resistor is practically close to loss-free. The LLR resistor can be widely used to replace the conventional resistor in order to save energy and to improve performance of the systems. The HTS wires are identified for this application, by considering their critical currents, ac loss and possibility to make a large HTS inductor winding. To make LLR resistors for practical applications is considered with the existing HTS wires.

AU9918227

A TEMPERATURE DEPENDENT STUDY OF THE RAMAN-ACTIVE PHONON MODES IN Ca and Zn doped $YBa_2Cu_3O_{7-x}$

J.W. Quilty*, A. Simpson‡, H.J. Trodahl*, N. Flower†, M. Staines†, J. Downes†

*Victoria University of Wellington, New Zealand

†Industrial Research Limited, New Zealand

‡Dalhousie University, Nova Scotia, Canada

The temperature dependent behaviour of the phonon modes in $YBa_2Cu_3O_{7-x}$ (Y–123) are of interest because the strong electron–phonon coupling within these materials yields information about the magnitude of the superconducting gap. The opening of a gap provides a new decay route for phonons, hence phonons near the gap energy show changes in their frequencies and widths as the temperature drops below T_c. The magnitude of the superconducting gap may be estimated from these changes.[1,2]

We report our temperature–dependent measurements of the Raman–active phonon modes in ceramic and preferentially oriented polycrystaline samples of Y–123, under a variety of doping regimes. The samples were made underdoped, optimally doped and overdoped by manipulation of the hole concentration on the Cu–O planes, achieved by changing the oxygen stoichiometry, substitution of Zn for Cu, and substitution of Ca for Y. As observed by others,[3] the 340cm^{-1} phonon, involving vibrations of the oxygen ions on the Cu-O planes, showed the greatest magnitude of change when the samples were cooled below T_c, indicating that the superconducting gap energy is close to that of the 340cm^{-1} phonon.

Figure 1 (right) is a plot of the 340cm^{-1} phonon frequency vs. temperature for an optimally doped (T_c around 90K), preferentially oriented Y–123 sample. Note the marked softening of the frequency that occurs below T_c, due to the opening of the superconducting gap.

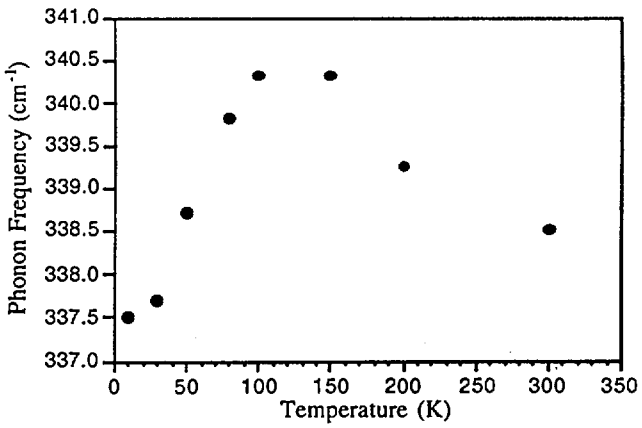

[1] C. Thomsen, in **Light Scattering in Solids VI**, edited by M. Cardona and G. Guntherodt (Springer, Berlin, 1991)

[2] B. Friedl, C. Thomsen, and M. Cardona, **Determination of the Superconducting Gap in $RBa_2Cu_3O_{7-\delta}$**, Phys. Rev. Lett. 65 (7), 915–918 (1990)

[3] Kyung–Min Ham, Jin–Tae Kim, R. Sooryakumar, and Thomas R Lemberger, **Raman study of the anomalous behaviour of the 340cm^{-1} CuO_2 planar–oxygen phonon in Ni–doped $YBa_2Cu_3O_{7-\delta}$ superconducting films**, Phys. Rev. B 47 (17), 11439–11446 (1993)

NORMAL STATE PHASE OF CuO PLANES IN HIGH Tc SUPERCONDUCTORS.

B.C. den Hertog and M.P. Das
Department of Theoretical Physics,
Research School of Physical Sciences and Engineering,
The Australian National University ACT 0200.

We[1] examine various aspects of the normal state phase of the copper oxide planes in high Tc superconductors. In particular, within the context of the three band Hubbard model, we study as a function of doping the competition between a charge density wave phase induced by the experimentally observed oxygen breathing modes, antiferromagnetic order, and paramagnetism. To account for the strong fermion interactions we use the finite U slave boson technique of Kotliar and Ruckenstein. Also[2], we discuss whether localisation of one hole per copper site is possible at finite doping in the paramagnetic phase. Here, we characterise localisation as a vanishing of the effective bandwidth. We obtain a metal insulator phase diagram at half filling.

---

[1] B.C. den Hertog and M.P. Das (preprint 1996)
[2] B.C. den Hertog and M.P. Das (preprint 1995)

CORRELATION OF MICRO-RAMAN AND OPTICAL MICROSCOPY ANALYSIS OF POLYCRYSTALLINE $YBa_2Cu_3O_{7-x}$

J.M. Long*, T.R. Finlayson†, C.S. Lim‡, and T.P. Mernagh§

*School of Engineering and Technology, Deakin University, Geelong, VIC 3217
†Department of Physics, Monash University, Clayton, VIC 3168
‡CSIRO Division of Minerals, Private Mail Bag 5, Menai, NSW 2234
§Australian Geological Survey Organisation, GPO Box 378, Canberra, ACT 2601

In our earlier presentations, we demonstrated that micro-Raman spectroscopy (MRS) was particularly suited for routine microstructural analysis of $YBa_2Cu_3O_{7-x}$ (YBCO) superconductors.[1,2] MRS may be employed to determine phases, oxygen stoichiometry, grain orientation, and impurities in YBCO and related materials. An important feature of this technique is that it examines a very small portion of material. Typically the region of a sample irradiated by the incident laser beam is a spot 2–10 microns wide. Thus analysis of individual grains or portions of grains is possible. However, obtaining more general information concerning an entire sample surface is difficult with this method, requiring one to obtain and analyse large numbers of spectra – a time consuming task.

Optical microscopy has proven to be a useful technique for obtaining general, qualitative information from the entire surface of YBCO samples. When observed through crossed polarisers, both orthorhombic and tetragonal YBCO show characteristic colours, allowing the observation and detection of superconducting and nonsuperconducting regions.[3-5] Certain impurities also have characteristic colours. Once the colours of the various phases are calibrated, one can determine their distribution throughout a whole surface. Both the observation of colour and the twin patterns can indicate textured regions, or grains of similar orientation in an untextured material.

We present an example of the complementary use of both techniques for a more complete analysis of polycrystalline YBCO. Observed colours of polarisation on YBCO were correlated with information provided by MRS on individual grains to deduce microstructural characteristics (including texture, chemistry, and impurities) across the whole surface of a sample. Grains of similar orientation were observed by both methods. It was also found that Raman results can be misleading unless the sample is also observed by polarised light microscopy and the two sets of results correlated. These techniques would be quite useful for the analysis of large, textured samples, especially where material is produced in large quantities.

[1] J.M. Long, *Light Scattering Studies of Microstructure in $YBa_2Cu_3O_{7-x}$ Superconductors*, Ph.D. thesis, Monash University (1994).
[2] J. M. Long, T.R. Finlayson, C.S. Lim, and T.P. Mernagh, Eighteenth Annual ANZIP Condensed Matter Physics Meeting (Wagga Wagga, NSW), 9–11 February 1994.
[3] H.A. Hoff and C.S. Pande, *JOM* **42**(6), pp. 10–15 (1990).
[4] H.A. Hoff, M. Rubinstein, M.S. Osofsky, A.K. Singh, L.E. Richards, W.L. Lechter, L.E. Toth, B.N. Das, and C.S. Pande, *Journal of Superconductivity* **2**, pp. 351–359 (1989).
[5] H.A. Hoff, A.K. Singh, J.S. Wallace, W.L. Lechter, and C.S. Pande, *Journal of Superconductivity* **1**, pp. 35–44 (1988).

AU9918230

XAS STUDY OF Pu AND Np INCORPORATION IN ZIRCONOLITE

Bruce D. Begg and Eric R. Vance,
Materials Division, ANSTO, PMB 1 , Menai, NSW 2234
Fax: (02) 543 7179
Email: bdb@nucleus.ansto.gov.au

Zirconolite is the key Synroc phase for the immobilisation of actinide-rich radioactive waste. The successful incorporation of actinide elements into zirconolite is critically dependent upon a knowledge of the prevailing valence state and site location for each of the elements under the selected processing atmosphere.

A series of Ce- (used as a nonradioactive simulant for Pu) Pu- and Np-bearing zirconolites representing the alternative valence states (+3 or +4) and site locations (Ca or Zr site) have been prepared and sintered under a range of oxygen pressures, prior to being analysed by XRD and analytical SEM. From these techniques the valence state and site locations of the actinide elements have been inferred. X-ray absorption spectroscopy (XAS) however offers an opportunity to determine these properties directly. These results will be discussed, and preliminary conclusions drawn about the role of cerium as a nonradioactive simulant for plutonium.

THERMAL REORIENTATION OF HYDROGENIC Pr^{3+} CENTERS

Glynn D Jones

Department of Physics and Astronomy
University of Canterbury, Christchurch, New Zealand

Sets of five multi-hydrogenic centers of both CaF_2:Pr^{3+} and SrF_2:Pr^{3+} show bleaching under selective polarized-light irradiation. Two forms of bleaching behaviour are observed. In reversible polarized bleaching, irradiation creates re-oriented equivalent centers, which can be restored to the original orientation by switching the laser polarization by 90°. Indefinite sequences of bleaching and recovery can be established. In photoproduct bleaching, inequivalent centers are produced, which can be reverted by subsequently selectively exciting their absorption lines.

Thermal recovery of the bleached centers on warming the crystals occurs abruptly over a 5 K range around 100 K and is noteworthy in occurring at essentially identical temperatures for H^-, D^- and T^- centers. The simplest model for this thermal recovery is thermal activation of the mobile hydrogenic ions over a double well potential barrier. If the mobile ion meets the barrier at a frequency $\nu = \frac{1}{\tau_0}$, the probability q of crossing the barrier is:

$$q = \nu \exp(\frac{-W}{kT}) \quad \text{or equivalently} \quad W = kT \ln(\frac{t}{\tau_0})$$

where W is the barrier potential to be surmounted, $t = \frac{1}{q}$ is the time for which the crystal is held at successively higher temperatures and T is the temperature for recovery to the $(1 - \frac{1}{e})$ level. Both the insensitivity of the ln function to the value chosen for τ_0 and the almost identical barrier heights W for H^-, D^- and T^- account for the isotopic independence of T. An alternative model proposed by Universität Regensburg requires the involvement of **high frequency excitations** in scattering processes for surmounting the barrier. These differing model ideas will be discussed, together with the general conclusions of a Polish paper[1].

[1] Cz. Koepke, A. Lempicki and A.J. Wojtowicz, Phys. stat. solidi (b) 179, 233 (1993).

AU9918232

THE FERMI SURFACE OF ORDERED AND DISORDERED Cu_3Au AS DETERMINED BY ANGLE RESOLVED PHOTOEMISSION

J. A. Con Foo, S. Tkatchenko and A. P. J. Stampfl
School of Physics, La Trobe University, Victoria 3083, Australia

A. Ziegler, B. Mattern, M. Hollering, R. Denecke and L. Ley
Universität Erlangen-Nürnberg, 91058 Erlangen, Germany

J. D. Riley and R. C. G. Leckey
School of Physics, La Trobe University, Victoria 3083, Australia

Cu_3Au is an interesting material which has been studied extensively for its alloying properties, its structural properties and for the bulk and surface order-disorder transition it displays. We have shown previously [1,2] that it is possible to accurately map the Fermi surface of Cu using photoemission spectroscopy. We present in this paper the bulk Fermi surfaces of the ordered and disordered phases of Cu_3Au which have been experimentally mapped using angle resolved constant initial state photoemission spectroscopy. The shape of the Fermi cross-section determined for the disordered phase has been found to be well described by a rigid band model. Comparison to previously reported de Haas-van Alphen results on the ordered phase has found that the neck radius is the same as the value determined for the disordered phase to within experimental error. It has been found however, that the Fermi surface belly radius of the disordered phase is $\approx 20 - 30\%$ larger than the corresponding calculated distance of the ordered material.

[1] A. P. J. Stampfl *et al.*, Surf. Sci. **331-333**, 1272 (1995).

[2] J. A. Con Foo *et al.*, Submitted to Phys. Rev. B .

AU9918233

SURFACE ELECTRICAL RESISTIVITY OF INSULATORS

B. C. Senn and J. Liesegang
School of Physics, Faculty of Sci. and Tech. La Trobe University, Bundoora VIC 3083

Surface electrical conductivity and charge transport in insulating materials, including strong insulating polymers is known to be very complex in mechanism [1,2]. Such electrical conductivity involves structure dependence, imperfections and impurities and also the problems associated with commonly used measuring techniques (e.g., difficulties in making good electrode contact and time delays due to the establishment of equilibrium charge displacement). The reproducibility of results has also been poor.

A method is presented here for measuring surface charge decay, and theory has been developed so as to produce determinations of resistivity in the surface region of insulator films or wafers [3]. This method incorporates the use of a coaxial cylindrical capacitor arrangement and an electrometer interfaced to a PC.

The charge transport theory given here is based on Mott-Gurney diffusion [4], and allows easy interpretation of the experimental data, especially for the initial phase of surface charge decay. Resistivity measurements are presented for glass, mica, perspex and polyethylene, covering a range of 10^9 to 10^{18} Ωm, as an illustration of the useful range of the instrument for static and antistatic materials, particularly in film or sheet form. Values for the surface charge diffusion constants of the materials are also presented.

The charge transport theory has also been extended to allow the experimental and computational theoretical comparison of surface charge decay not only over the initial phase of charge decay, but also over longer times. The theoretical predictions show excellent agreement with experiment using the values for the diffusion constants referred to above.

[1] D. A. Seanor "Electrical Properties of Polymers" Ch 17 in "Polymer Science" (North Holland Pub. Co. 1972).

[2] D. K. Das-Gupta, IEEE Trans. Electrical Insulation 27, 909, 1992.

[3] J. Liesegang, B. C. Senn and E. R. Smith "Resistivity of antistatic and static insulators from surface charge measurement" J. Appl. Phys. 77 1995 pp.5782-5785.

[4] N. F. Mott and R.W. Gurney "Electronic Processes in Ionic Crystals" (Oxford University Press, 1948).

TP16
AU9918234

IMAGING OF SURFACE STATES AND THE INTERPRETATION OF STM IMAGES FROM THE GaAs SURFACE.

L.D. Broekman, R.C.G. Leckey, J.D. Riley
School of Physics, La Trobe University, Bundoora 3083, Victoria, Australia

Atomic resolution STM images of Semiconductor surfaces are often formed by tunneling to or from the state density of a small number of surface electronic states. Images of the GaAs(001) surface not only show a large number of possible surface geometries but also show atomic resolution features identifiable with particular bonding or nonbonding states. Unfortunately the identification these states from images is not straight forward since the effect of a localised electric field resulting from a biased tip will cause the semiconducting surface band structure to shift in energy relative to the sample Fermi level. The effect of this 'tip induced band bending' will be discussed with reference to images acquired from the GaAs(001)-(2×4) reconstruction. These images show that factors such as dopant levels, surface defect concentration and bias voltage all contribute to the apparent resolution of the microscope by determining which energy levels contribute to image formation.

ELLIPSOMETRIC STUDIES OF ANISOTROPIC THIN FILMS

P. Moses, S. Dligatch and G.B. Smith
Department of Applied Physics, University of Technology, Sydney,
PO Box 123, Broadway, NSW 2007, Australia

Many structures of interest in modern devices, and many new optical materials, are intrinsically anisotropic. If one or two dimensions have quantum scale sizes this is certainly the case. Materials at these dimensions also have properties that depart from the bulk values. Films with very fine nanoscale features can be studied with ellipsometry to gain insights into size dependent properties. However accurate determination of intrinsic dielectric properties of the anisotropic films with absorptance is complicated but possible. We report initial results gained as part of this program.

Our measurements were performed on a Spectroscopic Phase Modulated Ellipsometer, UVISEL, in the visible range, for select angles of incidence between 30 and 80 degrees.

Data modelling and analysis were carried out using the optical analysis program, OPTICAN, developed by Optic Instruments Inc. This package allows users to construct a model for the multi-layered systems of anisotropic and isotropic layers and to fit the experimental spectral Photo-Ellipsometric data using a least-squares minimisation method. Desired layer and component parameters can be extracted in the program. Modelled results based on predicted optical constants were verified by comparison with the p- and s-polarised transmittance measurements performed on a Cary-05E spectrophotometer.

AU9918236

DIRECT DEPOSITION OF QUANTUM SCALE METAL STRUCTURES IN OXIDE MATRICES

S.Dligatch, M.R.Phillips, G.B.Smith and G.M.McCredie
Department of Applied Physics, University of Technology, Sydney,
PO Box 123, Broadway, NSW 2007 Australia

A special feature of obliquely deposited thin films is inclined columnar microstructure which leads to their optical anisotropy. When oblique metal-oxide composite films are produced the metal builds up in specific locations, often in very fine filamental structures, due to the difference in mobilities. Co-deposition from two sources either from the same or from opposite sides of the normal to the film surface is used. The oxide can come from the oxide target or bulk metal with reactive gas (oxygen). Different techniques were employed such as sputtering, cathodic arc, e-beam and thermal evaporation.

A high resolution field emission scanning electron microscope (JEOL JSM-6300F) was used to establish the microstructure of these films at the nano-level. Coated thin cover slip glass substrates were fractured to study the film's cross section parallel to the deposition direction. Secondary Electron and Back Scattering images for the same area of the film were compared to clarify the metal distribution in the oxide matrix. The metal inclusions resemble quantum scale "wires", whose properties can then be investigated.

Obliquely deposited thin films also have useful optical applications, for instance they can exhibit angular selectivity due to the difference in transmittance for the light incident at the same angle from the opposite sides of the surface normal. Angular selectivity is associated with the anisotropic optical absorption of p-polarised light at an oblique incidence. Angular selective glazing is considered to be the most advanced passive window coating available and well suited to hot climates. Its special feature is the ability to attenuate direct solar radiation hence reducing heating and glare while maintaining high forward vision and letting in more solar radiation in winter. It can be used in buildings and automobiles.

AU9918237

PARAMETER PREDICTION FOR MICROWAVE GARNETS

Rodica Ramer
Electrical Engineering, UNSW
Sydney 2052, Australia

Linearity of the microwave parameters (resonance linewidth ΔH and effective linewidth ΔH_{eff}) is demonstrated and their use in the CAD/CAM of new microwave garnets is proposed. Such an approach would combine a numerical database of microwave data and several computational programs.

The model is an applied formulation of the analysis of a wide range of microwave garnets. Experimental results were reported in *Electr. Power Syst. Res. 24(1992), 141-148.*

AU9918238

NITRIDATION OF SI USING MECHANO-FUSION METHOD

Z.L.Li, A.Calka and J.S.Williams

Department of Electronic materials and Engineering
Research school of Physics
Australian National University

It has been found that silicon nitride (Si_3N_4) can be formed by ball milling of Si in ammonia [1]. However only small fraction of Si can be transformed into Si_3N_4. The major milling effect is the formation of poly/nanocrystalline silicon. At this stage of research it is difficult to answer the question why ball milling causes only limited formation of Si_3N_4. It is due to little understanding of processes occurring during milling. Therefore, the purpose of this work was to study nitridation reaction during milling of Si in ammonia. In particular the effect of milling conditions such as milling energies, atmosphere and a form of starting material was studied.

The micro/macrostructural development during milling and subsequent annealing was studied using x-ray diffractometry, thermal analysis, elemental analysis measurement. It was found that the transformed fraction of Si_3N_4 compound is strongly dependent on milling energies and milling atmosphere.

Reference:

1. A.Calka, J.S.Williams and P.Millet, Scripta Metallurgica et Materialia **27**,185(1992)

AU9918239

PREPARATION OF TUNGSTEN-IRON CARBIDE BY BALL MILLING

G.M.Wang, S.J.Campbell, A.Calka* and W.A.Kaczmarek#

School of Physics, University College, University of New South Wales,
Australian Defence Force Academy, Canberra, ACT 2600

* Department of Electronic Materials and Engineering,
RSPhysSE, Australian National University, Canberra, ACT 0200

Department of Applied Mathematics, RSPhysSE,
Australian National University, Canberra, ACT 0200

Due to its beneficial effects on cold wear resistance, toughness and grindability, the η-carbide $(FeW)_6C$ plays an important role in high speed steels, hot working tool steels and superalloys. Conventionally, it is synthesized by argon arc melting followed by annealing at temperatures of over 1000°C [1]. With recent developments in ball milling techniques and the successful synthesis of tungsten carbides and iron carbides by mechanical alloying [eg 2,3 respectively], it is of interest to investigate the scope for preparation of Fe-W carbides by ball milling Fe-W-C mixtures.

Several sets of elemental powder mixtures of Fe-W-C ($W_{46}Fe_{46}C_8$, $W_{60}Fe_{20}C_{20}$ and $W_{34}Fe_{33}C_{33}$) were ball milled using Uni-Ball mill [4] for periods of up to 550 h in vacuum with a ball - to - powder ratio of about 35:1. Depending on the milling time, the main component of the as-milled materials was found to be solid solutions of Fe-W-C or Fe-C. Ternary phase W_3Fe_3C was obtained on annealing the as-milled materials at about 700°C. This product was then found to transfer to $(FeW)_6C$ on heat treatment at about 800°C. The resultant products of the annealing processes were found to depend not only on the annealing temperature, but also the starting composition, especially the initial carbon concentration. Detailed information on the structural and phase evolution during thermal treatment as measured using x-ray diffraction, Mössbauer spectroscopy and thermal analysis is presented. Special interest is focused on the competition for formation in this system between the Fe-C, W-Fe and W-C phases.

[1] M.Bergström, Mater. Sci. Eng., **27** (1977), 257.
[2] G.M.Wang, P.Millet, A.Calka and S.J.Campbell, Mater. Sci. Forum, **179-181** (1995), 183.
[3] P.Matteazzi and G.Le Caër, J. Am. Ceram. Soc., **74** (1991) 1382
[4] A. Calka and A.P. Radlinski, Mater. Sci. Eng. **A134**, (1991) 1350.

AU9918240

SOME IMAGE ARTEFACTS IN NON-CONTACT MODE FORCE MICROSCOPY

B.P. Dinte, G.S. Watson, J.F. Dobson, S. Myhra
School of Science, Griffith University
Nathan, Queensland 4111, Australia
B.Dinte@sct.gu.edu.au

Non-contact mode Atomic Force Microscopy (AFM), performed in air, of two-dimensional hexagonal close-packed (2DHCP) layers of 200nm diameter polystyrene spheres yields images containing artefacts ("ghost spheres") at layer edges and vacancy sites (Fig. 1) [1]. The origin of these artefacts is clearly not the simple convolution of the tip and sample geometries, but must be the interaction between them. A computer program was written to simulate the experimental contours, assuming that the only force between the tip and the sample is the van der Waals (dispersion) force, and that the contours traced by the AFM tip are those of constant force derivative. The energy was calculated by integrating R^{-6} over the volumes of the tip and the sample, with a (constant) arbitrary scaling factor. The experimental contours were reproduced by the simulations (Fig. 2), except for the "ghost" artefacts. The assumption that there is only a dispersion force is thus incorrect. The experiments were performed in air, so that all surfaces were coated by a layer of adsorbed moisture. It is proposed [2] that meniscus forces may be the origin of the artefacts.

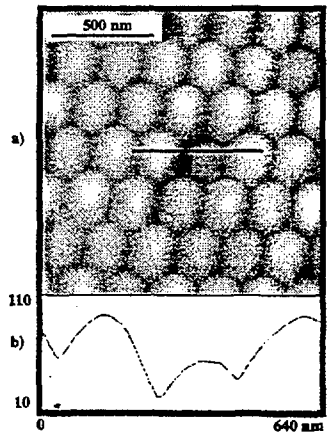

Fig. 1 vacancy (experiment)

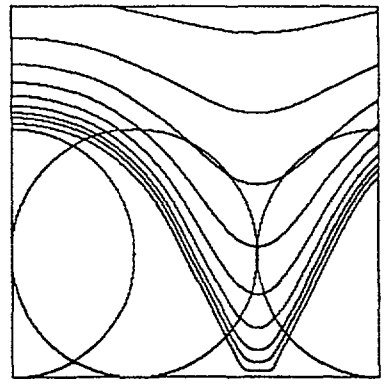

Fig. 2 vacancy (simulation)

[1] M. van Cleef, S.A. Holt, G.S. Watson, S. Myhra, *J. Micros.*, (in press)

[2] B.P. Dinte, G.S. Watson, J.F. Dobson, S. Myhra, *Ultramicroscopy*, (submitted)

Conductor Shape Optimisation Using Thermographic Imaging

D. Jinks and P. Owen
BHP Research, Port Kembla, PO Box 202, NSW 2505

An important consideration in the design of high frequency electromagnetic devices is the effect of conductor shape on current distribution. As a rule of thumb, at high frequency the cross-sectional current distribution resembles a charge distribution in a charged conductor, with current travelling along the surface and particularly along edges. However when other conductors are present the current distribution may change dramatically.

At BHP Research some novel electromagnetic devices are being developed. While the details are proprietary, in one of these the current distribution is an important factor in determining the ultimate performance of the device. Thus we required an experimental technique to analyse the current path. Thermographic imaging was considered because heating is proportional to I^2. The conductors carry very high currents (thousands of ampere) at high frequencies (thousands of hertz) and are water cooled through their hollow centers. Two conductor profiles were tested. These were circular and rectangular, with the rectangular section in two possible orientations, portrait and landscape as shown. Variations in temperature across the conductors of up to 40°C, with equilibrium times of less than one second were observed. It was found that for the circular conductor, the heating was almost exclusively along edge a. This was also the case for the portrait design. The landscape design however was heated fairly evenly about a,b and d, with less heating of c. Calculated current distributions in a finite element model provided qualitative support for these results as did power loss data which showed the landscape design as being the most efficient current carrier and the circular conductor as being the least efficient. For the particular application, the portrait shaped conductor proved to be most effective and this was largely attributable to the current distribution. This experience has shown that thermographic imaging when used appropriately, is a simple way of exploring the current distribution.

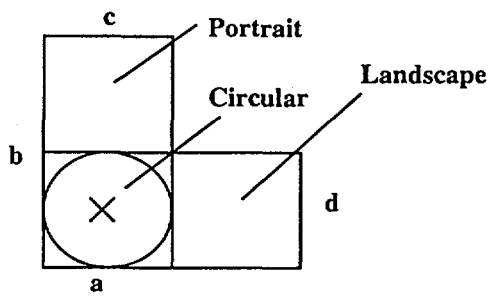

AN EPR STUDY OF THE LACQUER-TYPE BOTTLE DEPOSITS FROM RED WINES

G.J. Troup*, D.R. Hutton*, J.R. Pilbrow*, C.A. Hunter†, D.G. Hewitt††
*Physics Department, †Anatomy Department, ††Chemistry Department
Monash University, Clayton, Victoria 3168

Lacquer-type deposits from 4 naturally aged red wines and one 'artificially' aged wine (by heating for 16hrs at 84° C) were obtained from the Australian Wine Research Institute, Adelaide, and examined by EPR spectroscopy with a Varian E-12 spectrometer working at ~ 9.1 GHz. The naturally aged wine deposits showed Fe^{3+} in a low-symmetry site (g = 4.3), and Cu^{2+} in an axial symmetry site (as deduced from the hyperfine structure) showing superhyperfine structure from N nuclei. A strong free radical signal was also present. The artificially aged wine deposit spectrum was similar, except no superhyperfine structure was present. The deposits are known to be anthocyanines cross-linked to a protein[1]. The older the wine, the more intense was the superhyperfine structure, due to copper-amine interaction with the protein. The free radical signal is associated with the anthocyanines[2].

GT376JB.PA

---

[1] G.J. Troup et al, Australian Wine Industry Technical Conference 1995. Information and Abstracts p.42, Abstract No. 82.
[2] E.J. Waters, L. Peng, K.F. Pocock, G.P. Jones, P. Clarke, P.J. Williams, J.Agric.Food Chem (1994) 42: 1761-6.

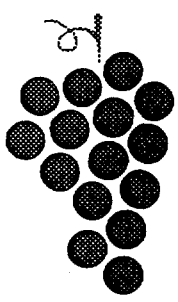

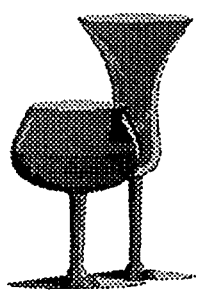

THE POSSIBLE USE OF EPR SPECTROSCOPY FOR PAINT PIGMENT IDENTIFICATION

G.J. Troup*, D.R. Hutton*, M. Bacci†, F. Lotti†, A. Casini†, M. Picollo†
*Physics Department, Monash University, Clayton 3168, Victoria
†Istituto di Ricerca sulle Onde Elettromagnetiche, Firenze, Italy

Visible and near-infra-red reflectance spectroscopy are now routinely used for the identification of paint pigments in Renaissance painting, thus playing a part in authentication and restoration. Since most of the pigments are minerals, and many minerals either contain traces of paramagnetic ions, or have paramagnetic ions in their main components (e.g., chromic oxide, haematite), it seemed logical to determine whether EPR could distinguish between different pigments.

14 pigments of different colours were tested in a Varian E-12 EPR spectrometer, at a frequency of ~ 9.1 GHz. Measurements were made at room (~ 20C) and liquid N_2 temperatures, in the standard special quartz sample tubes. The active volume is 0.15ml, but at most, a volume of sample (powder) one tenth of this was used.

The spectra (to be shown) clearly demonstrate that EPR can distinguish between different pigments. The power was 1 milliwatt, the modulation amplitude 4 gauss, the total field sweep 10,000 gauss, centred 5000 gauss and the amplification between 10^2 and 10^4, as indicated on the charts. The signal to noise ratio is excellent, and sensitivity could be increased (if necessary) by a factor of ~ 10^3, thus allowing much smaller samples to be tested.

Because the signals are so strong it should be possible to scan at least small painted canvases by the following non-destructive technique, using existing equipment. All that is required is a modified resonant cavity: it must have a high Q, and a slot where the magnetic field is maximum, and the electric field zero. The canvas can thus be placed flush with the waveguide, to interact with the microwave magnetic field emanating from the slot.

BLESSED NIELS STENSEN: DANE, FLORENTINE, AND BISHOP; A FOUNDING FATHER OF CRYSTALLOGRAPHY

A.E. Smith and G.J. Troup
Physics Department, Monash University, Clayton, Victoria 3168

Niels Stensen (Niccolo Stenone in Italian), 1636-1686, beatified in 1988, was a famous anatomist, geologist, palaeontologist and mineralogist in his day. He is one of the founding fathers of crystallography, and is generally regarded as the first to have published the law constancy of interfacial angle, in his work `De solids intra solidum naturaliter contento dissertations prodromus' (A pilot study for a dissertation on the solid naturally contained with a solid).

A brief account of his life and achievements will be given. His drawings of quartz crystals, and fibrous haematite crystals from Elba, which he studied, will be featured, together with his explanatory notes for them, and other selected statements on crystallography from the `Prodromus'.

Not Included

BACTERIAL LEACHING OF PYRITIC GOLD ORES

Frank M. Gagliardi[1], John D. Cashion[1], L. Joan Brown[1] and William H. Jay[2]

[1] Physics Department, Monash University, Clayton, Victoria, 3168

[2] Chemical Engineering Department, Monash University, Clayton, Victoria, 3168

Gold-containing pyritic ores (pyrite, pyrrhotite, arsenopyrite) are usually refractory to cyanidation. Concentrates can be obtained by flotation, with grades in excess of 50 g Au/t, but recovery of the gold requires the removal of the sulphur from the ore. This can be achieved by roasting (which produces sulphur dioxide emissions), pressure oxidation (expensive and thus only suitable for large high grade deposits), pressure leaching (not currently commercial) or bacterial oxidation.

The bacterial oxidation process is well known in nature but has only recently come under investigation as a viable and relatively clean method of gold recovery from ores. However there is currently little information about the process at an atomic scale. It is known that the bacterial attack progresses preferentially along grain boundaries which is precisely where the gold has been deposited from aqueous infiltration.

Samples have been obtained from the Wiluna mine in Western Australia consisting of the original ore, 2 pre-treatments, and from six successive bacterial reactors. ^{57}Fe Mössbauer spectra taken at room temperature show only two quadrupole split doublets which can be ascribed to pyrite, FeS_2, and arsenopyrite, FeAsS. However, the presence of any superparamagnetic oxide or oxyhydroxide species would be expected to give a spectrum very similar to that of pyrite and would be undetectable in small quantities. At a temperature of 5K, a broad magnetically split sextet is observable with a mean hyperfine field of approximately 50T. This field is characteristic of magnetically ordered ferric iron surrounded by an octahedron of oxygens. The intensity and characteristics of this subspectrum alters through the series and interpretations will be given on the oxidation products of the bacterial leaching.

TP28

CHEMICAL AND MORPHOLOGICAL CHANGES DURING PRODUCTION OF CONDUCTING CARBONS FROM FERROCENE-POLY(FURFURYL ALCOHOL)

J. Ozaki[1], J. D. Cashion[2] and L. J. Brown[2]

[1] Institute for Chemical Reaction Science, Tohoku University, Sendai, Japan

[2] Physics Department, Monash University, Clayton 3168 Australia

Carbons are obtained by heating organic substances up to 1000^{0}C under inert atmosphere. The electronic properties of carbons change dramatically during this carbonisation process. By controlled preparation, it is possible to obtain electronically functional materials. The addition of iron to the organic starting material has a strong modifying effect and, in particular, carbonising a ferrocene-poly(furfuryl alcohol) (PFA) mixture at 700^{0}C produces a carbon with a comparable electron transfer rate to platinum.

^{57}Fe Mössbauer spectra showed that the first transformation of the ferrocene is to magnetite, Fe_3O_4, at 200-300^{0}C. At 600^{0}C, the magnetite is converted to wustite, FeO, while at 650^{0}C α-iron starts to appear. The final products at 800^{0}C were α-iron, γ-iron and cementite, Fe_3C. Under the SEM, the material still showed a polymer-like appearance up to 500^{0}C and became charged under the beam. Between 600-650^{0}C the appearance resembled glassy carbons with hard and smooth surfaces, while the furry surface characteristic of high activity carbons was observed for temperatures above 700^{0}C. Arrhenius plots of the electrical conductivity of the various samples from 5-300K showed dramatic changes from temperature independence to extreme sensitivity and with linear and non-linear behaviour.

The tentative explanation for these results is that the iron promotes the elimination of oxygen from the initial PFA structure to produce magnetite. At 600-650^{0}C, the magnetite is carbothermically reduced to wustite and α-iron, forming glassy carbon. Above 700^{0}C, the iron dissolves carbon atoms to make a solid solution. On cooling, some of this fractionates into graphitic carbon, cementite and γ-iron stabilised by the carbon atoms. We believe that the furry surface is produced in this cooling process.

BALL MILLED MAGNETIC POWDERS

Sally G. Whitehead, John D. Cashion and L. Joan Brown
Physics Department, Monash University, Clayton, Victoria, 3168

Kneller and Hawig[1] have proposed the theory and technical realisation of a new type of permanent magnet known as an exchange-spring magnet. Such magnets consist of approximately 10% hard magnetic material and 90% soft magnetic phase, yet display remarkably good hard magnetic properties. The microstructure of exchange-spring magnets is that of ~10nm islands of the hard phase, separated by approximately the same distance, within a matrix of the soft phase.

To date, most exchange-spring magnets have been synthesised with both hard and soft phases containing iron, which makes it difficult to study the magnetic properties of each phase separately. We have attempted to synthesise exchange-spring magnets consisting of (i) Alnico and Fe, and (ii) $Nd_2Fe_{14}B$ and Gd, using the technique of ball milling. The composition and microstructure of the ball milled powders was investigated using XRD, SEM and TEM. The bulk magnetic properties of each sample were measured with a SQUID magnetometer, while ^{155}Gd and ^{57}Fe Mössbauer spectroscopy were used to measure the magnetisation of the phases which contained these elements.

Exchange-spring magnetic properties were not realised in either of the two systems studied. TEM analysis was inconclusive as to the dimensions of the phases within each sample. However, the SQUID and Mössbauer effect measurements both indicated that the two phases were acting as a coherent magnetic system. It is probable that the required microstructure was not formed in the case of the $Nd_2Fe_{14}B$ and Gd powder, where the particle size indicated by SEM was very large (~200μm). For the Alnico/Fe system, it is possible that ball milling undermined the microstructure of Alnico, destroying its hard magnetic properties.

[1] Kneller, E. H., and Hawig, R., *IEEE Trans Magn*, **27**, 4, 3588 (1991).

REVIEW OF METHODS FOR DETERMINING THE LOADED Q-FACTOR OF MICROWAVE RESONATORS.

Kenneth Leong*, Robert Grabovickic*, Janina Ceremuga*

*James Cook University of North Queensland, Department of Electrical and Computer Engineering, Townsville, Australia.

Abstract

Measurements of material properties such as loss tangent and surface resistance at microwave frequencies require the accurate determination of the quality factor Q of the resonating structure in which the sample is incorporated. We review various techniques used so far to determine the loaded quality factor Q_L of microwave resonators. We also present a method developed to accurately obtain Q_L from measurements of complex transmission coefficients S_{21} close to the resonant frequency using fractional linear curve-fitting. Verification of the technique was done using a sapphire rod resonator with $YBa_2Cu_3O_7$ end-plates.

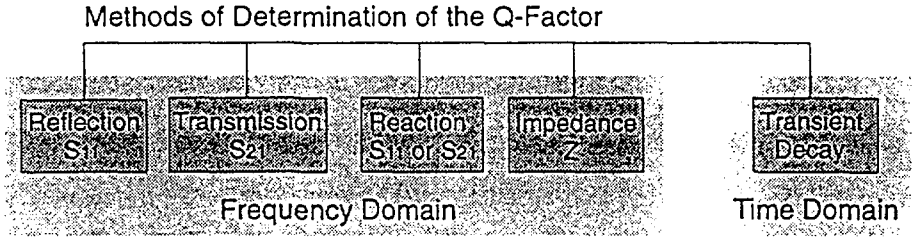

Figure 1 *Techniques used to find Q-factor*

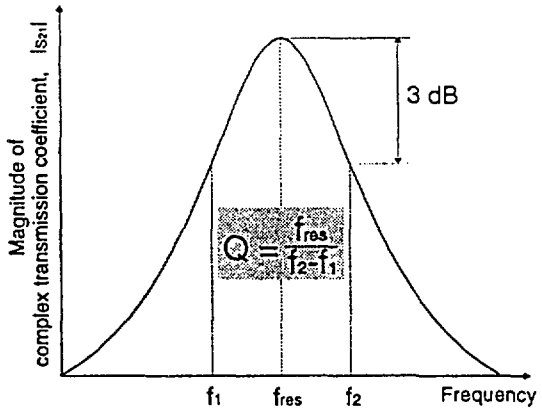

Figure 2 3 dB Method

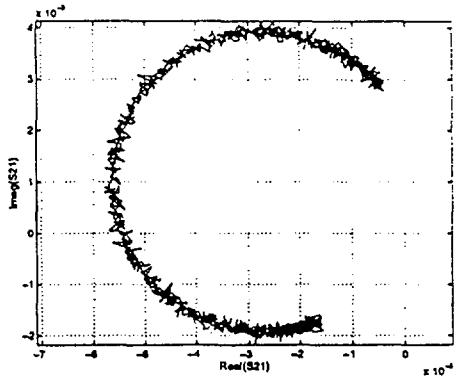

Figure 3 Experimental S_{21} Q-circle

References

[1] E.L. Ginzton, "Microwave measurements", McGraw Hill Book Co., pp 403-408, 1957.
[2] D. Kajfez And P. Guillon, "Dielectric resonators", Vector Fields, pp 53-63, 1990.
[3] D. Kajfez, "Q factor", Vector Fields, 1994.
[4] M.C. Sanchez, E. Martin, J.M Zamarro, IEE Proc. Vol. 137, Pt. H, pp 209-212, Aug. 1990.

TP31

INVAR FE-NI AND THE SANTA CATHARINA METEORITE

J. Chadwick

Department of Physics, Monash University, Clayton, Victoria 3168, Australia.

The Invar Effect phenomenon of length invariance in alloys was first observed in Fe-Ni by Guillaume in 1897 [1]. Since then, many models have been proposed to account for the behaviour [2]. It is believed that the very low thermal expansion coefficient is the result of a large, positive volume magnetostriction caused by moment-volume instabilities. However, the details of the underlying physical mechanism remain unclear. The Santa Catharina meteorite contains 62 at.% Fe and 35% Ni, placing it in the Invar range; thus, Mössbauer effect spectra of the meteorite are potentially relevant to understanding the Invar problem. The spectra show a component which has a drastic temperature-dependent line broadening, and other components which suggest that a phase of average composition $Fe_{0.72}Ni_{0.28}$ has more than one magnetic state. These features may shed some light on the mechanism responsible for Invar behaviour.

References

[1] Guillaume, C.E., Phys. Soc. Lond. Proc. **32**, 374 (1920).

[2] Wasserman, E.F., *Ferromagnetic Materials* **5**, ch. 3, Elsevier Science Pub. 1990.

AU9918250

MAGNETIC ANISOTROPY OF AMORPHOUS ALLOY RIBBONS

Xiang-Yuan Xiong, Paul L. Rossiter and Trevor R. Finlayson*
Department of Materials Engineering, and
*Department of Physics, Monash University, Clayton, Victoria. 3168

An amorphous alloy consists of a random, close-packed structure. The lack of any unique direction in the structure should lead to zero magnetocrystalline anisotropy and hence excellent soft magnetic properties. In practice, while amorphous alloy ribbons do generally exhibit high permeabilities and low losses, some are found to have in-plane magnetic anisotropy, K_u, with values for K_u as big as 10^4 erg/cm^3 determined using torque magnetometry.[1,2]

In amorphous alloy ribbons prepared by melt spinning, two types of magnetic anisotropy have been identified. One is perpendicular anisotropy which has an easy magnetisation axis normal to the ribbon plane; the other is in-plane anisotropy which usually has an easy magnetisation axis lying in the ribbon plane and showing two-fold symmetry. It has been confirmed that the perpendicular anisotropy is due to the coupling between magnetostriction and residual stress and causes the maze domains.[2] As for the in-plane anisotropy, by investigating the effect of annealing treatment on the magnetic torque curves and the dependence of K_u on temperature for Fe-based, FeNi-based and Co-based amorphous alloy ribbons, it is obtained that this in-plane anisotropy consists of two parts: One is stress anisotropy, $K_{u\sigma}$, associated with the coupling between magnetostriction and internal stress. This internal stress is a macroscopic internal stress, rather than the local stress. $K_{u\sigma}$ will affect the magnetisation process directly, but it can be eliminated by stress relief annealing.

The other is surface shape anisotropy, K_{us}, which is much bigger than $K_{u\sigma}$. By comparing K_{us} with the magnitude of the field-induced anisotropy, K_{in}[3], it is found that the surface-shape anisotropy, K_{us}, determined from the variation of the torque with θ, does not directly influence the magnetisation process. By 'does not directly influence' we mean that K_{us} can not be used as a variable to estimate the magnetisation process. It may reflect the surface topology and affect the motion of domain walls, to some extent, by means of pinning. In summary, we conclude that in amorphous alloy ribbons the value of K_{us} determined by torque magnetometry does not reflect the real magnetic anisotropy which governs the magnetisation process. It mainly reflects the surface shape anisotropy.

[1] Xiang-Yuan Xiong and Kai-Yuan Ho, Journal of Magnetism and Magnetic Materials 94 (1991) L29-L34.
[2] H. Fujimori, Amorphous Metallic Alloys, ed. F. E. Luborsky, (Butterworths, London, 1983) p300.
[3] Kai-Yuan Ho and Xiang-Yuan Xiong, Journal of Magnetism and Magnetic Materials 111 (1992) 71-74.

Nuclear Magnetic Resonance on Oriented Nuclei in $MnBr_2.4H_2O$

M. J. Prandolini, W. D. Hutchison, J. Leib[1] and D. H. Chaplin,

Department of Physics, University College, UNSW,

Australian Defence Force Academy, Canberra ACT 2600, Australia.

G. J. Bowden

School of Physics, University of New South Wales,

Sydney NSW 2052, Australia.

Precision Nuclear Orientation and NMRON studies have been undertaken on the antiferromagnetic insulator (^{54}Mn)$MnBr_2.4H_2O$ employing the concept of magnetic field induced enhanced nuclear spin–lattice relaxation to obtain working gamma anisotropies as large as -32% (35mK). The results reflect significant differences in detail to those obtained earlier on (^{54}Mn)$MnCl_2.4H_2O$ [1]. NMRON on (^{54}Mn)$MnBr_2.4H_2O$ was first obtained by Turrell [2], however fast magnon cooling was not applied, and so that study was limited to gamma anisotropies of about -5%. In this poster we present, (i) zero field quadrupolar split sub–resonances ($m = \pm3,\pm2$), ($\pm2,\pm1$) and ($\pm1,0$), with the latter two obtained through double and triple resonance techniques, (ii) a two–stage spin flop with the magnetic field aligned along the c-axis, confirming a previous result by Becerra [3] who first observed an intermediate phase between the antiferromagnetic and fully spin flopped phase down to 0.5K using differential magnetic susceptibility, and (iii) NMRON resonances in applied field, thus providing increased accuracy for the nuclear hyperfine parameters.

References

[1] A. L. Allsop *et al.*, Journal of Physics C: Solid State Physics **17**, 915 (1984).

[2] B. G. Turrell, Hyperfine Interactions **22**, 187 (1985).

[3] C. C. Becerra, A. P. Filho, and N. F. O. Jr., Solid State Communications **16**, 791 (1975).

---

[1]On leave from Department of Physics, Physikalisches Institut, Universität Bayreuth, Germany.

PARAMAGNETIC PROBES TO STUDY $PrNi_5$?

W D Hutchison, S J Harker, G A Stewart and D H Chaplin

School of Physics, University College, The University of New South Wales
Australian Defence Force Academy, Canberra ACT 2600, Australia

and

N Kaplan

Racah Institute of Physics, Hebrew University of Jerusalem
Jerusalem, Israel

The Van-Vleck paramagnet $PrNi_5$ has been the focus of many studies in the past as a result of its usefulness as a nuclear cooling agent (see for example [1]). Extensive continuous wave praseodymium NMR measurements have been carried out on this compound [2]. However pulsed NMR and therefore precise relaxation measurements particularly at mK temperatures have proved elusive. In this work we have proposed to use radiative gamma-ray detection to indirectly measure Pr NMR in $PrNi_5$ via cross relaxation to suitable paramagnetic impurity probes placed at Ni lattice sites. ^{57}Co was chosen as the most compatible nuclear orientation isotope with an appropriate nuclear g-factor. The choice of ^{57}Co also allows the use of Mössbauer spectroscopy to check the site occupancy.

This poster details the production of a ^{57}Co doped $PrNi_5$ single crystal specimen including the specimen preparation problems encountered, ^{57}Fe Mössbauer and preliminary nuclear orientation measurements.

[1] C Buchal, K J Fischer, M Kubota, R M Mueller and F Pobell, J. Phys. **39** (1978) L457.

[2] N Kaplan, D L Williams and A Grayevsky, Phys.Rev. B **21** (1980) 899.

THULIUM ENVIRONMENT IN THE CERAMICS Tm_2BaCoO_5 AND Tm_2BaNiO_5

S. J. Harker, G. A. Stewart and A. V. J. Edge

School of Physics, University College, The University of New South Wales, Australian Defence Force Academy, Canberra ACT 2600

It is well known that nearly all of the so-called "1:2:3 phases" $RBa_2Cu_3O_7$ (R = rare earth) are superconducting below approximately the same temperature, regardless of whether the rare earth atom is magnetic or not. This has stimulated interest in the nature of the very weak magnetic interaction between the copper and rare earth sublattices of related ceramic phases. The situation is complicated by the electrostatic interaction (the local crystal field) which distorts the rare earth ions' 4f shells and "quenches" their magnetic moments. One experimental approach is to investigate how the local magnetic and electrostatic interactions vary when the copper atoms are systematically replaced by other transition elements.

The green cuprates R_2BaCuO_5 are found often as impurity phases in the synthesis of the 1:2:3-type superconductors and have an orthorhombic structure (space group Pnma) with two distinct rare earth sites of monoclinic (m) point symmetry. Following on from a previous ^{169}Tm Mössbauer spectroscopy investigation of Tm_2BaCuO_5, this work presents new ^{169}Tm Mössbauer results for isostructural cobaltates and nickelates (in which the Cu atoms are replaced by Co and Ni atoms respectively). The temperatures at which the transition metal sublattice orders antiferromagnetically are observed to satisfy $T_N(Cu) > T_N(Ni) > T_N(Co)$. Whereas the previous ^{169}Tm measurements (for $T > T_N$) were unable to distinguish between the two Tm sites of the cuprate, the new results show that the crystal fields are markedly different for the the two sites of both the cobaltate and the nickelate. This is believed to be due to the stronger dependence of Co-O and Ni-O charge transfer on the type of site that the oxygen atom occupies. Although the Tm sites are structurally similar, their coordination polyhedra involve different combinations of oxygen equivalent sites.

Low-Field Magnetic Properties Of $Fe_{3-x}Mn_xSi$ Alloys

T. Ersez, G.T. Etheridge and T.J. Hicks

Department of Physics, Monash University, Clayton, Victoria 3168, Australia.

Low field dc susceptibility measurements (using the VSM, Faraday and SQUID magnetometers) have been made on an $Fe_{3-x}Mn_xSi$ alloy with composition $x = 1.14$ and on a single crystal with $x = 1$. The observed and calculated results show a demagnetising effect to be occuring in and around the ferromagnetic regime. This along with magnetic neutron diffraction evidence brings into question earlier assertions of spin-glass or mictomagnet like properties and the critical exponent estimates for these alloys because they lie within the region of significant demagnetisation. The results from single crystal measurements along separate crystallographic directions have shed some light on the magnetic anisotropy of the complex low temperature phase in these materials.

NANOSTRUCTURED HEXAGONAL FERRITES

W. A. Kaczmarek and B. W. Ninham
Institute of Advanced Studies, Research School of Physical Sciences and Engineering
Australian National University, Canberra, A.C.T. 0200, Australia. wak110@phys.anu.edu.au

Mechanical treatment of ferrite materials has become extremely important in many processes in technology of magnetic materials during last few decades. Most previous investigations describe improvements in 'classical' ceramic method in which premilled components(oxides and/or carbonates) are thermally treated-calcined to yield a final crystalline product.

Little research has used barium ferrite as a starting material, and little or no work has investigated the influence of milling time on crystal structure and magnetic properties. The crude milling devices used in such studies suffered from lack of control in prescribing milling conditions which have been neglected. While the nature of mechanochemical reactions involving nonmetallics has progressed the fundamental processes governing the evolution of structure, kinetics, and thermodynamics of induced chemical or physical transformations remain misunderstood. Our recent published results [1-3], together with new research will address the following changes in barium and strontium ferrites induced by mechanochemical processing: 1) generation of amorphous (disordered) and nanocrystalline phases, 2) mechanical activation and changes in solid surface properties, 3) mechanochemical solid state reactions either at the surface or in the bulk and 4) polymorphic transformations and alternations in magnetic properties.

References

[1] W. A. Kaczmarek and B. W. Ninham, Mater. Chem. Phys. 40 (1995) 21.

[2] W. A. Kaczmarek and B. W. Ninham, J. Appl. Phys. 76 (1994) 6065.

[3] W. A. Kaczmarek and B. W. Ninham, IEEE Trans. Magn. MAG-30 (1994) 717.

INTERBAND ABSORPTION IN THE PRESENCE OF A 2D ELECTRON GAS: FERMI EDGE SINGULARITIES AND THE ROLE OF NEGATIVELY CHARGED EXCITONS

S. A. Brown[a], Jeff F. Young[b], J. A. Brum[c], P. Hawrylak[d] and Z. Wasilewski[d]

[a] *School of Physics, University of New South Wales, Sydney 2052, Australia.*

[b] *Dept. of Physics, University of British Columbia, Vancouver, Canada.*

[c] *Instituto de Fisica, UNICAMP, Campinas, Brasil.*

[d] *Institute of Microstructural Sciences, National Research Council, Ottawa, Canada.*

It is well known that when light is incident on an *undoped* semiconductor, photo-created conduction electrons and valence holes form strongly bound pairs (excitons (X)) which dominate optical spectra. In 2D semiconductor systems the presence of a very small density of excess carriers causes the formation of negatively charged excitons (X^-)[1], which are an analogue of the negatively charged hydrogen atom (H^-). In contrast to bound states in 3D, which are completely screened by a large density of carriers, it is expected that in 2D the potential of a valence hole always contains a doubly occupied bound state (i.e. X^- always exists), even in the presence of high densities of carriers.

When a valence band hole is introduced (optically) into a *doped* n-type semiconductor system, the free conduction band electrons react by attempting to screen the hole and the result is a singularity in absorption and photoluminescence (PL) spectra at transition energies that correspond to electron states close to the Fermi level[2]. This enhancement of optical spectra, known as the Fermi-edge singularity (FES), was first understood in relation to the equivalent problem of X-ray absorption from localised atomic core states in simple metals[3]. This theory cannot be applied directly to two-dimensional electron systems in semiconductor heterostructures since it does not account for i) the presence of a doubly occupied bound state (X^-), ii) the existence of *gapless* plasmons in 2D, iii) the finite mass of the valence hole. and iv) electron-electron interactions, which are more important in 2D than in 3D due to i) and ii).

We have studied these problems experimentally using absolute absorption spectra from a series of modulation-doped GaAs/AlGaAs multiple quantum well samples with different carrier densities. We observe the evolution (as a function of carrier density) from the low density excitonic ground state to the FES at high carrier density and find that the results are in good agreement with theoretical calculations which include many-body effects and the doubly occupied bound state (X^-) in a *realistic* way. In particular, the evolution of the absorption lineshape in the experiment is found to be consistent with the predicted variation of the strength of the singularity (given by the calculated binding energy of the doubly occupied bound state).

1 A. J. Shields et al, Phys. Rev. B **51**, 18049 (1995).
2 M. S. Skolnick et al, Phys. Rev. Lett. **58**, 2130 (1987).
3 G. Mahan, 'Many Particle Physics', Plenum Press, New York (1981);
M. Combescot and P. Nozieres, J. Physique **32**, 913 (1971).

High Sensitivity to Temperature and Quantum Effects in Vanadium Oxide Diodes

V.A. Kuznetsov, D. Haneman

School of Physics, University of New South Wales, Sydney 2052, Australia

Vanadium is a metal with variable valence, forming a number of oxides. Some of the vanadium oxides exibit a semiconductor-metal phase transition accompanied by resistivity changes by a factor of 10^3 in thin films. The phase transition properties make such oxides suitable materials for fabrication of a variety of electrical and optical devices, including electrical switching devices, thermistors and bolometers. Morever, an 80000-element infrared bolometric detector array based on VO_2 film was recently fabricated by Honeywell, with noise equivalent temperature difference 0.1 °C. The temperature coefficient of resistance of the VO_2 used (in its semiconducting state) was 2 % per °C. We have developed a way of preparation of vanadium oxide films by the method of oxidation of evaporated vanadium films, and found it possible when used as a diode, to achieve a temperature coefficient of resistance of 25 % per °C. The nature of the contact influenced sensitivity.

We have also found quantised step-like features in the I-V characteristic in the switching vanadium oxide thin film devices, of the type reported in literature for vanadium oxide films, but not in the presence of switching. Quantised steps have also been reported for diode structures of hydrogenated amorphous silicon films. By removing parallel conductance, the quantized conductance in our case appeared to increase in integral and half integral multiples of $2e^2/h$. Optical transmission data show our vanadium oxide films to consists of a mixture of different oxides, mainly VO_2 and V_2O_5.

SPECTROSCOPY OF BERYLLIUM IMPURITY IN GALLIUM ARSENIDE*

R. A. Lewis
Department of Physics, University of Wollongong, Wollongong NSW 2522, Australia
T. S. Cheng, M. Henini and J. M. Chamberlain
Department of Physics, University of Nottingham, Nottingham, NG7 2RD, UK

Beryllium, substituting for gallium in gallium arsenide, is an acceptor impurity, whose behaviour can be described within the effective mass approximation. The energies of shallow substitutional acceptor impurities in gallium arsenide have recently been calculated by Fiorentini [1]. Fiorentini improves on earlier theory by including for the first time in the calculation the cubic term, split-off band coupling and dispersive impurity screening.

Far-infrared absorption due to Lyman transitions of the beryllium acceptor in gallium arsenide has been measured in bulk MBE-grown samples at various temperatures and under different illumination conditions. The transitions observed in the present spectra are much sharper and more intense than those observed in earlier work [2] and are believed to be the sharpest acceptor absorption lines observed to date in gallium arsenide. The G, D and C lines have energies (at 1.9 K) of 134.46±0.05, 166.76±0.05 and 182.30±0.05 cm^{-1}, respectively. Fiorentini's recent calculation of the acceptor energy spectrum in gallium arsenide is in good agreement with these results.

The absorption lines at 1.9, 5.1, 5.4, 10, 15, 20, 25, 30, 35 and 40 K were fitted with Lorentzian curves to allow precise evaluation of the line positions, widths and intensities. The energy of each line was found to decrease slightly with increasing temperature. The change observed is accounted for within the framework of the effective mass theory. At 1.9 K the G, D and C linewidths are 0.87±0.15, 1.16±0.04 and 1.86±0.05 cm^{-1}, respectively, and the integrated intensities are in the ratio 8.7±4.3:100:57.6±9.8. The overall areas decrease with temperature, but the ratio of line strengths remains fairly constant. External illumination during cooling or measurement had no effect on the observed spectra.

**Work supported by the Australian Research Council and the University of Wollongong.*

[1] V. Fiorentini, *Phys. Rev. B* **51**, 10161 (1995).

[2] A. A. Reeder, B. D. McCombe, F. A. Chambers and G. P. Devane, *Phys. Rev. B* **38**, 4318 (1988); A. A. Reeder, J.-M. Mercy and B. D. McCombe, *IEEE J. Quantum Elec.* **24**, 1690 (1988); A. A. Reeder, B. D. McCombe, F. A. Chambers and G. P. Devane, *Superlattices and Microstructures* **4**, 381 (1988); A. A. Reeder, B. D. McCombe, F. A. Chambers and G. P. Devane, *Inst. Phys. Conf. Series* **95**, 21 (1989).

EFFECT OF ACOUSTIC PHONON SCATTERING ON THE WIDTH OF THE ELECTRICAL MULTISTABILITY IN A DOUBLE BARRIER STRUCTURE

D. J. Fisher and C. Zhang

Department of Physics, University of Wollongong, New South Wales 2522, Australia

When electrons tunnel through a double barrier structure, there exists a region of bistablity (or tristability) in the current-voltage characteristics due to the dynamical charge feedback effect in the resonant well. That is, there is a range of the bias (ΔV) for which there are more than one stable current modes. We propose a mechanism of acoustic phonon assisted tunneling to explain the experimentally observed non-monotonic behaviour of this width of the tristable region with temperature[1]. By using the S-matrix scattering formalism, we have solved the energy and temperature dependent tunneling rate for electrons inelastically tunneling through a double barrier structure, similar to the LO phonon case[2]. It is found that the width of the region of electrical multistability has a single maximum as experimentally observed. Furthermore, contrary to the previous proposal, our result shows that electron thermal activation is not the dominant mechanism in controlling this temperature dependent width.

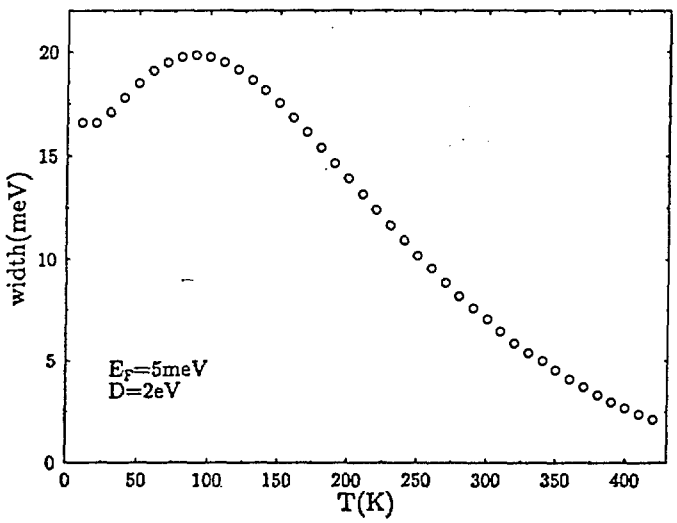

Figure 1: Plot of the calculated temperature dependent tristability width, ΔV. E_F is the Fermi energy, D is the deformation potential parameter. D sets the strength of the electron-acoustic phonon interaction.

Refs. [1] Lerch M L F *et al.* 1994 Solid State Electron. **37** 961
[2] Wingreen N S, Jacobson K W and Wilkins J 1988 Phys. Rev. Lett. **61** 1396

AU9918260

STRESS-ENHANCEMENT OF CERTAIN SPECTRAL LINES OF ANTIMONY IN GERMANIUM*

R.J. Baker and P. Fisher
The Department of Physics, University of Wollongong, Wollongong, NSW 2522, Australia

The optical spectroscopy of acceptors and donors in semiconductors has played a pivotal role in understanding these defects and their hosts.[1] Studies of the classic shallow group III and group V impurities in the archetypal semiconductors silicon and germanium led the way in this respect. The use of applied fields is important in this program[1,2] permitting very detailed comparisons to be made with the theoretical models.[3] One of the predictions in this area which, hitherto, has not been examined in any detail, relates to the stress dependence of the intensities of spectral lines of group V donors in germanium. In particular, a compressive force, **F**, applied along a <1 1 1> direction will, if large enough, cause all but one of the stress-induced transitions to m = 0 states and to m = ±1 states to be eliminated for E∥F ($E_{\parallel}$) and E⊥F ($E_{\perp}$), respectively.[4] Here **E** is the electric vector of the exciting radiation and m is the orbital magnetic quantum number. This large stress limit can be readily achieved for Sb in Ge since the valley-orbit splitting for this, the shallowest group V donor, is very small.[5,6] Part of the effect is due to thermal depopulation of the upper ground states as their separation from the lower ground state increases. In addition to this, the intensities of components arising from the valley-orbit split ground state change with stress as the combinations of conduction band valleys determining their eigenvectors change. As an example, for $E_{\parallel}$ these effects cause the lower energy np_0 components which arise from the lower ground state to increase in intensity by a factor of 4 while the other np_0components and the $np_{\pm}$ components, disappear.[4] In the earlier measurements,[4] the available experimental facility was not adequate to observe most of the details of this effect. These measurements have now been repeated using state-of-the art equipment. As will be seen, the predictions are borne out, producing spectacular results.

**Work supported by the Australian Research Council and the University of Wollongong Board of Research and Postgraduate Graduate Studies.*

1 A. K. Ramdas and S. Rodriguez, *Rep. Prog. Phys.* **44**, 1297 (1981).
2 R. E. M. Vickers *et al.*, *Solid State Commun.* **65**, 271 (1988); P. Fisher *et al.*, *Phys. Rev. B* **47**, 12999 (1993).
3 R. Buczko, *Nuovo Cimento* **9D**, 669 (1987); J. Broeckx, *Phys. Rev. B* **43**, 9643 (1991); W. O. G. Schmitt *et al.*, *J. Phys.: Condens. Matter* **3**, 6789 (1991).
4 J. H. Reuszer and P. Fisher, *Phys. Rev.* **165**, 909 (1968).
5 P. Fisher, *J. Phys. Chem. Solids* **23**, 1346 (1962); J. H. Reuszer and P. Fisher, *Phys. Rev.* **135**, A1125 (1964).
6 I. L. Beinikhes and Sh. M. Kogan, *Inst. Phys. Conf. Series* No. **95**, 161 (1989).

MINORITY CARRIER TUNNELING RESONANCES IN SEMICONDUCTOR DOUBLE BARRIER STRUCTURES.

M.L.F. Lerch, A.D. Martin, T. Silver, P.E. Simmonds
and L. Eaves#
Department of Physics, University Of Wollongong, Wollongong, NSW 2522.
 # Department of Physics, University Of Nottingham,
Nottingham, NG7 2RD, England

The phenomenon of resonant tunneling has been widely studied in semiconductor double barrier structures since its prediction by Tsu and Esaki [1]. Most studies have been on majority carrier tunneling in both p and n doped GaAs devices with AlGaAs barriers [2,3]. However, minority carriers can be created by above (GaAs) bandgap radiation and these also tunnel through the device under bias, giving rise to distinct resonances in the current vs. voltage characteristic. In standard device structures, above bandgap radiation floods the whole device with carriers of both signs, leading to a variety of effects which complicate the interpretation of results. Nevertheless, preliminary measurements on one device indicate minority carrier accumulation in the central quantum well near resonance, an effect which is known to cause intrinsic electrical multistability when the sheet charge density is sufficiently high [4]. This raises the intriguing possibility of optically induced electrical multistability in suitably designed devices.

This paper will report these results and also measurements made on a device with an InGaAs emitter pre-well which can be selectively excited using below bandgap radiation.

References.

[1] R. Tsu and L. Esaki, Appl. Phys. Lett. **22**, 562 (1973).

[2] M.L. Leadbeater *et al.* J. Phys.: Condens. Matter **1**, 10605 (1989).

[3] R.K. Hayden *et al.* Phys. Rev. B.**49**, 10745 (1994).

[4] C. Zhang *et al.* Phys. Rev. Lett. 72, 3397 (1994).

INTRODUCTION TO THE LA TROBE UNIVERSITY II-VI MBE FACILITY.

Y. Zhang, E. Huwald, J. D. Riley and R. C. G. Leckey
School of Physics, La Trobe University, Victoria 3083, Australia

Molecular Beam Epitaxy (MBE) is a versatile technique for growing thin epitaxial structures made of semiconductors, metals, or insulators. Compared with previous vacuum deposition techniques, MBE has much more precise control of the beam fluxes and deposition conditions. In this poster we will describe the construction of a II-VI MBE facility which has been designed and constructed by La Trobe University School of Physics. Consequently, we will provide a general view of researches which can be done based on the II-VI MBE machine.

ILLUMINATION EFFECT ON TRANSPORT PROPERTIES AND PHOTO CONDUCTIVITY MEASUREMENTS OF HIGH MOBILITY 2D HOLE GAS IN Si-SiGe HETEROSTRUCTURES

V.A. Stadnik[a], E.E. Mitchell[a], R.G. Clark[a], F.F. Fang[b], P.J. Wang[b] and B.S.Meyerson[b]
[a]National Pulsed Magnet Laboratory, University of NSW, Sydney 2052, Australia
[b]IBM T.J. Watson Research Center, Yorktown Heights, NY 10598, USA

Impressive progress in the growth of high quality Si-based semiconductor devices has lead to new physics in low dimensional electron and hole systems. For p-type Si-SiGe heterostructures, one of the most interesting features is an unusual spin degeneracy in the 2 dimensional hole gas (2DHG), which has been shown to be associated with important transport properties, particularly a low temperature insulating phase (IP) at Landau level filling factor ν=1.5 that is indicative of a new type of ground state for the 2D holes.

In this report we study the effect of illumination on transport and photoconductivity (PC) measurements of the 2DHG in Si-SiGe at temperatures 100mK-4.2K, magnetic fields 0-15T and extremely low level light excitation ~1nW, which avoids simple heating effects. Standard transport measurements carried out for dark and illuminated states of the samples demonstrate that illumination can significantly quench the resistance of the IP at ν=1.5 due to a lifting of the spin degeneracy of the 2DHG. The effect of illumination on transport properties of the 2DHG has irreversible character, which is analogous to the well-known persistent PC effect in GaAs devices.

Analysis of the experimental data allows us to obtain values of important physical parameters such as the 2D hole concentration, mobility, effective mass and momentum relaxation time, both before and after sample illumination, with relatively high precision ~1%. However evaluation of the g-factor is a difficult problem, because of the unusual 2DHG spin degeneracy in the Si-SiGe devices. Our PC data reveal more structure than conventional transport and we compare the PC data with numerical calculations of Shubnikov-de-Haas oscillations to derive the g-factor.

Yet another interesting property of the 2DHG is that low field oscillations in magneto-photoconductivity demonstrate a close resemblance to $d\rho_{xx}/dB$. We explain this observation in the framework of a recent Shubnikov-de-Haas model. We also report a PC study of the energy spectra of our Si-SiGe heterostructures. Development of the PC technique provides a spectroscopic method to investigate the low temperature (mK) ground states of the 2DHG in p-type Si-SiGe heterostuctures similar to photoluminescence in GaAs-based structures.

[1] R.B. Dunford, R.G. Clark, V.A. Stadnik *et al*, submitted to Phys Rev Lett., 1995.

DIFFERENTIAL REFLECTANCE SPECTROSCOPY OF QUANTUM WELL STRUCTURES

Patrick Burke and Michael Gal
School of Physics, The University of New South Wales, Sydney 2052

Differential Reflectance Spectroscopy (DR) is a sensitive, non-contact, non-destructive technique for probing the optical characteristics of semiconductor devices. The technique involves measuring the difference in reflectivity between different parts of a sample. When applied to quantum well (QW) structures, this technique displays derivative-like spectra related to the spatial inhomogeneities present. Spatial variations in the sample, whether they be deliberately induced, such as through an ion-implantation/annealing process, or inherent defects, such as a QW width variation, or constituent concentration variations due to growth processes, may be determined using this technique.

The sensitivity of DR has been shown to be comparable to or greater than similar techniques such as photoreflectance.

DIRECT AND INDIRECT OPTICAL TRANSITIONS IN STRAINED $In_{0.15}Ga_{0.85}As/GaAs$ AND IN $In_{0.15}Ga_{0.85}As/Al_{0.15}Ga_{0.85}As$ QUANTUM WELLS

E.M. Goldys[1], H. Zuo[1], M.R. Phillips[2], C.M. Contessa[2], M.R. Vaughan[3], and T.L. Tansley[1]

[1] Semiconductor Science and Technology Laboratories, Macquarie University, NSW 2109, Australia.

[2] Microstructural Analysis Unit, University of Technology, Sydney, 2007 NSW, Australia.

[3] CSIRO Radiophysics, P.O. Box 76, Epping, 2121 NSW, Australia.

We present results of photoluminescence and cathodoluminescence measurements of the strained undoped $In_{0.15}Ga_{0.85}As/GaAs$ and $In_{0.15}Ga_{0.85}As/In_{0.15}Al_{0.85}As$ quantum well structures and compare them with theoretical eight band effective mass approximation calculations of the confined state energies. The analysis shows that while in the case of $In_{0.15}$ $Ga_{0.85}As/GaAs$ the observed two transitions are consistent with both type I or type II alignment of the light hole band for the accepted band offset ratio of approximately 0.6, in the case of $In_{0.15}Ga_{0.85}As/In_{0.15}Al_{0.85}As$ the data are consistent with type II alignment only. We derive the offset ratio for the $In_{0.15}Ga_{0.85}As/In_{0.15}Al_{0.85}As$ system to be 0.84 and discuss it in the context of the common anion rule.

Fig 1. PL spectra at T $\approx$ 8K, (a) of the $In_{0.15}Ga_{0.85}As/GaAs$ QW structure, (b) of the $In_{0.15}Ga_{0.85}As/Al_{0.15}Ga_{0.85}As$ structure and the CL spectra at 80 K, of (c) of the $In_{0.15}Ga_{0.85}As/GaAs$ QW-s and (d) of the $In_{0.15}Ga_{0.85}As/Al_{0.15}Ga_{0.85}As$ QW-s.

Fig 2. The calculated 1hh-1lh energy (curve a) and the 1hh-valence band top in the barrier (curve b) for the $In_{0.15}Ga_{0.85}As/GaAs$ QW. The insert shows the type I and the type II band lineup for the lh band.

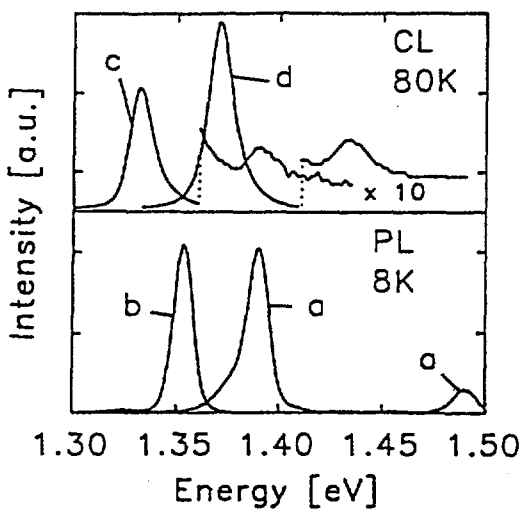

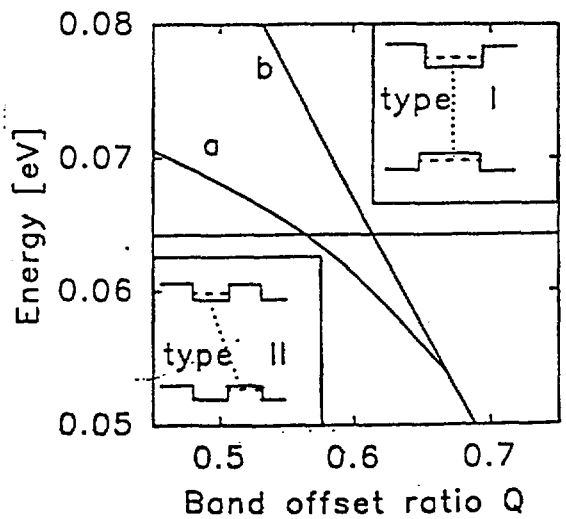

MOBILITY AND RESISTIVITY IN GaAs GROWN BY MBE AT LOW SUBSTRATE TEMPERATURE

P. Arifin, E.M. Goldys, T.L. Tansley
Semiconductor Science and Technology Laboratories,
Physics Department, Macquarie University, NSW 2109, Australia

M.R. Vaughan
CSIRO-Division of Radiophysics, P.O. BOX 76, Epping, NSW 2121, Australia

Abstract

An epitaxial layers of GaAs on semi-insulating substrate have been grown by MBE at temperature ~200° C (normally ~ 600°C), known as low temperature grown GaAs (LT GaAs). LT GaAs contains ~ 1% excess arsenic, and after annealing, the excess arsenic forms arsenic precipitates. To investigate annealing effect on mobility and resistivity, the sample was cut into several pieces and annealed at different temperatures, ranging from 200° C to 600° C. The resistivity and Hall mobility of the as grown and annealed samples were measured using Hall-van der Pauw methods at different temperatures. The Hall-van der Pauw measurement system was designed to suit the high-resistance measurement. The resistivity is dramatically increased as the annealing temperature is increased and the samples become highly resistive after annealed at 600° C. The as grown sample has very low mobility, however, after it is annealed the mobility is gradually increased.

The results of theoretical calculation of the mobility in annealed sample are also presented. The calculation was carried out using the Monte Carlo method, based on the 'internal Schottky barrier' model. We used a novel approach to overcome the problem of inhomogenety of internal electric field due to the presence of arsenic precipitates.

SCIENTIFIC PROGRAM OF THE SEMICONDUCTOR NANOFABRICATION FACILITY

A S Dzurak, B E Kane and R G Clark

School of Physics, University of New South Wales, Sydney NSW 2052

The Semiconductor Nanofabrication Facility at the University of New South Wales will be fully operational in early 1996. The philosophy underlying the research at this facility is that improvements in sample quality and the precision with which a potential may be imposed on electrons will be as important in elucidating 1D and 0D physics as they have been in 2D over the past decade. We are exploring undoped, gate-controlled variable density electron systems in GaAs in which the disorder that arises from modulation doping in conventional heterostructures is effectively eliminated [1,2]. Our initial focus is on the fabrication of ultra-clean quantum wires in these systems to investigate the anticipated Tomonaga-Luttinger liquid state in a truly 1D device [3]. We are also studying Si/SiGe devices [4] because these materials are rapidly approaching the quality of GaAs/AlGaAs, and SiGe has physical properties that may make it favourable for nanostructures. SiGe also introduces the possibility of integrating nanostructures with Si electronics. We will discuss the capabilities of our high-resolution 100 keV electron beam lithography system developed in a joint venture with industry and describe surface gate devices we have fabricated. Finally, we will describe the unique nano/micro facility at UNSW and the potential it offers to integrate nanostructures with existing microelectronics.

1. B.E. Kane, L.N. Pfeiffer and K.W. West, Appl. Phys. Lett. **67**, 1262 (1995).
2. B.E. Kane, L.N. Pfeiffer, K.W. West and C.K. Harnett, Appl. Phys. Lett. **63**, 2132 (1993).
3. C.L. Kane and M.P.A. Fisher, Phys. Rev. B **46**, 15233 (1992); C.L. Kane,Physica B **189**, 250 (1993).
4. R.B. Dunford, R.Newbury, F.F. Fang, R.G. Clark, R.P. Starrett, J. O. Chu, K.E. Ismail and B.S. Meyerson, Sol. Stat. Comm. **96**, 57 (1995).

UNDERSTANDING NOISE SUPPRESSION IN HETEROJUNCTION FIELD-EFFECT TRANSISTORS

F. Green
GaAs IC Prototyping Facility, CSIRO Division of Radiophysics
P.O. Box 76, Epping, N.S.W. 2121

The enhanced transport properties displayed by quantum-well-confined, two-dimensional, electron systems underpin the success of heterojunction, field-effect transistors. At *cryogenic* temperatures, these devices exhibit impressive mobilities and, as a result, high signal gain and low noise. Conventional wisdom has it that the same favourable conditions also hold for normal room-temperature operation. In that case, however, high mobilities are precluded by abundant electron-phonon scattering. Our recent study of nonequilibrium current noise shows that *quantum confinement*, not high mobility, is the principal source of noise in these devices; this opens up new and exciting opportunities in low-noise transistor design. As trends in millimetre-wave technology push frequencies beyond 100 Ghz, it is essential to develop a genuine understanding of noise processes in heterojunction devices.

A POSITRON ANNIHILATION LIFETIME SPECTROSCOPY STUDY OF POROUS SILICON USING A CONTINUOUS LIFETIME FITTING ALGORITHM

P. M. Derlet and T. C. Choy

Department of Physics, Monash University, Clayton, Victoria 3168

Porous silicon is a highly complex system containing disorder that exists over a range of scales. Positron Annihilation Lifetime Spectroscopy (PALS) provides a unique non-destructive probe into this disorder on the microscopic scale, through the identification of impurity concentrations and types; and on the mesoscopic scale at which the bulk of the porosity exists through the study of positronium lifetimes. Itoh[1,2] and Dannefaer[3] have done such an investigation for porous silicon using a discrete lifetime analysis. In the present work[4] we report on a PALS investigation of porous silicon using a continuous lifetime fitting algorithm. Our motivation lies in the underlying disadvantage in discrete lifetime fitting algorithms where the number of components must initially be assumed since in general a realistic spectrum does not uniquely determine this number. This becomes particularly apparent when looking at highly disordered systems where the notion of a discrete spectrum may be invalid and indeed crucial to an understanding of the optical absorption and photo-luminescence properties[5]. Using the PALS data collected from different porous silicon samples in conjunction with other methods of characterisation[6], we have extended the findings of previous work. In particular we resolve three rather than two ortho-positronium components, suggesting that there may be an additional intermediatory scale of porosity in which ortho-positronium annihilates. We also establish the existence of a very weak ortho-positronium component in the pre-anodised wafers at a time scale approximately equal to the longest time ortho-positronium component seen in porous silicon, suggesting that irregularities of a particular magnitude exist before anodisation and that these may, in part, be the catalyst for the initial pore formation process.

1 Y. Itoh *et al.*, Appl. Phys. Lett. 63 20 (1993) 2798.
2 Y. Itoh *et al.*, Journal de Physique IV, Colloque C4, supplement au Journal de Physics II 3 (1993) 193.
3 S. Dannefaer *et al.*, Thin Solid Films 255 (1995) 171.
4 P. M. Derlet and T. C. Choy, submitted to Journal of Material Science Letters.
5 P. M. Derlet, T. C. Choy & A. M. Stoneham, J. Phys.: Cond. Mat. 7 (1995) 2507
6 T. C. Choy *et al.* Third NUS Materials Science and Engineering Symposium Proceedings, Singapore 1994.

Green's Function calculation of STM on Graphite using a pseudo Tight-Binding Model

B.A. McKinnon¶ and T.C. Choy
Department of Physics
Monash University
Clayton, Victoria 3168

Abstract

We report results of a Green's function calculation of the scanning tunnelling microscopy on Graphite surfaces using a pseudo tight-binding model. The structures considered include simple hexagonal, Bernal and rhombohedral graphite. We found that due to the quadratic dependence of the tunnelling current on the relatively small tip-sample hopping parameter, a first order time-dependent peturbation treatment is adequate[1]. Our results are in reasonable accord with experiments, in that the current is found to increase markedly with applied voltage bias, the relative corrugation of the image is found to depend of the tip wavefunction, while the magnitude of the tip-height corrugation is about a third of that observed experimentally. The reason for this discrepancy is found to be due to the tip wavefunction and also to the neglect of atomic forces on the tip which lead to additional surface deformations[2].

References

1. J. Tersoff and D.R. Hamann, Physical Review **B31** (2), 805 (1985).
2. B.A. McKinnon, PhD thesis, Monash University, Sep 1995.

¶ Present address:
Department of Physics and Astronomy and
Materials Research Centre
University College,
University of London
London, UK

Non-orthogonality in tight-binding models - a derivation of the SWMc parameters for Graphite

B.A. McKinnon¶ and T.C. Choy
Department of Physics
Monash University
Clayton, Victoria 3168

The significance of the overlap of non-orthogonal atomic Slater-orbitals in the electronic band structure of solids was first appreciated by Löwdin in 1950 when he invented the transformation which now bears his name. We demonstrate in this work that when the effect of the overlapping Slater basis sets is included, then appropriate second and third neighbour hopping terms are obtained in the tight-binding model. In this way the Slonczewski and Weiss[1] and McClure[2] (SWMc) parametrization of the band structure of Graphite, which is known to agree well with experiments, is now given a microscopic derivation[3,4]. Similar results should hold for other systems, in particular for Si and Ge. Finally we shall use our formalism to give a simple derivation of the Orthogonality Catastrophe, first discovered by Anderson[5], using the model of an excited impurity atom on a tight-binding lattice.

References

1. J. Slonczewski and P. Weiss, Phys. Rev., **109**, 272 (1958).
2. J. McClure, Phys. Rev. **108**, 612 (1957).
3. B.A. McKinnon and T.C. Choy, Physical Review **B52**, 14531 (1995).
4. B.A. McKinnon, PhD thesis, Monash University Sep. 1995.
5. P.W. Anderson, Phys. Rev. Lett. **18**, 1049 (1967).

¶ Present address:
Department of Physics and Astronomy and
Materials Research Centre
University College,
University of London
London, UK

AU9918272

SERIES EXPANSION FOR THE J_1-J_2 HEISENBERG ANTIFERROMAGNET ON THE SQUARE LATTICE

J. Oitmaa and Zheng Weihong

School of Physics, The University of New South Wales, Sydney, NSW 2052, Australia

We present the first comprehensive series expansion study of the $S = \frac{1}{2}$ antiferromagnet with first and second neighbour antiferromagnetic interactions on the square lattice,

$$H = J_1 \sum_{\langle ij \rangle} \mathbf{S}_i . \mathbf{S}_j + J_2 \sum_{[ij]} \mathbf{S}_i . \mathbf{S}_j$$

The pure J_1 model ($J_2 = 0$) has Néel order in the ground state, reduced by quantum fluctuations. Increasing J_2 will act to destabilize the Néel order and at a value $J_2 / J_1 \approx 0.4$ we find a transition to a new phase. Conversely for large J_2 the ordered state is collinear and as J_2 is reduced this phase becomes unstable near $J_2 / J_1 \approx 0.6$. This is most clearly seen from magnetization series, as shown in the figure.

The Néel and collinear phases are gapless in the spin isotropic limit whereas the intermediate phase may have a small energy gap.

The full ground state phase diagram of the model with spin anisotropy has also been investigated, using the above methods as well as via perturbation theory at the Ising multiphase point at $J_2 / J_1 \simeq 0.5$.

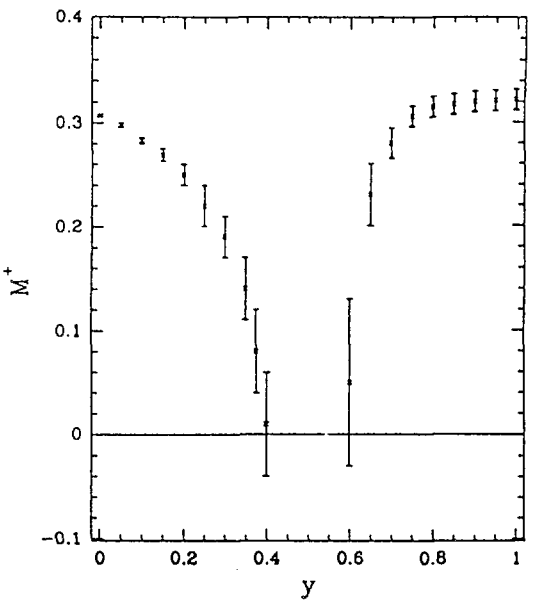

OPTICAL ABSORPTION OF A QUANTUM PLASMA IN A MAGNETIC FIELD AND A UNIDIRECTIONAL PERIODIC MODULATION

S. M. Stewart and C. Zhang

Department of Physics, University of Wollongong, NSW 2522, Australia

Free or quasi-free electrons or holes in metals and semiconductors under a constant magnetic field exhibit many interesting physical phenomena such as the de Haas-van Alphen effect, cyclotron resonance, helicon waves etc. The origin of these well-known physics can be mainly attributed to the energy level quantisation in the plane perpendicular to the magnetic field and the associated inverse-square-root divergence in the density of states. In this work we present a theoretical investigation of the electronic properties of these magneto-quantum plasma systems which in addition are subjected to a unidirectional periodic electrical potential. We have calculated, within the random phase approximation, the frequency dependent dielectric response function for a quantum plasma under a constant magnetic field and a one dimensional periodic modulation potential. It is found that the original inverse square root divergence in the density of states is removed by the modulation potential while periodic finite peaks and sudden steps are introduced. The electron-hole excitation exhibits two new features due to the periodic modulation, (i) the excitation contains double peaks at ω around ω_c and (ii) it also contains a series of kink like structures at the band edges.

THEORY OF 2D QUANTUM LIQUIDS

Miklos Gulacsi

Department of Theoretical Physics
Research School of Physical Sciences and Engineering
Institute of Advance Studies
The Australian National University
Canberra, ACT 0200

The properties of **2D** interacting electrons are described in terms of the well-known quasi particle picture borrowed from the Landau Fermi liquid theory. Within this theory, the excitations of the **1D** Fermi surface are described by the difference $\delta n(\mathbf{k})$ of the momentum distribution from the ground state. The free energy $F = E - \mu N$ of this interface is: $F = \Sigma\, [\varepsilon(\mathbf{k}) - \mu]\, \delta n(\mathbf{k}) + 1/2\, \Sigma\, f(\mathbf{k},\mathbf{k}')\, \delta n(\mathbf{k})\, \delta n(\mathbf{k}')$. In a classical linearized Boltzmann equation approach such an interface has well-known collective (sound) modes and a particle-hole continuum, which establish a Fermi liquid picture. However, the same type of linearized Boltzmann equations leads to the correct description of the excitations of the Tomonaga-Luttinger universality class. That is, at low energies and long wavelengths, the bosonic excitations are simply sound waves. Accordingly, a direct mapping of the Fermi surface into a true interface is possible. In the following I prove that the corresponding interface is *rough*.

1. Classical: For short-range $f(\mathbf{k},\mathbf{k}')$, the effective hamiltonian is of a solid-on-solid model form $\approx - \Sigma\, S(\mathbf{k})\, S(\mathbf{k}')$, where $S(\mathbf{k}) = 2\, \delta n(\mathbf{k}) - 1$ is an Ising 1/2 spin, which in **1D** is always rough. For a general 2N level model it is again always rough because of the broken symmetry. For long-range $f(\mathbf{k},\mathbf{k}')$, the effective hamiltonian is Gaussian which again gives a rough surface.

2. Quantum [1]: For short-range $f(\mathbf{k},\mathbf{k}')$, the excitations (being of the Tomonaga-Luttinger type) are described by a $c = 1$ conformal field theory, where c is the central charge of the Virasoro algebra, which is the well-known SU(2) Kac-Moody theory. This theory is critical; accordingly the corresponding surface is rough. For higher spin models the ferromagnetic region of the phase diagram remains unchanged, as can be proven by bosonizing the SU(N) massless Thirring model. For long-range $f(\mathbf{k},\mathbf{k}')$, the effective hamiltonian is of a Haldane-Shastry type which being equivalent to a Wess-Zumino-Witten model is a conformal field theory with $c = 1$, that is the model remains critical and the corresponding surface rough.

The only possibility to go out from the **2D** Fermi liquid picture is by generating a surface tension in F. That is, a Fermi to Luttinger liquid transition in **2D** can be accomplishes by doping. This process in case **1.** generates a gradient of the scalar field within the sine-Gordon theory. (This description is equivalent to the Ising, SOS or Gaussian models.) For case **2.** it corresponds to a mass generation. It is known [1] that in all SU(N) fermionic theories dynamical mass generation is possible without breaking its chiral symmetry and in particular for the system presently analysed this leads to a chiral Gross-Neveu theory [1]. Accordingly, a Fermi to Luttinger liquid transition will appear in **2D** quantum liquids.

[1] M. Gulacsi *et al.*, Phys. Rev. Lett. **72**, 2765 and **73**, 3239 (1994).

CRYSTALLIZATION AND MECHANICAL PROPERTIES OF THE ULTRAFINE FERRIC OXIDE-FILLED POLYPROPYLENE AND RHEOLOGY OF THE FILLED POLYPROPYLENE MELT

Gong Xiaoyi, Zeng Meizhen, and Song Rongzhao

Guangzhou Institute of Chemistry, Chinese Academy of Sciences, Guangzhou 510650, P.R.China
State Key Laboratory of Polymeric Materials Engineering, Chengdu University of Science and Technology, Chengdu, 610065, P.R.China

ABSTRACT

Polypropylene was first blended with a series of ultrafine powder of ferric oxide with average diameters 16.1nm, 41.3nm,73.0nm,184.0nm, and 660.6nm. The rheological property of the filled polypropylene melt was accessed in terms of equilibrium torques by using a Brabender plasticoder. The stress-strain behaviour was examined by using an Instron tensile tester. The crystallizing and melting processes of the filled polypropylene were followed by a Perkin-Elmer differential scanning calorimeter. And the crystallinities were determined by the WAXD analysis. The data showed that the filled polypropylene had crystallized at higher temperature than the unfilled polypropylene; the smaller the filler, the higher thecommencing temperature and the peak temperature of crystallization of the filled polypropylene. Whereas the α-form crystallinity of the polypropylene remained unchanged after it had been filled with the ultrafine ferric oxide. Young's modulus of the filled polypropylene at room temperature decreased with decreasing of the filler's average diameter. But tensile strength of the filled polypropylene increased, approaching to that of unfilled polypropylene as the filler's average diameter getting smaller. Elongation at break remained constant during changing of the filler size. Better fluidity was found for smaller filler filled polypropylene melt. All the results manifest more researches to be done into the promising ultrafine filler.

THE USE OF PIEZOELECTRIC BIMORPH TRANSDUCERS TO MEASURE FORCES IN COLLOIDAL SYSTEMS

A.M.Stewart, Department of Applied Mathematics, The Australian National University, Canberra ACT 0200: E-mail: andrew.stewart@anu.edu.au

The Surface Force Apparatus developed in this Department has proved useful for the measurement of colloidal forces between transparent surfaces in liquids and gases at surface separations of 1 nm up to 500 nm. The distance between the surfaces is measured by the interferometry of white light, and the force is measured from the movement of one of the surfaces that is attached to a cantilever spring which deflects under the influence of the force. Recently three new developments of technique have been applied to this instrument. The first is the magnetic force transducer [1] in which a force is applied externally to the cantilever, to which a small magnet is attached, by means of an electric current flowing in coils outside the apparatus. The second is to use a bimorph to measure the deflection of the cantilever. A bimorph is made of two thin sheets of piezoelectric ceramic fastened together with electrodes on their faces. When the bimorph is bent, one side expands and the other contracts; if the two halves of the bimorph are electrically polarised in opposite directions the resulting piezoelectric voltages add together to give an output voltage that is proportional to the deflection of the bimorph and hence to the force on it. The third development has been to connect the magnetic force transducer and the bimorph together in a feedback loop to control the position of the moving surface to have nominally zero displacement [2].

In a previous paper [2] an analysis has been given of the high frequency behaviour of such a system, which determines its dynamical stability. In the present work an analysis is made of the effect of the errors introduced at a longer time scale by bimorph drift and decay upon accuracy of measurement. For direct measurements the errors will be small provided that the time constant of the bimorph, given by the product of its capacitance and amplifier input impedance, is much larger than the total time of measurement. With the force-feedback technique the errors will be negligible provided that, in addition the integrator time constant is much smaller than the bimorph time constant, a condition easily satisfied. In is important to use an amplifier with a very high input impedance to buffer bimorphs used for this type of measurement.

[1] A.M.Stewart and H.K.Christenson, *Measurement Science and Techn.* (1990) **1** 1301.
[2] A.M.Stewart and J.L.Parker, *Review of Scientific Instruments* (1992) **63** 5626.
[3] A.M.Stewart, *Measurement Science and Techn.* (1995) **6** 114.

A Massively Parallel Molecular Dynamics Simulation of Phase Separation and Nucleation in a Simple Fluid

Steven Pickering and Ian Snook

Computational Physics Group, Department of Applied Physics, RMIT, Melbourne.

A recently developed Molecular Dynamics (MD) code for massively parallel computers was used to study an initially stable fluid which was subjected to a rapid quench to a temperature below the triple point. The atoms interacted according to a Lennard-Jones pair potential and the initial state of the 327,680 atoms system was at a density close to the critical density but at a temperature well above the critical temperature. The system was then rapidly cooled to below the triple point. The fluid initially showed density variations which were Gaussian in nature indicating a diffusive regime which was followed by decomposition of the fluid into gaseous and liquid regions with a well defined interface. Subsequently these regions grew in size by coalescence until at a certain size at certain stage growth ceased and nucleation of crystals occurred roughly from the centre of the liquid regions. The coarsening processes was shown to occur by two distinct mechanisms.

A Parallel Molecular Dynamics Code Based on the Liked-Cell Method and its Application to Liquids

Aaron McDonough, Salvy Russo and Ian Snook

Computational Physics Group, Department of Applied Physics, RMIT, Melbourne

Many problems in the Statistical Mechanics of materials may be solved by use of the Molecular Dynamics (MD) technique involving the numerical solution of Newton's equations of motion for a few hundred interacting particles. However, some problems require many thousands to millions of atoms in order to accurately represent the length and/or time scales involved. Examples of such problems are nucleation, phase separation, extended defects and crack propagation. Such large numbers of atoms cannot be treated using existing serial computers and computer codes. Thus, new methods must be sought to tackle such problems. One such method is the use of parallel computers which involves the development of MD codes which will work on computers with parallel architectures. Here we discuss one such implementation of the MD method which uses the linked cells method of Hockney and Eastwood. As an illustration we show how this method performs on a TRANSPUTER array and discuss some applications to problems in liquid state physics.

ELECTRONIC CHARGE DENSITY OF Si(111)2x1

B. Chen, Y. Zhao

School of Materials Science and Engineering, University of New South Wales, Sydney, NSW 2052 Australia

and

D. Haneman

School of Physics, University of New South Wales, Sydney 2052 NSW, Australia

The total electron charge densities of various regions of Si(111)2x1 were calculated using Hartree-Fock Linear Combination of Atomic Orbital program CRYSTAL-92. The amplitude of charge density corrugation was found to decay rapidly from the surface. The corrugation amplitudes at 5 Å from the surface for the Three-Bond Scission (TBS) model [1] was found to be close to that of the Pandey π-bonded chain (Pandey) model [2] and Scanning Tunnelling Microscopy (STM) measurements [3]. STM would therefore not be able to distinguish between the two models. Charge was found to transfer from higher buckled surface atom to lower one. The electronic images of TBS and Pandey models were also computed using Local Density-Molecular Dynamics program and may be compared directly with STM images, both in constant current and constant height modes. The top π-bonded chains of both models are clearly shown in charge density contour map.

Reference:

1. D. Haneman, Rep. Prog. Phys. **50** 1045 (1987)

2. K. C. Pandey, Phys. Rev. Lett. **47** 1913 (1981)

3. R. M. Feenstra, W. A. Thompson, and A. P. Fein, Phys. Rev. Lett. **56** 608 (1986),

A LABORATORY BASED X-RAY REFLECTIVITY SYSTEM

S.A. Holt,* I.M. Jamie,+ T.L. Dowling,# A.S. Brown# and D.C. Creagh*

* Department of Physics, ADFA, University College, UNSW, Canberra, ACT, 2600.

\+ Department of Chemistry, University of Wollongong, Wollongong NSW 2522.

\# Research School of Chemistry, ANU ACT 0200.

X-ray Reflectivity (XRR) over the last decade has proved to be a versatile and powerful technique by which the thickness of thin films, surface roughness and interface roughness can be determined. The systems amenable to study range from organic monolayers (liquid or solid substrates) to layered metal or semiconductor systems. Access to XRR has been limited by the requirement for synchrotron radiation sources. The development of XRR systems for the laboratory environment was pioneered by Weiss *et al.*[1]

An X-ray Reflectometer has been constructed by the Department of Physics (Australian Defence Force Academy) and the Research School of Chemistry (Australian National University). The general principles of the design were similar to those described by Weiss *et al.*[1] The reflectometer is currently in the early stages of commissioning, with encouraging results thus far. The reflectivity of a 31 layer Ba-Arachidate film can be seen in Fig. 1. The diffraction pattern of Mobil Catalytic Material (MCM), consisting primarily of SiO_2, is displayed in Fig. 2. The poster will describe the reflectometer, its operation and present a summary of the most important results obtained to date.

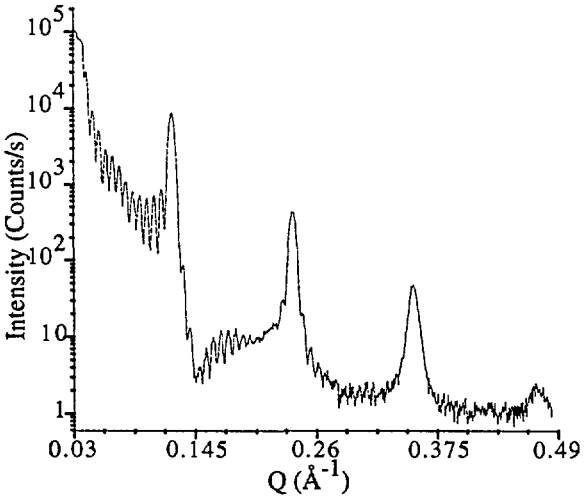

Fig. 1 Reflectivity of a Ba Arachidate film.

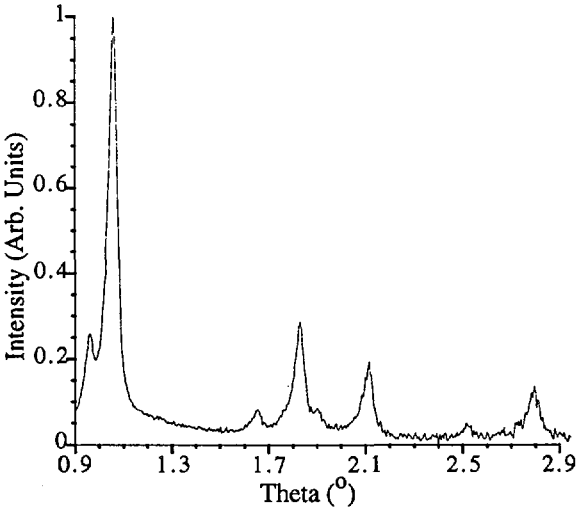

Fig. 2 Diffraction pattern from MCM.

1. A.H. Weiss, M. Deutsch, A. Braslau, B.M. Ocko, and P.S. Pershan (October 1986) Rev. Sci. Instrum. **57(10)**, 2554 - 2559.

A MOLECULAR DYNAMICS STUDY OF HYDROCARBONS ON THE (001) SURFACES OF Si AND β-SiC.

A. J. Dyson and P. V. Smith
Department of Physics, University of Newcastle
Callaghan, NSW 2308, Australia

An empirical many-body potential has recently been developed for systems containing silicon, carbon and hydrogen atoms [1,2]. We have used this potential to simulate the interactions between hydrocarbon molecules and the silicon surface.

This study has encompassed a number of unsaturated hydrocarbon molecules and neutral radicals, incident upon the Si(001):2x1 dimerized surface and the Si-terminated (001) surface of β-SiC. The role of atomic and molecular hydrogen in the gas phase has also been investigated.

---

[1] A. J. Dyson and P. V. Smith, *Surf. Sci.* submitted for publication.

[2] D. W. Brenner, *Phys. Rev. B* 42(1990) 9458.

THE JAHN-TELLER EFFECT AND ITS OBSERVATION IN TITANIUM ALUM

Philip Tregenna-Piggott
Department of Physics, Monash University,
Clayton, Victoria 3168, Australia.

A fundamental assumption, often employed to problems in solid state physics, is that a system may be well described within the confines of the Born-Oppenheimer approximation. As a consequence of the substantial difference of masses, the electrons are assumed to follow the motion of the nuclei adiabatically; hence, the motion of the electrons and nuclei are solved separately. As Jahn and Teller showed in 1936, any non-linear molecule having orbital degeneracy will be unstable to at least one assymetric displacement which lifts the degeneracy. The wave equation must then be solved taking into account coupling between the electronic and nuclear motion. The $\mathbf{E} \times \beta$ system, an electronic doublet coupled to a single mode of vibration, is introduced as an elementry example and is used to illustrate features characteristic of Jahn-Teller systems. The $\mathbf{E} \times \epsilon$ system is discussed in conjunction with work currently being undertaken on $CsTi(SO_4)_2.12H_2O$. In this alum, the $[Ti(OH_2)_6]^{3+}$ cation ($3d^1$) is subject to an axial field which acts to leave a doubly degenerate electronic ground term. Spectroscopic and Crystallographic data show the salt to undergo a phase transition at 12 K which we associate with a Co-operative Jahn-Teller Effect manifested by the interaction of the Jahn-Teller electrons with the crystal lattice. Also presented are EPR and SQUID data which illustrate how the Jahn-Teller effect leads to quenching of orbital angular momentum and spin-orbit coupling.

STRUCTURAL and MAGNETIC FEATURES of the NOVEL QUATERNARY COMPOUNDS - $NdTM_8SiB_3$ (TM=Co, Ni)

Heng Zhang, S J Campbell, A V J Edge and E Wu*

School of Physics, University College, University of New South Wales
Australian Defence Force Academy, Canberra , ACT 2600

* School of Science, University of Griffith, Brisbane, QLD 4111

The interesting range of magnetic properties exhibited by ternary R-TM-Si and R-TM-B compounds (R= rare earth), some with technological applications as permanent magnets, has resulted in their extensive investigation in recent years [eg 1]. Recently, a link between these two series has been established with the discovery of a new quaternary compound based on Nd-Co-Si-B [2]. Here, we present further information on $NdCo_8SiB_3$ along with preliminary results for $NdNi_8SiB_3$, as part of a systematic study of RTM_8SiB_3.

The samples were prepared by arc melting high purity elements followed by annealing under vacuum at 900 °C for two weeks. The structure was analysed by x-ray diffraction using a Philips diffractometer with CuKα radiation. ^{57}Fe Mössbauer spectroscopy was carried out in transmission mode using a ^{57}CoRh source from 4.2 K to room temperature for ^{57}Fe(0.5 wt%) doped $NdCo_8SiB_3$ and $NdNi_8SiB_3$. The magnetic transition temperature of $NdCo_8Sib_3$ was determined by ac susceptibility measurements from 4.2 K to room temperature.

The x-ray patterns indicated that the dominant phase for both $NdCo_8SiB_3$ and $NdNi_8SiB_3$ exhibits the same crystal structure which can be indexed as a tetragonal structure (P4m2). The lattice parameters are a=11.150(5) Å, c=7.953(5) Å for $NdCo_8SiB_3$, and a=11.136(5) Å, c=7.930(5) Å for $NdNi_8SiB_3$.

The room temperature Mössbauer spectra for both the $NdCo_8SiB_3$ and the $NdNi_8SiB_3$ systems comprise predominantly a single line, indicating that the ^{57}Fe atoms which replace the Co or Ni atoms, are located in sites of high cubic symmetry. The 4.2 K spectrum for $NdCo_8SiB_3$ exhibits primarily (~95.3% spectral area) a unique magnetic hyperfine field B_{hf} =27.9(3) T, with a small fraction (~4.7% area) of B_{hf}=26.(4) T. On the other hand, the 4.2 K spectrum of $NdNi_8SiB_3$ reveals a distribution of magnetic hyperfine fields of mean value $\langle B_{hf} \rangle$ = 13.8 T and width σ_B = 7.2 T . The initial results and analysis, with main interests centred both on the type of magnetic order exhibited below the transition temperatures and the differences in magnetic behaviours between the Co and Ni systems, of this continuing project will be presented.

1. H. -S. Li and J. M. D. Coey, in *Handbook of Magnetic Materials*, Vol.6 ed. by K. H. J. Buschow, (Elsevier, Amsterdam, 1991) p.1
2. E Wu, G. H. J. Wantenaar, S. J. Campbell, and H.-S. Li, J Phys. Cond. Matter 5 (1993) L457.

AU9918284

LEACHING OF SYNROC IN D_2O

E.R Vance, N. Dytlewski, B.D.Begg, K Prince and G. J. Thorogood,
Materials Division, ANSTO, Menai, NSW 2234.
Fax: (02) 543 7179
Email:erv@nucleus.ansto.gov.au

The use of D_2O rather than H_2O for leaching Synroc and its constituent phases allows the study of hydration and hydroxylation reactions without the contaminating influence of atmospheric moisture. For Synroc leached at 190°C for 5-30 days, the penetration of D into the Synroc is found as ~30 nm from both energy recoil analysis using 1.5 MeV He ions from a Van de Graaff accelerator and secondary ion mass spectroscopy near mass 18(OD-).

Analogous studies have been carried out on single crystals of $SrTiO_3$ which have the perovskite (a constituent phase of Synroc) structure, and augmented by additional atomic force and scanning electron microscope studies of secondary TiO_2 alteration products. Alteration products on single crystals of $CaTiO_3$ have also been studied.

Neutron and Resonant X-ray Diffraction from Cuprate Superconductors

B. A. Hunter and C. J. Howard
A.N.S.T.O., Neutron Scattering Group,
Private Mail Bag 1, Menai, N.S.W., 2234, Australia.
bah@atom.ansto.gov.au, cjh@atom.ansto.gov.au.

Many areas of condensed matter physics and chemistry rely on the study of materials that are chemically doped at one or more sites in their atomic structures. Powder diffraction is a powerful technique to determine the site positions and occupancies of such dopants. However in many systems the dopant has a neutron scattering length and/or x-ray form factor closely related to the host atom, such as substitution of Fe for Ni, where both the neutron scattering lengths and form factors are practically the same for both elements. This problem can be overcome by 1) using joint x-ray/neutron refinements and/or 2) using x-ray resonant (anomalous) scattering. The latter technique uses synchrotron radiation where the wavelength is tuned to energies near the absorption edge of a particular element, typically the absorption edge of the host or dopant element, thereby changing its form factor.

There has been much interest in the doping of cuprate superconductors, where Cu is substituted by other transition elements such as Mn, Fe, Co, Ni and Zn. In particular the doping effects of Zn and Ni on the CuO_2 layers are important to the understanding of the superconductor mechanism. We present here a study of neutron and resonant x-ray scattering from $YBa_2Cu_{3-x}(Zn,Ni)_xO_7$ to determine the site location and occupations of the dopants Ni and Zn. Multiple wavelengths around the Cu absorption edge at 1.381Å were collected and used in conjunction with neutron diffraction data to determine the occupations and site positions. The use of simultaneous refinement of both the neutron and x-ray data allows more unambiguous site occupancies to be determined in contrast to standalone neutron or x-ray refinement. The novel use of x-ray image plates at the Australian National Beamline Facility at Tsukuba, Japan to produce 30 wavelengths on 4 images plates (totalling 120 powder patterns) is also examined and it's implications for simultaneous Rietveld refinements addressed.

A NEUTRON DIFFRACTION STUDY OF THE KINETICS OF SETTING CEMENT

L. C. Jones, S. J. Kennedy and L. P Aldridge*

Neutron Scattering Group & *Advanced Materials Division, Australian Nuclear Science and Technology Organisation, Private Mail Bag 1, Menai NSW, 2234

The performance of cement compounds depends critically on the initial composition of constituent phases and on the particle size distribution of those constituents. These factors largely determine the rate and degree of hydration during setting and the strength and durability of the compound when set. There are a variety of conventional techniques available to monitor the hydration process (eg calorimetry, microscopy, X-ray diffraction), however none can provide an 'in situ' continuous assessment of the chemical state during hydration. Neutron diffraction is a technique which can yield quantitative information on the chemical changes that occur during setting, provided that hydrogen is substituted by its chemical equivalent deuterium. Reasons for this application include the unique ability of neutrons to locate deuterium in the lattice and their ability to penetrate deeply into condensed matter. The deep penetration allows us to probe into the bulk of the material and therefore not to be misled by surface effects. Also because the kinetics of the chemical reaction are relatively slow, it is not difficult to attain sufficient statistical quality for real time quantitative phase analysis.

We report a neutron powder diffraction study on a sample of high purity portland cement as it set. The experiments were performed on the medium resolution powder diffractometer (MRPD) at the HIFAR research reactor immediately after deuteration with 40% (wt) of D_2O. Diffraction patterns were collected every few hours over the first 5 days, and then 12 days and 29 days after deuteration. A pattern of the initial dry cement was also collected on the high resolution powder diffractometer (HRPD) to aid in the accurate determination of constituent phases. The diffraction patterns were analysed using the Rietveld method to determine the rate of chemical reaction in the major constituent phases. The Rietveld analysis shows that the main constituents of the dry powder are Ca_3SiO_5 (Alite) and Ca_2SiO_4 (Belite) with a lesser amount of Ca_2AlFeO_5 (calcium-ferrite) and $Ca_3Al_2O_6$ (calcium-aluminate). The chemical reaction during setting results mainly in the growth of Portlandite ($Ca(OD)_2$) from the Alite and Belite phases. The kinetics of the reaction have been determined and compared to data obtained from other techniques.

PLASTIC DEFORMATION OF Ce-ZrO_2 STUDIED BY IN-SITU NEUTRON DIFFRACTION

E H Kisi, C J Howard and S J Kennedy

Most ceramics are brittle because the energy cost of producing new cracked area is less than the released elastic strain energy. Zirconia ceramics are as fracture resistant as some metal alloys (eg cast Mg alloys). The predominant microstructural mechanism responsible for their high toughness is the martensitic transformation of tetragonal zirconia (*t*) to monoclinic zirconia (*m*). The ferroelastic switching of tetragonal domains under the action of an applied stress is another potential toughening mechanism. The precise nature and relative importance of each mechanism is unknown.

We have used a 200kN mechanical testing device to study a ceria stabilised tetragonal zirconia polycrystal (Ce-TZP) at compressive stresses up to 1.6 GPa using neutron diffraction [1]. The use of neutrons ensures the results are free from surface artifacts caused by sample preparation and decay of stress fields at the free surface. The stress-strain diagram is hysteretic, with some plastic deformation. Rietveld analysis of the neutron diffraction patterns has confirmed both substantial $t \rightarrow m$ transformation and ferroelastic switching in the *t* phase. Both mechanisms are partially reversible on removal of the load.

The $t \rightarrow m$ transformation and ferroelasticity are strongly coupled and we are unable to ascribe a 'primary' or 'secondary' role to either. Analysis of the neutron diffraction patterns prior to transformation gives some insight into the elastic anisotropy of the t-phase and the mechanisms which cause the $t \rightarrow m$ transformation and ferroelasticity.

[1] "Neutron Diffraction Observation of Ferroelastic Domain Switching and $t \rightarrow m$ Transformation in Ce-TZP", E H Kisi, S J Kennedy and C J Howard, J. Am. Ceram. Soc. (submitted).

DEVELOPMENT OF SOFTWARE IN *LabVIEW* FOR MEASUREMENT OF TRANSPORT PROPERTIES OF HIGH T_C SUPERCONDUCTORS

David Reilly and Nick Savvides

CSIRO Applied Physics, Sydney 2070

The gathering of data and their analysis are vital processes in experiments. We have used LabVIEW (National Instruments) to develop programs to measure transport properties of high - T_c superconductors, eg. resistivity, ac susceptibility, I-V characteristics. Our systems make use of GPIB (IEEE - 488.2) programmable instruments and a personal computer.

LabVIEW is a graphical programming system for instrument control and data acquisition, data analysis and presentation. A key feature of LabVIEW is the ability to graphically assemble software modules or virtual instruments (VIs) and 'wire' them together.

In this paper we describe the development of several programs and will offer advice to colleagues wanting to explore LabVIEW.

Electron Emission from Materials at Low Excitation Energies

Nicoleta Urma, Dr. Marek Kijek, Prof. J. J. Millar
Department of Applied Physics, RMIT, Melbourne

An experimental system has been designed and developed with the purpose of measuring the total electron emission yield from materials at low energy excitation. In the first instance the reliability of the system was checked by measuring the total electron emission yield for a well defined surface (aluminium 99.45%). The obtained data was in the expected range given by the literature, and consequently the system will be used further for measuring the total electron yield for a range of materials with interest in the instrumentation industry. We intend to measure the total electron emission yield under electron bombardment as a function of incident electron energy up to 1200 eV, angle of incidence, state of the surface and environment to which the surface has been exposed. Dependence of emission on total electron irradiated dose is also of interest. For many practical application of the "Secondary Electron Emission", the total electron yield is desired to be as large as possible. The above phenomenon has practical applicability in electron multiplier tube and Scanning electron microscopy - when by means of the variation of the yield of the emitted electrons one may produce visible images of small sample areas. The electron multiplier tube, is a device which utilises the above effect to detect and amplify both single particles and low currents streams of charged particles. The majority of electron tubes use electrons with low energy, hundreds of eV. Not a lot has been published in the literature about this regime and also about the emission when the impinging electrons have small energy, up to 1 KeV. The information obtained from the experimental measurements concerning the total electron emission yield is used to asses the investigated materials as a potential electron emitting surfaces or dynodes in an electron multiplier tube.

REGISTRANTS

Mr		Afifuddin	MPCE, Macquarie University	afifud@mpce.mpce.mq.edu.au	WP59
Dr	Arthur	Anderson	St George Campus, University of NSW	A.Anderson@unsw.edu.au	WP06
Mr	Chris	Andrikidis	CSIRO Division of Applied Physics	chrisa@dap.csiro.au	WM02, WP67, TP01
Mr	Pepen	Arifin	MPCE, Macquarie University	pepen@mpce1.mpce.mq.edu.au	TP48
Mr	Nigel	Attwood	Alphatec International Pty Ltd, Sydney		
Dr	Phil	Back	AMPL/RSPhysSE, ANU	pjb107@rsphy7.anu.edu.au	
Mr	Peter	Bain	Materials Engineering, University of Wollongong	apb28@uow.edu.au	WP04, WP12
Mr	Richard	Baker	Physics, University of Wollongong	richard.baker@uow.edu.au	TP42
Prof	Eugene	Bashkin	Physics Department, University of Western Australia		FM5
Mr	Joe	Beer	Electric Power Engineering, University of NSW	tombeer@mpx.com.au	WP07, WP08, TP06, TP07
Mr	Bruce	Begg	ANSTO	bdb@nucleus.ansto.gov.au	TP12, TP66
Mr	Rajesh	Bhasale	Materials Engineering, University of Wollongong	drb04@uow.edu.au	WP05
Ms	Laure	Bourgeois	Physics, University of Melbourne	lnb@tauon.ph.unimelb.edu.au	WP40
A/Prof	Graham	Bowden	Physics, University of NSW	gjb@newt.phys.unsw.edu.au	WA2, TP33
Mr	Leonard	Broekman	Physics, La Trobe University	phyldb@lure.latrobe.edu.au	TP16
Dr	Simon	Brown	Physics, University of NSW	sab@newt.phys.unsw.edu.au	TP38
Dr	Tony	Brown	Research School of Chemistry, ANU	abrown@rschp1.anu.edu.au	TM4, TA1, TP62
Dr	Victor	Buntar	Atomic Institute, Vienna	Buntar@ati.ac.at	WE1
Dr	Iko	Burgar	BHP Research, Melbourne Laboratories	iko@resmel.bhp.com.au	
Mr	Patrick	Burke	Physics, University of NSW	ptb@newt.phys.unsw.edu.au	TP46
A/Prof	Stewart	Campbell	Physics, ADFA	s-campbell@adfa.oz.au	WP31, TP21, TP65
Dr	S	Canney	Electronic Structure of Materials Centre, Flinders University		WP16, WP17
Ms	Marina	Capponi	University of Technology, Sydney	perezm@phys.uts.edu.au	
A/Prof	John	Cashion	Physics, Monash University	john.cashion@sci.monash.edu.au	WP01, TP27, TP28, TP29
Ms	Julia	Chadwick	Physics, Monash University	julia.chadwick@sci.monash.edu.au	TP31
A/Prof	Don	Chaplin	Physics, ADFA	d-chaplin@adfa.oz.au	WA3, WP32, TP33, TP34
Dr	Bo	Chen	Materials Science and Engineering, University of NSW	bc@newt.phys.unsw.edu.au	WP53, TP01, TP61
Dr	Tuck	Choy	Physics, Monash University	tuck@sci.monash.edu.au	WP58, TP51, TP52, TP53,

					FM3
Dr	John	Collins	CSIRO Division of Applied Physics	collins@dap.csiro.au	
Dr	Stephen	Collocott	CSIRO Division of Applied Physics	steve@dap.csiro.au	
Ms	Jenice	Con Foo	Physics, La Trobe University	elejcf@lure.latrobe.edu.au	WP33, WP49, TP14
Mr	Rick	Craig	Physics, PSET, Murdoch University	craig@central.murdoch.edu.au	FM7
Mr	Ning	Cui	Materials Engineering, University of Wollongong	nc42@uow.edu.au	WP19, WP20
Dr	Craig	Davis	Plasma Physics, ANU		
Dr	Rod	Day			
Mr	Byron	den Hertog	Theoretical Physics, RSPhysSE, ANU	bdh105@rsphy2.anu.edu.au	TP10
Dr	Peter	Derlet	Physics, Monash University	phs216J@vaxc.cc.monash.edu.au	TP51
Dr	David	Dew-Hughes	Engineering Science, Oxford University	david.dew-hughes@eng.ox.ac.uk	WM01
Mr	Bradley	Dinte	Science and Technology, Griffith University	sctdinte@kraken.itc.gu.edu.au	TP22
Ms	Svetlana	Dligatch	Applied Physics, University of Technology, Sydney		TP17, TP18
A/Prof	John	Dobson	School of Science, Griffith University	j.dobson@sct.gu.edu.au	TM6, TM7, TP22
Prof	S	Dou	CSEM, University of Wollongong	s.dou@uow.edu.au	WM03, WM05, WP04, WP05, WP07, WP08, WP09, WP12, WP19, WP20, WP67, TP03, TP04, TP05, TP06, TP07, TP08
Dr	John	Dunlop	CSIRO Division of Applied Physics	jbd@dap.csiro.au	
Mr	Tony	Dyson	Physics, University of Newcastle	tony@schroeder.newcastle.edu.au	TP63
Dr	Andrew	Dzurak	Physics, University of NSW	ad@newt.phys.unsw.edu.au	TP49
Dr	Andy	Edgar	Physics, Victoria University, Wellington	andy.edgar@vuw.ac.nz	FM6
Dr	Margaret	Elcombe	Neutron Scattering Group, ANSTO	mme@atom.ansto.gov.au	TA4
Mr	Tunay	Ersez	Physics, Monash University		TP36
Mr	Geoff	Facer	Physics, University of NSW	gfacer@newt.phys.unsw.edu.au	WP50
Dr	Mike	Fee	Industrial Research Ltd, Lower Hutt	m.fee@irl.cri.nz	WP14
A/Prof	Trevor	Finlayson	Physics, Monash University	trevor.finlayson@sci.monash.edu.au	WM09, WP03, WP24, WP25, WP26, TP11, TP32
Mr	Duncan	Fisher	Physics, University of Wollongong,	duncan@davinci.sci.uow.edu.au	TP41
Prof	Peter	Fisher	Physics, University of Wollongong	p.fisher@uow.edu.au	WP47, TP42
Prof	Neville	Fletcher	RSPhysSE, ANU	Neville.Fletcher@anu.edu.au	

Mr	Adam	Forsyth	Physics, Monash University	adam.forsyth@sci.monash.edu.au	WP64
Dr	Dennis	Fowler	Physics, ADFA	d-fowler@adfa.oz.au	WA3
Mr	Frank	Gagliardi	Physics, Monash University		TP27
Dr	Ewa	Goldys	MPCE Physics, Macquarie University	ewa@mpce1.mpce.mq.edu.au	WP45, TP47, TP48
Dr	Xiaoyi	Gong	CSIRO Division of Chemicals and Polymers	x.gong@chem.csiro.au	TP57
Mrs	B-J	Green			
Dr	Fred	Green	CSIRO Division of Radiophysics	fgreen@rp.csiro.au	TP50
Dr	Miklos	Gulacsi	Theoretical Physics, RSPhysSE, ANU	miklos.gulacsi@anu.edu.au	TP56
Dr	X	Guo	Electronic Structure of Materials, Flinders University	phxg@cc.flinders.edu.au	WP17
Dr	Yuan	Guo	CSEM, University of Wollongong	yuancg@uow.edu.au	WM03, WP12, TP03, TP04, TP05
Mr	Paul	Gwan	CSIRO Division of Applied Physics	paulg@dap.csiro.au	
Miss	Yvette	Hancock	Physics, Monash University	yvette.hancock@sci.monash.edu.au	WP35
Mr	Stephen	Harker	Physics, ADFA	sjh@phadfa.ph.adfa.oz.au	WP02, TP34, TP35
Mr	Rodney	Harris	Oxford Scientific Pty Ltd, Sydney		
Ms	Rachael	Heron	Physics, University of Wollongong	rjh@newt.phys.unsw.edu.au	WP48
Mr	Timothy	Heseltine	Physics, University of NSW	thh@newt.phys.unsw.edu.au	WA2
Dr	Trevor	Hicks	Physics, Monash University	t.j.hicks@sci.monash.edu.au	WP34, TA3, TP36
Dr	Stephen	Holt	Physics, ADFA	s-holt@adfa.edu.au	TP62
Mr	Graeme	Honner	RSPhysSE, ANU	gbh105@rsphy2.anu.edu.au	WP55
Dr	Josip	Horvat	Materials Engineering, University of Wollongong	jhorvat@uow.edu.au	WP05, WP12, TP05
Dr	Chris	Howard	Neutron Scattering Group, ANSTO	cjh@atom.ansto.gov.au	TP67, TP69
Dr	Brett	Hunter	Neutron Scattering Group, ANSTO	bah@atom.ansto.gov.au	TP67
Dr	Wayne	Hutchison	Physics, ADFA	wayne@phadfa.ph.adfa.oz.au	WP32, TP33, TP34
Dr	Mike	James	Neutron Scattering Group, ANSTO	mja@atom.ansto.gov.au	TP02
Mr	J	Jin	Materials Engineering, University of Wollongong	jj97@uow.edu.au	WP07, WP08, TP06, TP07, TP08
Mr	Damien	Jinks	BHP Research, Port Kembla	damienj@resptk.bhp.com.au	WP01, TP23
Dr	Leigh	Johnson	CSIRO Division of Applied Physics	leighj@dap.csiro.au	WP11
Dr	Glynn	Jones	Physics and Astronomy, University of Canterbury	g.jones@phys.canterbury.ac.nz	TP13
Ms	Lois	Jones	Neutron Scattering Group, ANSTO	-	TP68

Dr	Wieslaw	Kaczmarek	RSPhysSE, ANU	wak110@phys.anu.edu.au	WP22, WP23, TP21, TP37
Mr	Alex	Katsaros	CSIRO Division of Applied Physics	alexk@dap.csiro.au	WP69, WP70, WP71
Ms	Georgina	Kelly	Physics, Monash University	g.l.kelly@sci.monash.edu.au	WM09
Dr	Shane	Kennedy	Neutron Scattering Group, ANSTO	sjk@atom.ansto.gov.au	TA3, TA6, TP68, TP69
Dr	Michael	Kenny	CSIRO Division of Applied Physics	michaelk@dap.csiro.au	WM07
Dr	Peter	Killen	Physics, QUT	p.killen@qut.edu.au	WP21
Dr	Robert	Kinnear	Physics, ADFA	r-kinnear@adfa.oz.au	
Dr	Erich	Kisi	Mechanical Engineering, University of Newcastle	meehk@cc.newcastle.edu.au	TP69
Dr	Mark	Knackstedt	RSPhysSE, ANU	mark110@rsphy3.anu.edu.au	FM2
Dr	Yoshihiro	Kuroiwa	Physics, Monash University	yoshihiro.kuroiwa@sci.monash.edu.au	WP26
Mr	Valerian	Kuznetsov	Physics, University of NSW	vk@newt.phys.unsw.edu.au	TP39
Dr	George	Lazarev	Physics, Monash University	georgii.lazarev@sci.monash.edu.au	WP27
Mr	H	Le	Science and Technology, Griffith University	sctle@kraken.itc.gu.edu.au	TM7
Prof	Robert	Leckey	Physics, La Trobe University	leckey@latrobe.edu.au	WP33, WP49, TP14, TP16, TP44, FM8
Mr	Kenneth	Leong	Electrical and Computer Engineering, James Cook University	eng-ktml@jcu.edu.au	WP71, TP30
Dr	Roger	Lewis	Physics, University of Wollongong	r.lewis@uow.edu.au	WP48, TP40
Ms	Zhongli	Li	Electronic Materials Engineering, RSPhySE, ANU	lzl@rsphysse.anu.edu.au	TP20
Mr	Roman	Liebach	Physics, Monash University	roman.liebach@sci.monash.edu.au	
A/Prof	John	Liesegang	Physics, La Trobe University	Liesegang@latrobe.edu.au	TP15
Dr	Michael	Ling	Physics, Monash University	michael.ling@sci.monash.edu.au	WA4, WP34, WP54
Dr	C-J	Liu	Physics, Victoria University of Wellington	Chia-Jyi.Liu@vuw.ac.nz	WP10, WP60
A/Prof	H	Liu	CSEM, University of Wollongong	h.liu@uow.edu.au	WM03, WM05, WP04, WP05, WP09, WP12, WP19, WP20, WP67, TP03, TP04, TP06, TP07
Dr	Mao	Liu	Physics, Monash University	Liu.mao@sci.monash.edu.au	WP25, WP26
Dr	John	Long	Engineering, Deakin University	jlong@deakin.edu.au	TP11
Dr	Nick	Long	Industrial Research Ltd, Lower Hutt	n.long@irl.cri.nz	WP14
Mr	Don	Lowe	Physics, Monash University	don.lowe@sci.monash.edu.au	WP03

Ms	Linda	Macks	Physics, University of NSW	ldm@newt.phys.unsw.edu.au	TM4
Dr	David	Maddison	DSTO-AMRL	maddison@connexus.apana.org.au	WP72
Dr	Hiroshi	Maeda	Tsukuba Magnet Laboratories, Tsukuba	maedah@nrim.go.jp	WA1, WP36
Mr	Craig	Marshall	Balzers Australia	-	
Dr	Dougal	McCulloch	EM Unit, University of Sydney	dougal@emu.su.oz.au	WP13, WP57, TM9
Mr	Alex	Merchant	EM Unit, University of Sydney	merchant@physics.usyd.edu.au	WP13
Mr	Phil	Miles	University of NSW	pam@newt.phys.unsw.edu.au	TA6
A/Prof	David	Miller	Physics, University of NSW	d.miller@unsw.edu.au	WP51
Dr	David	Mills	Physics, Monash University	david.mills@sci.monash.edu.au	
Ms	Emma	Mitchell	Physics, University of NSW	emma@newt.phys.unsw.edu.au	TM3, TP45
Mr	Perez	Moses	Applied Physics, University of Technology Sydney	perezm@phys.uts.edu.au	TP17
Dr	Karl	Müller	CSIRO Division of Applied Physics	karl@dap.csiro.au	WP67, WP68
Mr	Keith	Murray	Oxford Instruments Pty Ltd, Sydney		
Dr	Peter	Norman	Physics, Monash University		WP30
Mr	Graeme	Nott	MPCE, Macquarie University	gnott@mpce.mq.edu.au	WP45
A/Prof	John	O'Connor	Physics, University of Newcastle	PHJOC@cc.newcastle.edu.au	WM06
Mr	Brendan	O'Malley	Applied Physics, RMIT	brendan@giroc.ph.rmit.edu.au	WP57
Prof	Jaan	Oitmaa	Physics, University of NSW	otja@newt.phys.unsw.edu.au	TM8, TP54
Mr	Derek	Oliver	Physics, Monash University	derek.oliver@sci.monash.edu.au	WP24
Mr	Bill	Palmer	AINSE		
Dr	Mark	Prandolini	Physics, ADFA	mjp@phadfa.ph.adfa.oz.au	TP33
Mr	Tony	Puclin	Applied Maths, RSPhysSE, ANU	tpp110@rsphysse.anu.edu.au	WP23
Mr	James	Quilty	Physics, Victoria University of Wellington	james.quilty@vuw.ac.nz	WM04, TP09
Dr	Rodica	Ramer	Electrical Engineering, University of NSW	r.ramer@unsw.edu.au	TP19
Dr	Marlene	Read	Physics, University of NSW	m.read@unsw.edu.au	WP66
Mr	David	Reilly	CSIRO Division of Applied Physics	davidr@dap.csiro.au	WP71, TP70
Dr	Philip	Reynolds	Research School of Chemistry	phil@rschp1.anu.edu.au	TA2
Dr	John	Riley	Physics, La Trobe University	riley@latrobe.edu.au	WP33, WP43, WP49, TP14, TP16, TP44, FM8
Prof	Terry	Sabine	ANSTO	lpa@ansto.gov.au	TA5
Dr	Nick	Savvides	CSIRO Division of Applied Physics	savv@dap.csiro.au	WP69, WP70, WP71, TP70
Dr	Jeff	Sellar	Materials Engineering, Monash University	-	
Mr	Bradley	Senn	Physics, La Trobe University	phybcs@lure.latrobe.edu.au	TP15

Prof	Edie	Sevick	Research School of Chemistry, ANU	sevick@escarides.colorado.edu	WM08
A/ Prof	L	Shakhmuratova	Physics, ADFA	lns@phadfa.ph.adfa.oz.au	WA3, WP32
Mr	Wayne	Sheils	Physics, La Trobe University		FM8
Mrs	Tania	Silver	Physics, University of Wollongong	tania.silver@uow.edu.au	WP46, TP43
Dr	Antony	Simpson	Physics, Victoria University of Wellington	asimpson@ac.dal.ca	TP09
Dr	Jagriti	Singh	Applied Physics, RMIT	jagriti@bunyip.ph.rmit.edu.au	WP37, WP38
Dr	Andrew	Smith	Physics, Monash University	andrew.edward.smith@sci.monash.edu	WP35, WP63, WP64, TP26
Prof	Fred	Smith	La Trobe University	vcomr@lure.latrobe.edu.au	WP25, WP26
Prof	Geoff	Smith	Applied Physics, University of Technology Sydney	G.Smith@uts.edu.au	TP17, TP18
Prof	Phil	Smith	Physics , University of Newcastle		WP61, WP62, TP63
Prof	Ian	Snook	Applied Physics, RMIT	ian@epheron.ph.rmit.edu.au	WP56, WP57, TP59, TP60
Dr	Spiro	Spiliopoulos	Australian Geological Survey		
Dr	Vadim	Stadnik	Physics, University of NSW	vs@newt.phys.unsw.edu.au	TM3, TP45
Mr	Bill	Stanton	Stanton Scientific, Byron Bay		
Dr	Andrew	Stewart	Applied Mathematics, RSPhysSE, ANU	andrew.stewart@anu.edu.au	TP58
Dr	Glen	Stewart	Physics, ADFA	g-stewart@adfa.oz.au	WP02, WP18, TP34, TP35
Mr	Sean	Stewart	Physics, University of Wollongong	sean@davinci.sci.uow.edu.au	TP55
Mr	Agus	Subekti	MPCE, Macquarie University	subekti@mpce1.mpce.mq.edu.au	WP41
Mr	John	Tann	Physics, University of NSW	J.Tann@unsw.edu.au	TM2
Dr	Jagdish	Thakur	Physics, University of NSW	thakur@newt.phys.unsw.edu.au	WP52
Mrs	G	Thurgate			
Dr	Steve	Thurgate	PSET, Murdoch University	thurgate@murdoch.edu.au	WP65, FM7
Mr	Stan	Tkatchenko	Physics, La Trobe University	elest@lure.latrobe.edu.au	WP33, TP14
Dr	Philip	Tregenna-Piggott	Physics, Monash University		TP64
Dr	Gordon	Troup	Physics, Monash University		WP28, WP29, TP24, TP25, TP26
Prof	Tien	Tsong	Institute of Physics, Academia Sinica, Taipei	phTsong@ccvax.sinica.edu.tw	TM1
Dr	Alfred	Uhlherr	CSIRO Division of Chemicals and Polymers	a.uhlherr@chem.csiro.au	FM4
Mrs	Nicoleta	Urma	Applied Physics, RMIT	nicoleta@bunyip.ph.rmit.edu.au	TP71
Dr	Brian	Usher	Electronic Engineering , La Trobe Unversity	bfu@ee.latrobe.edu.au	WP44

Dr	Lou	Vance	Materials Division, ANSTO	erv@nucleus.ansto.gov.au	TP04, TP12, TP66
Dr	Rodney	Vickers	Physics, University of Wollongong	r.vickers@uow.edu.au	WP47
Dr	Nghia	Vo	CSEM, University of Wollongong	vnv56@uow.edu.au	WM03, WM05
Mr	Russell	Walker	Physics, University of Melbourne	rjw@tauon.ph.unimelb.edu.au	WM10
Mr	Genmiao	Wang	Physics, ADFA	gmw@phadfa.ph.adfa.oz.au	TP21
Dr	Hao	Wang	CSEM, University of Wollongong		TP03
Mr	Sanwu	Wang	Physics, University of Newcastle	sanwu@schroeder.newcastle.edu.au	WP62
Mr	Wei	Wang	CSEM, University of Wollongong	gww47@uow.edu.au	WM03, WP12
Dr	Guy	White	CSIRO Division of Applied Physics	guyw@dap.csiro.au	
Prof	John	White	Research School of Chemistry, ANU	jww@rschpl.anu.edu.au	TA1
Ms	Sally	Whitehead	Physics, Monash University	sally.whitehead@DSTO.defence.gov.au	TP29
Dr	Barry	Williams	Australian Skeptics	skeptics.spot.tt.sw.oz.au	
Dr	David	Williams	Applied Maths, I.A.S., ANU	drwll0@rsphy3.anu.edu.au	WM08, TM5
Mr	Xiang-Yuan	Xiong	Materials Engineering, Monash University	xiong@eng2.eng.monash.edu.au	TP32
Ms		Yarovsky			
Dr	Irene	Yarovsky	BHP Research, Melbourne Laboratories	jul@resmel.bhp.com.au	FM1
Mr	M	Yavuz	CSEM, University of Wollongong		TP04
Dr	Gideon	Yoffe	Electronic Engineering, La Trobe University	g.yoffe@ee.latrobe.edu.au	WP44
Mr	Jinning	Yuan	Physics, University of NSW	yuan@newt.phys.unsw.edu.au	WP39
Mr	Bernhard	Zeimetz	CSEM, University of Wollongong	bzeimetz@uow.edu.au	WM03, WP09, WP12
Mr	Heng	Zhang	Physics, ADFA	hgz@phadfa.ph.adfa.oz.au	TP65
Mr	Yu	Zhang	Physics, La Trobe University	phyyu@lure.latrobe.edu.au	WP49, TP44
Ms	Dong	Zhao	Physics, University of NSW	dz@newt.phys.unsw.edu.au	WP15
Mr	Xiaoli	Zhao	Physics, ADFA	xlz@phadfa.ph.adfa.oz.au	WP31
Dr	Yong	Zhao	Materials Science and Engineering, University of NSW	y.zhao@unsw.edu.au	WM02, WP53, TP01, TP61
Mr	Bing	Zhou	SSTL Physics Department, Macquarie University	bing@mpce1.mpce.mq.edu.au	WP42
Ms	Helen	Zuo	School of MPCE, Macquarie University	hyzuo@mpce.mq.edu.au	WP42, TP47